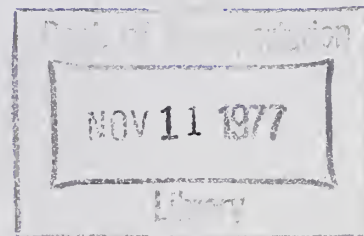


TE  
662  
.A3  
no.  
FHWA-  
RD-  
77-5

No. FHWA-RD-77-5

# - A MODERN APPROACH FOR THE STRUCTURAL AND ANALYSIS OF BURIED CULVERTS



**October 1976**

**Final Report**

Document is available to the public through  
the National Technical Information Service,  
Springfield, Virginia 22161

**Prepared for**  
**FEDERAL HIGHWAY ADMINISTRATION**  
**Offices of Research & Development**  
**Washington, D. C. 20590**

## NOTICE

This document is disseminated under the sponsorship of the Department of Transportation in the interest of information exchange. The United States Government assumes no liability for its contents or use thereof.

The contents of this report reflect the views of the contracting organization, which is responsible for the facts and the accuracy of the data presented herein. The contents do not necessarily reflect the official views or policy of the Department of Transportation. This report does not constitute a standard, specification, or regulation.

The United States Government does not endorse products or manufacturers. Trade or manufacturers' names appear herein only because they are considered essential to the object of this document.

1. Report No. FHWA-RD-77-5	2. Government Accession No.	3. Recipient's Catalog No.	
4. Title and Subtitle CANDE - A MODERN APPROACH FOR THE STRUCTURAL DESIGN AND ANALYSIS OF BURIED CULVERTS		5. Report Date October 1976	
		6. Performing Organization Code	
7. Author(s) M. G. Katona, J. M. Smith, R. S. Odello, J. R. Allgood		8. Performing Organization Report No.	
9. Performing Organization Name and Address Civil Engineering Laboratory Naval Construction Battalion Center Port Hueneme, California 93043		10. Work Unit No. (TRAIS) FCP#	
		11. Contract or Grant No. I.A. 3-1170-(P.O.#)	
12. Sponsoring Agency Name and Address Office of Research Federal Highway Administration Washington, D.C. 20590		13. Type of Report and Period Covered Final Report 1973-1976	
		14. Sponsoring Agency Code 3513-112 S0648	
15. Supplementary Notes Computer program "CANDE" available from the Federal Highway Administration, Washington, D.C. 20590, with System Manual and User Manual. Project Manager: G. W. Ring, HRS-14			
16. Abstract A unified computer methodology is presented for the structural design, analysis, and evaluation of buried culverts made of corrugated steel, aluminum, reinforced concrete, and a class of plastic pipe. Through proper representation of soil-structure interaction, the engineer can test and evaluate either old or new culvert design concepts. The engineer may select any of three solution levels in the computer program, depending on the complexity of the problem and vigor of solution derived. Level 1 is a closed-form elasticity solution (Burns), whereas levels 2 and 3 are based on finite element methods. Each solution characterizes the culvert-soil system by plain strain geometry and loading. Analytical modeling features incremental construction and non-linear constitutive models for characterizing culvert and soil behavior. Culvert material models account for ductile yielding and brittle cracking. CANDE designs are compared with traditional design solutions for both corrugated metal and reinforced concrete pipe. Field experimental data compared to CANDE predictions demonstrate good condition.			
17. Key Words culverts soil-structure interaction		18. Distribution Statement No restrictions. This document is available to the public through the National Technical Information Service, Springfield, Virginia 22161.	
19. Security Classif. (of this report) Unclassified	20. Security Classif. (of this page) Unclassified	21. No. of Pages 475	22. Price

## SUMMARY

### CANDE: A MODERN APPROACH FOR THE STRUCTURAL DESIGN AND ANALYSIS OF BURIED CULVERTS

A unified methodology is presented for the structural design, analysis, and evaluation of buried culverts, including corrugated steel, corrugated aluminum, reinforced concrete, and a class of plastic pipe. Through proper representation of soil-structure interaction, this tool enables design engineers to test and evaluate old or new culvert concepts and, thereby, achieve a keen insight into the relative merits of one culvert-soil configuration versus another. The methodology is embodied in a computer program called CANDE, which has three solution levels corresponding to successive increases in analytical sophistication. Level 1 is based on a closed-form elasticity solution, whereas Levels 2 and 3 are based on the finite element method. Level 2 employs a completely automated finite element mesh generation scheme that permits consideration of both embankment and trench installations. Level 3 applies to any arbitrary culvert installation, but requires a user-defined mesh topology. The solution level concept permits the design engineer to choose a degree of rigor and cost commensurate with a particular project and confidence in input parameters. For each solution level the culvert-soil system is characterized by plane strain geometry and loading so that the loads on the culvert are determined by principles of soil-structure interaction as opposed to assuming the soil loads on the culvert.

CANDE operates in either an analysis or design mode. In the analysis mode the objective is to obtain structural responses of a specified soil-culvert system and to evaluate the culvert in terms of factors-of-safety against potential modes of failure associated with the type of culvert specified. Alternatively, in the design mode, the objective is to ascertain the required wall properties of the culvert such that specified safety factors are satisfied.

Analytical modeling features include incremental construction and nonlinear constitutive models for characterizing the culvert and soil behavior. Culvert material models account



for ductile yielding and brittle cracking, and soil models range from linear to fully nonlinear. In addition, a special interface element permits frictional sliding, separation, and rebonding of two subassemblies meeting at a common junction, such as, the culvert-soil interface.

Parametric studies obtained from CANDE include the influence of soil stiffness, culvert stiffness, culvert geometry, frictional interfaces, bedding configurations, imperfect trench configurations, and other system variations. Also, CANDE designs are compared with traditional design solutions for both corrugated metal and reinforced concrete pipe. Finally, the experimental data are compared with CANDE predictions to demonstrate good correlation.

## ACKNOWLEDGMENTS

Representatives of the pipe industry, state highway departments, universities, and research groups have been very helpful in providing information and constructive criticism for this research effort. Specifically, Professor L. Herrmann of the University of California at Davis graciously provided help with aspects of his finite element computer program, HEROIC, which was modified and incorporated into the CANDE program. Messrs. D. Spannagel and R. Davis of the California Department of Transportation provided experimental data from prototype test culverts discussed herein.

Members of the CEL staff provided suggestions and counsel on aspects of the CANDE methodology. In particular, the author's colleague Mr. J. Crawford was instrumental in establishing automated finite element mesh generating schemes.

Most of all, a debt of gratitude is extended to the Federal Highway Administration and to Mr. George W. Ring, III, the Project Technical Monitor, for the opportunity to work on this fascinating problem. Mr. Ring provided direction, numerous technical papers and reports, and helpful comments on the writing.

# CONTENTS

	page
CHAPTER 1 – INTRODUCTION . . . . .	1
1.1 PURPOSE . . . . .	1
1.2 OBJECTIVE . . . . .	2
1.3 STATEMENT OF PROBLEM . . . . .	3
1.4 BACKGROUND . . . . .	4
1.4.1 Traditional Methods . . . . .	5
1.4.2 Modern Methods . . . . .	7
1.5 SCOPE AND APPROACH . . . . .	9
CHAPTER 2 – CULVERT ASPECTS AND BEHAVIOR . . . . .	13
2.1 GENERAL . . . . .	13
2.2 STRUCTURAL CONSIDERATION OF PIPE-SOIL SYSTEM . . . . .	15
2.2.1 Scope of Boundary Value Problem . . . . .	15
2.2.2 Pipe Definitions and Behavior . . . . .	17
2.2.3 Pipe-Soil System, Definitions and Behavior . . . . .	20
2.2.4 Techniques of Culvert Installation . . . . .	24
2.3 FAILURES OF CULVERTS . . . . .	27
CHAPTER 3 – STRUCTURAL DESIGN CRITERIA AND CONSIDERATION . . . . .	29
3.1 DESIGN DEFINITIONS . . . . .	29
3.2 DESIGN CRITERIA SCOPE . . . . .	30
3.2.1 Flexible Pipe . . . . .	30
3.2.2 Rigid Pipe . . . . .	34
3.3 HANDLING CRITERIA . . . . .	38
3.3.1 Definition . . . . .	38
3.3.2 Traditional Criteria . . . . .	38
3.3.3 Proposed Criteria . . . . .	40
CHAPTER 4 – OVERVIEW OF CANDE . . . . .	45
4.1 CANDE DEFINITION . . . . .	45
4.2 PURPOSE AND PHILOSOPHY . . . . .	45
4.3 CANDE STRUCTURE . . . . .	46
4.3.1 Execution Mode . . . . .	48
4.3.2 Solution Level Concept . . . . .	49
4.3.3 Pipe Library Concept . . . . .	50

	page
CHAPTER 5 – SOLUTION METHODS . . . . .	53
5.1 ELASTICITY SOLUTION (LEVEL 1) . . . . .	54
5.1.1 Conceptualization of Level 1 . . . . .	54
5.1.2 Nonlinear Aspects of Level 1 . . . . .	56
5.1.3 Summary of Level 1 . . . . .	59
5.2 FINITE ELEMENT METHOD . . . . .	59
5.2.1 Finite Element Formulation . . . . .	60
5.2.2 Incremental Form . . . . .	63
5.2.3 Element Types . . . . .	66
5.2.4 Level 2 Operation . . . . .	69
5.2.5 Level 3 Operation . . . . .	74
5.3 BUCKLING APPROXIMATION . . . . .	76
CHAPTER 6 – SOIL MODELS . . . . .	79
6.1 CHARACTERISTICS OF SOIL MODELS . . . . .	80
6.1.1 General Concepts . . . . .	80
6.1.2 Incremental Form . . . . .	82
6.1.3 Constitutive Modeling, Finite Element Versus Closed Form . . . . .	83
6.2 LINEAR SOIL MODEL . . . . .	85
6.3 OVERBURDEN-DEPENDENT MODEL . . . . .	87
6.4 NONLINEAR SOIL MODELS . . . . .	95
6.5 EXTENDED-HARDIN MODEL . . . . .	98
6.5.1 Hardin Shear Modulus Development . . . . .	99
6.5.2 Verification of Shear Model . . . . .	103
6.5.3 Poisson Ratio Function . . . . .	107
6.5.4 Extended-Hardin Versus $K_0$ Test. . . . .	112
6.5.5 Parameters for Extended-Hardin Model . . . . .	115
6.5.6 Computer Algorithm for Extended-Hardin Model . . . . .	120
6.5.7 Summary of Extended-Hardin Model . . . . .	125
CHAPTER 7 – INTERFACE MODEL . . . . .	127
7.1 INTRODUCTION . . . . .	127
7.1.1 Background . . . . .	128
7.1.2 Scope . . . . .	129
7.2 CONSTRAINT EQUATIONS AND VIRTUAL WORK . . . . .	130
7.2.1 Restricted Virtual Work . . . . .	131
7.2.2 General Virtual Work . . . . .	133
7.2.3 Constraint Partitioning . . . . .	135
7.3 CONSTRAINT EQUATIONS FOR INTERFACE MODEL . . . . .	139
7.3.1 Interface Definition . . . . .	139
7.3.2 Interface States . . . . .	141



	page
7.4 FINITE ELEMENT ASSEMBLY OF CONSTRAINT ELEMENTS . . . . .	150
7.4.1 Constraint Assembly . . . . .	150
7.4.2 Constraint Element . . . . .	153
7.5 SUMMARY OF SOLUTION STRATEGY . . . . .	158
CHAPTER 8 - PIPE MODELS AND DESIGN LOGIC . . . . .	161
8.1 PIPE SUBROUTINES . . . . .	162
8.1.1 Data Specification . . . . .	162
8.1.2 Nonlinear Model . . . . .	164
8.1.3 Pipe Evaluation . . . . .	172
8.1.4 Design Update . . . . .	174
8.2 SPECIFIC DESIGN CRITERIA . . . . .	175
8.2.1 Corrugated Steel . . . . .	175
8.2.2 Corrugated Aluminum . . . . .	186
8.2.3 Reinforced Concrete . . . . .	191
8.2.4 Plastic Pipe . . . . .	215
8.2.5 Basic Pipe . . . . .	220
CHAPTER 9 - A TECHNICAL SUMMARY AND RECOMMENDATIONS . . . . .	221
9.1 TECHNICAL SUMMARY . . . . .	221
9.2 LIMITATIONS AND DEFICIENCIES . . . . .	223
9.3 MODELING RECOMMENDATIONS . . . . .	224
9.3.1 Selection of Solution Level . . . . .	225
9.3.2 Selection of Pipe and Soil Model . . . . .	225
9.3.3 Load Representation . . . . .	226
9.4 EXTENSIONS OF CANDE . . . . .	230
CHAPTER 10 - APPLICATIONS OF CANDE . . . . .	231
10.1 PARAMETRIC STUDIES . . . . .	231
10.1.1 Basic Soil-Structure Interaction for Simple Systems . . . . .	232
10.1.2 Effects of Wall Corrugations . . . . .	239
10.1.3 Effects of Pipe Nonlinearity . . . . .	243
10.1.4 Effects of Friction on Pipe-Soil Interface . . . . .	247
10.1.5 Influence of Bedding Parameters . . . . .	252
10.1.6 Influence of Imperfect Trench Parameters . . . . .	257
10.1.7 Influence of Various System Parameters . . . . .	262
10.2 DESIGN COMPARISONS . . . . .	266
10.2.1 Reinforced Concrete . . . . .	267
10.2.2 Corrugated Steel . . . . .	274

	page
10.3 EXPERIMENTAL COMPARISONS . . . . .	279
10.3.1 CANDE and D-Load Comparisons . . . . .	279
10.3.2 California Experimental Test Culverts . . . . .	284
10.3.3 CANDE Model of Test Culverts . . . . .	285
10.3.4 CANDE Predictions and Experimental Data . . . . .	289
CHAPTER 11 - FINDINGS AND CONCLUSIONS . . . . .	297
APPENDIXES	
A - Durability (Corrosion and Abrasion) . . . . .	303
B - Embankment Considerations . . . . .	309
C - Longitudinal Bending . . . . .	315
D - Review of State Highway Department Practices . . . . .	321
E - Recent Culvert Technology . . . . .	345
F - Culvert Failures . . . . .	363
G - Yield-Hinge Theory . . . . .	397
H - Incremental Construction Technique . . . . .	415
I - Element Stiffness Derivations . . . . .	427
J - Soil Test Data and Soil Model Restrictions . . . . .	447
REFERENCES . . . . .	455

# METRIC CONVERSION FACTORS

## Approximate Conversions to Metric Measures

Symbol	When You Know	Multiply by	To Find	Symbol
<b>LENGTH</b>				
in	inches	*2.5	centimeters	cm
ft	feet	30	centimeters	cm
yd	yards	0.9	meters	m
mi	miles	1.6	kilometers	km
<b>AREA</b>				
in <sup>2</sup>	square inches	6.5	square centimeters	cm <sup>2</sup>
ft <sup>2</sup>	square feet	0.09	square meters	m <sup>2</sup>
yd <sup>2</sup>	square yards	0.8	square meters	m <sup>2</sup>
mi <sup>2</sup>	square miles	2.6	square kilometers	km <sup>2</sup>
	acres	0.4	hectares	ha
<b>MASS (weight)</b>				
oz	ounces	28	grams	g
lb	pounds	0.45	kilograms	kg
	short tons (2000 lb)	0.9	tonnes	t
<b>VOLUME</b>				
tsp	teaspoons	5	milliliters	ml
Tbsp	tablespoons	15	milliliters	ml
fl oz	fluid ounces	30	milliliters	ml
c	cups	0.24	liters	l
pt	pints	0.47	liters	l
qt	quarts	0.95	liters	l
gal	gallons	3.8	liters	l
ft <sup>3</sup>	cubic feet	0.03	cubic meters	m <sup>3</sup>
yd <sup>3</sup>	cubic yards	0.76	cubic meters	m <sup>3</sup>
<b>TEMPERATURE (exact)</b>				
°F	Fahrenheit temperature	5/9 (after subtracting 32)	Celsius temperature	°C

## Approximate Conversions from Metric Measures

Symbol	When You Know	Multiply by	To Find	Symbol
<b>LENGTH</b>				
mm	millimeters	0.04	inches	in
cm	centimeters	0.4	inches	in
m	meters	3.3	feet	ft
m	meters	1.1	yards	yd
km	kilometers	0.6	miles	mi
<b>AREA</b>				
cm <sup>2</sup>	square centimeters	0.16	square inches	in <sup>2</sup>
m <sup>2</sup>	square meters	1.2	square yards	yd <sup>2</sup>
km <sup>2</sup>	square kilometers	0.4	square miles	mi <sup>2</sup>
ha	hectares (10,000 m <sup>2</sup> )	2.5	acres	
<b>MASS (weight)</b>				
g	grams	0.035	ounces	oz
kg	kilograms	2.2	pounds	lb
t	tonnes (1000 kg)	1.1	short tons	
<b>VOLUME</b>				
ml	milliliters	0.03	fluid ounces	fl oz
l	liters	2.1	pints	pt
l	liters	1.06	quarts	qt
l	liters	0.26	gallons	gal
m <sup>3</sup>	cubic meters	35	cubic feet	ft <sup>3</sup>
m <sup>3</sup>	cubic meters	1.3	cubic yards	yd <sup>3</sup>
<b>TEMPERATURE (exact)</b>				
°C	Celsius temperature	9/5 (then add 32)	Fahrenheit temperature	°F



\*1 in = 2.54 (exactly). For other exact conversions and more detailed tables, see NBS Misc. Publ. 286, Units of Weights and Measures, Price \$2.25, SD Catalog No. C13.1-0-286.





# CHAPTER 1

## INTRODUCTION

### 1.1 PURPOSE

Culverts are transverse drains under highways, railroads, and other embankments which are manufactured from a variety of materials in a variety of shapes and sizes, most commonly being corrugated metal and reinforced concrete circular pipe. Applications number in the tens of thousands at an annual cost estimated between \$100 to \$500 million [1-1, 1-2], not including installation. It is reasonably certain, therefore, that improvements in design and installation could result in significant cost savings. Therein lies the economic purpose of the effort reported herein.

However, besides the objective of achieving economy, understanding and insight of soil-structure interaction for buried culverts are of utmost importance for advancing culvert technology. Soil-structure interaction is the recognition that culvert and soil act as a synergistic unit, and new innovations in culvert technology can only be achieved by proper application of the principles of soil-structure interaction.

The culmination of this study is "CANDE," which is both a philosophy and an automated computer program for the design and analysis of buried pipe culverts. CANDE fulfills the above purposes by providing a modern design tool that not only demonstrates potential for economic savings,

but also greatly enhances insight into soil-structure interaction and allows evaluation of new culvert-soil concepts.

## 1.2 OBJECTIVE

The objective of this project was to synthesize and extend state-of-the-art analytical techniques into a user-oriented computer program, CANDE, that would provide the capability of both analyzing and designing buried culverts made of corrugated steel, corrugated aluminum, reinforced concrete, or plastic (or brittle) pipe. The specific objectives of CANDE were to:

- (1) Utilize finite element technology and continuum mechanics to characterize the culvert-soil system.
- (2) Properly represent soil-structure interaction, including incremental construction, nonlinear soil models, nonlinear culvert models, and culvert-soil interface models.
- (3) Establish an automated design algorithm for finding the required culvert wall properties based on potential modes of failure and to evaluate culvert performance by factors of safety.

- (4) Structure CANDE for ease-of-use, provide automated finite element mesh routines, and minimize all input.

In addition to the development of CANDE, colateral objectives were to compare CANDE predictions with experimental field data and to conduct parametric studies to evaluate and optimize various culvert installation techniques and procedures.

### 1.3 STATEMENT OF PROBLEM

Heretofore, most culvert designs were based on semiempirical methods that employed "lumped" parameters to represent the influence of loading, soil stiffness-to-pipe stiffness, bedding type, etc. Because one must rely on the empirical lumped parameters, confidence in these methods are limited to situations where the pipe-soil system properties are similar to the test studies defining the lumped parameters.

Fortunately, advances in soil-structure interaction, soil mechanics, and finite element technology permit improved design-analysis methods. These modern methods are timely in that current trends are toward ever-larger culverts under ever-deeper fills. For example, less than 40 years ago, 4-foot-diameter pipes would have been considered "large diameter" pipes and 10 feet of fill would have been referred to as "high fill." Today "large diameter" implies 15 to 30 feet, while

“high fill” means 100 to 200 feet. Another modern trend is toward large-span (50 feet or more), culvert-soil bridges used as an economical replacement for traditional bridges. These recent applications, which are well outside the valid domain of traditional design procedures, require new methods based on sound principles of soil-structure interaction and rational mechanics.

Even for the design of common culverts, substantial benefits should accrue from modern design procedures, such as CANDE, including uniformity, accuracy, speed, and, most importantly, creativity and insight for testing new configurations and installation concepts.

It is recognized that culvert installations often suffer from poor quality control and uncertainties of field construction. Naturally, every effort should be made to insure proper construction procedures are employed and the installation meets all specifications. However, modern analysis methods, such as CANDE, have the ability to assess the consequences of improper construction procedures, such as poor soil compaction under the pipe haunches or moving construction equipment over the pipe in the early stages of construction.

#### 1.4 BACKGROUND

In this section various approaches for designing and analyzing buried culverts are briefly summarized; more thorough discussions are reported



in Reference 1-2. This summary will serve the dual purpose of providing an appreciation of past thinking and establishing a "yardstick" to judge the approach offered herein.

It is convenient to classify the design methods as traditional or modern. Modern means the culvert and soil system are analyzed together so that the load distribution on the pipe is determined in the course of the solution. Contrarily, traditional methods a priori assume the load distribution on the pipe through semiempirical lumped parameters. In short, traditional methods do not properly represent soil-structure interaction. These and other shortcomings of traditional methods have been pointed out by contemporary investigators [1-2,1-3,1-4].

#### 1.4.1 Traditional Methods

Most of the traditional design procedures in use today can be traced back to the pioneering work done at Iowa State University by Marston and Spangler during the first part of this century [1-5 through 1-8]. The Marston-Spangler method is comprised of Marston's estimation of effective vertical load acting on the pipe and Spangler's assumption for the load distribution around the pipe. Effective load is assumed to be the weight of a sliding vertical soil column above the pipe plus or minus the shearing resistance on the sides of the soil column. The sign and magnitude of the shearing resistance are in part dependent

on a rather abstract lumped parameter known as the settlement ratio, which is a relative measure of pipe stiffness to soil stiffness.

Culverts are historically classified as rigid (e.g., reinforced concrete) or flexible (e.g., corrugated metal) with separate design procedures for both groups.

In the case of rigid culverts, the design methodology is intimately connected with the so-called D-load test for reinforced concrete pipe (ASTM-C-497-65T). The D-load test is a standardized procedure for measuring the pipe's load capacity (for either ultimate load or a load causing an 0.01-inch flexural crack) under a three-edge bearing test.

The current design practice for reinforced concrete is well documented by the American Concrete Pipe Association [1-9], whereby the Marston-Spangler approach is used to determine an "equivalent" D-load on the buried pipe. Then, a suitable pipe wall design is selected whose load capacity satisfies the "equivalent" D-load.

For flexible pipe, the Marston-Spangler approach is used to estimate the load distribution around the pipe and predict the relative deflection or flattening of the pipe by means of the well-used Iowa formula [1-8]. Design is achieved by adjusting the pipe's in-plane bending stiffness to limit deflection to 5% or less of the diameter.

In later work Watkins and Spangler [1-10] re-examined the Iowa formula and offered improvements in a controversial characterization of the soil stiffness.

In 1960 White and Layer [1-11] proposed to treat flexible culverts as compression rings where the wall thrust is equal to the weight of the supported soil column. Design is achieved by supplying sufficient pipe wall area such that the thrust stress is safely below the wall strength.

Also in the 1960s extensive consideration was given to elastic buckling, and several prediction techniques were put forth for buckling of buried cylinders in an elastic confining medium with a hydrostatic loading assumption [1-12, 1-13, 1-14, 1-15, 1-16].

Other design concepts have also been proposed [1-2, 1-17]; however, the major design manuals in current use, e.g., AISI [1-18], AASHTO [1-19], and USDOT [1-20], generally employ the Iowa-formula, ring compression, and/or buckling equations for designing flexible pipe.

The traditional design methods for both rigid and flexible pipe are long overdue for a modern design approach [1-2].

#### 1.4.2 Modern Methods

As defined herein, modern methods represent the soil system as a continuum and the conduit as a shell (or continuum). The combined soil-conduit system is the boundary value problem. Solution techniques for the combined boundary value problem can be categorized as analytical or numerical. Analytical approaches use classical elasticity and shell

theory to obtain "exact" solutions, whereas, numerical methods use approximating techniques, such as finite differences or finite elements.

Analytical solutions have been offered by Savin [1-21], Hoeg [1-22], and Burns [1-23]. The latter solution by Burns provides a closed-form solution for a thin shell encased in an infinite elastic medium with overburden loading. Even though this theory has several simplifying assumptions, it nonetheless offers an accurate assessment of soil-structure interaction. Several investigators, including Kay and Krizek [1-24], Dar and Bates [1-25], Nielson and Statish [1-26], and Lew [1-27], have examined Burn's solution and proposed design methods based on this theory.

In the realm of numerical techniques, the finite element method has received the greatest attention in the field of culvert-soil interaction. The method permits description of a wide variety of culvert installation variables, such as embankment or trench conditions, various bedding configurations, and arbitrary pipe shapes, to name but a few. Also, the method is well suited for modeling incremental construction and nonlinear behavior.

Initial applications of finite elements to culverts were performed by Brown [1-28, 1-29] for both rigid and flexible culverts. Other finite element applications include investigations by Allgood and Takahashi [1-30], Nataraja [1-4], Kirkland and Walker [1-31], Anand [1-32], Duncan [1-33], Abel and Mark [1-34], and Spannagel, Davis, and Bacher [1-35].



Utilization of finite element technology to aid in culvert design is currently being developed by Duncan [1-36] for aluminum culverts, by Parmalee [1-37] for reinforced concrete culverts, and by Kay and Abel [1-38] for steel culverts. Each of these approaches is under separate development and employ different mathematical models for characterizing the soil system as well as the culvert. However, one point in common is the intent to develop design charts and graphs as opposed to automated design with the computer. Charts and tables (or regression equations) are only valid for a subset of parameters varied in the finite element solution to create the curves. Extrapolations must be viewed with suspicion. On the other hand, direct design with the computer allows each design to be "tailor made" with no worry of extrapolation. More importantly, the designer can examine the design responses and ascertain how and why different parameters, e.g., bedding shapes, soil placement, pipe types, soft inclusions, etc., influenced the design. Armed with this information the designer can fulfill his real function of conceiving a better culvert installation.

## 1.5 SCOPE AND APPROACH

The ensuing chapters present the philosophy, development, limitations, and application of the CANDE design methodology. The backbone of CANDE is built on three optional solution strategies: (1) the elasticity solution of Burns with nonlinear modifications, (2) the finite element

method with completely automated mesh configurations, and (3) the finite element method with user-defined mesh. In all cases, small displacement theory, time-independent responses, and plane-strain geometry is assumed.

Wherever feasible and proper, existing theories and formulations were synthesized into the CANDE methodology. However, many new innovations or theoretical formulations were developed in the course of this work to meet the objectives. Listed below are some of the more important developments herein:

- (1) A general interface element allowing for frictional sliding, separation, and rebonding of two bodies meeting at a common interface, such as, the pipe-soil interface or the soil-soil interface (Chapter 7).
- (2) A nonlinear soil law employing a variable shear modulus and variable Poisson's ratio dependent on maximum shear strain and hydrostatic pressure (Chapter 6).
- (3) Nonlinear pipe models for concrete cracking, metal yielding, and plastic hinging (Chapter 8 and Appendix G).
- (4) Direct search design strategy based on desired versus actual safety factors for potential modes of failure (Chapter 4 and Chapter 8).

This presentation of CANDE is self-contained; consequently, the writing is lengthy. The following synopsis will aid the reader in locating chapters of interest to him.

Chapter 2 is a brief review of terminology and general considerations of culvert behavior and aspects. Supportive information on durability, longitudinal bending, current practices, and failures are provided in Appendixes A through F. Chapter 3 identifies the design criteria for each pipe type employed in the CANDE program. Chapter 4 is an overview of the CANDE methodology, while Chapter 9 is a corresponding summary. For readers not interested in detail these two chapters describe the essence of CANDE. The intervening Chapters, 5, 6, 7, and 8, detail the solution methods, soil model, interface model, and pipe models with design logic. Supplementary analytical developments are given in Appendixes G through J. The remaining chapters illustrate and discuss applications of CANDE. User input instructions and program documentation are given in separate reports [1-39, 1-40].



## CHAPTER 2

### CULVERT ASPECTS AND BEHAVIOR

#### 2.1 GENERAL

The design and installation of buried culverts is unique in that it requires engineering know-how from almost every field and speciality in civil engineering - structural engineering, soil mechanics, hydraulics, material science, construction methods, transportation, surveying, etc. This study is primarily concerned with the aspects of structural engineering and soil mechanics, hereafter referred to as soil-structure interaction.

In practice, however, the concepts of soil-structure interaction cannot be applied in a "vacuum" independent of other engineering aspects. To illustrate, consider a typical sequence of engineering tasks for culvert design and installation:

- (1) Surveying and Planning. Determine culvert location, optimum alignment, depth of burial, etc.
- (2) Hydraulics. Determine requirements for culvert inside diameter (or shape) and pipe roughness based on flow considerations.



- (3) Structural Design. Determine required pipe wall sizing to support all loads based on soil-structure interaction.
- (4) Durability. If necessary provide protective measures for corrosion and abrasion.
- (5) Field Construction. Employ proper construction procedures, and insure the pipe-soil system conforms to design specifications.

Although task (3), structural design, is the area of interest, it is evident all the engineering tasks are interrelated and influence the structural design. For example, surveying and planning establish the burial depth, which is a key structural design parameter. Likewise, hydraulic considerations dictate requirements for inside pipe diameter (or flow area).

Durability is a measure of the pipe's resistance to material loss due to corrosion and abrasion. Naturally, loss of pipe material compromises the structural integrity of the pipe-soil system and must be considered in the overall design process. Appendix A discusses the durability problem along with recommendations and references.

Undoubtedly the most important and yet most elusive influence on structural design is achieving conformance of field installation with design specifications. Here the problem is generally not with

the pipe itself, but rather with construction of the soil embankment, including bedding and backfill. Appendix B discusses the importance of proper soil compaction and uniform bedding along with a list of potential problem areas. It is emphasized that improper field installations are seldom if ever due to a lack of adequate design specifications. Rather, it is a problem of adequately enforcing these specifications.

In the remainder of this writing, the focus is on soil-structure interaction and structural design. However, the influence of other engineering aspects should be kept in mind for proper perspective.

## 2.2 STRUCTURAL CONSIDERATIONS OF PIPE-SOIL SYSTEM

### 2.2.1 Scope of Boundary Value Problem

In the Introduction it was mentioned that traditional design methods view the pipe as a plane-strain cylinder (or ring) upon which a load distribution is assumed. On the other hand, the CANDE design methodology models both pipe and soil configuration as a plane-strain unit so that the loads carried by the pipe-soil system are determined in the course of the solution.

In reality, of course, culverts are three-dimensional structures, and it is well to emphasize the limitations of plane-strain assumptions. Plane strain implies the culvert installation is a long, prismatic

configuration with no variation in the pipe-soil system or loading along the longitudinal direction of the pipe. Consequently, any cross-sectional view of the pipe-soil system represents the entire system. Clearly, prototype installations do not conform to these ideal prismatic conditions, and the adequacy of plane strain becomes a question of suitable approximation. For example, loading is probably the most dubious prismatic assumption. In the case of an embankment culvert, the fill soil is generally the most significant load component. The soil surface profile measured vertically above the longitudinal pipe axis may vary from a few inches at the toe of an embankment to hundreds of feet at the center of the embankment. To deal with this load variation in a plane-strain context, maximum fill heights are used for conservative design.

For shallow-buried pipes, live surface loads, such as wheel tire pressures and construction equipment, also produce nonprismatic loading. To approximate concentrated loads, equivalent plane-strain strip and pressure loads can be employed (see Chapter 9).

By and large the plane-strain load approximations are adequate and perhaps conservative with regard to in-plane responses. However, from a three-dimensional viewpoint, nonprismatic loading produces longitudinal bending not unlike a beam on an elastic foundation. Fortunately, in most culvert installations longitudinal bending is minimized due to the segmented construction of the pipe or the "bellows" type action of the pipe wall circumferential corrugation. That is, the transmittal of longitudinal bending moments along rigid pipes (e.g., reinforced

concrete) is mitigated at the joints of adjoining pipe segments, and, in the case of corrugated pipes, the bellows action of the corrugation negates any significant transfer of moment. Consequently, for properly installed systems, longitudinal bending is generally not a major design consideration. Nonetheless, in some instances where bedding is nonuniform or consolidation of soil is significant, longitudinal bending cannot be ignored. Appendix C presents techniques for determining structural responses due to longitudinal bending.

To summarize, plane strain is an adequate and perhaps at times conservative description of the culvert boundary value problem. Three-dimensional effects are minimized by the low capacity of pipes to transmit longitudinal bending moments. In all subsequent discussion reference is made only to plane-strain behavior.

#### 2.2.2 Pipe Definitions and Behavior

Although the plane strain cylindrical conduit (or pipe) is a well-studied structural configuration, it is worthwhile to review some basic definitions and structural behavior patterns of the pipe itself independent of the soil system.

Figure 2-1 illustrates a typical circular conduit cross section with commonly defined areas identified. The crown and invert (regardless of pipe shape) are the top and bottom of the pipe, respectively, and the springline is an imaginary line connecting left and right extremities.

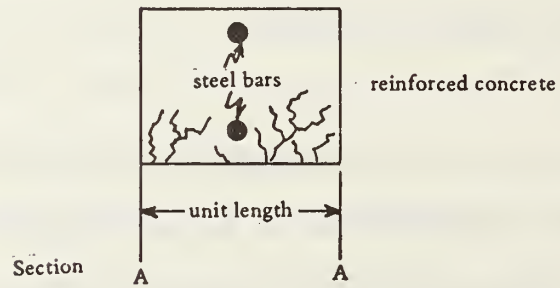
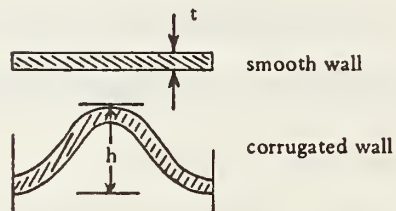
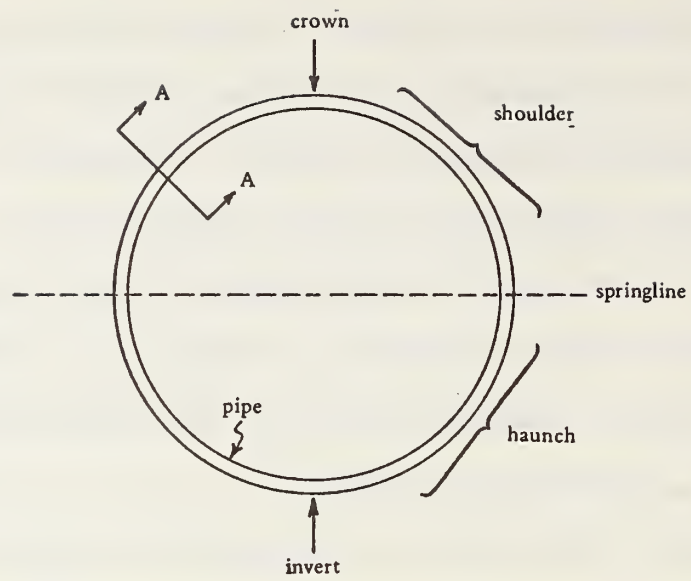


Figure 2-1. Pipe definitions and wall types.



The area between crown and springline is called the shoulder, while the area between the springline and invert is called the haunch.

At any cross section (e.g., A-A in Figure 2-1) the pipe wall is described by four properties:

$E$  = Young's modulus

$\nu$  = Poisson's ratio

$I$  = moment of inertia of wall per unit length

$A$  = thrust area of wall per unit length

The material properties  $E$  and  $\nu$  can be combined into an equivalent plane-strain modulus given by  $E_e = E/(1 - \nu^2)$ . Thus, for a pipe of radius  $R$ , two useful measures of stiffness are given as: hoop stiffness,  $E_e A/R$ , and bending stiffness,  $E_e I/R^2$ . Naturally, the type of material and wall construction greatly influence these stiffnesses as does the pipe radius. For example, if the wall is homogeneous and of uniform thickness,  $t$ , (see Figure 2-1), then  $A = t$  and  $I = t^3/12$ , and if  $t \ll 1.0$ , the bending stiffness becomes very small. However, by corrugating the pipe wall (see Figure 2-1) the bending stiffness is increased on the order of  $(h/t)^2$ , where  $h$  is the height of the corrugation.

As a general rule for most culverts (including thick-walled reinforced concrete), bending stiffness is substantially less than hoop stiffness because of the radius influence. Consequently, visible deformations are primarily in the bending mode as opposed to hoop compression as illustrated next.

Basic notions of structural behavior of pipe can be illustrated by considering two extreme load distributions - hydrostatic and concentrated. In the hydrostatic case (Figure 2-2), only hoop or thrust forces exist in the pipe wall, and deformation is radially inward and inversely proportional to hoop stiffness.

In the second load case, the same total load is applied to the culvert, but is concentrated at the crown and invert. This loading produces moment, thrust, and shear forces in the pipe wall, and deformation takes on an oval shape inversely proportional to bending stiffness (as shown in Figure 2-3).

Comparison of the two load cases dramatizes the importance of properly assessing the load distribution. In the first case the pipe material is fully utilized both through the cross section and around the pipe circumference. However, in the second case large bending deformations occur that produce large tensile stresses (material cracking and rupture) at the crown and invert, thereby inviting premature failure.

In later chapters it is demonstrated that even small perturbations from hydrostatic loading can cause significant bending deformation, emphasizing the need for proper representation of soil-structure interaction.

### 2.2.3 Pipe-Soil System, Definitions and Behavior

“The whole is greater than the sum of its parts.” Although the philosopher Gestalt did not have soil-structure in mind, the above

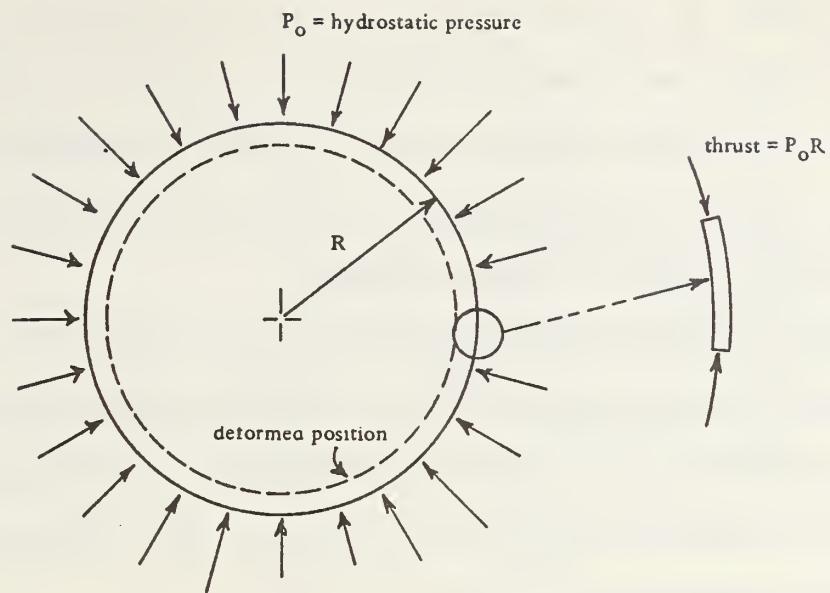


Figure 2-2. Hydrostatic loading and response.

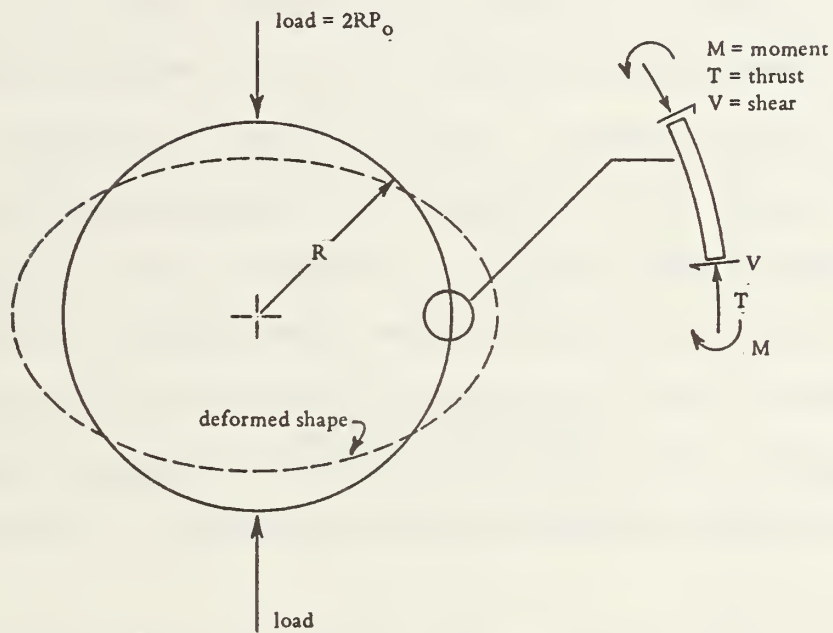


Figure 2-3. Concentrated loading and response.

credo is a most apt description of soil-structure interaction. Pipe and soil working in tandem is one of the most remarkably synergistic systems in engineering. When the soil is properly compacted around the pipe, the load-carrying capacity of the pipe-soil system far exceeds the individual capacity of each component.

Soil-structure interaction analysis is the recognition that both pipe and soil are structural materials, and the purpose of soil-structure interaction theories (like those in CANDE) is to determine the correct magnitude and distribution of loads carried by each component and to assess the consequences.

The role of the engineer is to devise new concepts and configurations that fully utilize the capacity of the pipe-soil system. One fundamental measure for assessing the magnitude of the load carried by the pipe is the "arching" concept. Positive arching is a favorable condition wherein a portion of the overburden load is diverted around the pipe in a compression arch of soil, i.e., the pipe "ducks" the load. The amount of positive arching is measured by the percent reduction of total springline thrust as compared to the weight,  $W$ , of the soil column above the pipe. This concept is illustrated in Figure 2-4a by a freebody of the system above the springline where the thrust,  $N$ , in each wall satisfies  $N < W/2$ .

On the other extreme, negative arching is unfavorable and implies that the pipe is drawing load in excess of the soil column weight so that wall thrust has the relation  $N > W/2$ . The transition case, neutral

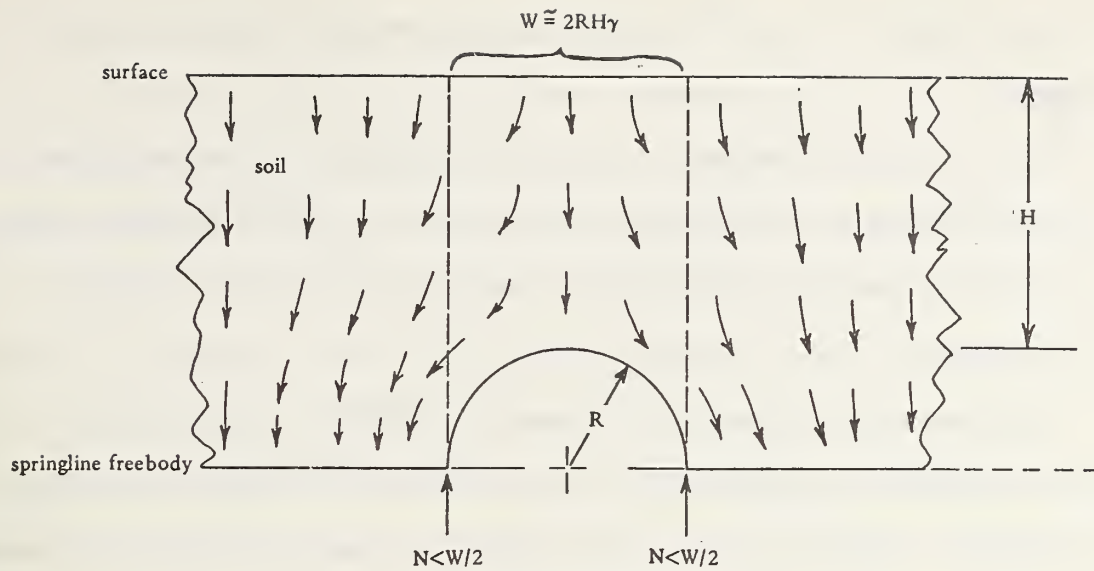


Figure 2-4a. Positive arching.

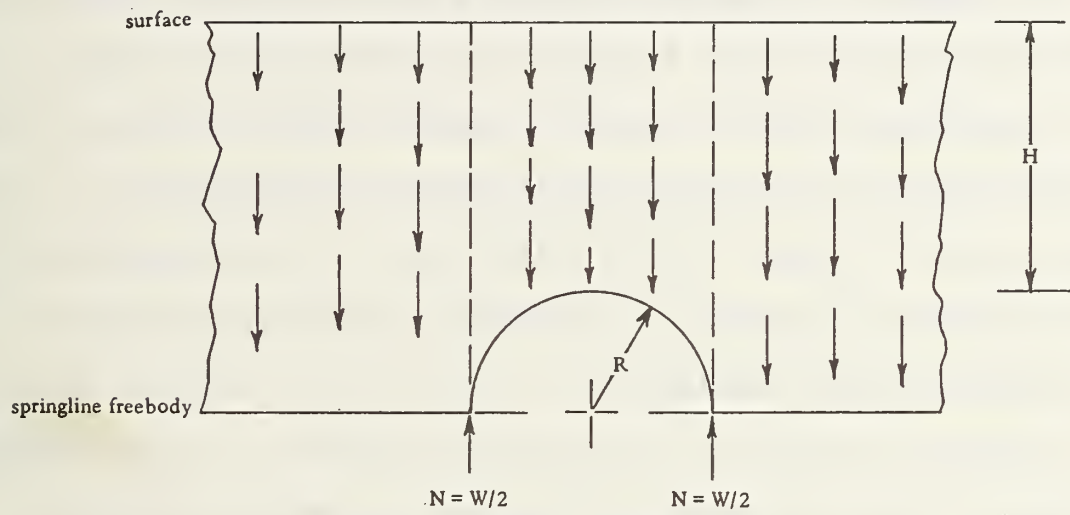


Figure 2-4b. Neutral arching.

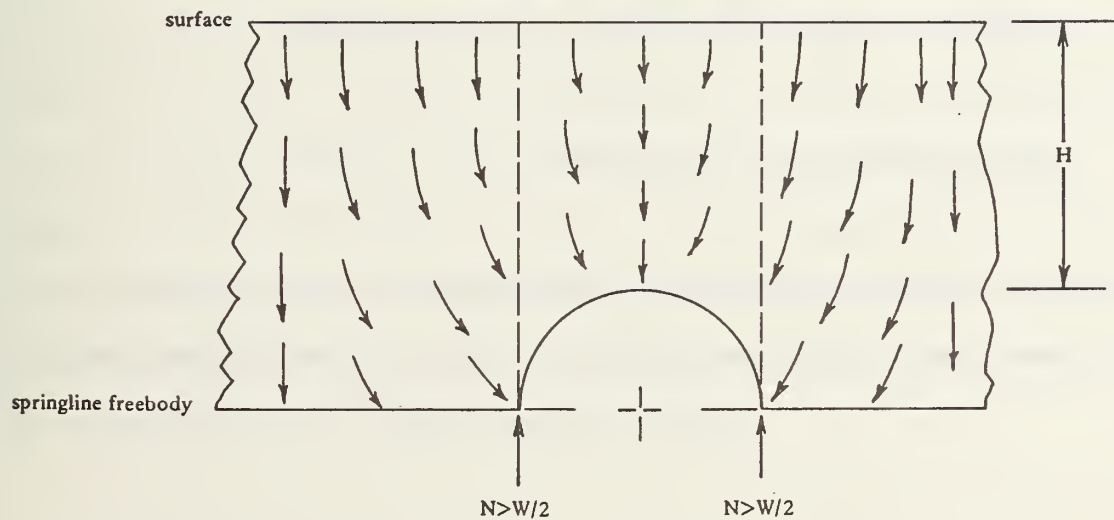


Figure 2-4c. Negative arching.



arching, is given by  $N = W/2$ . Figures 2-4b and 2-4c illustrate these concepts.

Quantitative predictions for arching require solution techniques like CANDE. However, qualitatively it may be said that positive arching is enhanced as the soil stiffness is increased and/or pipe stiffness is decreased.

Based on this reasoning pipes are traditionally classified as rigid or flexible. Rigid pipes, e.g., reinforced concrete, cast iron, or clay tile, typically have large stiffnesses compared to soil stiffness and induce negative arching unless special construction methods are employed. On the other hand, flexible pipes, such as smooth, thin-wall, low stiffness conduits, generally engender positive arching. Corrugated metal pipes are traditionally called "flexible pipe"; however, in many instances they are stiff enough to promote negative arching. This last statement is controversial and will be discussed in the results of this investigation.

To summarize, arching is a fundamental consequence of soil-structure interaction. Arching can work for or against the designer, depending on the installation technique employed as discussed next.

#### 2.2.4 Techniques of Culvert Installation

Two basic culvert installation types are the embankment condition and the trench condition. These designations are self-descriptive, denoting

in the latter case the pipe is set into a trench prior to backfilling, while in the former case the pipe is set at ground surface then covered with a soil embankment. Appendix D illustrates these conditions and variations thereof in detail. For either condition, fill soil is placed around and over the pipes in a series of soil lifts or construction increments. Initially, soil is placed and compacted around the pipe sides so that the pipe experiences lateral pressure and elongates in the vertical direction. This compaction operation is very important because sufficient soil density (and hence stiffness) must be achieved to initiate the soil arch. After subsequent soil lifts are placed and compacted, the pipe flattens or elongates in the horizontal direction, mobilizing soil resistance to lateral movement. Thus, in its final position the load on the pipe is dependent on the construction sequence and load history.

Three common inclusions used in pipe-soil systems are bedding, imperfect trenching, and backpacking; these concepts are illustrated in Figure 2-5.

Traditionally, bedding has been composed of stiff materials, such as dense granular aggregates or concrete, to provide a hard uniform platform to support the pipe. As a mechanism to restrict unequal settlement and longitudinal bending, stiff beddings are useful; however, with regard to soil arching, they represent a stiff inclusion that promotes negative arching and stress concentrations in the pipe. In recognition of this problem, recent trends are to simply carve out a cradle in the undisturbed soil to form a natural bedding.

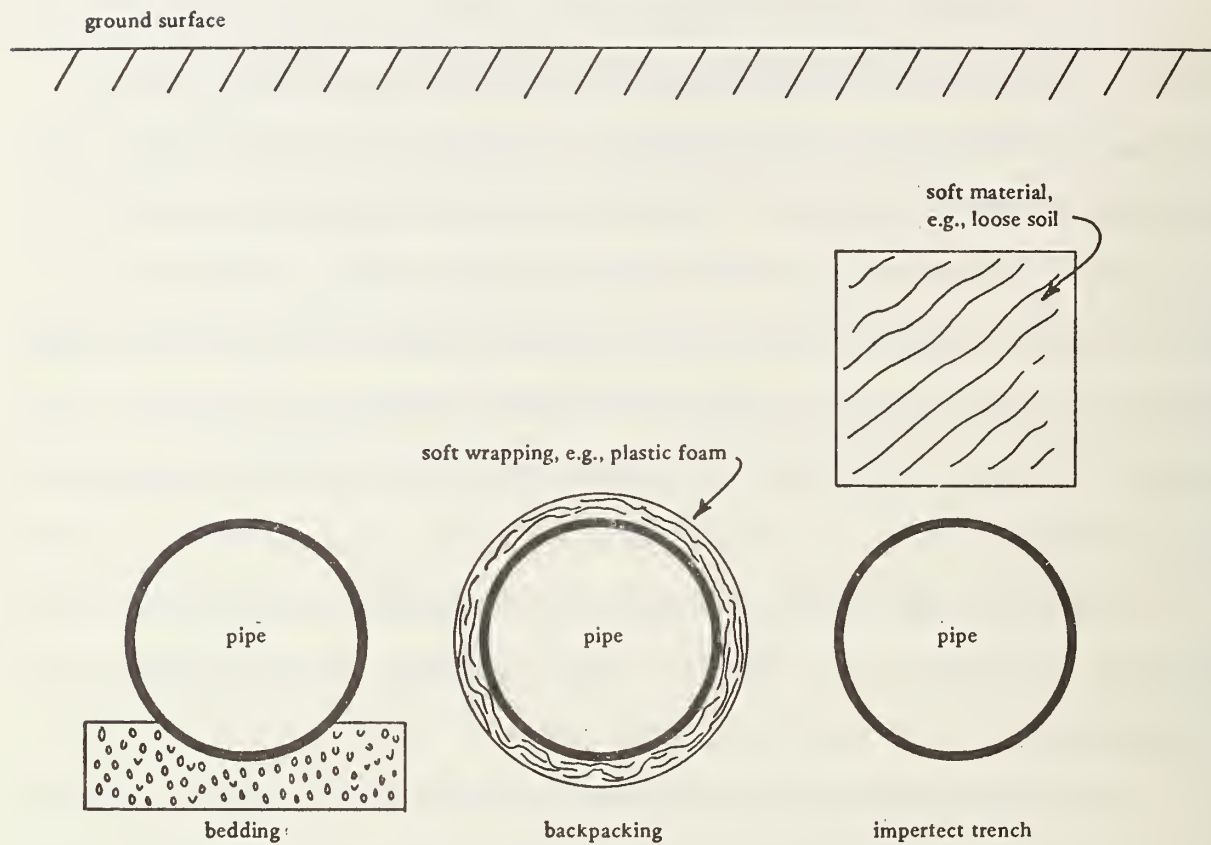


Figure 2-5. Illustrations of culvert inclusions: bedding, backpacking, and imperfect trench.

The imperfect trench concept is intended to promote positive arching by constructing a soft inclusion above the pipe. The method was proposed by Spangler in the 1930s, wherein it was recommended to use straw, hay, cornstalks, and other organic material for the soft element. Theoretically the concept is sound; however, the method has drawn criticism, because decomposition of the organic material can cause caving of the soil arch. Accordingly, some states specify nonorganic material (i.e., loose soil) for the imperfect trench design. Appendix D summarizes current state practices and materials for bedding, backfill, and imperfect trench construction.

Backpacking is a relatively new construction technique and has not as yet been accepted into regulatory design manuals. Like the imperfect trench, backpacking promotes positive arching by soft inclusions. However, the soft material is placed immediately next to the pipe extrados and is nonorganic, such as plastic foam. The material need not be a complete wrap as suggested in Figure 2-5. Optimum distribution can be determined with CANDE. Additional discussion on backpacking along with other recent innovations in culvert technology is provided in Appendix E.

## 2.3 FAILURES OF CULVERTS

A discussion of all known causes of culvert failures is given in Appendix F along with a survey study of reported failures from state highway departments and other sources.

The conclusions from the above study are: (1) most failures occur during the construction process due to poor soil compaction, equipment on the pipe, or construction accidents; (2) failure of functioning culverts is most often attributed to extenuating circumstances, such as corrosion, fire, undermining, floods, and natural disasters; (3) structural failures due to anticipated design loads are extremely rare; and (4) the number of failures that have occurred are exceedingly small compared to the large number of culvert installations, indicating the conservative nature of most traditional design procedures. This conservatism seems particularly true for reinforced concrete pipe.

Potential modes of distress for culverts can be assessed by deflections, wall stresses, buckling loads, and other measures, such as crack width for reinforced concrete. Identification of potential failure modes constitutes design criteria. Each pipe material has its own peculiarities and, hence, its own design criteria. In the next chapter design criteria for each pipe material are established along with suggested safety factors.



## STRUCTURAL DESIGN CRITERIA AND CONSIDERATIONS

## 3.1 DESIGN DEFINITIONS

The intent of this chapter is to establish and define the structural design criteria to be used in the CANDE design methodology. It is important to distinguish between design criteria and design methodology. Design criteria are a minimum set of acceptable standards (or response levels) against which the viability of the culvert designs can be measured. The design methodology is the analytical process of finding culvert wall properties such that predicted structural responses satisfy the design criteria.

The ratio of a design criterion to the corresponding response prediction is termed a safety factor or a performance factor and is a convenient measure to evaluate the pipe design. The term safety factor is proper when the design criterion is a measure of pipe distress tantamount to failure. Accordingly, safety factors should be substantially greater than 1 for safe design. On the other hand, a performance factor implies the design criterion is a measure of an allowable level of response; thus, performance factors can be equal to (and sometimes less than) 1 for safe design. A prime example of performance factors are the handling design criteria discussed at the end of this chapter.

### 3.2 DESIGN CRITERIA SCOPE

The design criteria developed over the years form the basis for the criteria employed in this investigation. Traditional design criteria have withstood the test of time and, for the most part, are tried and true measures of pipe distress. The job at hand is to identify these criteria and introduce additional criteria where necessary. To this end, the design criteria of traditional methods are examined. However, the traditional design methodologies (i.e., prediction techniques) are discussed only in so far as it helps to understand the criteria.

It would be convenient if one set of design criteria was applicable to all pipe materials. Unfortunately, this is not the case now or in the past. Different design criteria are applied to flexible and rigid pipes. In this study the concept of flexible and rigid will be retained to provide a convenient format for discussing design criteria.

#### 3.2.1. Flexible Pipe

3.2.1.1. Traditional Criteria. Historically, the first widely accepted design criterion of flexible pipe was a displacement limit based on a study by the American Railway Engineering Association in 1926 [3.1]. From inspecting numerous large-diameter installations,

the average deflection at the threshold of failure was found to be 20% of the vertical diameter. Recommendations were made for 5% deflection (i.e., safety factor = 4) for functional culverts, and this criterion remains today. Most notably the well-used Iowa formula (3-2) is keyed to the deflection criterion and has served as the major design methodology.

In 1960 White and Layer [3-3] proposed a different design criterion based on ring compression. Simply stated, if maximum thrust stress (or ring stress) in the pipe wall exceeds the pipe wall strength (i.e., either yield stress of metal or seam strength), then the pipe is said to be unsafe. Their prediction technique to determine maximum wall stress is based on the simple equilibrium concept that the pipe must carry the weight of the soil column directly above the pipe. This gives wall stress at the springline as  $\sigma = \lambda_s RH/A$ , where  $\lambda_s$  is soil density, R is pipe radius, H is height of soil column, and A is the area per unit length of pipe wall.

Also in the 1960s a third consideration, elastic buckling, was proposed as a design criterion for flexible pipe along with a host of buckling prediction techniques [3-4 through 3-7]. Actually, an elastic buckling failure of an in-service corrugated metal culvert has never been reported, except where excessive deformation preceded failure. Nonetheless, with increased useage of smooth-wall plastic pipe and large-diameter corrugated metal pipe, buckling considerations should not be dismissed.

Current design procedures for flexible pipe are typified by the AASHTO design approach [3.8] where displacement, wall strength, and buckling are all considered.

3.2.1.2 Proposed Criteria. Table 3-1 summarizes the design criteria used in this investigation (CANDE) for corrugated steel, corrugated aluminum, and a class of plastic pipe that is linear up to brittle rupture. Traditional concepts for displacement and buckling are adopted uniformly for each pipe material, only the values of the suggested safety factors differ slightly.

Stress criteria concepts differ among pipe materials due to different ductile behavior. That is, because steel is highly ductile, yielding due to bending stresses (plastic hinging) is permitted. The only concern for steel is to limit thrust stress,  $\sigma_N$  (average over section), below wall yield stress,  $\sigma_y$ , with a suitable safety factor. This criterion is identical to the traditional concept of ring compression.

Contrari-wise, brittle types of plastic pipe cannot yield in bending, but rather will rupture under excessive outer fiber strain. Accordingly, the design criterion is to limit the maximum strain (bending plus thrust) to less than the ultimate strain,  $\epsilon_u$  of the material.

The behavior of aluminum is between that of highly ductile steel and brittle plastic. Like steel, aluminum exhibits some ductility after the material initially yields; however, unlike steel, the ductile range terminates in rupture without significant strain

Table 3-1. Proposed Design Criteria for Flexible Pipe

Flexible Pipe	Design Criteria for --			
	Thrust Stress, $\sigma_N$	Outer Fiber Strain, $\epsilon$	Relative Pipe Displacement, $\Delta X$	Buckling Pressure, $P_a$
Corrugated steel	$\leq \sigma_y / SF$ SF = 2.0 to 3.0		$\leq 0.2D / SF$ SF = 3.5 to 4.0	$\leq P_{cr} / SF$ SF = 2.0 to 3.0
Corrugated aluminum	$\leq \sigma_y / SF$ SF = 2.0 to 3.0	$\leq \epsilon_u / SF$ SF = 2.0 to 3.0	$\leq 0.2D / SF$ SF = 3.0 to 4.0	$\leq P_{cr} / SF$ SF = 2.0 to 3.0
Smooth plastic		$\leq \epsilon_u / SF$ SF = 2.5 to 3.5	$\leq 0.2D / SF$ SF = 3.0 to 4.0	$\leq P_{cr} / SF$ SF = 2.5 to 3.5

SF = Safety Factor

$\sigma_y$  = Initial yield stress

$\epsilon_u$  = Strain at rupture

$P_{cr}$  = Critical buckling pressure



hardening. Thus, both the thrust and outer fiber strain criterion are employed for aluminum.

A more detailed discussion on material behavior is given in Chapter 8 for each pipe material.

### 3.2.2 Rigid Pipe

3.2.2.1 Traditional Criteria. The first accepted criterion for reinforced concrete pipe was based on the work of Marston, Schliek, and Spangler at Iowa State University in the 1920s. Simply stated, the criterion is: the allowable longitudinal crack width of a functional reinforced concrete culvert is 0.01 inch. Reasoning for this criterion remains controversial. Originally, the Iowa State investigators choose 0.01 inch as a convenient measure for evaluating the pipe. Subsequently, other investigators proposed that 0.01 inch is the tolerable crack width beyond which the reinforcing steel would become vulnerable to corrosive attack. This crack width criterion is employed in the well-used design methodology offered by ACPA (American Concrete Pipe Association) [3-9].

An alternate design criterion also offered by ACPA is ultimate load capacity. Ultimate load is the load producing complete collapse by any failure mechanism.

These criteria are intimately connected with the design methodology of ACPA which employs a D-load rating of the pipe. The D-load rating is a standard method for determining the adequacy of a pipe by employing

a three-edge bearing test (ASTM C497-65T). Under the three-edge bearing method of loading, the pipe is subjected to concentrated line loads at the crown and invert. The load per foot of length of the pipe at which a 0.01-inch-wide crack occurs over a length of 1 foot is divided by the inside pipe diameter to form the D-load rating for crack width which is denoted as  $D_{01}$ . A D-load rating for ultimate load (collapse load) is determined in a similar manner and is termed  $D_{ult}$ . ASTM C76-66T for culvert pipes describes five strength classes for both  $D_{01}$  and  $D_{ult}$ .

To correlate the D-load rating with actual load distribution of a buried culvert, the design procedure estimates the vertical load on the buried pipe and reduces this load by a load factor. The reduction of load is intended to account for the more favorable load distribution and strength characteristics of the buried pipe as opposed to the unconfined D-load pipe. Once the equivalent D-load on the buried pipe is determined, a suitable pipe is obtained from ASTM C-76 tables.

A criterion for allowable diametrical displacement was proposed by Lum [3-10]. The criterion is given as  $d_L = D^2/1200h$ , where  $D$  is pipe diameter and  $h$  is wall thickness. This is seldom used in any design procedures; however, it is a useful performance factor for evaluating the pipe.

3.2.2.2 Proposed Criteria. Whether or not one agrees with the 0.01-crack criterion, it is, nonetheless, a well-defined measure of pipe performance and is one of the few criteria that can be readily measured

in functional pipes. In keeping with the CANDE philosophy the crack-width criterion is retained but can be optionally excluded. Because a 0.01-inch crack represents allowable cracking, it defines a performance factor rather than a safety factor. Table 3-2 shows the crack criterion and the suggested performance factor equal to 1.

Ultimate load capacity is an elusive criterion. It is not well defined from a mechanistic viewpoint, because it does not indicate the mode of failure, such as, concrete crushing, diagonal cracking, tension steel yielding, and/or bowstringing (i.e., a tendency of interior reinforcing steel to separate from concrete under high tensile stress).

In place of the ambiguous ultimate load concept, design criteria for each of the above failure modes are adopted into the CANDE design consideration, as shown in Table 3-2, along with suggested safety factors. The last entry in this table is the allowable displacement criterion of Lum, and the entire table constitutes the design criteria for reinforced concrete pipe.

The above design criteria and failure mechanisms are elaborated upon in Chapter 8 along with a special discussion on bowstringing and reasons for classifying it as a performance factor.

Table 3-2. Design Criteria for Reinforced Concrete Pipe

Parameter	Design Criteria	Relationship*
Concrete Crushing	Maximum compressive stress, $\sigma_c$	$\sigma_c \leq f'_c/SF$ $SF = 1.5 \text{ to } 2.0$
Diagonal Cracking	Maximum shear stress, $v$	$v \leq f'_t/SF$ $SF = 2.0 \text{ to } 3.0$
Steel Yielding	Maximum steel stress, $f_s$	$f_s \leq f_y/SF$ $SF = 1.5 \text{ to } 2.0$
Crack Width	Maximum crack width, $C_w$	$C_w \leq 0.01 \text{ in./PF}$ $PF = 1.0$
Bowstringing	Maximum radial stress along steel-concrete bond, $f_b$	$f_b \leq f'_t/PF$ $PF = 1.0$
Displacement	Maximum diametrical displacement, $\Delta X$	$\Delta X \leq d_L/PF$ $PF = 1.0$

\* $f'_c$  = Concrete compressive strength

$d_L = D^2/1200h$  = Allowable deflection

$f'_t$  = Concrete tensile strength

SF = Safety Factor

$f_y$  = Steel yield stress

PF = Performance Factor

### 3.3 HANDLING CRITERIA

#### 3.3.1 Definition

Handling is the consideration of all loads and shocks which pipes may receive prior to the backfilling operation. In other words, handling requirements insure pipes are sufficiently robust to withstand loads from transportation, unloading, and setting them into place. Once backfilling begins, proper design methodologies (e.g., CANDE) can adequately consider construction loads; therefore, handling criteria must account for all loads prior to the initiation of the boundary value problem.

#### 3.3.2 Traditional Criteria

The traditional handling criterion for flexible pipe is measured by ring deflection rigidity of the pipe. However, the handling relationship is not the result of a specified handling boundary value problem, but rather is established on experience. The relationship is:

$$FF \geq D^2/EI \quad (3-1)$$



where  $D$  = pipe diameter

$E$  = Young's modulus of pipe material (psi)

$I$  = moment of inertia of pipe wall ( $\text{in.}^4/\text{in.}$ )

The term  $FF$  is the so-called flexibility factor whose value is established from experience and is the maximum allowable pipe flexibility. In other words, for a given pipe diameter, the pipe wall bending stiffness,  $EI$ , must be large enough so that Equation 3-1 is satisfied.

The concept of  $FF$  was introduced for corrugated steel design, and it is fairly well standardized among the major steel design codes. The accepted value is  $FF = 0.0433$  for all steel pipe corrugations, except for 6 X 2-inch, where  $FF = 0.02$  is recommended.

In the case of corrugated aluminum, the  $FF$  value is not well established. Typical values range from  $FF = 0.06$  to  $0.09$ .

For plastic pipe, many design procedures do not consider handling at all, and those that do, show little uniformity.

Lastly, reinforced concrete pipe designs generally do not employ a handling criterion in the form of a mathematical relationship. Of course, many handling precautions must be observed to avoid serious concrete cracking, but the rigidity of the concrete pipe wall is assumed sufficient to withstand normal handling loads.

In view of the disparity of current handling criteria among different pipe materials, a desirable goal would be to establish a uniform handling

consideration among the pipe types. This endeavor is attempted in the next section.

### 3.3.3 Proposed Criteria

The handling criterion for corrugated steel is well accepted, and experience has shown that stiffness values for EI not satisfying Equation 3-1 are probably not wise. Thus, to achieve a uniform approach for establishing handling criteria, corrugated steel criterion is used as a basis.

Equation 3-1 can be considered as a measure of percent deflection due to bending. This can be observed from the elastic solution for deflection of a circular ring with diametrically opposed concentrated loads, given as:

$$\frac{\Delta X}{D} = \beta P \frac{D^2}{EI} \quad (3-2)$$

where  $\Delta X$  = diametrical displacement

$\beta$  = 58.8, numerical constant

$P$  = concentrated load

Note the term  $D^2/EI$  is proportional to percent deflection,  $\Delta X/D$ , and, in turn, is proportional to FF in Equation 3-1.

To extend the steel handling flexibility concept uniformly to each pipe material, the viewpoint is taken that Equation 3-1 is a measure of allowable percent deflection for a specified concentrated loading on the circular ring boundary value problem, Equation 3-2. Consider two pipe materials: corrugated steel and a second pipe material. Let  $EI_{\text{steel}}$  represent the typical (or average) stiffness of corrugated steel pipe, and let  $EI_{\text{new}}$  be the typical stiffness of the second pipe material. Clearly, if all things are equal except for the pipe stiffness, and if the new pipe is to be restricted to the same allowable deflection, the new flexibility factor must be defined as:

$$FF_{\text{new}} = \left( \frac{EI_{\text{steel}}}{EI_{\text{new}}} \right) FF_{\text{steel}}$$

Next, it is asserted that allowable percent deflection is not and should not be an absolute constant for all pipe materials under handling loads. Rather, it should be based on the relative deflection strength of each material, so that  $FF_{\text{new}}$  is further scaled by the ratio: (displacement-strength, new)  $\div$  (displacement-strength, steel). These concepts are compactly expressed as:

$$FF_{\text{new}} = r_1 r_2 FF_{\text{steel}} \quad (3-3)$$

where  $FF_{\text{new}}$  = flexibility factor of new pipe material  
 $FF_{\text{steel}}$  = flexibility factor of steel  
 $r_1 = EI_{\text{steel}}/EI_{\text{new}}$ , steel-to-new stiffness ratio  
 $r_2 = (\text{displacement-strength, new}) \div (\text{displacement-strength, steel})$

Equation 3-3 provides a convenient and consistent format for establishing handling flexibility factors for different pipe materials and constructions. Table 3-3 summarizes the proposed flexibility factors for corrugated steel, corrugated aluminum, plastic, and reinforced concrete pipe. Estimates for  $r_1$  and  $r_2$  are based on the following reasoning.

For the flexible pipe group, the characteristic moments of inertias are assumed equivalent so that  $r_1$  is determined from moduli ratios using  $E_{\text{steel}} = 30 \times 10^6$  psi. The ratio  $r_2$  is based on ratios of yield strength, where steel yield is 33 ksi. However, in this study plastic pipe is considered brittle and does not yield, its yield value is taken as 1/2 of ultimate rupture stress ( $\frac{1}{2}$  25 ksi).

With regard to reinforced concrete, the characteristic moment of inertia ratio of corrugated steel to cracked transformed concrete is of the order  $I_{\text{steel}}/I_{\text{conc}} = 1/10$ . At the same time the modulus ratio has the opposite relationship,  $E_{\text{steel}}/E_{\text{conc}} = 10$ , so that  $r_1 = 1$ .

Table 3-3. Handling Flexibility Factors

Type of Pipe	Flexibility Factor		
	$r_1$	$r_2$	FF*
Corrugated steel	1.0	1.0	0.043 (0.02)**
Corrugated aluminum	3.0	0.73	0.09 (0.042)**
Plastic (fiberglass)	18.5	0.38	0.30
Reinforced concrete	1	0.167	0.0072

$$*FF \geq D^2/EI$$

\*\*For structural plate corrugations

The ratio  $r_2$  is based on allowable deflections. The allowable percent deflection for corrugated steel is 5%, and, for reinforced concrete, it is given by  $\Delta X/D = D/1200h$ . For standard reinforced concrete pipe the ratio of inside diameter to wall thickness is  $D/h = 10.0$ , giving the allowable percent deflection as  $\Delta X/D = 0.83\%$ . Therefore,  $r_2$  is given by  $r_2 = 0.83/5.0 = 0.167$ .

The handling criteria of Table 3.3 should be viewed as a design aide and not necessarily as absolute design requirements. In automated design procedures, such as CANDE, the handling criteria provide convenient relationships for starting the design process as detailed in Chapter 8.





## CHAPTER 4

### OVERVIEW OF CANDE

#### 4.1 CANDE DEFINITION

An overview of the CANDE methodology is presented in this chapter to provide the reader with a birdseye view of the purpose, philosophy, and structure of CANDE and to set the stage for detailed analytical developments of subsequent chapters. The acronym CANDE is derived from Culvert ANALysis and Design and is the name of the computer program associated with this work. However, in this writing, the term CANDE does not simply imply a set of computer cards, but rather the name is used in a broader sense to signify the goals, objectives, theories and limitations of a modern approach for the design and analysis of buried pipe culverts.

#### 4.2 PURPOSE AND PHILOSOPHY

The purpose of CANDE is to synthesize and extend modern analytical techniques into a single computer program that is readily usable by a broad spectrum of engineers for culvert design and analysis.

The concept of usability is the key factor in the philosophy of the CANDE methodology. All too often, computer-aided design procedures

require a high level of expertise and experience to correctly define the boundary value problem (input) and interpret the results (output), thereby limiting the applicability of the program to a small subset of the engineering community. To deal with this problem, CANDE is structured to operate in a range of usage from "black box" to "grey box." "Black box" implies the engineer need know nothing of the solution methodology (e.g., finite element mesh) to design or analyze a culvert installation. Input consists of pipe dimensions and engineering properties, while output includes safety factors against potential modes of failure and required pipe wall properties.

On the other end of the scale, "grey box" signifies a close contact between the engineer and CANDE, such that, the engineer can construct his own finite element mesh or add new pipe and soil models to the program. The modular nature of CANDE permits relatively easy additions and/or modifications. This will be apparent in the CANDE structure discussed next.

#### 4.3 CANDE STRUCTURE

Figure 4-1 is a schematic overview of CANDE wherein three main areas are identified: the main control at top, the pipe library at bottom left, and the solution library at bottom right.

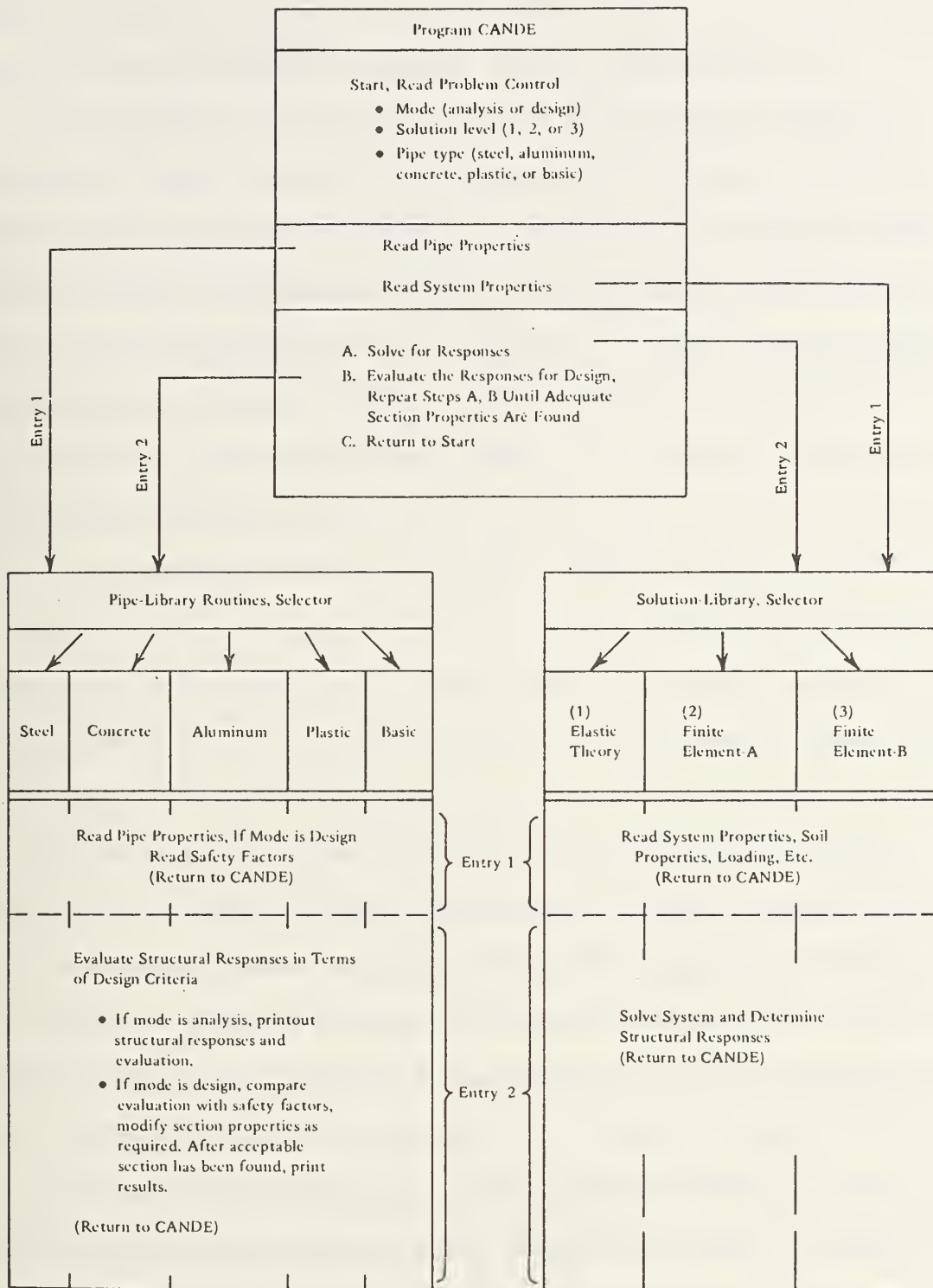


Figure 4-1. Schematic diagram for CANDE.

The main control identifies the problem to be considered and acts as a switchboard to shift information back and forth between the pipe library and the solution library. Three basic selections in the main control identify the problem to be considered: (1) execution mode, (2) solution level, and (3) pipe type. The "mix-and-match" feature of CANDE is apparent. Any pipe type from the pipe library can be matched with any solution level from the solution library, and the pair can be run in either a design or analysis mode. Not apparent from Figure 4-1 are the analytical modeling techniques, which include: incremental construction, nonlinear soil models, nonlinear interface models (e.g., pipe-soil interface), and nonlinear pipe models ranging from ductile yielding to brittle cracking. These features are discussed in turn in Chapters 5 through 8.

#### 4.3.1 Execution Mode

The execution mode is the decision between design or analysis. Analysis means a particular pipe-soil system is completely defined and then solved by the chosen solution level. Output consists of the structural responses (displacements, stresses, strains) as well as an evaluation of the pipe performance in terms of safety factors against potential modes of failure.

The alternative execution mode, design, requires the same input definition, except that the pipe wall geometrical section properties



are unknown. Instead, desired safety factors are input, and CANDE achieves a design by a direct search approach. That is, a series of analyses are performed such that an initial trial section is successively modified until the desired safety factors are achieved. Design output includes required wall properties, actual safety factors, and structural responses. Naturally, required wall properties depend on the pipe type. For example, properties for metal pipes are given in corrugation and gage sizes, while reinforced concrete pipe properties are given in wall thickness and steel area.

#### 4.3.2 Solution Level Concept

In the solution library there is a choice of three solution levels corresponding to successively increased levels of analytical sophistication. The successive increase in analytical power is accompanied by an increase in the input preparation and computer cost. Level 1 is based on a closed-form elasticity solution, while Levels 2 and 3 are based on the finite element method. Level 2 provides completely automated finite element meshes suitable for the vast majority of culvert installations, whereas Level 3 requires a user-defined mesh for special installations. All solution levels assume plane-strain geometry and are cast in incremental form to accommodate nonlinear processes.

The solution level concept allows the engineer to select a degree of rigor and cost commensurate with the confidence of input parameters and relative worth of the project. Chapter 5 is devoted to the full

development of each solution level, including applications and limitations.

#### 4.3.3 Pipe Library Concept

Like the solution library, the pipe library offers a selection of pipe types. Each pipe type resides in a separate subroutine and contains a constitutive model (stress-strain law) and design logic representative of the pipe material. Currently, the pipe library contains subroutines for corrugated steel, corrugated aluminum, plastic, and reinforced concrete. In addition, a subroutine, called BASIC, allows for the description of nonstandard or built-up pipe properties. However, this routine is intended for analysis only.

The pipe subroutines are the key control areas of CANDE and monitor the design process. Referring to Figure 4-1, the information flow goes back and forth from the solution level through the main control switchboard to the pipe routine in a solve-evaluation loop. That is, the pipe routine evaluates the structural integrity of the pipe from the structural responses of the current solution. If the pipe wall properties are inadequate (either over or underdesigned), the wall properties are modified and passed back to the solution level for another trial. When at last the design criteria are satisfied, the wall design and evaluation of the culvert system are printed out, and the next problem is considered.

Nonlinear stress-strain laws for pipe material are also accommodated by the same solve-evaluation loop. Nonlinear treatment requires an iteration loop within the design loop. Chapter 8 provides a full discussion on the design logic and stress-strain modeling for each pipe type.



## CHAPTER 5

### SOLUTION METHODS

The solution methods consist of two distinct solution theories: a closed-form elastic solution by Burns [5-1], called Level 1, and a finite element program modified and extended from Herrmann [5-2]. The finite element program is fashioned to operate in either of two input options. In one option, called Level 2, a completely automated mesh generator is employed to model the pipe-soil system. The second option requires user-defined input for describing mesh topology. This latter option is called Level 3 and is used when the pipe-soil system cannot be adequately described with Level 2.

Basic assumptions common to all three solution levels are: plane-strain geometry and loading, small displacement theory, and quasi-static responses. Naturally, the elasticity theory, Level 1, is more restrictive than the finite element Levels 2 and 3 with regard to the scope of the boundary values that can be considered. Also Level 2 is more restrictive than Level 3. However, this ordering is reversed with regard to ease of data preparation and computer costs. Detailed capabilities and restrictions of each level are discussed in the following sections.



## 5.1 ELASTICITY SOLUTION (LEVEL 1)

The elasticity formulation [5-1] provides an exact solution for an elastic cylindrical conduit encased in an isotropic, homogeneous, infinite, elastic medium (soil) with a uniformly distributed pressure acting on horizontal planes at an infinite distance. Thin-shell theory is assumed for the conduit, and continuum elastic theory is employed for the surrounding infinite medium. The conduit-medium interface is modeled with a choice of two boundary conditions: bonded interface, where both normal and tangential forces are transmitted across the interface and frictionless interface, where only normal forces are transmitted across the interface.

Table 5-1 summarizes the elasticity solutions for conduit responses, including radial and tangential soil pressure on conduit, radial and tangential displacements of conduit wall, along with moment and thrust resultants. The responses are a function of the angle,  $\theta$ , measured from the springline of conduit, and are identified for the two interface conditions -- bonded or frictionless.

### 5.1.1 Conceptualization of Level 1

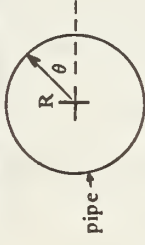
At first encounter, the applicability of the infinite regions described above to model culvert systems with finite burial depths may seem questionable. However, it has been shown [5-1] that the interaction

Table 5-1. Elasticity Solution Equations for Pressures on Pipe and Pipe Responses for Bonded and Frictionless Interfaces

Soil Properties  
 $M_s$  = confined modulus\*  
 $K$  = lateral pressure coef.\*\*  
 $P_o$  = overburden pressure

Pipe Properties  
 $\tilde{E}$  = effective Young's modulus\*\*\*  
 $I$  = moment of inertia p.u.l.  
 $A$  = thrust area p.u.l.  
 $R$  = average radius

Dimensionless Parameters  
 $B = (1 + K)/2$   
 $C = (1 - K)/2$   
 $U = M_s R/E A$   
 $V = M_s R^3/6 E I$

Structural Responses of Pipe	Common Factor	Bonded Interface	Frictionless Interface
		$a_o = C(2BU - 1) \div B(1 + 2CU)$ $a_2 = [CV(2BCU - C) + C^2 U/2 - B] \div d$ $b_2 = [CV(B + 2BCU) - BC U/2 - B] \div d$ $d = CV(1 + B + 2BCU) + C U(1 + C/2) + C + 1$	$a_o = C(2BU - 1) \div B(1 + 2CU)$ $a_2 = (4BCV + C) \div d$ $b_2 = (4BCV - B) \div d$ $d = 4BCV + C + 2$
Radial pressure on pipe: $P_r =$	$P_o \times$	$B(1 - a_o) - C(1 + 3a_2 - 4b_2) \cos 2\theta$	$B(1 - a_o) - C(1 + 3a_2 - 4b_2) \cos 2\theta$
Tangential pressure on pipe: $P_\theta =$	$P_o \times$	$C(1 - 3a + 2b_2) \sin 2\theta$	0.0
Radial displacement of pipe: $w =$	$\frac{P_o R}{M_s} \times$	$B U(1 - a_o) - C V(1 + a_2 - 2b_2) \cos 2\theta$	$B U(1 - a_o) - \frac{2}{3} C V(1 + 3a_2 - 4b_2) \cos 2\theta$
Tangential displacement of pipe: $v =$	$\frac{P_o R}{M_s} \times$	$\frac{1}{2} (1 + a_2 + 2b_2 C/B) \sin 2\theta$	$\frac{1}{3} C V(1 + 3a_2 - 4b_2) \sin 2\theta$
Moment on pipe wall: $M =$	$P_o R^2 \times$	$B U(1 - a_o)/6 V + \frac{1}{2} C(1 + a_2 - 2b_2) \cos 2\theta$	$B U(1 - a_o)/6 V + \frac{1}{3} C(1 + 3a_2 - 4b_2) \cos 2\theta$
Thrust on pipe wall: $N =$	$P_o R \times$	$B(1 - a_o) + C(1 - a_2) \cos 2\theta$	$B(1 - a_o) + \frac{1}{3} C(1 + 3a_2 - 4b_2) \cos 2\theta$

\*Soil confined modulus is related to Young's modulus and Poisson's ratio by:  $M_s = E_s(1 - \nu_s)/[(1 + \nu_s)(1 - 2\nu_s)]$

\*\*Soil lateral pressure coef. is related to Poisson's ratio by:  $K = \nu_s/(1 - \nu_s)$

\*\*\*Pipe effective Young's modulus is related to Young's modulus and Poisson's ratio by:  $\tilde{E} = E/(1 - \nu^2)$

between conduit and medium (or pipe and soil) occurs primarily within a three-radius area of the pipe center. Beyond this area the soil response is practically unaffected by the pipe inclusion for overburden loading. Therefore, the pipe-soil system can be visualized with the finite boundaries and overburden loading as shown in Figure 5-1.

In this representation,  $P_o$  is the equivalent overburden pressure of the fill soil above the pipe, and the remaining system parameters are identified in Figure 5-1. The elasticity solution becomes progressively less valid when the free surface (depth of cover) is less than three pipe radii and should not be used for cover depths less than one radius.

#### 5.1.2 Nonlinear Aspects of Level 1

Although Level 1 is based on a linear elasticity solution, a fair degree of nonlinear modeling is achieved for both soil and pipe in the following manner. First, with regard to the soil, the overburden pressure,  $P_o$ , is divided into several load increments, and the load is applied in a series of load steps. During each load step the material properties of the soil can be redefined in accordance with current overburden pressure. The structural responses of the pipe-soil system are summed in a running total providing a load history record. This procedure and the concept of overburden-dependent soil properties are elaborated upon in Chapter 6.

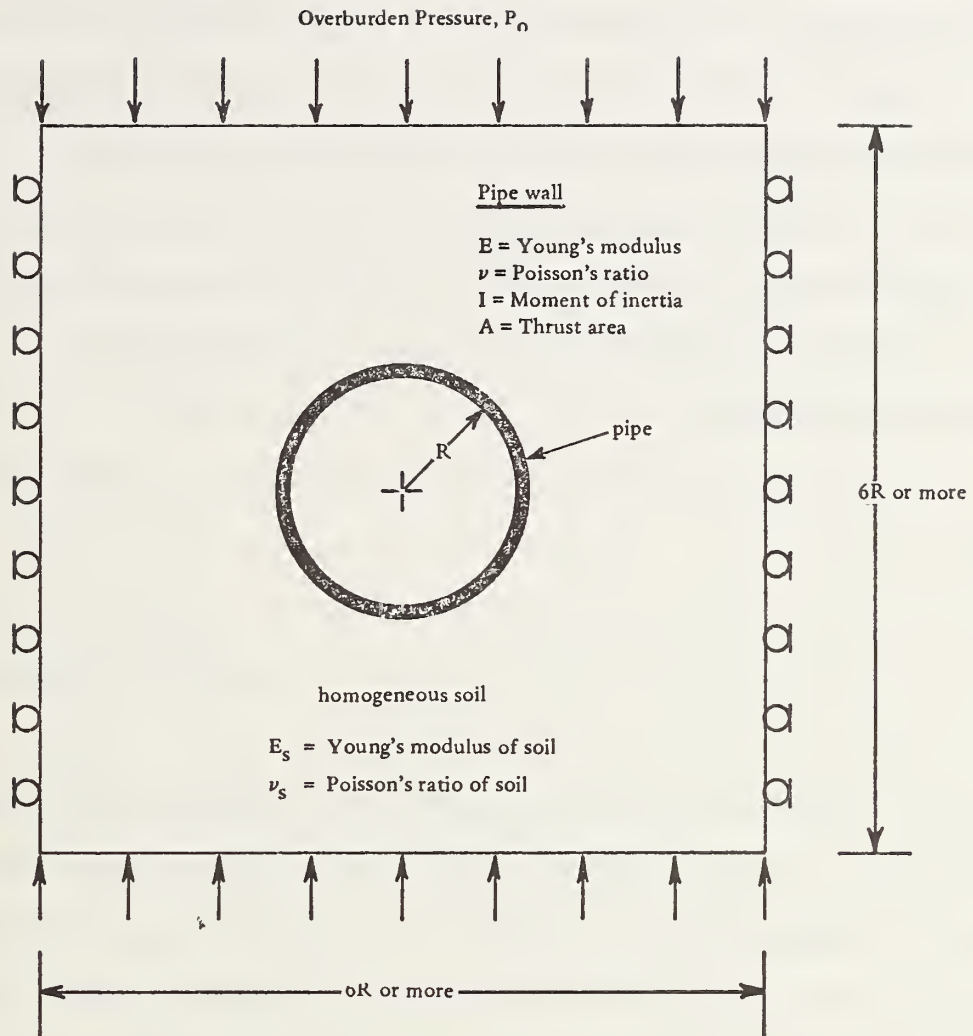


Figure 5-1. Conceptual approximation of elasticity boundary value problem.

With regard to nonlinear behavior of the pipe, two approaches are considered. First, the nonlinear material law of each pipe type (developed in detail in Chapter 8) produces changes in the effective stiffness at each point around the pipe periphery. These modified properties are used directly to predict stress and strain at each pipe point; however, to predict displacements and resultants (i.e., moment, thrust, and shear) a smeared average of the modified properties is used for the Level 1 equations presented in Table 5-1.

The above approach works surprisingly well for most problems; however, in the case of flexible, ductile pipes under very deep fill soil, it is likely that bending stresses at the quarter points of the pipe will produce significant plastic hinging (say more than 50% of the wall section in yield). In these cases, the "smeared stiffness" approach is not well-suited for predicting displacements and resultants. As an alternative, the "yield hinge theory" is provided. The "yield hinge theory" is a correctional solution that is adjoined to the elasticity solution and is developed in detail in Appendix G. Briefly, the approach is to utilize a correctional boundary value problem idealized by four equal segments of a circular pipe joined by hinges and embedded in the soil medium. Assumed hinge rotations are prescribed in an iterative manner until the assumed rotations are in agreement with rotations from the plastic hinge theory.



### 5.1.3 Summary of Level 1

The Level 1 approach does not have the versatility, and generality of the Level 2 and 3 counterparts. Nonetheless, its efficiency and applicability, particularly for design, cannot be overemphasized. From a design viewpoint, the exact nature of the soil system, loading, and boundary conditions are seldom known a priori. Thus, the simplifying assumptions of Level 1 are often commensurate with knowledge of the design problem. It follows that the simple data preparation and small computer cost make Level 1 an attractive and powerful design tool.

## 5.2 FINITE ELEMENT METHOD

As previously mentioned Level 2 and Level 3 share a common finite element solution program and differ only with respect to the mode of input: automatic or user-defined. The development and formulation of the finite element method is well- established [5-3]; a summary will be given herein as it applies to the culvert problem.

### 5.2.1 Finite Element Formulation

A static formulation of the finite element method can be equivalently derived from virtual work or from variational principles. The virtual work approach is outlined below.

The virtual work in a structural system can be expressed in matrix notation as:

$$\int_V \delta\{\epsilon\}^T \{\sigma\} dV = \int_S \delta\{u\}^T \{t\} dS + \int_V \delta\{u\}^T \{f\} dV \quad (5-1)$$

where     $\{\sigma\}$  = stress vector  
          $\{\epsilon\}$  = strain vector  
          $\{u\}$  = displacement vector  
          $\{t\}$  = surface traction vector  
          $\{f\}$  = body force vector  
          $\{ \}^T$  = transpose of vector  
          $\delta\{ \}$  = virtual vector  
          $S$  = surface of body  
          $V$  = volume of body

Equation 5-1 states, “virtual strain energy is equal to the virtual external work of body and traction loads undergoing virtual movements compatible with the kinematic constraints of the system.” (Note: in Chapter 7 this principle is extended.)

In preparation for the so-called finite element displacement formulation, the strain energy term of the virtual statement is written in terms of displacements by use of the constitutive relationship and strain-displacement relationship; i.e.,

$$\{\sigma\} = [C] \{\epsilon\} \quad (5-2)$$

$$\{\epsilon\} = [Q] \{u\} \quad (5-3)$$

where  $[C]$  = constitutive matrix (stress-strain law)  
 $[Q]$  = strain-displacement operator (derivative matrix)

Using the above relationships, virtual strain energy can be written as:

$$\int_V \delta\{\epsilon\}^T \{\sigma\} dV = \int_V \{[Q] \delta\{u\}\}^T [C] [Q] \{u\} dV \quad (5-4)$$

The actual form of  $[C]$  and  $[Q]$  is dependent on material and kinematic assumptions and will differ between soil and pipe models. These points will be discussed later; for now, the concern is with the general formulation.

At this juncture, the finite element approximation is introduced by subdividing the domain  $V$  into a discrete set of elements interconnected at common nodal points such that continuity is maintained at all points on the boundary of the elements. The assemblage of elements and nodes is termed the finite element mesh.

Within each element displacements are selected as the primary dependent variable, such that the displacements are characterized by a specified interpolation function with unknown nodal displacements on the element exterior; i.e.,

$$\{u\}_e = [h]_e \{\hat{u}\} \quad (5-5)$$

where  $\{u\}_e$  = displacement vector within element

$[h]_e$  = interpolation matrix of prescribed functions

$\{\hat{u}\}$  = nodal displacement vector (unknowns)

Again, the form of the interpolation matrix and nodal displacement vector is dependent on element type and will be addressed later.

By (1) inserting Equations 5-4 and 5-5 into the virtual work statement (Equation 5-1), (2) allowing the integration over the entire domain  $V$  to be represented by a summation of element integrations, and (3) noting the virtual displacement of each node is independent, the virtual work equation yields the familiar global equilibrium equation:

$$[K] \{\hat{u}\} = \{P\} \quad (5-6)$$

$$\text{where } [K] = \sum [k]_e \quad (5-7)$$

$$\{P\} = \sum \{p\}_e \quad (5-8)$$

Global stiffness matrix  $[K]$  and load vector  $\{P\}$  are the ordered summation of the element stiffness matrix and load vector, respectively, given by:

$$[k]_e = \int_{V_e} [B]_e^T [C]_e [B]_e dV_e \quad (5-9)$$

$$\{p\}_e = \int_{S_e} [B]_e^T \{t\} dS_e + \int_{V_e} [B]_e^T \{f\} dV_e \quad (5-10)$$

$$\text{where } [B]_e = [Q]_e [h]_e \quad (5-11)$$

The element stiffness matrix,  $[k]_e$ , is the heart of the finite element formulation and provides the flexibility for modeling complex boundary value problems by assigning any group of elements special material characteristics, loadings, and/or boundary conditions. However, before pursuing these concepts it is convenient to recast the above derivation in incremental form.

### 5.2.2 Incremental Form

Thus far, discussion has been slated toward linear systems, because the constitutive matrix in Equation 5-9 was implied to be constant. To provide for material nonlinearity an incremental approach is commonly used to approximate nonlinear behavior by a summation of linear solutions.



However, in the case of culvert-soil systems, the incremental approach takes on a larger meaning than is generally inferred. To wit, not only the load, but also the structural system is incremented. This process is termed "incremental construction technique" and is the mathematical analogue of the physical process of constructing the soil system in a series of compacted layers or lifts. At first encounter with the concept of incremental construction, several natural questions arise; e.g., how do the analytical responses of a "single-lift" system compare with the same system composed of "multilifts." This question and further discussion on the incremental construction technique are discussed in Appendix H.

To extend the linear formulation to include incremental construction and without loss of generality, all vector quantities are prefixed with an incremental symbol  $\Delta$  so that Equation 5-6 is written as:

$$[K]_i \{\Delta \hat{u}\}_i = \{\Delta P\}_i \quad i = 1, 2, \dots N \quad (5-12)$$

where  $\{\Delta \hat{u}\}_i$  = unknown nodal displacement increments due to construction increment "i"  
 $\{\Delta P\}_i$  = load increment associated with construction increment "i"  
 $[K]_i$  = combined stiffnesses of construction increments up to and including "i"  
*i* = construction increment number, *i* = 1, 2, ... N,  
 where N = number of increments

Each incremental solution is solved as a linear system. That is, the current stiffness matrix,  $[K]_i$ , is triangularized by Gaussian elimination, taking full advantage of positive definiteness and the banded nature of the stiffness matrix. Thereafter, the solution increment  $\{\Delta\hat{u}\}_i$  is added to the summation of all previous increments; i.e.,

$$\{\hat{u}\}_i = \sum_{j=1}^i \{\Delta\hat{u}\}_j \quad (5-13)$$

where  $i$  = current construction increment  
 $j$  = history counter of construction increments  
 $\{\hat{u}\}_i$  = net nodal displacements after increment  $i$

Similarly, stress, strain, and other response increments are calculated and summed into running totals so that complete response records are available after each loading increment.

In conjunction with the above incremental construction, material nonlinearities can be directly accommodated by the so-called tangent method. After each construction increment the material properties of each element (i.e.,  $[C]_e$ ) are re-evaluated in accordance with the chosen nonlinear model and current state of stress. The element stiffness is recalculated, and the solution process continues as previously described. Thus, the concepts of incremental construction and material tangent nonlinearity are treated simultaneously. The shortcoming of the tangent modeling method is that relatively small load increments must be used

so that evaluation of the nonlinear model at the beginning of the load step is representative of the material during the entire step.

In many instances, the tangent method is sufficiently accurate for typical culvert applications; however, if large load steps are employed or if the material model is highly nonlinear, a more accurate technique is required; i.e., iterating within the load step. Iteration implies the load step is repeated and solved several times, such that the material properties are representative of the stress state over the entire load step.

The CANDE algorithm is structured to operate in either the tangent or iterative method. The choice of operation is dependent on the nonlinear model and input specifications. Nonlinear material models are a dominant feature of CANDE and are discussed throughout this report.

### 5.2.3 Element Types

The heart of any finite element formulation is the description of the elements themselves. There are three basic element types employed in the CANDE program.

1. Quadrilateral element, for soil, bedding, etc.
2. Interface element, for interface assemblies.
3. Bending-thrust element, for pipe.

The quadrilateral element is a nonconforming element developed by Herrmann [5-4] that has superior qualities in all basic deformation modes. The quadrilateral is composed of two triangles with complete quadratic interpolation functions initially specified within each triangle. Upon applying appropriate constraints and static condensation procedures a four node quadrilateral with an  $8 \times 8$  stiffness matrix is formed such that the eight external degrees of freedom are the horizontal and vertical displacements of each node. The complete derivation of this element is given in Appendix I.

Associated with the quadrilateral element are three constitutive forms for material characterization: (1) linear elastic (isotropic or anisotropic); (2) incremental elastic, wherein elastic moduli are dependent on current overburden pressure; and (3) variable modulus model employing a shear modulus and Poisson's ratio, which are dependent on hydrostatic pressure and maximum shear strain. Each of these soil models is developed in Chapter 6.

The interface element allows consideration of two subassemblies meeting at a common interface, such that under loading the subassemblies may slip relative to each other with Coulomb friction, or separate, or rebond. The natural application of this element is the treatment of the pipe-soil interface; however, other applications include trench soil-to-in-situ soil interface.

The interface element is composed of two nodes, each associated with one subassembly and initially meeting at a common contact point. Each

contact node has two degrees of freedom - "horizontal and vertical displacement. In addition, a third node is assigned to the "interior" of the contact point to represent normal and tangential interface forces. The three nodes produce a 6 x 6 element "stiffness" matrix in a mixed formulation. Actually, the element stiffness is a set of constraint equations with Lagrange multipliers. Constraint equations impose conditions on normal and tangential displacements, and Lagrange multipliers are interface forces. This element was developed during this investigation and is presented in detail in Chapter 7.

The bending-thrust element is the familiar beam/column element in a plane strain formulation. It is defined by two nodes with three degrees of freedom per node - horizontal and vertical displacement and a rotation. The assumed interpolation functions and element stiffness matrix derivation are developed in Appendix I.

The element derivation employs a general nonlinear stress-strain model for characterizing a variety of material behavior ranging from brittle cracking to ductile yielding. In all cases the nonlinear formulation takes proper account of moment-thrust interaction by determining the axis of bending in a consistent manner.

The general nonlinear stress-strain model is presented in Chapter 8 followed by specializations of the model for each pipe material.



#### 5.2.4 Level 2 Operation

The purpose of Level 2 operation is to eliminate the need of "node counting" and mesh construction by means of a versatile canned mesh routine. The canned routine is restricted to symmetric geometry and loadings about the vertical centerline of the pipe. Thus, only half of the system is modeled with finite elements. The basic mesh topology employs 86 quadrilateral elements for soil, bedding, etc., and ten bending-thrust elements for the pipe. Figure 5-2 illustrates the basic mesh topology and boundary conditions, wherein all nodal coordinates are referenced to the major and minor radii ( $R_1$ ,  $R_2$ ) of the pipe.

From the basic mesh configuration, Level 2 considers two fundamental culvert installation conditions - the embankment condition and the trench condition. These conditions are modeled by assigning material numbers and construction increment numbers to appropriate element groupings of the basic mesh. Typically, Level 2 operations require four to ten data cards.

5.2.4.1 Embankment Mesh. Figure 5-3 illustrates the material zones and construction increment layers for the Level 2 embankment mesh. In addition to specifying the pipe shape by  $R_1$  and  $R_2$ , input geometry includes thickness and angle of wrap of the backpacking ring and height of fill soil over pipe. Each of the material Zones,

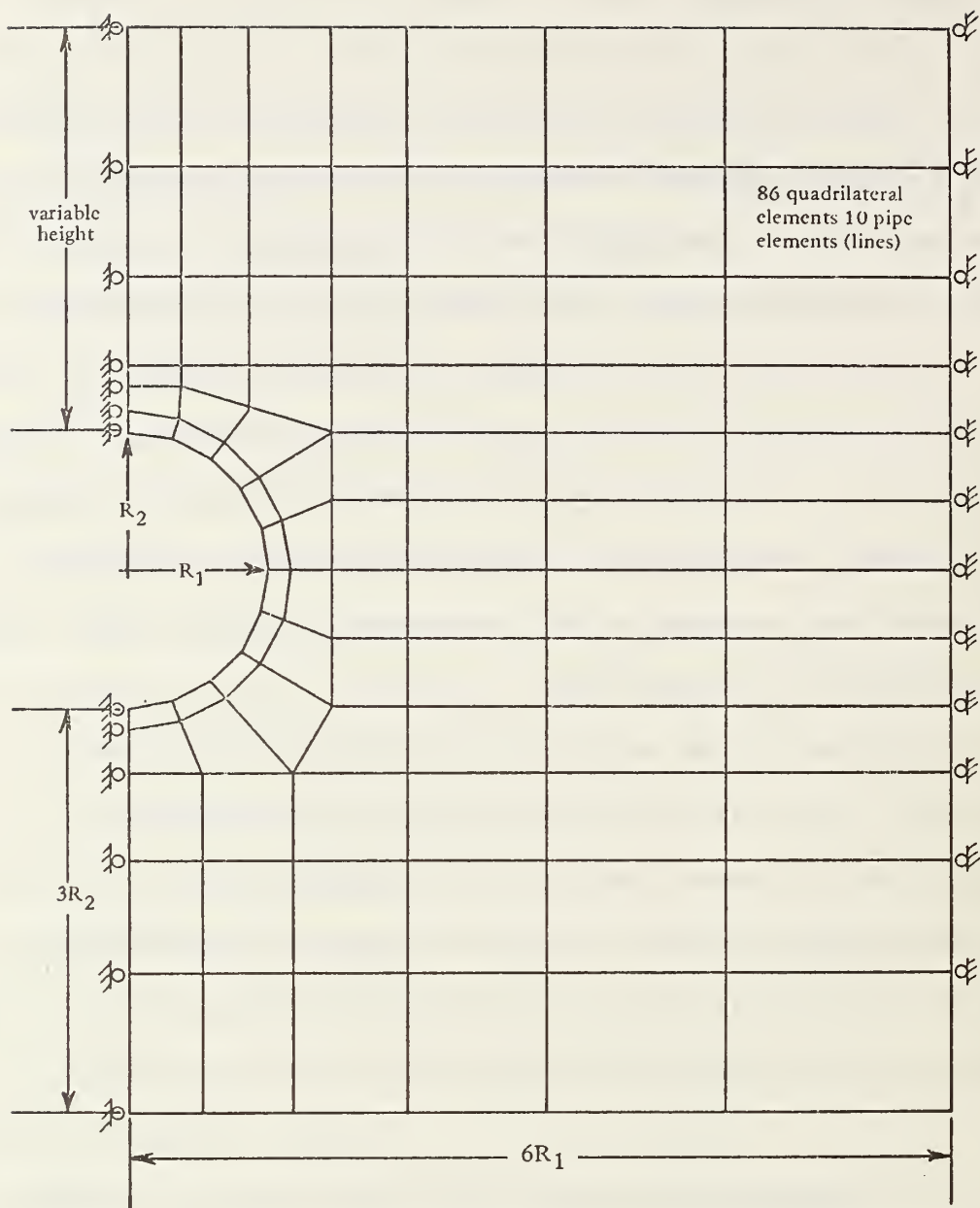


Figure 5-2. Basic Level 2 mesh topology.

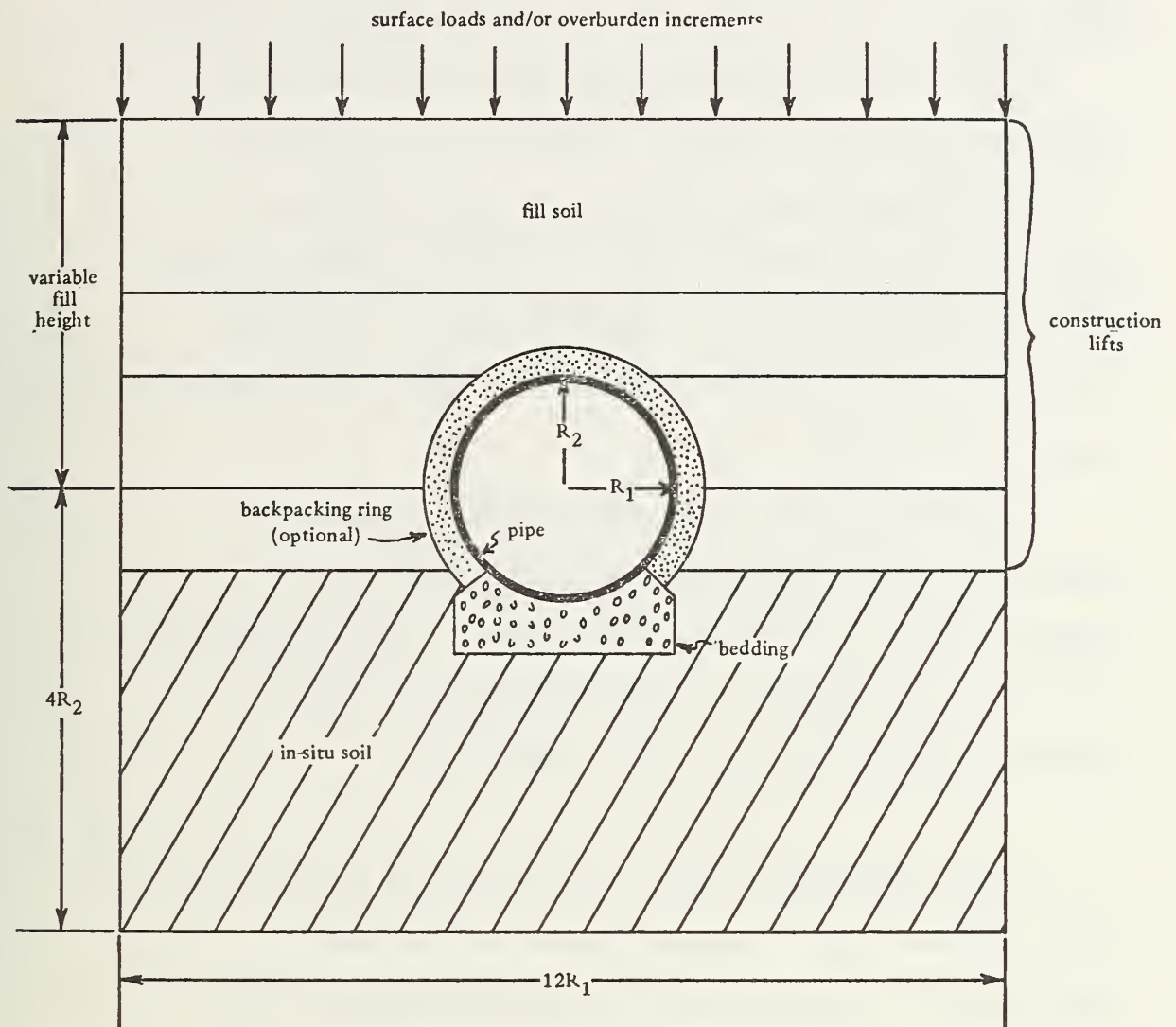


Figure 5-3. Embankment mesh configuration.

in-situ soil, bedding, backpacking, and fill soil can be assigned a separate constitutive model (see Chapter 6) or can be declared homogeneous.

The incremental construction schedule begins with the initial setup of pipe, bedding, and in-situ soil followed by a series of four lifts of fill soil up to an elevation of  $4R_2$  above the pipe center. If the fill height is greater than  $4R_2$ , each remaining lift is treated as equivalent overburden pressure applied to the mesh surface. The lifts can be combined as desired.

In addition to gravity loading from soil weight, live pressure and point loads can be assigned anywhere in the system by means of a special access subroutine. The access routine also allows reassignment of material zones, construction increments, geometry, and boundary conditions.

5.2.4.2 Trench Mesh. Figure 5-4 illustrates the material zones and construction increment layers for the trench mesh of Level 2. Here the geometry specifications are pipe shape ( $R_1$ ,  $R_2$ ), trench depth, trench width, and fill height over the trench. The material zones are in-situ soil, bedding, trench fill soil, and overfill soil. Each zone can be assigned the same or different constitutive models.

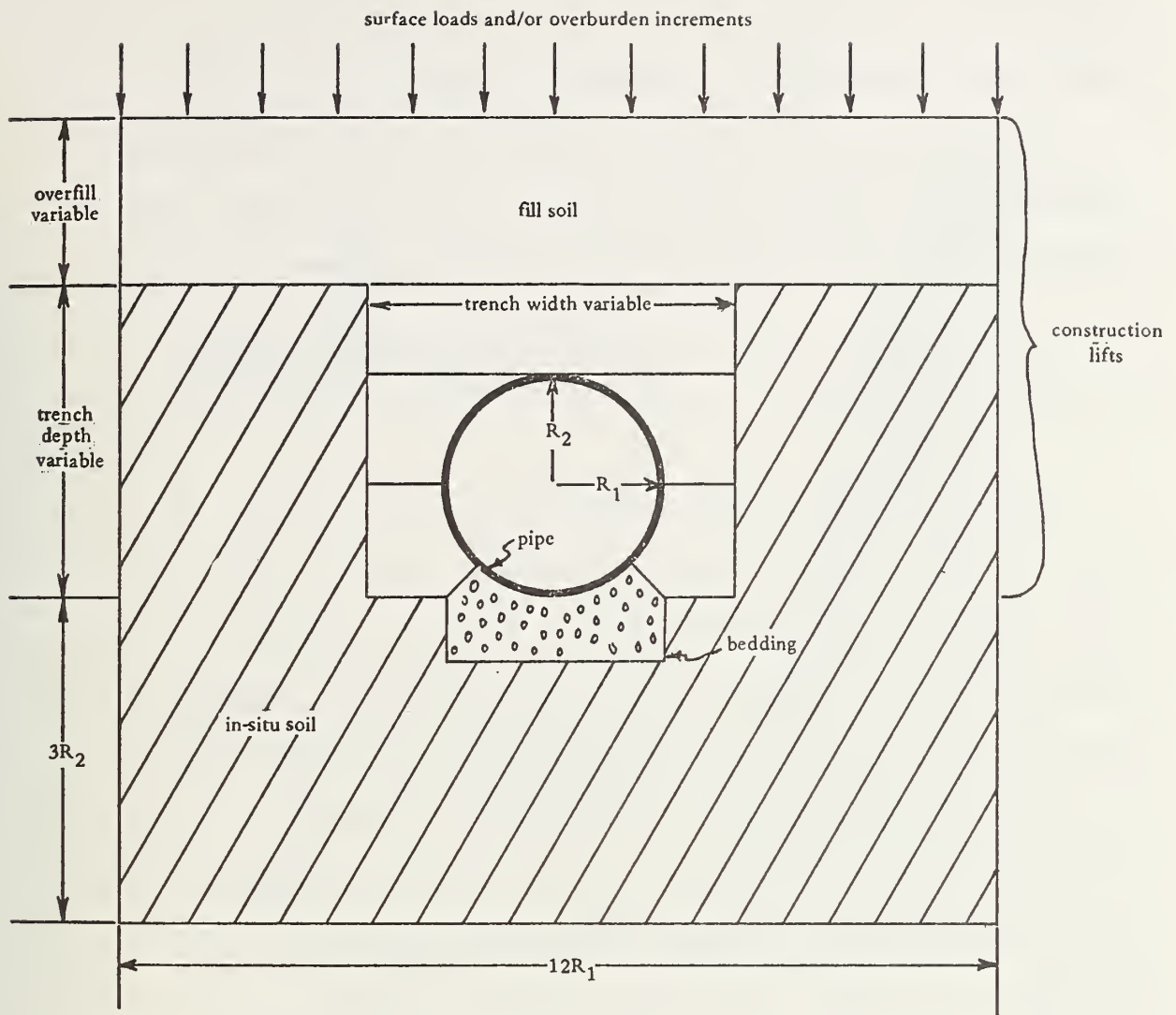


Figure 5-4. Trench mesh configuration.



As before, the construction schedule begins with in-situ soil, bedding, and pipe, followed by a series of fill soil lifts applied individually or combined as desired. Soil lifts above an elevation of  $4R_2$  from pipe center are treated as equivalent increments of overburden pressure applied to the mesh surface. The special access routine allows arbitrary loading and mesh alterations.

#### 5.2.5 Level 3 Operation

Level 3 operations provide the full power of the finite element method to model culvert installations. However, the finite element mesh must be completely defined, i.e., nodal coordinates, element connectivity, boundary conditions, element material properties, and construction schedules. To aid in this task many unique mesh generation aids have been provided, including straight, curve, and Laplace generation schemes for nodal point definition. Also plotting programs have been interfaced with CANDE to facilitate debugging and data evaluation. Nonetheless, Level 3 operation is at best tedious and should only be used when Level 2 is not applicable.

An illustration of a generalized culvert installation requiring Level 3 is shown in Figure 5-5. Due to the nonsymmetrical distribution of materials Level 2 is not applicable. Note, the only

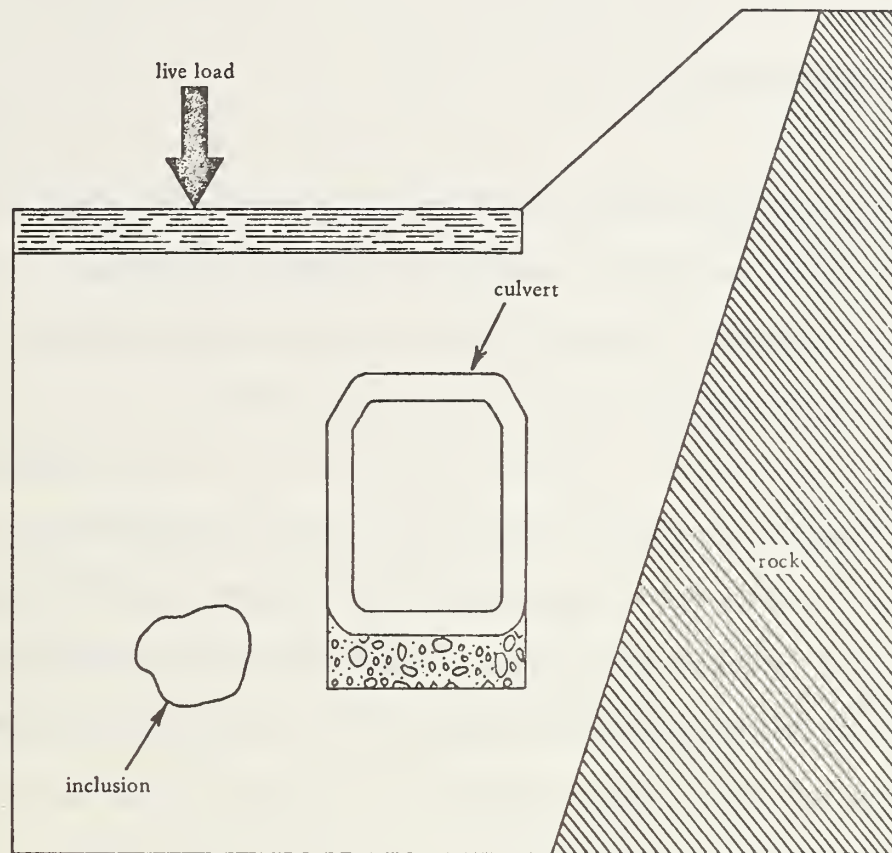


Figure 5-5. Example culvert installation for Level 3.

restriction on Level 3 with regard to design is that the pipe wall must be prismatic; thus, Level 3 could design the installation in Figure 5-5.

### 5.3 BUCKLING APPROXIMATION

A general elastic buckling formulation is not included in this investigation, because no report of an elastic buckling failure of an in-service circular culvert has been found unless the failure was preceded by excessive deflection [5-5]. However, for large-diameter culverts with relatively weak in-plane bending stiffness (e.g., smooth wall pipe), elastic buckling should not be dismissed. To this end a closed-form solution for elastic buckling based on energy concepts was adopted from Chelapati and Allgood [5-6]. The limitations and applications of this theory are addressed below.

For long cylinders deeply embedded in an elastic medium, the critical hydrostatic buckling pressure is given as [5-6]:

$$p_{cr} = 6 \sqrt{M_s (1 - K_s) EI / D^3} \quad (5-14)$$

where  $M_s$  = confined modulus of soil  
 $K_s$  = lateral coefficient of soil  
 $EI$  = in-plane bending stiffness of pipe  
 $D$  = pipe diameter

Inherent limitations in the above are: soil is linear elastic with no free surface influence, pipe is circular and linear elastic, and loading is a uniform compression ring.

In this study some of the above limitations have been mitigated as follows. For each load step, average elastic soil properties representative of the current stress state are used to define  $M_s$  and  $K_s$ . Similarly, the pipe stiffness  $EI$  is continually adjusted to represent the current stiffness. However, the assumption of uniform compression loading and circular geometry is retained. These assumptions should be kept in mind in defining buckling safety factors.

For most corrugated pipe and all thick wall pipe, elastic buckling is seldom a controlling design factor, and usually deflection predictions will foreshadow any potential buckling problem. Further discussion on the buckling design approximation is given in Chapter 8.





As part of this research effort a literature study was conducted to determine appropriate soil model(s) for characterizing soils typical of culvert installations. Based on this study, it became evident that there is no unanimity of opinion on soil models. With this in mind, it was concluded that as a first prerequisite the framework of the program CANDE should be structured in a general way to readily accommodate new soil models rather than be exclusively tied to the models presented in this chapter. To this end, CANDE was programmed to operate on an incremental loading basis where, within each load step, the solution process could be iterated as many times as desired. This general framework allows consideration of soil models ranging from linear to highly nonlinear and provides the capability of utilizing various types of solution strategies commensurate with the desired accuracy. The algorithms for each soil model are isolated in subroutines allowing relatively easy incorporation of new or improved models.

In keeping with the spirit of the solution level concept (i.e., a choice of solution methodology, Levels 1, 2, or 3), a second prerequisite of the modeling philosophy was the provision for a spectrum of soil model types from which to choose. The spectrum includes linear, overburden dependent, and fully nonlinear forms. Each of which are discussed and developed in subsequent sections.

## 6.1 CHARACTERISTICS OF SOIL MODELS

Prior to developing particular constitutive forms some general concepts of soil models are reviewed. The term soil model and constitutive form are used interchangeably in this discussion.

### 6.1.1 General Concepts

A soil model defines the relation between stress and strain based on phenomenological observations. That is, soil responses are measured from a "macroscopic" level as opposed to "microscopic" measurements of individual particle movements. Accordingly, at any "point" in the soil mass the stress-strain relationship is the average of a neighborhood of the point.

The phenomenological approach permits tractable solutions to the field equations of continuum mechanics; however, it also implies the constitutive form is to be treated like a "black box." That is, a general relationship for stress (in the absence of thermodynamic effects) is expressed as a functional of state variable histories.

$$\underset{\sim}{\sigma} = \underset{\sim}{F} \left( \underset{\sim}{\epsilon}(t'), T(t'), \dots \underset{\sim}{X}, t \right), \quad \text{for } t' \in [0, t] \quad (6-1)$$

This functional  $\underset{\sim}{F}$  is actually a confession of ignorance. It simply says, stress  $\underset{\sim}{\sigma}$  is somehow functionally related to state variable

histories, such as strain  $\epsilon(t')$ , temperature  $T(t')$ , moisture content  $W(t')$ , etc.. History is implied by the dummy time parameter,  $t'$ , ranging from time origin to current time  $t$ , and the inclusion of  $t$  and  $X$  in the functional denotes aging and material anisotropy, respectively.

The form of the functional is chosen to represent phenomenological observations. However, the choice of the functional is not completely arbitrary and must satisfy certain axioms detailed in Reference 6-1.

Complete identification of the parameters and functional forms implied in Equation 6-1 is extremely difficult to determine for soils over the entire range of state variables. Thus, the first job for soil model development is to restrict the domain of interest and eliminate state variables considered unessential to the boundary value problem. In this study time-dependent effects are not considered; therefore, time histories and aging are excluded. This also implies changes in intrinsic properties, such as water content, temperature, density, etc., must be considered as transformations to new materials as opposed to one material described by a functional relationship.

Certainly there are instances in culvert installations where time-dependent effects are significant. Moreover, current research efforts show great promise for modeling time-dependent effects with viscoplastic models [6-2, 6-3] or coupled field theories [6-4]. However, these techniques require further research before they can be meaningfully applied to the culvert problem. In the interim the influence of the

time-dependent effects can be approximated by selecting material parameters and moduli representative of long term-loading.

The outcome of the above limitations can be stated as follows: stress is a functional relationship of strain and independent of real-time history. However, by writing the stress-strain relationship in incremental form, a quasi-history of loading can be achieved by incrementing the loads and summing the stresses and strains. This technique is discussed fully later; for now the incremental form is introduced.

#### 6.1.2 Incremental Form

In computational applications, generally small increments of loading that follow the load path are considered as opposed to single-step loadings. Accordingly, the stress-strain relationship is expressed in an incremental form as:

$$\Delta \underset{\sim}{\sigma} = \underset{\sim}{C} \Delta \underset{\sim}{\epsilon} \quad (6-2)$$

where  $\Delta \underset{\sim}{\sigma}$  = increment of stress vector

$\Delta \underset{\sim}{\epsilon}$  = increment of strain vector

$\underset{\sim}{C} = \underset{\sim}{C}(\underset{\sim}{\sigma}, \underset{\sim}{\epsilon})$ , incremental constitutive matrix whose properties can be dependent on the current total values of stress and strain

In effect Equation 6-2 is a linearization of the functional relationship (Equation 6-1). The degree of linearization depends on the treatment of the constitutive matrix  $\underset{\sim}{C}$ , whose components are dependent upon the total stress-strain state. For example, if  $\underset{\sim}{C}$  is determined solely on the known stress-strain state at the beginning of the load step, then the load increments must be kept small so that  $\underset{\sim}{C}$  can be frequently updated to avoid significant error. Naturally, this treatment of the  $\underset{\sim}{C}$  matrix is highly linearized. On the other end of the scale, if the  $\underset{\sim}{C}$  matrix is not considered predetermined but rather is determined in an iterative fashion during the load step, then large load steps (or even single-load steps) can be achieved.

All of the constitutive forms considered herein - linear, overburden-dependent, and fully nonlinear - can be expressed by Equation 6-2. However, before illustrating these forms, it is well to recognize the differences between material modeling for the elasticity solution versus the finite element solutions.

### 6.1.3 Constitutive Modeling, Finite Element Versus Closed Form

For the elasticity solution (Level 1), the soil description is limited to homogeneous, isotropic media such that  $\underset{\sim}{C}$  is composed of linear elastic material properties (e.g., Young's modulus and Poisson's ratio). However, as noted in Chapter 5, soil nonlinearity can be approximated with Level 1 by dividing the total overburden load into several increments such that



for each load increment the "elastic" properties are changed to reflect changing soil stiffness. After each increment, the structural responses are summed in a running total, thereby providing a history of responses. This procedure implies that for any given load increment, the entire soil mass is assigned a single, constant, constitutive matrix  $\tilde{C}$ . With this limitation it seems reasonable to determine  $\tilde{C}$  based on the current overburden stress state in the vicinity of the culvert, say at the springline.

On the other hand, the finite element formulation (Levels 2 and 3) provides a great deal more flexibility in describing the soil. First, the soil mass need not be considered homogeneous but can be composed of several material zones, such as in-situ, bedding, backfill, etc., as described in Chapter 5. Moreover, each element within a material zone takes on material properties peculiar to the stress-strain state of that particular element. For fully nonlinear forms several iterations are required for each load step before every element attains converged material properties.

The differences between material modeling for the elasticity solution and the finite element solution should be kept in mind for the following constitutive forms.

The linear model is the most simplistic of the models considered and implies the matrix  $\underset{\sim}{C}$  is constant for all time regardless of the stress-strain state. Thus, if other nonlinearities are not present, the load could be applied in a single step if desired.

The linear form for plane-strain geometry is shown in Equation 6-3, where  $\{\sigma_x, \sigma_y, \tau\}^T$  and  $\{\epsilon_x, \epsilon_y, \gamma\}^T$  are stress and strain vectors, and  $C_{11}$ ,  $C_{12}$ ,  $C_{22}$ , and  $C_{33}$  are material constants.

$$\begin{Bmatrix} \sigma_x \\ \sigma_y \\ \tau \end{Bmatrix} = \begin{bmatrix} C_{11} & C_{12} & 0 \\ & C_{22} & 0 \\ & \text{Sym} & C_{33} \end{bmatrix} \begin{Bmatrix} \epsilon_x \\ \epsilon_y \\ \gamma \end{Bmatrix} \quad (6-3)$$

For isotropic materials the components  $C_{11}$ ,  $C_{12}$ ,  $C_{22}$ , and  $C_{33}$  are all defined by any two elastic parameters. Table 6-1 provides elastic relationships for some common elastic pairs: Young's modulus and Poisson's ratio ( $E$ ,  $\nu$ ), confined modulus and lateral pressure coefficient ( $M_s$ ,  $K_o$ ), and bulk modulus and shear modulus ( $B$ ,  $G$ ).

For orthotropic materials (e.g., stratified soil layers),  $C_{11}$ ,  $C_{12}$ ,  $C_{22}$ , and  $C_{33}$  can be specified independently of each other to reflect responses dependent on the material axis. However, the resulting  $\underset{\sim}{C}$  matrix

Table 6-1. Elastic Equivalents for Isotropic, Plane-Strain Models

Components of Constitutive Matrix	Elastic Equivalent Pairs		
	E = Young's Modulus $\nu$ = Poisson's Ratio (E, $\nu$ )	$M_s$ = Confined Mod $K_o$ = Lateral co-efficient ( $M_s$ , $K_o$ )	B = Bulk Modulus G = Shear Modulus (B, G)
$C_{11} = C_{22}$	$\frac{E(1 - \nu)}{(1 + \nu)(1 - 2\nu)}$	$M_s$	$B + 4/3 G$
$C_{12}$	$\frac{E \nu}{(1 + \nu)(1 - 2\nu)}$	$M_s K_o$	$B - 2/3 G$
$C_{33}$	$\frac{E}{2(1 + \nu)}$	$\frac{M_s (1 - K_o)}{2}$	G

must be positive definite to avoid violation of energy principles.

Orthotropic representation of materials only applies to the finite element solution levels.

Two significant questions with respect to linear models are: (1) when, if ever, are they applicable, and (2) if they are applicable, what are reasonable values for the elastic moduli. With regard to the first question, it is true that soils seldom if ever behave in a linear fashion; nonetheless, linear approximations can provide a reasonable representation of soil behavior, particularly in design situations where soil information is scanty. Moreover, in parametric studies it is often justifiable to utilize linear soil properties when studying the effect of culvert geometry and stiffness or inclusions, such as bedding and backpacking.

As to the second question, the selection of appropriate elastic moduli should be based on type of soil, degree of compaction, and overburden pressure on the soil zone of interest. In the next section graphs are presented depicting reasonable ranges of elastic parameters.

### 6.3 OVERBURDEN-DEPENDENT MODEL

The overburden-dependent model is the application of the linear model in a series of steps. Each step represents an increment of soil fill or overburden pressure so that the elastic moduli are modified at each step to account for an increased stiffness due to increased overburden.

Implicit in the above model is the assumption that soil stiffness increases with overburden pressure. Here a red flag must be waved to point out the limitations of this assumption. It will be demonstrated in the development of the nonlinear model that soil stiffness does increase with confining pressure so that, if the soil is essentially in a state of confined compression (one-dimensional straining), then increased overburden pressure will be tantamount to increased confining pressure and soil properties will stiffen. On the other hand, if the soil is in the state of unconfined compression (e.g., triaxial test), then increased overburden (axial load) will not stiffen the soil but, on the contrary, stiffness will be reduced due to shear straining.

The significant point is, that overburden-dependent models are only valid insofar as the soil is predominantly in a state of confined compression. Generally, gravity loading of the soil promotes states of confined compression; however, in regions of interaction, such as certain areas in the vicinity of the pipe or around other inclusions, the assumption of confined compression is questionable.

Keeping the above limitations in mind, the overburden-dependent model is best illustrated by considering a typical soil specimen undergoing a confined compression test. For example, consider Figure 6-1 which typifies the stress-strain path of overburden pressure versus axial strain. Three important concepts are illustrated in this figure. First, the upward shape of the curve illustrates increased stiffness with overburden. Second, the relationship between overburden stress,  $\sigma_y$ , and axial strain,  $\epsilon_y$ , is measured by the "secant" confined modulus,  $M_s$ ; i.e.,

$$\sigma_y = M_s \epsilon_y \quad (6-4)$$

From the measurements of Figure 6-1, it is a simple matter to plot  $M_s$  for various values of  $\sigma_y$  ( $M_s = \sigma_y / \epsilon_y$ ) such that  $M_s$  is a known function (pointwise) of  $\sigma_y$ , as depicted in Figure 6-2.



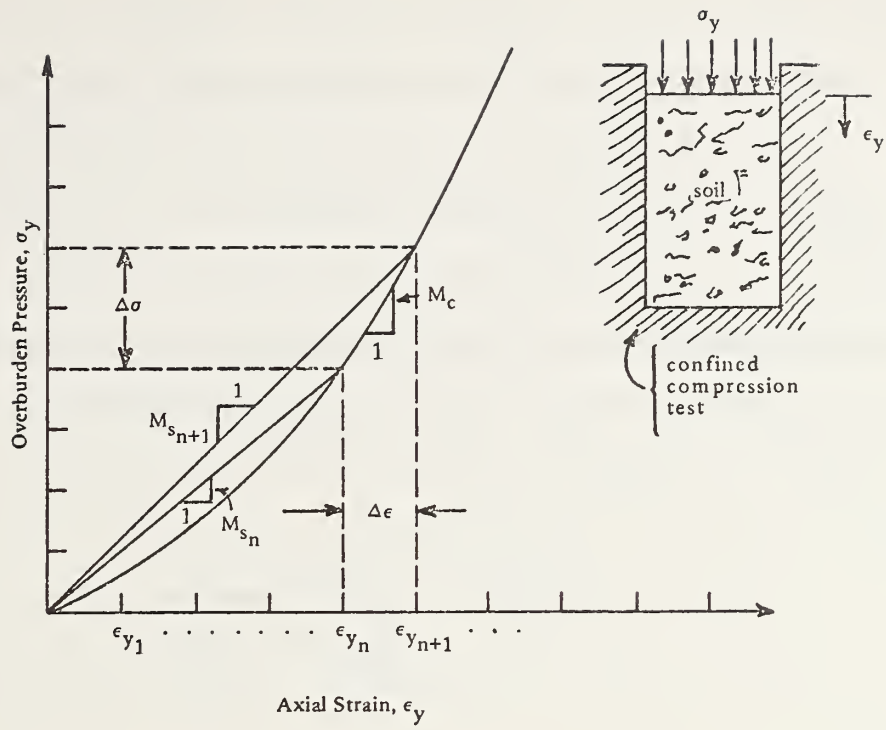


Figure 6-1. Typical confined compression stress-strain path.

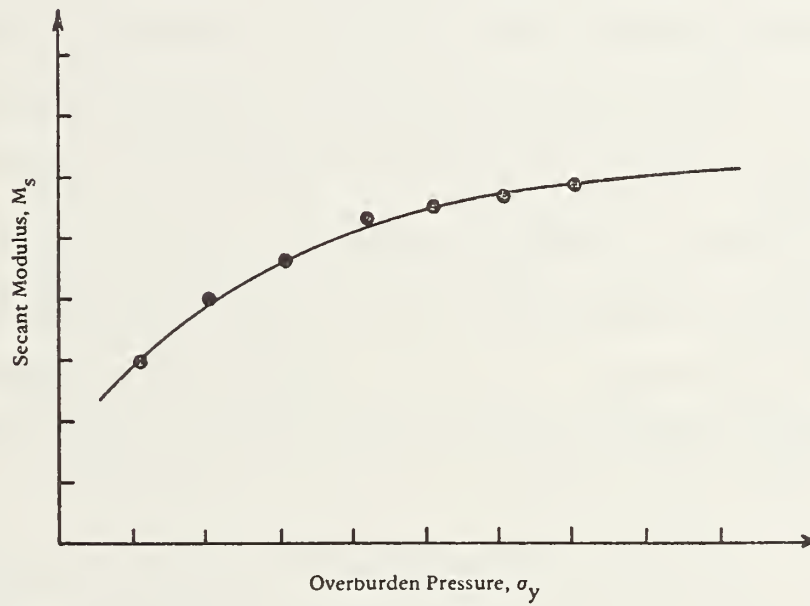


Figure 6-2. Typical plot of secant modulus versus overburden pressure.

Third, increments of overburden stress are related to increments of axial strain by the "chord" of the confined modulus,  $M_c$ ; i.e.:

$$\Delta\sigma_y = M_c \Delta\epsilon_y \quad (6-5)$$

The "chord" modulus,  $M_c$ , (or average tangent) can be determined directly from the secant modulus,  $M_s$ , for any increment  $n$  to  $n+1$  by:

$$M_c = \frac{\Delta\sigma_y}{\Delta\epsilon_y} = \frac{\sigma_{y_{n+1}} - \sigma_{y_n}}{\left( \frac{\sigma_{y_{n+1}}}{M_{s_{n+1}}} - \frac{\sigma_{y_n}}{M_{s_n}} \right)} \quad (6-6)$$

Herein lies the advantage of an overburden-dependent model over the fully nonlinear model (described later). That is, to advance the solution from step  $n$  to  $n+1$  the chord modulus,  $M_c$ , can be determined directly by estimating  $\sigma_{y_{n+1}} = \Delta\sigma_y + \sigma_{y_n}$ , where  $\Delta\sigma_y$  is estimated as the increment of overburden pressure (fill height equivalent). Since the secant modulus function,  $M_s(\sigma_y)$ , is known input data,  $M_c$  can be directly computed from Equation 6-6. Note however, in the fully nonlinear model several iterations within each load step are required to determine the correct material properties.

Thus far, only the elastic parameter,  $M_s$ , has been discussed. The complete description of the  $\underset{\sim}{C}$  matrix requires a second elastic parameter,

such as the lateral pressure coefficient,  $K_0$ , or, equivalently, Poisson's ratio, since  $K_0 = \nu/(1 - \nu)$ . In later sections, it is shown that Poisson's ratio remains practically constant in the environment of confined compression (but not in other loading environments). Therefore, as a general recommendation for overburden-dependent models, a constant value for Poisson's ratio is suggested. Furthermore, it is generally more common to describe the  $\underset{\sim}{C}$  matrix with Young's modulus and Poisson's ratio. Since Young's modulus is related to the confined modulus by a simple factor of Poisson's ratio [i.e.,  $E_s = r M_s$ , where  $r = (1 + \nu)(1 - 2\nu)/(1 - \nu)$ ] and with Poisson's ratio constant,  $E_s$  has all the same characteristics as  $M_s$ , including the concept of secant and chord relationships.

For reference, reasonable ranges of Young's secant modulus are provided in Figures 6-3, 6-4, and 6-5 along with suggested values of Poisson's ratio. The curves consider three broad categories of soil: granular, mixed, and cohesive for compaction ranging from fair to good. The curves are based on a composite of references [6-5 through 6-12] as well as experimental data from this investigation. On the whole, the curves are conservative and can be used for design, if no soil data are available for the problem at hand.

The linear model is a special case of the overburden-dependent model in that only one load step is considered; thus, the secant modulus corresponding to the maximum overburden pressure is the proper linear representation.

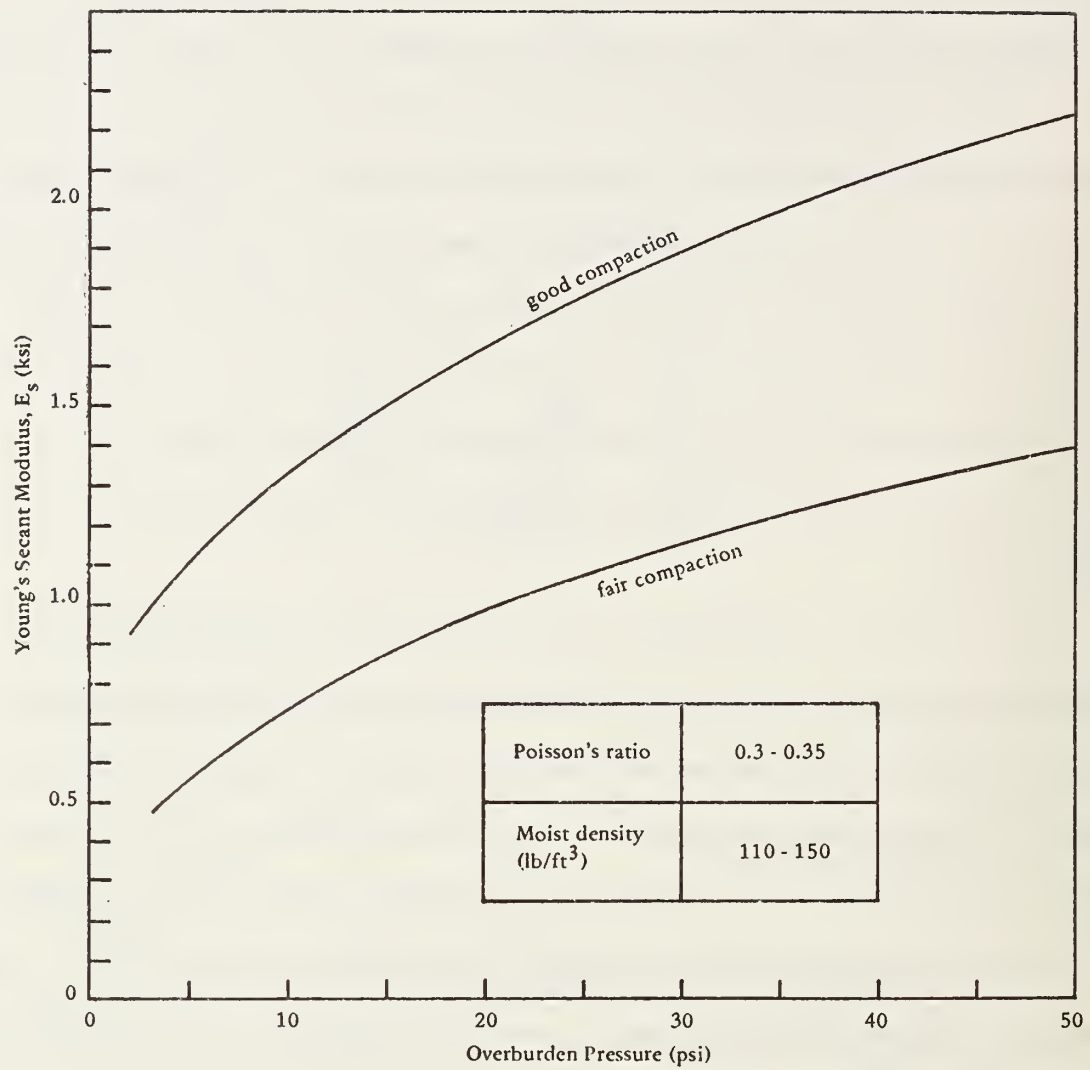


Figure 6-3. Secant modulus versus overburden pressure for granular soil (e.g., gravel, sand).

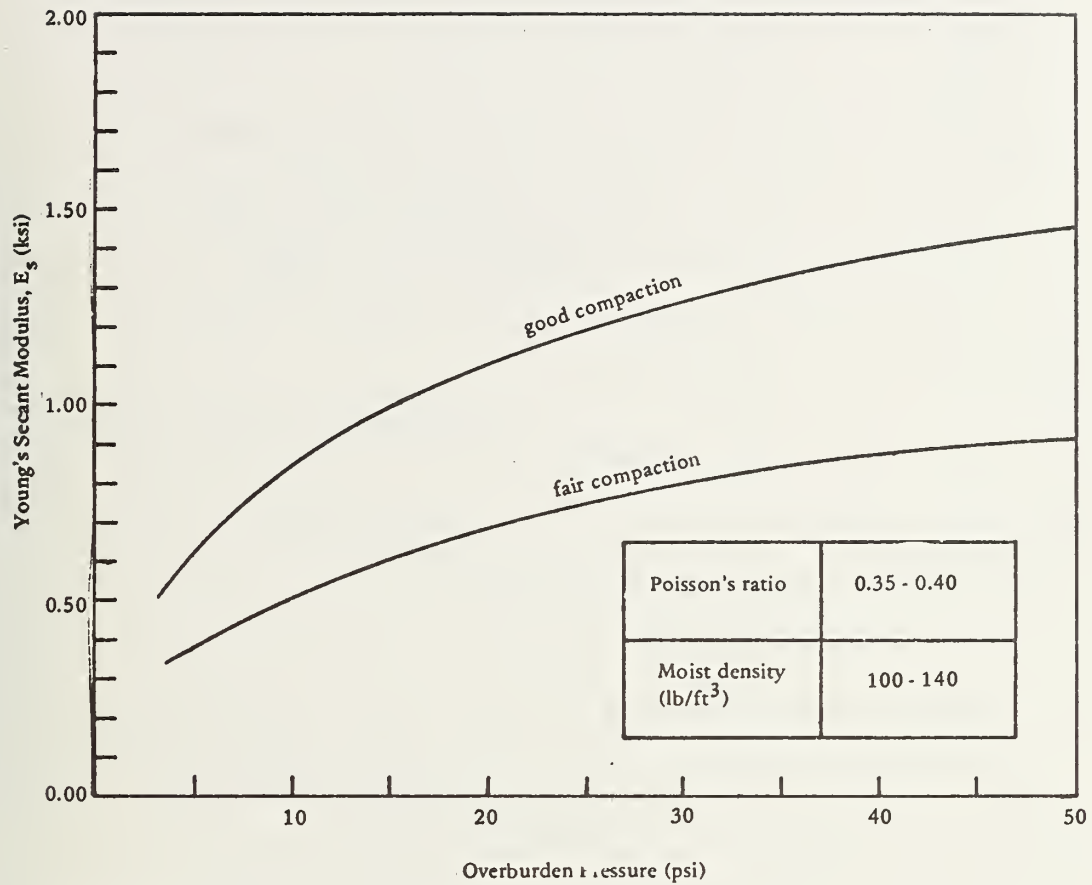


Figure 6-4. Secant modulus versus overburden pressure for mixed soils (e.g., silty sand, clayey sand).



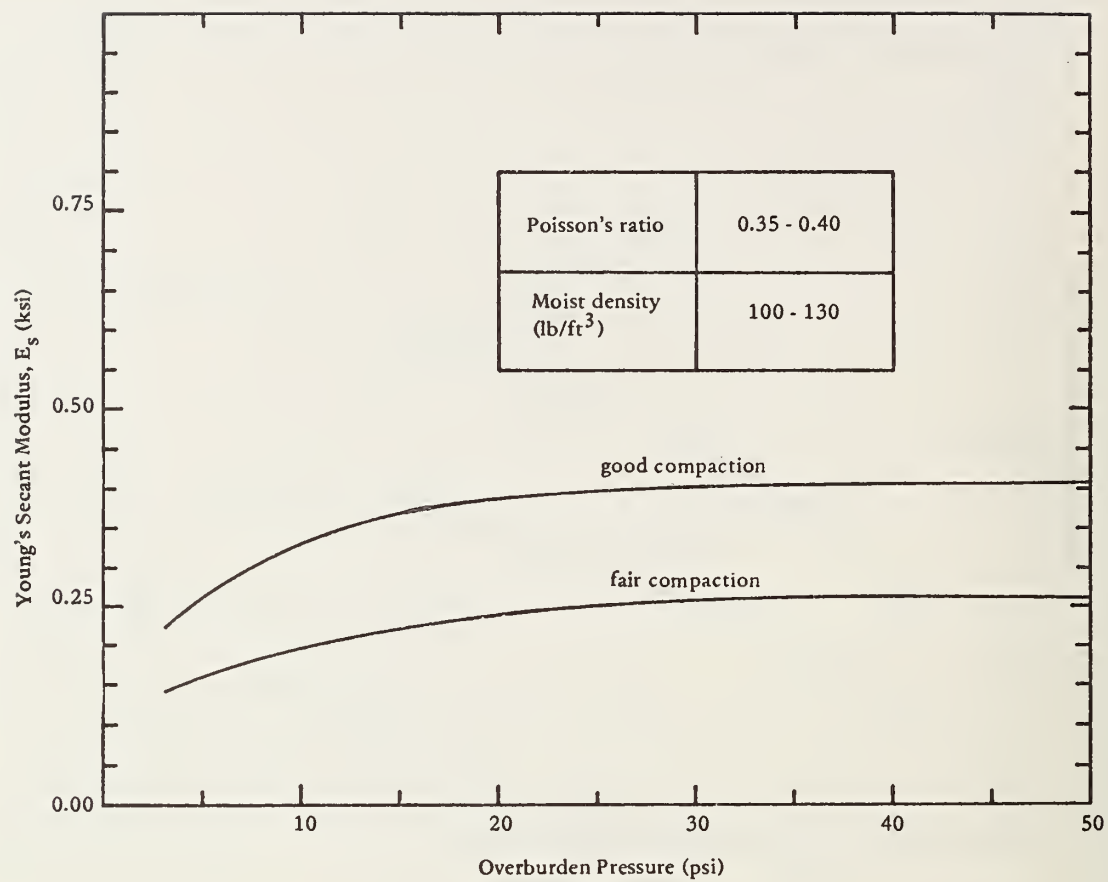


Figure 6-5. Secant modulus versus overburden pressure for cohesive soils (e.g., silt, clay).

In this section a brief overview of time-independent nonlinear soil models is presented. A more thorough development can be obtained from References 6-6 and 6-13. For purpose of this discussion it is convenient to classify nonlinear soil models into two groups: plasticity models and variable modulus models. The former group is based on the theory of plasticity, which in general requires a yield criterion, a hardening rule, and a flow rule. A yield criterion defines the onset of plastic yielding and is usually assumed to be a function of the stress invariants. The hardening rule redefines the yield criterion after plastic deformation has occurred and is usually assumed to be a function of plastic work and stress level. The flow rule relates increments of plastic strain to increments of stress after the yield criterion has been satisfied. Examples of plastic models applied to soils are the Drucker-Prager, Mohr-Coulomb, and capped models [6-14].

From an academic viewpoint, the plasticity models are more attractive than the variable modulus models (discussed next), because they generally satisfy rigorous theoretical requirements of continuity, uniqueness, and stability, and are inherently capable of treating unloading. On the negative side, plasticity models are generally difficult to correlate with triaxial test data, thereby making it relatively difficult to determine their parameters.

Variable modulus models are based on the hypothesis that stress increments can be related to strain increments by an "elastic" constitutive matrix, wherein the components of the constitutive matrix are dependent on the level of stress and strain; i.e.,  $\{\Delta\sigma\} = [C]\{\Delta\epsilon\}$ , where  $\{\Delta\sigma\}$  and  $\{\Delta\epsilon\}$  are increments of stress and strain, and  $[C]$  is the "elastic" constitutive matrix whose components,  $C_{ij}$ , are dependent on the current total level of stress and strain. The variable modulus models represent materials of the so-called "hypoelastic" classification; that is, the constitutive components are dependent upon initial conditions and the stress path. Consequently, the term "nonlinear elastic" is not appropriate for variable modulus models, since "nonlinear elastic" implies path independence.

Variable modulus models differ among themselves in two important ways. First and foremost is the particular material law or relationship used to define the elastic parameters. Second is the associated methodology for updating the constitutive matrix. With regard to the latter, four methods are most commonly employed: secant, tangent, modified tangent, and chord. In the secant method the total load is applied in one step, and the solution is iterated to find the secant constitutive components satisfying both equilibrium and the associated material law. For the tangent method the load is applied in a series of steps. At the end of each step the tangent of the material law is evaluated at the accumulated stress-strain level to provide the constitutive components for the next load step. Note that the stress and

strain responses calculated by this method increasingly diverge from the material law under monotonic loading. The modified tangent method avoids this divergency by iterating within the load step to determine constitutive components that are based on weighted averages of the material law tangents evaluated at both the beginning and the end of the load step. The chord method is the secant method applied in a step-by-step fashion. Thus, the chord method satisfies equilibrium and the material law at every load step and is generally the most accurate method.

The significant advantages of the variable modulus models are their inherent ability to closely approximate experimental data and the relative ease by which the parameters of the model are determined. For these reasons and their computational simplicity, variable modulus models are more commonly employed in culvert soil systems than plasticity models. Accordingly, the variable modulus technique is employed in this investigation.

Many variable modulus models have been reported in the literature [6-6 through 6-12]. Some of these are based on tangent moduli, while others are based on secant moduli. However, the application of these models all illustrate the same fundamental trends: increased confining pressure produces increased stiffness, and increased shear strain (or stress) produces decreased stiffness. In this investigation, the Hardin model [6-6, 6-7] was chosen for further study and was incorporated into CANDE. The selection of the Hardin model does not mean the other

models are inferior, but rather the author preferred to work with secant models and that the Hardin model employs some unifying concepts that will be discussed in subsequent sections.

## 6.5 EXTENDED-HARDIN MODEL

The Hardin soil model [6-6, 6-7] provides a relationship for the secant shear modulus as a function of maximum shear strain and spherical stress pressure. More significantly, Hardin presents relationships for the parameters of the model dependent on soil type, void ratio, percent saturation, and plasticity index. In order to adapt the Hardin model to a general variable modulus approach, two extensions of the model were undertaken. First, a secant relationship for Poisson's ratio was developed in a manner similar to Hardin's shear modulus. Second, the secant formulations were recast into chord formulations to provide greater flexibility in modeling the load path.

In the ensuing discussion, the original Hardin development is presented, discussed, and compared with experimental data. Similarly, the extended version of the Hardin model is developed, discussed and compared with test data. The model is valid for monotonically increasing states of stress as discussed in Appendix J. No consideration is given to cyclic loading.



### 6.5.1 Hardin Shear Modulus Development

The original Hardin relationship relates accumulated maximum shear stress to accumulated maximum shear strain by Equation 6-7, and is shown graphically in Figure 6-6.

$$\tau = G_s \gamma \quad (6-7)$$

where  $\tau$  = accumulated maximum shear stress  
 $\gamma$  = accumulated maximum shear strain  
 $G_s$  = secant shear modulus

The heart of Hardin's model is the relationships for the secant shear modulus,  $G_s$ , expressed in a hyperbolic form as:

$$G_s = \frac{G_{\max}}{1 + \gamma_h} \quad (6-8)$$

$G_{\max}$  is the maximum value of the shear modulus dependent on spherical stress;  $\gamma_h$  is the so-called hyperbolic shear strain dependent on the ratio of shear strain to reference shear strain as defined below:

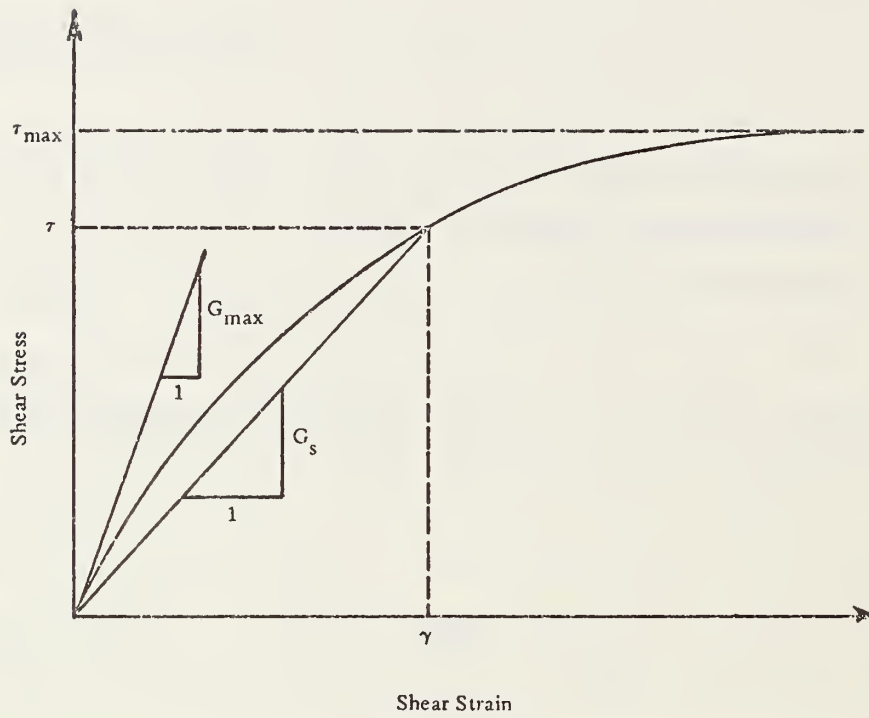


Figure 6-6. Idealized shear stress-strain relationship.

$$G_{\max} = S_1 \sqrt{\sigma_m} \quad (6-9)$$

$$\gamma_h = \frac{\gamma}{\gamma_r} \left[ 1 + \frac{a}{\exp(\gamma/\gamma_r)^{0.4}} \right] \quad (6-10)$$

$$\gamma_r = G_{\max}/C_1 \quad (6-11)$$

where  $\sigma_m$  = spherical stress; i.e.,  $|\sigma_{11} + \sigma_{22} + \sigma_{33}|/3$   
(compressive states only)

$\gamma_r$  = reference shear strain

$S_1$  = soil parameter (related to void ratio)

$a$  = soil parameter (related to soil type and percent saturation)

$C_1$  = soil parameter (related to void ratio, percent saturation, and plasticity index)

Equations 6-7 through 6-11 embody the general form of Hardin's soil model for shear modulus. To utilize the model for a particular soil, it only remains to specify values for the soil parameters  $S_1$ ,  $a$ , and  $C_1$ . One way of accomplishing this is to perform a series of triaxial tests and curve fit these parameters to the model. This approach is discussed at the end of this chapter. However, the advantage of Hardin's work is that he presents relationships for these parameters in terms of fundamental soil characteristics which are readily

measurable or readily available: void ratio, plasticity index, and percent saturation.

Below are the expressions for  $S_1$ ,  $a$ , and  $C_1$  for one cycle of loading at a slow loading rate, applicable for the inch-pound-second system of units.

$$S_1 = 1230 F \quad (6-12)$$

$$a = \begin{cases} 3.2 & \text{for granular soil} \\ 2.54 (1 + 0.02 S) & \text{for mixed soil} \\ 1.12 (1 + 0.02 S) & \text{for cohesive soil} \end{cases} \quad (6-13)$$

$$C_1 = \frac{F^2 R^2}{0.6 - 0.25 (PI)^{0.6}} \quad (6-14)$$

where  $F = (2.973 - e)^2 / (1 + e)$

$R = \begin{cases} 1100 & \text{for granular soil} \\ 1100 - 6 S & \text{for mixed or cohesive soil} \end{cases}$

$e =$  void ratio

$S =$  percent saturation ( $0 \leq S \leq 100$ )

$PI =$  plasticity-index/100 ( $0 \leq PI \leq 1$ )

With Equations 6-12, 6-13, and 6-14 the Hardin model for the shear modulus can be specified without need of triaxial tests. Of course, the worth of any soil model is not only gaged by its ease of use, but also

by its ability to correctly capture the soil responses. Here too, the Hardin model performs well as demonstrated in the following section.

#### 6.5.2 Verification of Shear Model

It would be of little significance to demonstrate the validity of the Hardin model by comparing it to the same test data on which Hardin developed his model because the parameters of his model were chosen to best fit his data. However, it is significant to compare Hardin with test data not previously "built in" to the model. To this end, an independent and comprehensive set of experimental data [6-15] on a uniform sand was obtained for purposes of the soil study. The tests, which were performed in a triaxial testing apparatus, included two hydrostatic tests, two uniaxial strain tests ( $K_0$  test), and five standard triaxial tests with measurements of lateral strain. Appendix J contains a tabularized listing of these tests along with a discussion of the test specimens and testing procedure.

Graphs of secant shear versus shear strain for the five triaxial tests are displayed in Figure 6-7. It is easily observed that the measured secant shear modulus,  $G_s$ , is dependent upon shear strain and stress state in that  $G_s$  increases with increasing confining pressure and decreases with increasing shear strain.

To directly compare Hardin's model with this test data, the soil parameters  $S_1$ ,  $a$ , and  $C_1$  were evaluated by Equations 6-12, 6-13, and



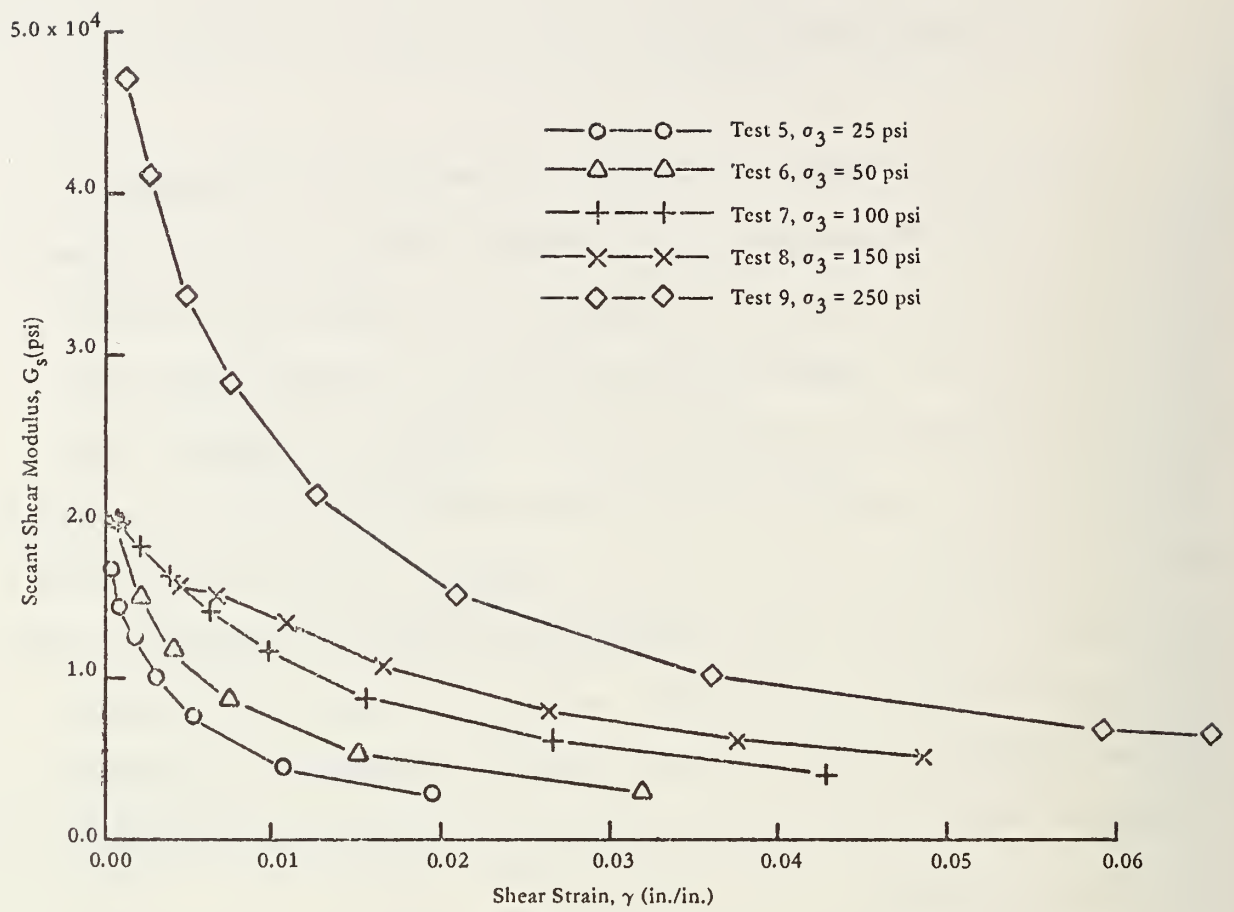


Figure 6-7. Secant shear modulus versus shear strain for confining pressures.

6-14 using these reported values: void ratio = 0.5, percent saturation = 0.0, and plasticity index = 0.0. For each data point in Figure 6-7 a corresponding value for  $G_{\max}$  and  $\gamma_h$  can be determined by means of Equations 6-9, 6-10, and 6-11. Figure 6-8 illustrates the comparison between the Hardin model and the experimental data, wherein the solid line represents the Hardin model (Equation 6-8) in the normalized form  $G_s/G_{\max} = 1/(1 + \gamma_h)$ . The accompanying data points are plotted in the same form using measured values of  $G_s$  together with the corresponding computed values of  $G_{\max}$  and  $\gamma_h$ .

The agreement between the Hardin prediction and the test data is quite remarkable over the entire range of  $\gamma_h$ . The significant result of Hardin's model is that it condenses the observed secant shear modulus into a single general relationship which provides a means to establish a computational algorithm for determining the shear modulus as a function of the stress and strain state.

It is re-emphasized that the above comparison was not based on curve fitting, but rather on a straightforward application of Hardin's shear model. In the next section a proposed relationship for Poisson's ratio is introduced to form the extended Hardin soil law.

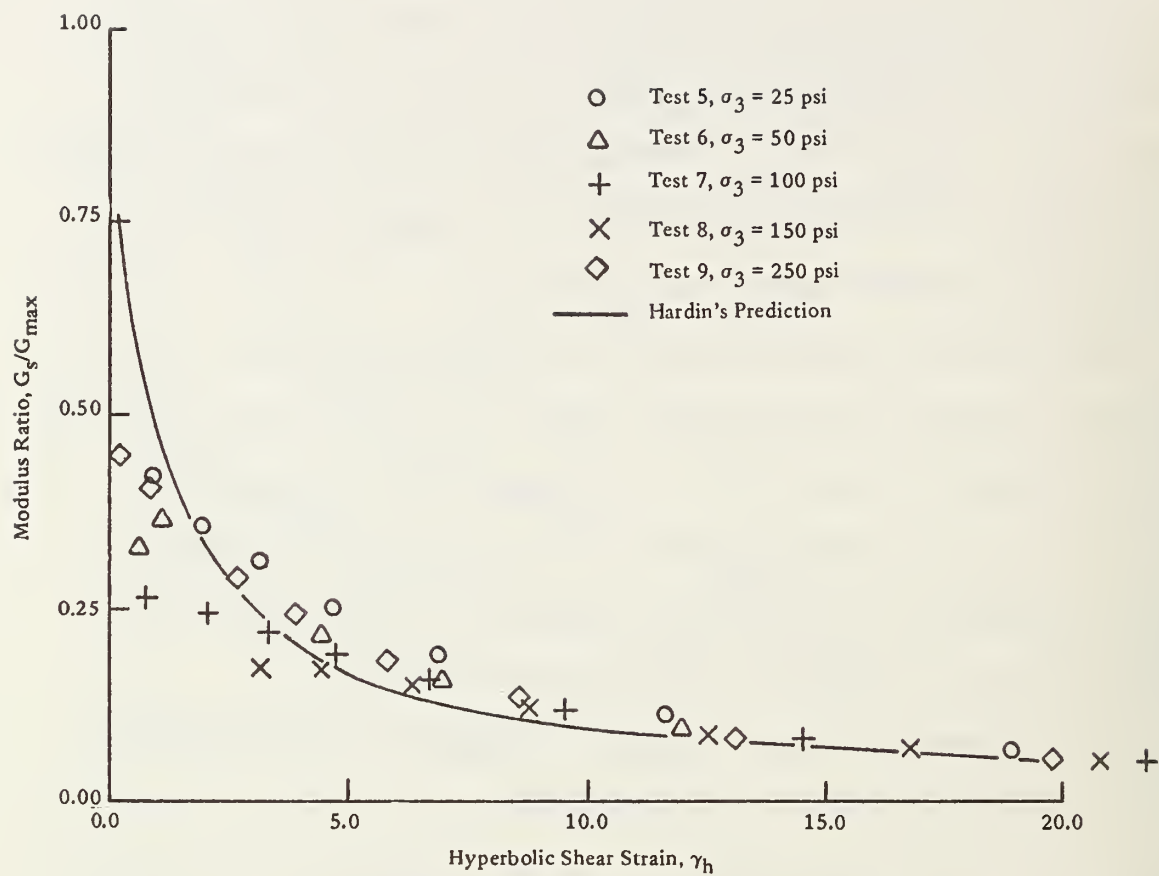


Figure 6-8.  $G_s/G_{max}$  versus hyperbolic shear strain.

### 6.5.3 Poisson Ratio Function

For isotropic materials two "elastic" parameters (functions) must be specified. The secant shear modulus,  $G_s$  (Equation 6-8), supplies one of these parameters. For the second parameter, any one of several common measures can be selected, e.g., Young's modulus, bulk modulus, or Poisson's ratio. The specification of any two elastic parameters automatically infers the specification of the remaining parameters through well-known elastic relationships.

The bulk modulus is the natural choice to compliment the shear modulus,  $G_s$ . However, any candidate bulk modulus relationship,  $B_s = B_s(\sigma, \epsilon)$ , must be such that  $B_s > (2/3)G_s$  in order to avoid an undesired inverse Poisson effect. That is, if  $B_s$  is specified less than  $(2/3)G_s$ , the model would respond with transverse dialation under uniaxial tension, which is clearly unrepresentative of soil behavior. Because of this potential problem, it is difficult to directly specify an independent function for  $B_s$  that will at all times satisfy the above requirements. However, it can be done indirectly by first specifying an admissible function for Poisson's ratio,  $\nu_s$ , and then using elastic relationships to define  $B_s$ . This point is developed in a later section.

Based on the above, the secant Poisson's ratio was selected as the second "elastic" functional relationship to be developed in a form similar to Equation 6-8. Note, if the Poisson's ratio function,

$\nu_s = \nu_s(\sigma, \epsilon)$ , is such that the range is within the limits  $0 \leq \nu_s < 0.5$  and  $G_s > 0$ , then the theoretical energy considerations are satisfied providing the stresses increase monotonically during the loading schedule as discussed in Appendix J.

For the first step in developing the functional relationship, observed values of Poisson's ratio are examined from experimental tests. From Hooke's law the observed value of Poisson's ratio can be determined from a known stress-strain state by:

$$\nu_s = \frac{(\sigma_m/3 \phi) - (2 \tau/\gamma)}{(2 \sigma_m/3 \phi) + (2 \tau/\gamma)} \quad (6-15)$$

where  $\nu_s$  = secant Poisson ratio

$\sigma_m$  =  $(1/3)(\sigma_{11} + \sigma_{22} + \sigma_{33})$ , average normal stress

$\phi$  =  $(\epsilon_{11} + \epsilon_{22} + \epsilon_{33})$ , volume change

$\tau$  = maximum shear stress

$\gamma$  = maximum shear strain

Equation 6-15 reduces to  $\nu_s = -\epsilon_1/\epsilon_2$  for a one-dimensional stress state.

To examine the nature of the secant Poisson's ratio, the test data of the five triaxial tests of Appendix J were used to calculate Poisson's ratio from Equation 6-15. Note, in Appendix J the tabularized values of axial and radial strain do not include hydrostatic straining due to



confining pressure. Therefore, in order to obtain the total strains,  $\phi$  and  $\gamma$ , the corresponding hydrostatic strains from the two hydrostatic tests must be averaged and added to the tabularized values.

Figure 6-9 shows the calculated values of Poisson's ratio as a function of shear strain for each triaxial test. It is readily observed that Poisson's ratio varies dramatically over the range of shear strain, and is also dependent on confining pressure.

Motivated by Hardin's approach for the shear modulus, the data in Figure 6-9 were re-plotted as a function of the ratio of shear strain to reference shear strain,  $\gamma/\gamma_r$  (see Equation 6-11). These results are illustrated in Figure 6-10, wherein it is observed the data collapse into a single curve. This suggests that a relationship for Poisson's ratio using  $\gamma/\gamma_r$  as the independent variable is reasonable. Again paralleling Hardin's work, a hyperbolic relationship given by Equation 6-16 is hereby proposed as a general relationship for Poisson's ratio.

$$v_s = \frac{v_{\min} + \gamma_p v_{\max}}{1 + \gamma_p} \quad (6-16a)$$

and

$$\gamma_p = q \gamma/\gamma_r \quad (6-16b)$$

where  $v_s$  = Poisson's as function of  $\gamma_p$

$v_{\min}$  = Poisson's ratio at zero shear strain

$v_{\max}$  = Poisson's ratio at large shear strain (failure)

$q$  = dimensionless parameter for curve shape

The terms  $v_{\min}$ ,  $v_{\max}$ , and  $q$  are parameters dependent on the type and characteristics of the soil, and are selected by simple curve-fitting techniques discussed at the end of this chapter. The solid line in Figure 6-10 represents Equation 6-16 for the parametric values:

$$v_{\min} = 0.10$$

$$v_{\max} = 0.49$$

$$q = 0.258$$

It is observed that the proposed curve for Poisson's ratio is in good agreement with the test data over the entire range of shear strain.

Of course, the general validity of Equation 6-16 is by no means substantiated by a single set of tests. Confidence in the model can only be obtained through further testing of many types of soils in different loading environments. Nonetheless, it is felt Equation 6-16 is sufficiently general to model most soils. Certain features are particularly useful. For example, the theoretical limits of Poisson's ratio,  $0 \leq v_s < 0.5$ , are easily maintained by the parameters  $v_{\min}$  and

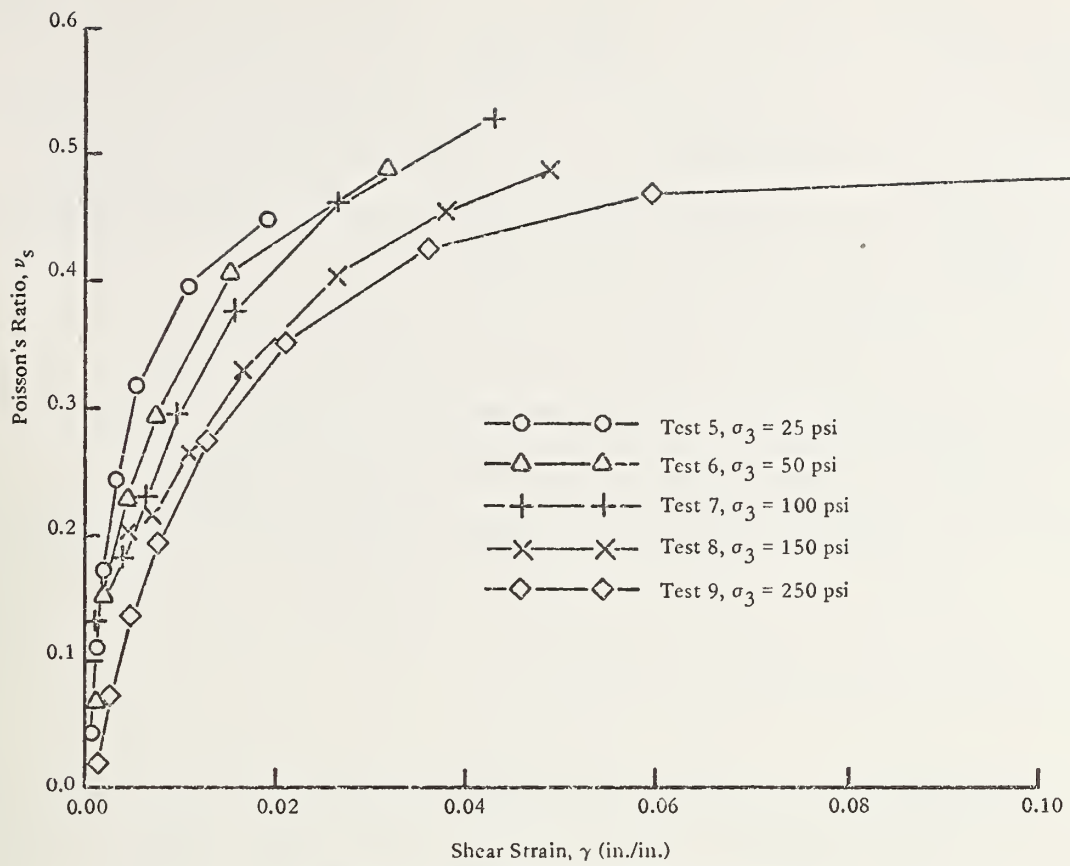


Figure 6-9. Poisson's ratio versus shear strain.

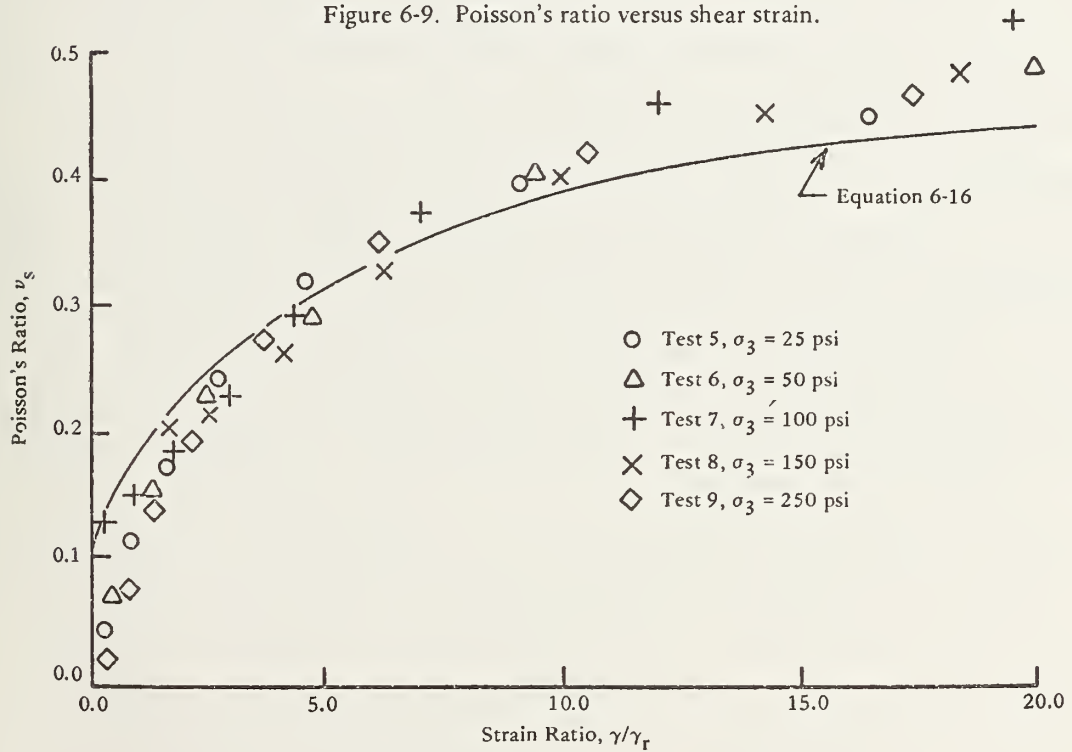


Figure 6-10. Poisson's ratio versus strain ratio.

$v_{\max}$ . Also, the shape of the curve can be varied from concave to convex by the parameter  $q$ . Carried to its logical end, expressions for  $v_{\min}$ ,  $v_{\max}$ , and  $q$  can be developed in terms of basic soil characteristics such as void ratio, saturation and plasticity index, thereby eliminating the need of triaxial testing.

The combination of the shear modulus and Poisson's ratio relationships constitute the Extended-Hardin soil model. In the next section the versatility of the Extended Hardin model is demonstrated on a one-dimensional confined compression test ( $K_o$  test).

#### 6.5.4 Extended-Hardin Versus $K_o$ Test

A severe test of any soil model is to compare it to test data from a load environment different from the one upon which the model was based. To this end, the  $K_o$  tests of Appendix J provide experimental data for determining the coefficient of lateral earth pressure,  $K_o$ , and the confined modulus,  $M_s$ .  $K_o$  is determined by the ratio of lateral stress to axial stress (i.e.,  $\sigma_3/\sigma_1$ ), and  $M_s$  is determined by the ratio axial stress to axial strain (i.e.,  $\sigma_1/\epsilon_1$ ). The corresponding Extended-Hardin prediction is determined by solving a one-dimensional plane-strain boundary value problem characterized by the following set of nonlinear equations:

$$\tau = \sigma_1 \frac{1 - 2\nu_s}{2(1 - \nu_s)} \quad (6-17a)$$

$$\sigma_m = \sigma_1 \frac{1 - 2\nu_s}{3(1 - \nu_s)} \quad (6-17b)$$

By utilizing the Extended-Hardin model (Equations 6-7 through 6-16), the above equations can be solved in an iterative manner to determine the predicted responses for each axial load,  $\sigma_1$ . Figure 6-11 shows the comparison between measured and predicted values for the coefficient of lateral earth pressure as a function of axial stress. It is observed that the agreement is good. More significantly, the results indicate that  $K_o$  is constant for this load environment. Since  $K_o$  is directly related to Poisson's ratio by the expression  $K_o = \nu_s / (1 - \nu_s)$ , one could be led to conclude from this type of test that Poisson's ratio remains constant for soils regardless of the load environment. Of course, this conclusion is invalid as previously demonstrated in Figure 6-9. The reason Poisson's ratio remains practically constant for this type of test can be understood by examining the variable,  $\gamma_p$ , of Equation 6-16b. Since Poisson's ratio is constant, it follows that  $\gamma_p$  is constant. But  $\gamma_p$  is directly proportional to shear strain and inversely proportional to the square root of the spherical stress ( $\gamma_r \sim \sigma_m$ ). Consequently, in this loading environment the shear



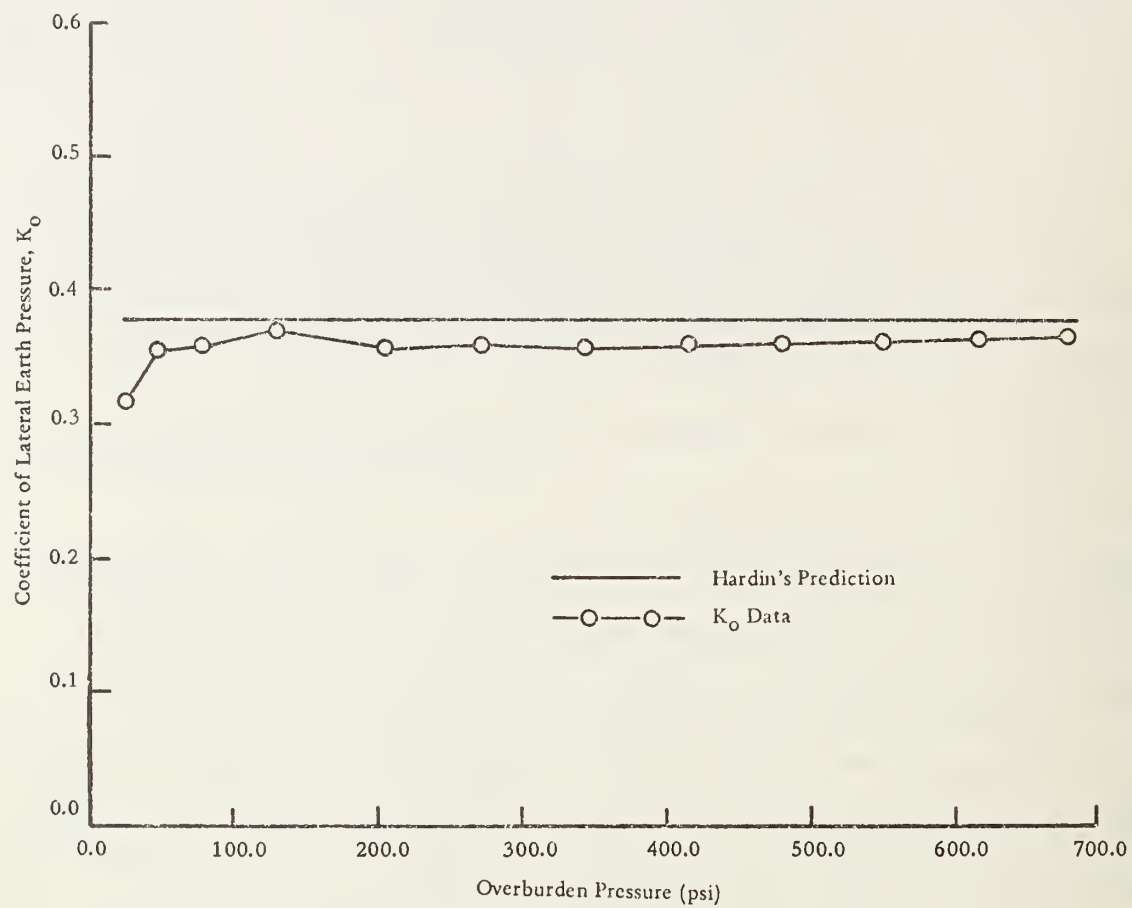


Figure 6-11.  $K_o$  versus overburden pressure.

strain increases directly with the square root of spherical stress, producing a relatively constant Poisson's ratio.

For the last comparison, Figure 6-12 depicts the measured and predicted value of the confined modulus,  $M_s$ , as a function of axial stress. In this instance, the predicted values have the same trend as the measured values, but differ by a constant amount. The important observation is that the soil model stiffens under one dimensional straining as does most soils.

#### 6.5.5 Parameters for Extended-Hardin Model

Complete identification of the Extended-Hardin model requires specifying the parameters  $S_1$ ,  $a$ , and  $C_1$  for defining the secant shear modulus (Equations 6-9, 6-10, and 6-11), and the parameters  $v_{min}$ ,  $v_{max}$ , and  $q$  for Poisson's ratio (Equation 6-16).

As a general rule, it is always more desirable to determine the parameters directly from soil test specimens taken from the field under investigation. Moreover, the specimens should be tested in a load environment closely resembling actual field conditions. However, all too often engineers are faced with analyzing soil-structure systems without available test data of soil specimens. In such cases Equations 6-12, 6-13, and 6-14 can be used directly to determine  $S_1$ ,  $a$ , and  $C_1$ . Unfortunately, similar expressions for  $v_{min}$ ,  $v_{max}$ , and  $q$  are not

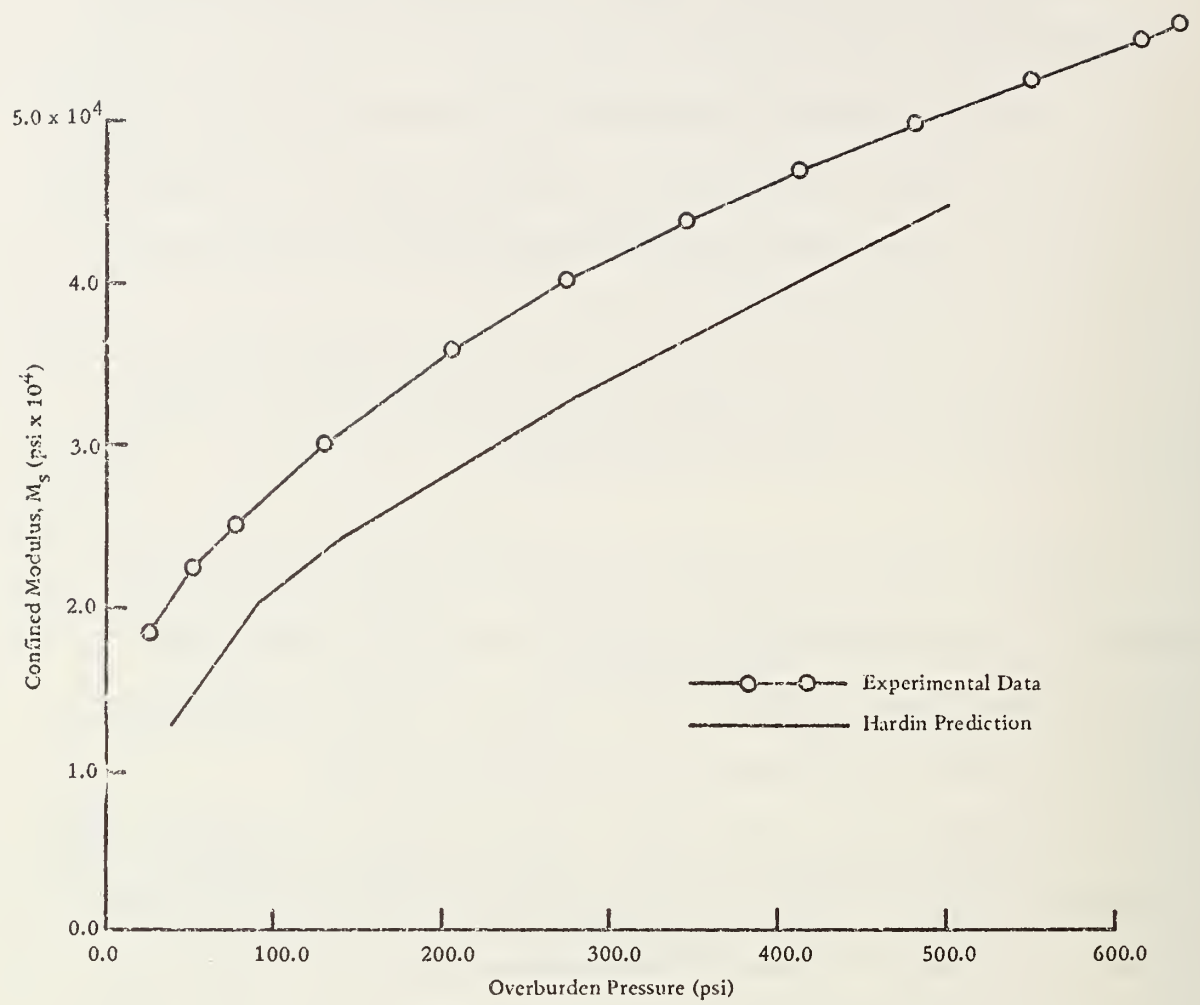


Figure 6-12.  $M_s$  versus overburden pressure.

yet developed. It is hoped that this report will stimulate further work toward that end. In the meantime, the Poisson's ratio parameters will have to be determined from test data similar to Appendix J and/or engineering judgment.

Outlined below is a step-by-step procedure for determining the complete set of parameters for the Extended-Hardin model based on a triaxial test with axial strain,  $\epsilon_1$ , and radial strain,  $\epsilon_3$ , measurements.

A. Shear modulus parameters. To begin with, a graph of shear stress,  $\tau = (\sigma_1 - \sigma_3)/2$ , versus shear strain,  $\gamma = \epsilon_1 - \epsilon_3$ , is plotted similar to Figure 6-6

1. Construct the initial tangent at zero shear strain, and denote its value as  $G_{\max}$ . The parameter  $S_1$  is given by:

$$S_1 = G_{\max} / \sqrt{\sigma_3} \quad (6-18)$$

2. Determine the maximum shear stress,  $\tau_{\max}$ , at failure. The parameter  $C_1$  is computed by:

$$C_1 = S_1^2 \left( \frac{2}{3} + \frac{\sigma_3}{\tau_{\max}} \right) \quad (6-19)$$

3. At the shear stress level,  $\bar{\tau} = \tau_{\max}/2$ , determine the corresponding measured shear strain, and denote it as  $\bar{\gamma}$ . Also compute the reference shear,  $\bar{\gamma}_r$ , at this stress level given by the expression:

$$\bar{\gamma}_r = \frac{s_1}{c_1} \sqrt{(\sigma_3 + \tau_{\max})/3} \quad (6-20)$$

Then, the parameter  $a$  is given by:

$$a = \exp(r)^{0.4} \left[ \left( \frac{6\rho + 2}{3\rho + 2} \right) - \left( \frac{1 + r}{r} \right) \right] \quad (6-21)$$

where  $r = \bar{\gamma}/\bar{\gamma}_r$ , ( $r > 0$ )

$\rho = \sigma_3/\tau_{\max}$ , ( $\rho > 0$ )

B. Poisson ratio parameters. Poisson's ratio can be computed from the results of a triaxial test by the relationship:

$$v_s = \frac{(\sigma_3/\sigma_1) - (\epsilon_3/\epsilon_1)}{1 + (\sigma_3/\sigma_1)(1 - 2\epsilon_3/\epsilon_1)} \quad (6-22)$$



In the above equation,  $\epsilon_3$  and  $\epsilon_1$  must include the volumetric strain due to confining pressure. Also the signs of  $\epsilon_3$  and  $\epsilon_1$  must be strictly observed. Hence, the ratio  $\epsilon_3/\epsilon_1$  varies from positive to negative with increased axial stress.

1. Equation 6-22 is undefined at the origin, i.e., at hydrostatic loading. Therefore, to obtain the value of the parameter  $v_{\min}$ , it is necessary to evaluate Equation 6-22 at the first few data points and extrapolate to the origin (see Figure 6-9). Any error arising from this extrapolation will generally be diminished, since the influence of  $v_{\min}$  on the Poisson's ratio function decreases with increasing shear strain.

2. To obtain  $v_{\max}$ , Equation 6-22 is evaluated at maximum failure stress; i.e.,  $\sigma_1 = \sigma_{1\max}$  and  $\epsilon_1 = \epsilon_{1\max}$ .

3. Lastly, to compute the parameter  $q$ , the data obtained at the stress level,  $\bar{\tau}$ , defined in Step 3 of Part A, are used as follows: Equation 6-22 is evaluated for  $\bar{v}_s$  using  $\bar{\epsilon}_1 = \bar{\gamma} + \bar{\epsilon}_3$ , and  $\bar{\sigma}_1 = \bar{\sigma}_3 + 2\bar{\tau}$ , then  $q$  is given by:

$$q = \frac{1}{r} \left( \frac{\bar{v}_s - v_{\min}}{v_{\max} - \bar{v}_s} \right) \quad (6-23)$$

The above procedure is only one of a multitude of possible curve-fitting techniques. For example, a least-squares procedure could also be used. For different types of soil tests similar procedures can readily be developed to define the parameters.

#### 6.5.6 Computer Algorithm for Extended-Hardin Model

Equations 6-8 and 6-16 are the functional relationships for the secant "elastic" parameters,  $G_s$  and  $\nu_s$ . For solving boundary value problems these relationships require an iterative approach wherein initial values of  $G_s$  and  $\nu_s$  are assumed and then revised based on the resulting stress-strain state. The procedure is repeated until the revisions are negligible.

The above approach is adequate for one-step loading; i.e., the total load is assumed to be applied monotonically in one step. In such cases, the secant relationships,  $G_s$  and  $\nu_s$ , can be utilized directly.

A more general case is where the loads are applied in a series of steps, such as soil lifts, temporary construction loads, and live loads. This type of loading requires an incremental formulation to account for the varied loading history.

To adapt the Extended-Hardin model to an incremental formulation, it is convenient to use the elastic parameters  $G_s$  and  $B_s$  instead of  $G_s$  and  $\nu_s$ . The parameter  $B_s$  is the secant bulk modulus and is related to  $G_s$  and  $\nu_s$  by:

$$B_s = \frac{2}{3} G_s \frac{1 + \nu_s}{1 - 2\nu_s} \quad (6-24)$$

Accordingly, Equation 6-24 provides a secant bulk modulus function by replacing  $G_s$  and  $\nu_s$  with Equations 6-8 and 6-16.

For a given state of stress-strain,  $G_s$  and  $B_s$  must satisfy the prescribed functions (Equations 6-8 and 6-24) and at the same time satisfy the fundamental stress-strain laws,  $\tau = G_s \gamma$  and  $\sigma_m = B_s \phi$ ; where  $\tau$ ,  $\gamma$ ,  $\sigma_m$ , and  $\phi$  are defined in Equation 6-15 and represent total accumulated values of stress and strain.

The incremental equivalent of the above is given by a chord relationship, i.e.:

$$\Delta\tau = G_c \Delta\gamma \quad (6-25)$$

$$\Delta\sigma_m = B_c \Delta\phi \quad (6-26)$$

where  $G_c$  = chord shear modulus  
 $B_c$  = chord bulk modulus  
 $\Delta\tau$  = maximum shear stress increment  
 $\Delta\gamma$  = maximum shear strain increment  
 $\Delta\sigma_m$  = average stress increment  
 $\Delta\phi$  = volume change increment

The chord quantities,  $G_c$  and  $B_c$ , are illustrated graphically in Figures 6-13 and 6-14. They are piecewise continuous curves inscribing the response path of the secant functions,  $G_s$  and  $B_s$ .

The objective of the incremental procedure can be stated as follows: Given a body in a state of equilibrium under a set of external loads, find values for  $G_c$  and  $B_c$  at every point in the body (every finite element) such that when an external load increment is applied, the resulting total accumulated stress and strains satisfy the functional relationships for  $G_s$  and  $B_s$  and at the same time satisfy  $\tau = G_s \gamma$  and  $\sigma_m = B_s \phi$  at every point in the body.

A methodology for achieving the above objective is outlined below, wherein it is assumed that the point (element) is in a state of equilibrium at load step  $n$  denoted by the stress and strain vectors  $\{\sigma_n\}$  and  $\{\epsilon_n\}$ .

1. Estimate trial values for  $G_c$  and  $B_c$  for the next load step  $n+1$ . For example, the final values of the previous load step could be used.
2. Construct the stiffness matrix of the system using  $G_c$  and  $B_c$  as elastic material properties in the generalized Hooke's law.

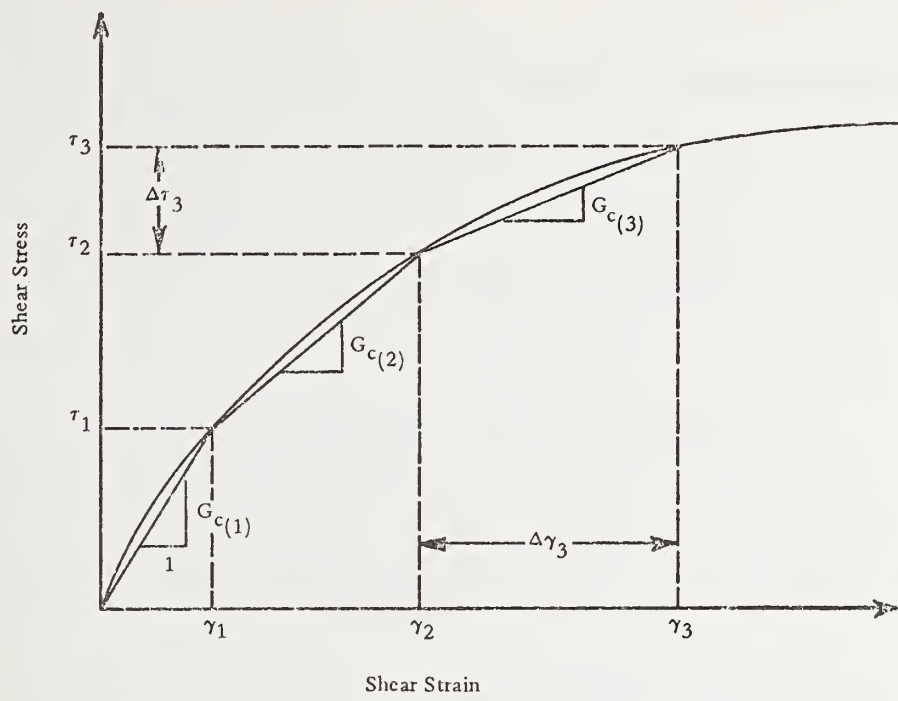


Figure 6-13. Chord approximation of shear modulus.

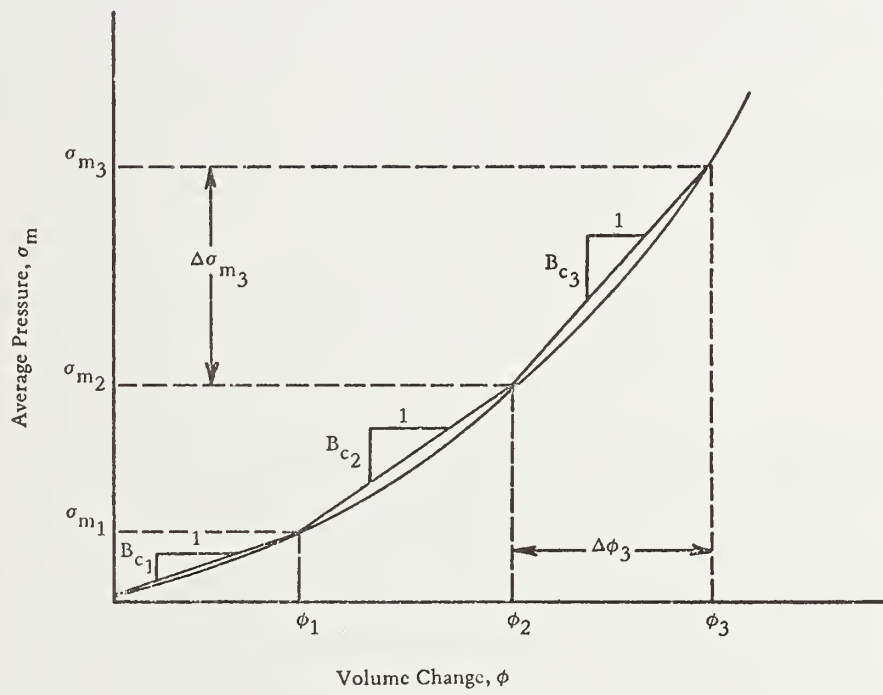


Figure 6-14. Chord approximation of bulk modulus.

3. Apply load increment  $n+1$  and obtain the trial solution for stress and strain increments denoted as  $\{\Delta\sigma_{n+1}\}$  and  $\{\Delta\epsilon_{n+1}\}$ . Compute the trial accumulated stress and strain vectors:

$$\{\sigma_{n+1}\} = \{\sigma_n\} + \{\Delta\sigma_{n+1}\}$$

$$\{\epsilon_{n+1}\} = \{\epsilon_n\} + \{\Delta\epsilon_{n+1}\}$$

and record the values for shear strain  $\gamma_{n+1}$  and the volume change  $\phi_{n+1}$ .

4. Evaluate the Extended-Hardin secant predictions  $\tau^* = G_s \gamma_{n+1}$  and  $\sigma_m^* = B_s \phi_{n+1}$ , where  $G_s$  and  $B_s$  are evaluated at the current accumulated stress-strain level by Equations 6-8, 6-16, and 6-24.

5. Estimate new chord values for  $G_c$  and  $B_c$  by:

$$G_c = \frac{\tau^* - \tau_n}{\gamma_{n+1} - \gamma_n}$$

$$B_c = \frac{\sigma_m^* - \sigma_{m_n}}{\phi_{n+1} - \phi_n}$$



6. If  $G_c$  and  $B_c$  are sufficiently close to the previous estimates, the load step has converged; therefore, control shifts back to Step 1 and the load step is advanced. Otherwise the solution increment is discarded, and control shifts back to Step 2 to repeat the load increment using the new  $G_c$  and  $B_c$ .

The speed of convergence for the above procedure is dependent on the initial trial estimates and the updating procedures for  $G_c$  and  $B_c$  given in Steps 1 and 5. To enhance convergence, the initial estimates for  $G_c$  and  $B_c$  could be based on the tangent values of the previous load step rather than the chord values. With regard to the updating estimates it is observed that the new estimate for  $G_c$  and  $B_c$  in Step 5 is based on the assumption  $\gamma_{n+1}$  and  $\phi_{n+1}$  are correct. However, it may be more expedient to assume  $\tau_{n+1}$  and  $\sigma_{n+1}$  are correct, and estimate a new  $G_c$  and  $B_c$  on this basis.

#### 6.5.7 Summary of Extended-Hardin Model

The results presented in this chapter illustrate how the Extended-Hardin model closely approximates the response data of the uniform sand specimens in Appendix J. Although different types of soils were not considered in this study, the Hardin shear modulus function includes predefined relationships for cohesive and mixed as well as

granular soil classifications. Moreover, these relationships are based on fundamental soil properties, including void ratio, percent saturation, and plasticity index. A similar set of predefined relationships has not been developed for the Poisson's ratio function. Thus, for the present, triaxial test data are required to define the Poisson's function parameters. However, with further research, relationships for the parameters of the Poisson's ratio function could be established analogous to the shear modulus parameters. At such a time the Extended-Hardin model could be used independently of triaxial tests, thereby providing an extremely powerful and versatile soil model.

As a last reminder, the limitations of the Extended-Hardin model are recanted. The model was developed on the premise of monotonic loading. Unloading is not considered in this development.

When the model is used in a secant fashion (i.e., one load step), the range of Poisson's ratio is always within the limits of  $v_{\min}$  to  $v_{\max}$ . However, when the incremental loading procedure is used, it is possible to obtain chord values for Poisson's ratio that exceed  $v_{\max}$ . In applications to date this has not occurred. However, to preclude numerical and theoretical problems it is recommended to arbitrarily limit the chord value of Poisson's ratio to  $v_{\max}$ .

## CHAPTER 7

### INTERFACE MODEL

#### 7.1 INTRODUCTION

In general interface conditions can be considered as the interaction between two substructures as they come together or separate under loading. In culvert installations there are numerous instances of interface interactions. Some important examples are: (1) relative movement of the soil with respect to the pipe at the soil-pipe interface, and (2) relative movement of fill soil with respect to in-situ soil at common interfaces. The latter example is particularly important in trench installations, wherein frictional movement of the fill soil past the trench wall can significantly alter the load on the pipe. Clearly an analytical model for interface conditions is desirable for a better understanding of the culvert problem.

The elasticity solution developed by Burns provides a first step in this direction by supplying solutions for two cases: (1) full bond between pipe and soil, and (2) bonded in normal direction across pipe-soil interface, but free to slip in tangent direction (frictionless). Although these two solutions are useful for bracketing a partial slip (frictional) condition, the limitations of Burn's theory do not allow for the more general considerations of interface problems noted above.

To achieve sufficient generality, the interface conditions will be developed in the context of a finite element formulation. Thus, an objective is to develop an "interface element" that responds to a general loading schedule, such that tensile separation, frictional movement, or complete bond of the interface are possible at any load step.

#### 7.1.1 Background

There are two fundamental approaches to treat interfaces in the context of a finite element formulation. First is the method of stiffness, and second is the method of constraints.

The method of stiffness is basically the simple concept of using "bar" elements (or directionally stiff elements) across the interface in both the normal and tangent direction. For example, if it is desired to model frictionless slippage across an interface, the normal stiffness would be specified arbitrarily large to force near compatibility of normal displacements, while the tangent stiffness would be specified extremely small (or zero) to allow independent movement in the tangent direction. Although this method has been used successfully in culvert applications [7-1, 7-2], it has certain inconsistencies that are difficult to overcome. For example, nodes on either side of a zero-width interface will penetrate each other under compressive loading, because the normal stiffness is finite. Moreover, this relative movement (penetration)

is required in order to recover the normal force in the interface element. However, if a normal stiffness is selected too large with respect to computer word length, the significant digits of the relative displacement become truncated, and the calculation of interface forces is in error. On the other hand, if the normal stiffness is selected too low, significant penetration will occur, and the kinematics will be in error.

These same inconsistencies apply to the tangent direction when frictional resistance is modeled. That is, the stiffness approach requires some relative tangential slip to occur at each load step whether or not the frictional resistance has been exceeded.

The alternative approach, method of constraints, eliminates the above inconsistencies and provides a more general capability of modeling interface interactions. The concept of using constraint equations to model interfaces has been addressed in References 7-3 and 7-4; for impact-contact, an elegant development is given by Hughes, Taylor, and Sackman [7-5].

#### 7.1.2 Scope

For this study the constraint approach is adopted and is presented in three steps:

- (1) Development of a general theory for treating constraint equations in a finite element formulation based on a generalized principle of virtual work.



(2) Development of constraint equations and decision logic suitable for characterizing the culvert interface problem.

(3) Incorporation of these constraint equations into the global stiffness matrix using standard finite element assembly techniques; i.e., the constraints are treated as "element stiffnesses."

## 7.2 CONSTRAINT EQUATIONS AND VIRTUAL WORK

In most finite element applications, constraint equations prescribe the displacement boundary conditions and generally have the simple form:

$$\begin{matrix} \hat{u}_s & - & a & = & 0 \\ (r \times 1) & & (r \times 1) & & (r \times 1) \end{matrix} \quad (7-1)$$

where  $\hat{u}_s$  are  $r$ -constrained degrees of freedom, and  $a$  are the specified values. If constraints are specified in a local coordinate system (e.g., skewed boundaries), then it is necessary to rotate the associated degrees of freedom from the global to the local coordinate system before applying Equation 7-1. Whenever constraints can be written in the form of Equation 7-1 (in either local or global coordinates), it is usually most efficient to eliminate these degrees of freedom by direct substitution and, thereby, reduce the size of the system matrix. This approach is in accord with



the restricted statement of virtual work wherein constrained degrees of freedom are assumed to be satisfied.

Contrary to the above, there are cases where retention of the constraint equations in the governing equations is extremely useful. A case in point is the treatment of interface conditions. Moreover, a more general form of constraints may be required:

$$\underset{\sim}{C} \quad \underset{\sim}{\hat{u}} \quad - \quad \underset{\sim}{a} \quad = \quad \underset{\sim}{0} \quad (7-2)$$

$$(r \times m) \quad (m \times 1) \quad (r \times 1) \quad (r \times 1)$$

The constraint matrix  $\underset{\sim}{C}$  allows consideration of arbitrary coupling of the total  $m$  degrees of freedom as well as simple constraints.

Retention of these coupled constraints in the governing equations can be formulated by evoking a general statement of virtual work. To this end, the restricted virtual work statement is reviewed followed by the general statement.

### 7.2.1 Restricted Virtual Work

The restricted virtual work principle can be stated as: "If a system of forces is in equilibrium, the net work done by all forces (external and internal) through virtual displacements compatible with constraints is zero."

From the finite element formulation of Chapter 5, the virtual work is symbolically expressed as:

$$\begin{matrix} \delta \hat{\underline{u}}^T & (\underline{K} & \hat{\underline{u}} & - & \underline{P}) & = & \underline{0} \\ (m \times 1) & (m \times m) & (m \times 1) & & (m \times 1) & & (m \times 1) \end{matrix} \quad (7-3)$$

In the above,  $\underline{K}\hat{\underline{u}}$  are the internal forces due to deformation,  $\underline{P}$  are all external forces, and  $\delta \hat{\underline{u}}$  are virtual displacements consistent with the constraints. For clarity the following system sizes are defined:

$m$  = number of all degrees of freedom

$r$  = number of constraints

$n$  =  $m - r$ , number of unknown degrees of freedom

The virtual displacement vector,  $\delta \hat{\underline{u}}$ , is of dimension  $m$ ; however, since  $r$  constraints are implied, only  $n$  arbitrary virtual movements are independent. Accordingly, Equation 7-3 can only produce  $n$  independent equilibrium equations of the form  $\underline{K}_{nn} \hat{\underline{u}}_n = \underline{P}_n$ . This point is often ignored in reducing the system from  $m$  to  $n$  degrees of freedom. That is, the conventional approach is to momentarily assume that the equilibrium equations embedded in Equation 7-3 apply to the total  $m$  degrees of freedom so that the system of equations can be written in matrix form as:

$$\begin{bmatrix} \underline{K}_{nn} & \underline{K}_{nr} \\ \underline{K}_{rn} & \underline{K}_{rr} \end{bmatrix} \begin{bmatrix} \hat{\underline{u}}_n \\ \hat{\underline{u}}_r \end{bmatrix} = \begin{bmatrix} \underline{P}_n \\ \underline{P}_r \end{bmatrix} \quad (7-4)$$

Using the top partition, the reduced system can be written as:

$$\underset{\sim}{K}_{nn} \hat{\underset{\sim}{u}}_n = \underset{\sim}{P}_n - \underset{\sim}{K}_{nr} \hat{\underset{\sim}{u}}_r \quad (7-5)$$

If the constraints can be put in the form of Equation 7-1, then  $\hat{\underset{\sim}{u}}_r$  is directly specified and Equation 7.5 can be solved by standard methods.

Although Equation 7-5 is correct, it was obtained in an ambiguous manner, i.e., by assuming Equation 7-4 provides  $m$  equations. In the next section it is shown that the general virtual work statement not only removes the above ambiguity, but also provides the mechanism for retaining all, some, or none of the constraint equations in the system matrix.

#### 7.2.2 General Virtual Work

“If a system of forces is in equilibrium, the net work done by internal, external, and constraint forces through any virtual displacement is zero.” This general statement differs from the restricted statement in that the virtual displacements need not be compatible with the constraints. Consequently, to maintain balance of virtual work the work of unknown constraint forces through virtual constraint displacements must be included in the summation of virtual work.

The virtual work of constraints is defined as “the work of constraint forces undergoing a virtual movement in violation of the

constraint." Identifying the constraints by Equation 7.2, the virtual work of constraints is:

$$V.W._c = \delta(\underline{\hat{C}} \underline{\hat{u}} - \underline{a})^T \underline{\lambda} = \delta \underline{\hat{u}}^T \underline{\hat{C}}^T \underline{\lambda} \quad (7-6)$$

where  $V.W._c$  = virtual work of constraints

$\underline{\lambda}$  = vector of  $r$  unknown constraint forces

There is one constraint force for each constraint equation; thus,  $\underline{\lambda}$  is of dimension  $r$ . Furthermore, the constraint forces are in the direction of the constraints and not necessarily in the direction of a global degree of freedom. Using Equation 7-6, the general virtual work principle can be expressed as follows.

$$\delta \underline{\hat{u}}^T (\underline{\hat{K}} \underline{\hat{u}} + \underline{\hat{C}}^T \underline{\lambda} - \underline{P}) = 0 \quad (7-7)$$

Since  $\delta \underline{\hat{u}}$  is not restrained to be compatible with constraints, it represents  $m$  arbitrary virtual movements. Therefore, unlike the restricted method, the entire set of  $m$  equilibrium equations is valid. In addition to the  $m$  equilibrium equations, there are  $r$  constraint equations providing  $m + r$  equations for  $m + r$  unknowns composed of  $\underline{\hat{u}}_m$  and  $\underline{\lambda}_r$ . Thus, the general virtual work principle plus constraint equations gives:

$$\left[ \begin{array}{c|c} K_{mm} & C_{mr}^T \\ \hline C_{rm} & 0 \end{array} \right] \left\{ \begin{array}{c} \hat{u}_m \\ \lambda_r \end{array} \right\} = \left\{ \begin{array}{c} P_m \\ a_r \end{array} \right\} \quad (7-8)$$

The development of Equation 7-8 does not have the ambiguities that arose in the derivation of Equation 7-5. However, Equation 7-8 represents a system of  $2r$  more equations. If there is no interest in the constraint forces, Equation 7-8 can be directly reduced to Equation 7-5 as shown subsequently.

### 7.2.3 Constraint Partitioning

For purposes of this development it is convenient to selectively retain some constraint relationships in the governing equations (e.g., those defining interface conditions) while eliminating other constraints by direct substitution (e.g., boundary conditions). To this end, the  $r$  constraint equations and associated forces are subdivided into  $p$  and  $q$ , ( $r = p + q$ ) where  $p$  represents the subset of constraints to be retained, and  $q$  denotes the subset to be eliminated by substitution. In like manner, the  $m$  degrees of freedom are selectively partitioned into  $n$  and  $q$  ( $m = n + q$ ), where  $n$  represents the retained degrees of freedom to be determined, and  $q$  denotes the subset to be removed prior to solving the system of equations.

With the above understanding, Equation 7-8 can be equivalently expressed in partitioned form as:



$$\begin{bmatrix} K_{nn} & K_{nq} & C_{pn}^T & C_{qn}^T \\ K_{qn} & K_{qq} & C_{pq}^T & C_{qq}^T \\ C_{pn} & C_{pq} & 0 & 0 \\ C_{qn} & C_{qq} & 0 & 0 \end{bmatrix} \begin{bmatrix} \hat{u}_n \\ \hat{u}_q \\ \lambda_p \\ \lambda_q \end{bmatrix} = \begin{bmatrix} P_n \\ P_q \\ a_p \\ a_q \end{bmatrix} \quad (7-9)$$

where the subscripts of the partitioned matrices and vectors denote their dimensions.

Equation 7-9 is in the appropriate form to eliminate  $\hat{u}_q$  and  $\lambda_q$  by standard matrix manipulations. For simplicity it will be assumed that the q subset of constraint equations has the simple form  $\hat{u}_q = a_q$ . Therefore,  $C_{qq}$  is the identity matrix, and  $C_{qn}$  contains all zeros. With this assumption, the first and third partitioned rows of Equation 7-9 provide the reduced set of equilibrium equations:

$$\begin{bmatrix} K_{nn} & C_{pn}^T \\ C_{pn} & 0 \end{bmatrix} \begin{bmatrix} \hat{u}_n \\ \lambda_p \end{bmatrix} = \begin{bmatrix} P_n - K_{nq} a_q \\ a_p - C_{pq} a_q \end{bmatrix} \quad (7-10)$$

Note, if all constraints are assumed simple (i.e.,  $p = 0$  and  $q = r$ ), Equation 7-10 reduces to Equation 7-5, verifying the conventional method of handling constraints with the restricted statement of virtual work.

There is one further partition of Equation 7-10 that is extremely useful. This applies to the case where some of the constraint forces,



$\lambda_p$ , are known and the corresponding subset of constraint equations is to be suppressed. Formally, the  $p$  constraints and constraint forces are partitioned into  $p_1$  and  $p_2$  ( $p = p_1 + p_2$ ), where  $p_1$  denotes the subset of unknown constraint forces,  $\lambda_{p_1}$ , or specified constraint equations, while  $p_2$  denotes the subset of prescribed constraint forces,  $\lambda_{p_2}$ , or suppressed constraint equations.

Performing this partition on Equation 7-10 yields:

$$\begin{bmatrix} K_{nn} & C_{p_1 n}^T & C_{p_2 n}^T \\ C_{p_1 n} & 0 & 0 \\ C_{p_2 n} & 0 & 0 \end{bmatrix} \begin{bmatrix} \hat{u}_n \\ \lambda_{p_1} \\ \lambda_{p_2} \end{bmatrix} = \begin{bmatrix} P_n - K_{nq} a_q \\ a_{p_1} - C_{p_1 q} a_q \\ a_{p_2} - C_{p_2 q} a_q \end{bmatrix} \quad (7-11)$$

Since  $\lambda_{p_2}$  is specified, say  $\lambda_{p_2} = \bar{\lambda}_{p_2}$ , Equation 7-11 can be directly reduced to:

$$\begin{bmatrix} K_{nn} & C_{p_1 n}^T \\ C_{p_1 n} & 0 \end{bmatrix} \begin{bmatrix} \hat{u}_n \\ \lambda_{p_1} \end{bmatrix} = \begin{bmatrix} P_n^* \\ a_{p_1}^* \end{bmatrix} \quad (7-12)$$

where  $P_n^* = P_n - K_{nq} a_q - C_{p_2 n}^T \bar{\lambda}_{p_2}$

$a_{p_1}^* = a_{p_1} - C_{p_1 q} a_q$

Equation 7-12 is a general set of equilibrium equations that permit all, some, or none of the constraint equations to be retained in the system matrix. Furthermore, any portion of the retained constraint equations can be suppressed by specifying the constraint forces. The generality afforded in this development is the outcome of the general virtual work principle. Motivation for this generality will be apparent in the development of the interface element.

It is emphasized that the formal partitioning indicated in Equation 7-12 is merely for ease of presentation. In computational practice the constraint matrices can be treated as "element stiffnesses," utilizing standard finite element assembly techniques. This will be demonstrated in a later section.

Lastly, it is noted that Equation 7-12 can be written directly in incremental form with no loss of generality:

$$\begin{bmatrix} K_{nn} & C_{p_1 n}^T \\ C_{p_1 n} & 0 \end{bmatrix} \begin{bmatrix} \Delta \hat{u}_n \\ \Delta \lambda_{p_1} \end{bmatrix} = \begin{bmatrix} \Delta P_n^* \\ \Delta a_{p_1}^* \end{bmatrix} \quad (7-13)$$

The incremental form is convenient for handling the nonlinear aspects of the interface constraint conditions discussed next.

## 7.3 CONSTRAINT EQUATIONS FOR INTERFACE MODEL

### 7.3.1 Interface Definition

The interface model will be restricted to planar degrees of freedom, and it is assumed that in the undeformed state the interface is defined by a set of "paired" nodes joining two bodies, as shown in Figure 7-1. Thus, prior to deformation the paired nodes occupy the same position in space but are assigned to separate bodies (elements).

Upon deformation the response of the interface as a whole is composed of the individual responses of each node pair. Thus, attention can be focused on one node pair, hereafter called contact points. Figure 7-2 illustrates a single contact point for bodies I and J. Let the respective points,  $i$  and  $j$ , be contact points such that they share a common interface plane defined by the direction  $s$ . Let the normal of the interface be positive in the direction  $n$  from point  $i$  to  $j$ , thereby defining an angle  $\theta$  with respect to the global  $x$ -axis. In other words,  $\theta$  is the angle the local  $n - s$  system is rotated with respect to the global  $x - y$  system.

In Figure 7-3 a microscopic view of the contact interface is shown to illustrate forces and displacements in the local  $n - s$  system. Here,  $u_{n_i}$  and  $u_{s_i}$  are the normal and tangential displacements of point  $i$ , while  $u_{n_j}$  and  $u_{s_j}$  are the normal and tangential displacements of point  $j$ . The interface forces are denoted as  $\lambda_n$  and  $\lambda_s$  for normal and shear

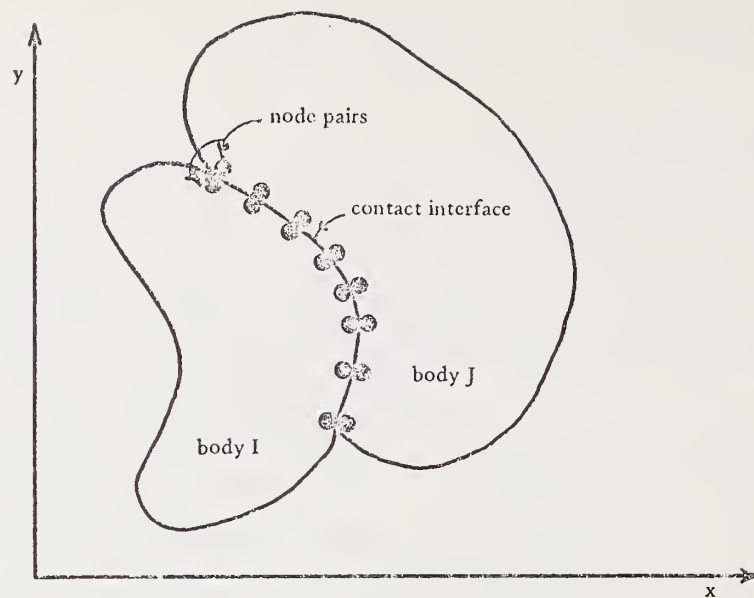


Figure 7-1. Interface points between body I and J.

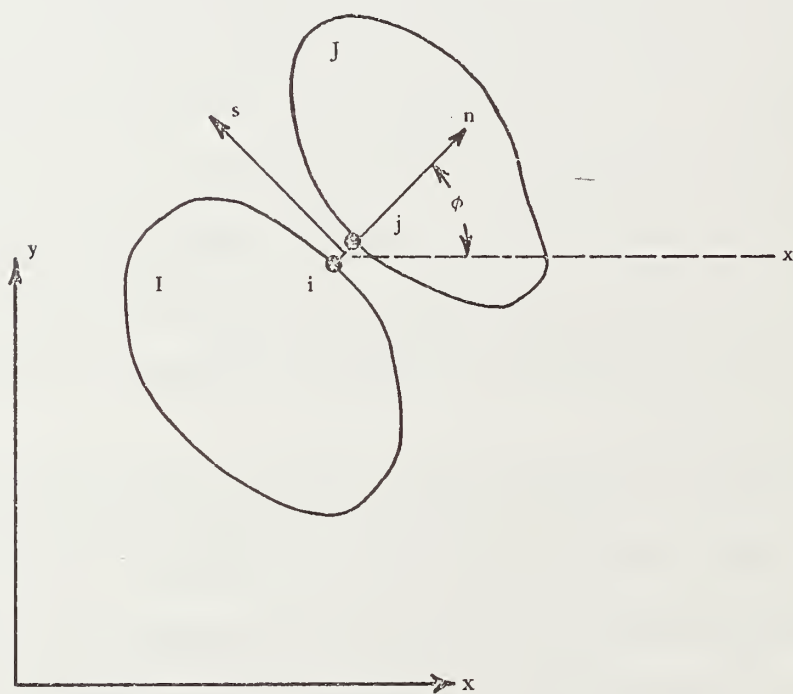


Figure 7-2. Local  $n - s$  system of contact points.

forces existing between points i and j. Note a positive value of  $\lambda_n$  implies tension across the interface. It should be observed that these forces arise solely from the contact interaction and are in addition to any other external force existing at points i and j.

### 7.3.2 Interface States

For any particular load increment the interface condition between points i and j can be characterized by the state of the normal and tangential displacement components of the contact points. That is, by using the descriptors "fixed" and "free" for describing the relative movement of the contact points in the normal and tangential directions, four states can be defined: fixed-fixed, fixed-free, free-fixed, and free-free. These states are clarified in Figure 7-4 and are designated as states A, B, C, and D, respectively.

State A implies the contact points are constrained to move together in both the normal and tangential direction, while State D implies the constraints are suppressed which allows independent movement of nodes i and j.

State B characterizes the case for sliding movement (with or without friction) so that relative normal movement is constrained while the tangential constraint is suppressed and a frictional force is specified.

State C is discarded because it has no physical significance for this model. That is, it implies a separation in the normal direction

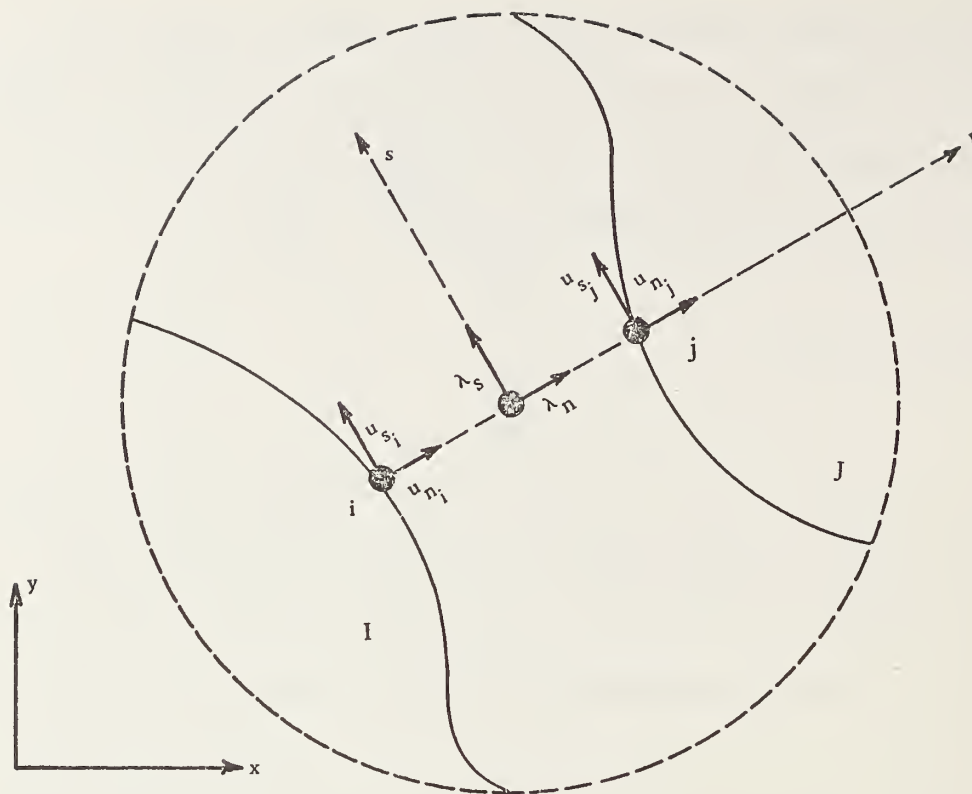


Figure 7-3. Sign convention of contact forces and displacements.

		Relative Tangent Movement	
		Fixed	Free
Relative Normal Movement	Fixed	A fixed-fixed	B fixed-free
	Free	C free-fixed	D free-free

Figure 7-4. Designation of potential kinematic states.



while retaining contact in the tangential direction. For this development, whenever normal separation occurs, state D is automatically implied, thereby eliminating State C.

The job at hand is to quantify the above concepts for States A, B, and D in terms of constraint equations and/or constraint forces. For generality it is convenient to consider incremental quantities of the interface responses caused by increments of loading. Let the load step number be designated by the superscript  $k$  and let incremental quantities be prefixed with the symbol  $\Delta$  so that the following definitions hold:

$$\Delta u_{n_i} = u_{n_i}^{k+1} - u_{n_i}^k$$

$$\Delta u_{n_j} = u_{n_j}^{k+1} - u_{n_j}^k$$

$$\Delta u_{s_i} = u_{s_i}^{k+1} - u_{s_i}^k$$

(7-14)

$$\Delta u_{s_j} = u_{s_j}^{k+1} - u_{s_j}^k$$

$$\Delta \lambda_n = \lambda_n^{k+1} - \lambda_n^k$$

$$\Delta \lambda_s = \lambda_s^{k+1} - \lambda_s^k$$

Further, the relative tangential and normal movements between nodes

i and j are defined as:

$$a_s^k = u_{s_j}^k - u_{s_i}^k$$

$$a_n^k = u_{n_j}^k - u_{n_i}^k$$

With increments:

(7-15)

$$\Delta a_s = a_s^{k+1} - a_s^k$$

$$\Delta a_n = a_n^{k+1} - a_n^k$$

7.3.2.1 State A Interface. To impose State A during the load increment k to k + 1, the resulting normal relative displacement must be zero;  $a_n^{k+1} = 0$ . By definition this implies the incremental constraint relationship,  $\Delta u_{n_j} - \Delta u_{n_i} = -a_n^k$  must hold. For the tangent direction the constraint is not quite so obvious. Unlike the normal displacements, bonding or rebonding does not require the total tangential displacements to be identical. Thus, the constraint is imposed on the tangential increments,  $\Delta u_{s_j} - \Delta u_{s_i} = \bar{a}_s$ , where  $\bar{a}_s$  is the relative tangential movement within the load step and is dependent on the state of the previous load step. If States A or B existed previously then  $\bar{a}_s = 0$ . On the other hand, if D was the previous state,  $\bar{a}_s$  is generally nonzero and is determined from geometrical considerations. This point is deferred until later. Table 7-2 contains a summary of constraints to impose State A.

7.3.2.2 State B Interface. To impose State B during the load increment  $k$  to  $k + 1$ , the normal displacements have the same constraint as in State A, i.e.,  $\Delta u_{n_j} - \Delta u_{n_i} = -a_n^k$ .

For the tangent direction the displacement constraint is suppressed, and a frictional interface force is specified. Assuming Coulomb friction, the passive friction resistance at the end of the load step is:

$$S_{\max}^{k+1} = (\text{sign})\mu |\lambda_n^{k+1}| \quad (7-16)$$

where  $(\text{sign}) = \lambda_s^{k+1} / |\lambda_s^{k+1}|$

$\mu$  = coefficient of friction

$S_{\max}$  is the maximum passive shear resistance obtainable for a given normal (compressive) force,  $\lambda_n$ . Naturally, the direction (sign) of  $S_{\max}$  is in the direction of the impending tangential force,  $\lambda_s$ .

With the above understanding, the interface tangent force at the end of the load step must be (for State B)  $\lambda_s^{k+1} = S_{\max}^{k+1}$ . This requires the tangent force increment to be specified as  $\Delta \lambda_s = S_{\max}^{k+1} - \lambda_s^k$ . Note if  $\mu \neq 0$ ,  $S_{\max}^{k+1}$  depends on responses at the end of the load step; thus, the specification of  $\Delta \lambda_s$  requires an iterative solution. State B equations are summarized in Table 7-1.

7.3.2.3 State D Interface. Imposing State D during the load step  $k$  to  $k + 1$  requires suppressing displacement constraints and demanding

Table 7-1. Equations to Impose States A, B, and D

State	Constraint Equations
A (fixed-fixed)	$\Delta u_{n_j} - \Delta u_{n_i} = a_n$ $\Delta u_{s_j} - \Delta u_{s_i} = a_s$
B (free-fixed)	$\Delta u_{n_j} - \Delta u_{n_i} = a_n$ $\Delta \lambda_s = S_{\max}^{k+1} - \lambda_s^k$
D (free-free)	$\Delta \lambda_n = -\lambda_n^k$ $\Delta \lambda_s = -\lambda_s^k$

$$\text{where: } S_{\max}^{k+1} = (\text{sign})u|\lambda_n^{k+1}|$$

$$(\text{sign}) = \lambda_s^{k+1}/|\lambda_s^{k+1}|$$

$$a_n = -a_n^k$$

$$a_s = \begin{cases} 0, & \text{if state of previous load step} = A \text{ or } B \\ \Delta a_s |a_n^k / \Delta a_n|, & \text{if state of previous load} \\ & \text{step} = D \end{cases}$$

$\lambda_n^{k+1} = \lambda_s^{k+1} = 0$ . Consequently, constraint force increments are specified as:  $\Delta\lambda_n = -\lambda_n^k$ , and  $\Delta\lambda_s = -\lambda_s^k$ . In other words, all pre-existing constraint forces are removed. Table 7-1 summarizes these equations.

7.3.2.4 Selection of Correct State. As yet no criteria have been presented to decide what state is the correct choice to impose during a given load increment. This decision requires a trial and error approach, wherein a particular state is assumed and a set of trial responses are obtained. The trial responses are used to determine if the assumed state was correct, and, if not, what state is more likely.

Figure 7-5 contains an exhaustive set of decision parameters to aid in determining the correct state. The diagram is in the form of a 3 x 3 matrix, where each row is associated with the assumed state, and the columns denote new candidate states based on the responses of the assumed state. If the assumed state and the new candidate state are identical, the solution increment is valid, and the next load step can be considered. Otherwise, the new candidate state is assumed, and the load step is repeated.

Consider the first row of Figure 7-5 where the trial solution is based on State A. State A is the correct choice, if the total normal force  $\lambda_n^{k+1}$  is less than or equal to the tensile breaking force,  $\beta$ , (normally  $\beta = 0$ ), and the absolute value of the total interface shear force,  $|\lambda_s^{k+1}|$ , is less than the maximum shear resistance,  $|S_{\max}^{k+1}|$ . If not, State B becomes the new candidate, if tensile rupture does not

		New Candidate State From Decision Matrix		
		A	B	D
Assumed State of Contact for Current Trial Solution	A →	$\lambda_n^{k+1} \leq \beta$ and $ \lambda_s^{k+1}  <  S_{\max}^{k+1} $	$\lambda_n^{k+1} \leq \beta$ and $ \lambda_s^{k+1}  \geq  S_{\max}^{k+1} $	$\lambda_n^{k+1} > \beta$
	B →	$\lambda_n^{k+1} \leq \beta$ and $\Delta a_s \cdot S_{\max}^{k+1} < 0$	$\lambda_n^{k+1} \leq \beta$ and $\Delta a_s \cdot S_{\max}^{k+1} \geq 0$	$\lambda_n^{k+1} > \beta$
	D →	$a_n^{k+1} < 0$		$a_n^{k+1} \geq 0$

$\beta$  = tensile rupture resistance of interface (positive)

Figure 7-5. Decision matrix for testing assumed state.



occur, but shear resistance is exceeded. Otherwise, if tensile rupture occurs, State D becomes the candidate state.

Next consider row 2 where State B is the assumed state. The decision parameters are tensile rupture,  $\beta$ , and relative tangential movement,  $\Delta a_s$ . State B is the correct choice, if tensile rupture is not exceeded, and the relative tangential movement,  $\Delta a_s$ , has the same sign as the imposed frictional forces,  $S_{\max}^{k+1}$ ; i.e.,  $(S_{\max}^{k+1} \cdot \Delta a_s \geq 0)$ . If the latter criterion is not satisfied, the solution will not be valid because relative movement cannot reverse its direction until the passive resistance reverses direction. Instead, relative movement is restrained, and State A is the new candidate. If tensile rupture is exceeded, State D is the candidate.

Finally, row 3 implies State D is assumed. If the total relative normal displacement,  $a_n^{k+1}$ , is greater than or equal to zero, then penetration has not occurred, and State D is the correct choice. Otherwise, if penetration does occur, State A is the candidate state. This does not imply State B cannot be reached from State D; it simply means State B must be reached by an iterative path such as  $D \rightarrow A \rightarrow B$ . The event of moving from State D to State A requires the calculation of the relative tangential movement,  $\bar{a}_s$ , which has been deferred until now.

7.3.2.5 Determination of  $\bar{a}_s$ . Consider the situation where the interface is in State D at step k, and, upon assuming State D for the next load increment, it is found that State A is the new candidate

state (i.e.,  $a_n^{k+1} < 0$ ). Let this sequence of events be denoted as:  $D^k \rightarrow D^{k+1} \rightarrow A^{k+1}$ . Although  $D^{k+1}$  represents an invalid trial solution, the results of  $D^{k+1}$  are used to determine  $\bar{a}_s$  in preparation for the new candidate State  $A^{k+1}$ . Figure 7-6 illustrates the geometrical concepts for determining  $\bar{a}_s$  by considering the relative normal and tangential movements from the States  $D^k \rightarrow D^{k+1}$ . Since the normal relative displacement increment is constrained to be  $\bar{a}_n = -a_n^k$  for State  $A^{k+1}$ , the corresponding proportional tangential increment is  $\bar{a}_s = \Delta a_s |a_n^k / \Delta a_n|$ .

This completes the development of the constraint/force equations and decision logic. In the next section a strategy for implementing these relationships at the element level is presented.

## 7.4 FINITE ELEMENT ASSEMBLY OF CONSTRAINT ELEMENTS

### 7.4.1 Constraint Assembly

The constraint/force equations of Table 7-1 will now be assimilated into the general equilibrium Equation 7-13 by means of finite element assembly techniques. To demonstrate the "element nature" of the constraint matrix, the coefficient matrix of Equation 7-13 is written as:

$$\left[ \begin{array}{c|c} K_{nn} & C_{pn}^T \\ \hline C_{pn} & 0 \end{array} \right] = \underline{\underline{K^*}} + \underline{\underline{C^*}} \quad (7-17)$$

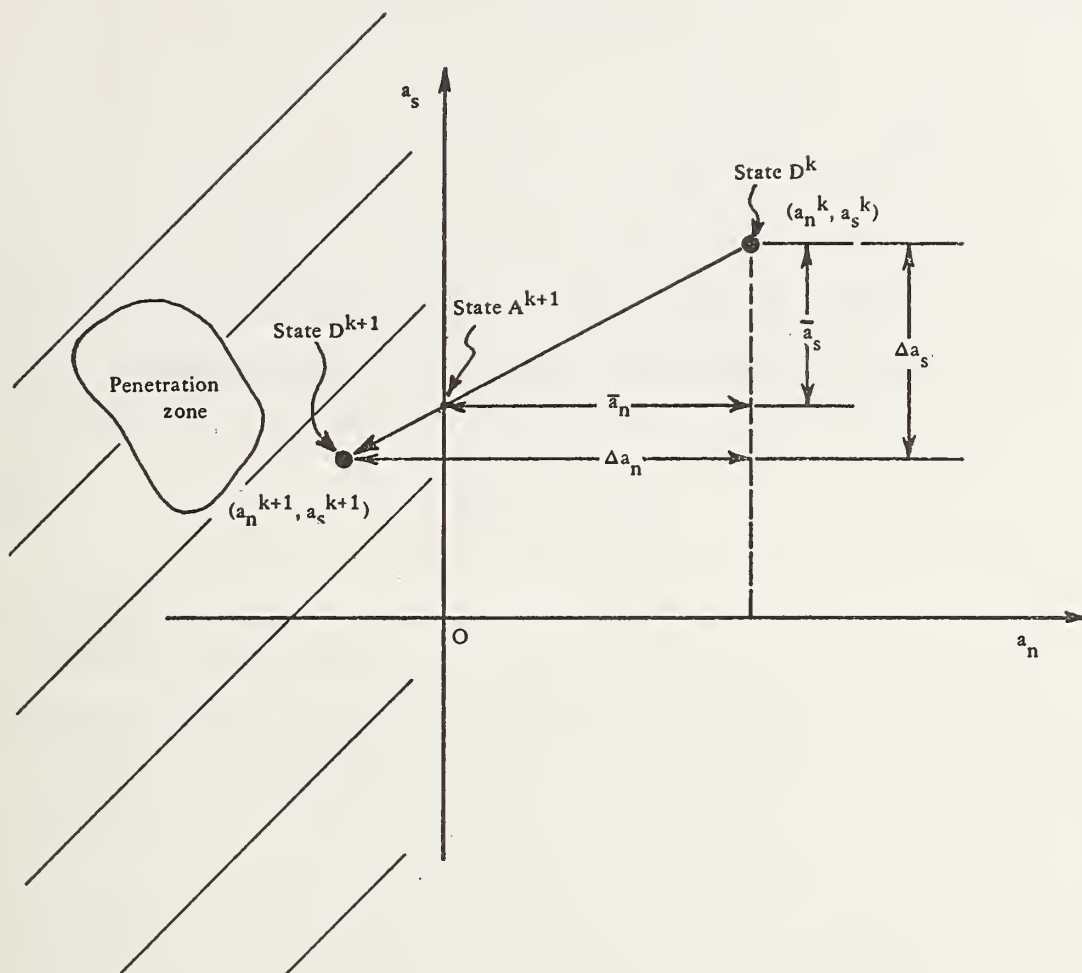


Figure 7-6. Geometric representation of  $\bar{a}_s$ .

$$\text{where } \underline{\underline{K}}^* = \begin{bmatrix} K_{nn} & 0 \\ 0 & 0 \end{bmatrix}$$

$$\underline{\underline{C}}^* = \begin{bmatrix} 0 & C_{pn}^T \\ C_{pn} & 0 \end{bmatrix}$$

$\underline{\underline{K}}^*$  is the stiffness portion of the coefficient matrix and is constructed by standard procedures of assembling element stiffnesses, i.e.,

$$\underline{\underline{K}}^* = \sum k_c \quad (7-18)$$

where  $k_c$  is the element stiffness, and  $\sum$  is a summation operator with the special understanding that contributions of each element are properly assigned to the correct locations of the nodal displacement vector,  $\Delta \hat{u}$ .

In an identical fashion, the constraint portion of the coefficient matrix,  $\underline{\underline{C}}^*$ , can be constructed by an ordering of "constraint elements," i.e.,

$$\underline{\underline{C}}^* = \sum c_e \quad (7-19)$$

where  $c_e$  is the element constraint matrix and has the simple symmetric form:

$$\underline{\underline{c}}_e = \begin{array}{c} \Delta \tilde{u} \quad \Delta \tilde{\lambda} \\ \left[ \begin{array}{c|c} 0 & c^T \\ \hline c & 0 \end{array} \right]_e \end{array} \quad (7-20)$$

where  $c$  are constraint equation coefficients that pertain to element  $e$ . The operator  $\tilde{E}$  assigns the element constraint coefficients to the associated nodal displacements and interface forces. No summation occurs, because the constraint forces are unique to each element. The above concepts are better understood by formally developing the interface element.

#### 7.4.2 Constraint Element

The constraint element consists of the nodes  $i$  and  $j$  as previously suggested in Figures 7-2 and 7-3. Node  $i$  is associated with an element or group of elements on the negative side of the interface, while node  $j$  is associated with elements on the positive side of the interface. It is convenient to define a third node,  $l$ , so that the interface element is defined by the nodes  $i-l-j$ , as shown in Figure 7-7. The spatial location of node  $l$  is immaterial; its sole purpose is to provide unique equation numbers for the interface forces. Accordingly, node  $l$  cannot be shared with any other element. (Note, if storage is provided for the interface forces by increasing the degrees of freedom at nodes  $i$  and  $j$ , the ability to use either node  $i$  or node  $j$  in a second constraint

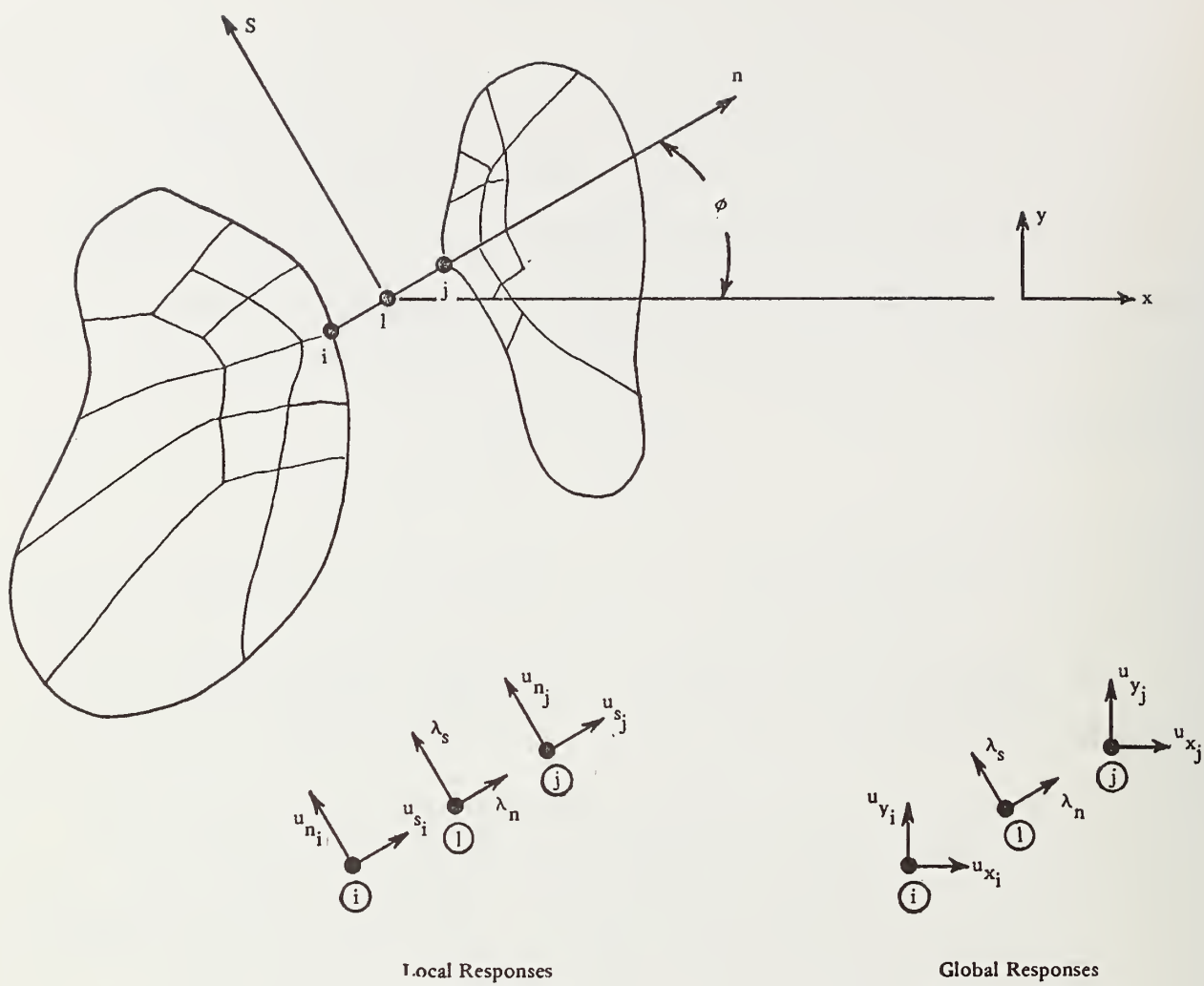


Figure 7-7. Nodes for constraint element.



element is lost. Corners often require two constraint elements with common nodes.)

The interface constraint equations for State A in Table 7-1 can be written in matrix notation as:

$$\begin{bmatrix} -1 & 0 & 1 & 0 \\ 0 & -1 & 0 & 1 \end{bmatrix} \begin{Bmatrix} \Delta u_{n_i} \\ \Delta u_{s_i} \\ \Delta u_{n_j} \\ \Delta u_{s_j} \end{Bmatrix} = \begin{Bmatrix} \bar{a}_n \\ \bar{a}_s \end{Bmatrix} \quad (7-21)$$

For compatibility with the stiffness matrix, the displacement degrees of freedom must be rotated to the x - y system through the angle  $\phi$ . The transformation for both node i and j is:

$$\begin{Bmatrix} \Delta u_n \\ \Delta u_s \end{Bmatrix} = \begin{bmatrix} \cos\phi & \sin\phi \\ -\sin\phi & \cos\phi \end{bmatrix} \begin{Bmatrix} \Delta u_x \\ \Delta u_y \end{Bmatrix} \quad (7-22)$$

Performing this simple transformation, Equation 7-21 becomes:

$$\begin{bmatrix} -\cos\phi & -\sin\phi & \cos\phi & \sin\phi \\ \sin\phi & -\cos\phi & -\sin\phi & \cos\phi \end{bmatrix} \begin{Bmatrix} \Delta u_{x_i} \\ \Delta u_{y_i} \\ \Delta u_{x_j} \\ \Delta u_{y_j} \end{Bmatrix} = \begin{Bmatrix} \bar{a}_n \\ \bar{a}_s \end{Bmatrix} \quad (7-23)$$

The leading matrix in Equation 7-23 contains the constraint coefficients, denoted as  $\underline{c}$  in Equation 7-20. Therefore, the constraint element stiffness  $\underline{c}_e$ , for State A is given by:

$$\underline{c}_e = \begin{matrix} & \begin{matrix} \text{i} & & \text{j} & & \text{l} \end{matrix} & \\ & \begin{matrix} \Delta u_{x_i} & \Delta u_{y_i} & \Delta u_{x_j} & \Delta u_{y_j} & \Delta \lambda_n & \Delta \lambda_s \end{matrix} & \\ \begin{matrix} 0 & 0 & 0 & 0 & -\cos\phi & \sin\phi \\ 0 & 0 & 0 & 0 & -\sin\phi & -\cos\phi \\ 0 & 0 & 0 & 0 & \cos\phi & -\sin\phi \\ 0 & 0 & 0 & 0 & \sin\phi & \cos\phi \\ -\cos\phi & -\sin\phi & \cos\phi & \sin\phi & 0 & 0 \\ \sin\phi & -\cos\phi & -\sin\phi & \cos\phi & 0 & 0 \end{matrix} & \end{matrix} \quad \begin{matrix} (7-24) \\ (State A) \end{matrix}$$

The associated State A element "load" vector to be added to the right-hand side of the system of equations is:

$$\Delta \underline{f}_e = \begin{Bmatrix} 0 \\ 0 \\ 0 \\ 0 \\ \bar{a}_n \\ \bar{a}_s \end{Bmatrix} \quad \begin{matrix} (7-25) \\ (State A) \end{matrix}$$

To construct State B,  $\Delta \lambda_s$  is specified as  $\Delta \lambda_s = \bar{\lambda}_s$  (where from Table 7-1,  $\bar{\lambda}_s = S_{\max}^{k+1} - \lambda_s^k$ ), and the tangential constraint is suppressed to give:

$$\begin{aligned}
\mathbf{c}_e &= \begin{bmatrix} \Delta u_{x_i} & \Delta u_{y_i} & \Delta u_{x_j} & \Delta u_{y_j} & \Delta \lambda_n & \Delta \lambda_s \\ 0 & 0 & 0 & 0 & -\cos\phi & 0 \\ 0 & 0 & 0 & 0 & -\sin\phi & 0 \\ 0 & 0 & 0 & 0 & \cos\phi & 0 \\ 0 & 0 & 0 & 0 & \sin\phi & 0 \\ -\cos\phi & -\sin\phi & \cos\phi & \sin\phi & 0 & 0 \\ 0 & 0 & 0 & 0 & 0 & 1 \end{bmatrix} \quad (7-26) \\
&\quad \text{(State B)}
\end{aligned}$$

The associated element "load" vector for State B is:

$$\begin{aligned}
\Delta \mathbf{f}_{\sim e} &= \begin{Bmatrix} -\sin\phi \bar{\lambda}_s \\ \cos\phi \bar{\lambda}_s \\ \sin\phi \bar{\lambda}_s \\ -\cos\phi \bar{\lambda}_s \\ \bar{a}_n \\ \bar{\lambda}_s \end{Bmatrix} \quad (7-27) \\
&\quad \text{(State B)}
\end{aligned}$$

And, finally, to construct State D, both  $\Delta \lambda_n$  and  $\Delta \lambda_s$  are specified as  $\Delta \lambda_n = \bar{\lambda}_n$  and  $\Delta \lambda_s = \bar{\lambda}_s$ , where Table 7-1 gives  $\bar{\lambda}_n = -\lambda_n^k$  and  $\bar{\lambda}_s = -\lambda_s^k$ .

Suppressing both constraints gives:

$$\begin{aligned}
\mathbf{c}_e &= \begin{bmatrix} \Delta u_{x_i} & \Delta u_{y_i} & \Delta u_{x_j} & \Delta u_{y_j} & \Delta \lambda_n & \Delta \lambda_s \\ 0 & 0 & 0 & 0 & 0 & 0 \\ 0 & 0 & 0 & 0 & 0 & 0 \\ 0 & 0 & 0 & 0 & 0 & 0 \\ 0 & 0 & 0 & 0 & 0 & 0 \\ 0 & 0 & 0 & 0 & 1 & 0 \\ 0 & 0 & 0 & 0 & 0 & 1 \end{bmatrix} \quad (7-28) \\
&\quad \text{(State D)}
\end{aligned}$$

And the associated "load" vector is:

$$\Delta \tilde{f}_e = \begin{Bmatrix} \bar{\lambda}_n \cos \phi - \bar{\lambda}_s \sin \phi \\ \bar{\lambda}_n \sin \phi + \bar{\lambda}_s \cos \phi \\ -\bar{\lambda}_n \cos \phi + \bar{\lambda}_s \sin \phi \\ -\bar{\lambda}_n \sin \phi - \bar{\lambda}_s \cos \phi \\ \bar{\lambda}_n \\ \bar{\lambda}_s \end{Bmatrix} \quad \begin{matrix} (7-29) \\ \text{(State D)} \end{matrix}$$

## 7.5 SUMMARY OF SOLUTION STRATEGY

The developments of this chapter are summarized in the following solution methodology for treating interface conditions within a finite element framework. The problem is posed as follows. At load step  $k$  the system is in equilibrium, and the constraint elements are in the correct state. The objective is to determine the system responses and correct states of the constraint elements after applying the loads from step  $k$  to  $k + 1$ :

1. Initially assume that each constraint element "stiffness" remains as in the previous step (i.e.,  $\tilde{c}_e^{k+1} = \tilde{c}_e^k$ ), and assign the element "load" vector,  $\Delta \tilde{f}_e = 0$ .

2. Construct the global "stiffnesses,"  $\tilde{K}^*$  and  $\tilde{C}^*$ , and load vector,  $\Delta P^*$ , i.e.,

$$\begin{aligned}\tilde{K}^* &= \sum \tilde{k}_e && \text{(standard stiffness)} \\ \tilde{C}^* &= \sum \tilde{c}_e && \text{(constraint "stiffness") } \\ \Delta P^* &= \Delta P + \sum \Delta f_e && \text{(applied + constraint loads)}\end{aligned}$$

3. Solve the system:

$$[\tilde{K}^* + \tilde{C}^*] \begin{Bmatrix} \Delta \hat{u} \\ \Delta \hat{\lambda} \end{Bmatrix} = \begin{Bmatrix} \Delta P^* \end{Bmatrix}$$

for  $\Delta \hat{u}$  and  $\Delta \hat{\lambda}$ , and get trial solution for total responses:

$$\hat{\lambda}^{k+1} = \Delta \hat{\lambda} + \hat{\lambda}^k \quad \text{and} \quad \hat{u}^{k+1} = \Delta \hat{u} + \hat{u}^k$$

4. Evaluate the validity of the assumed state for each element by the decision logic of Figure 7-5.

(a) If every interface element was assumed in the proper state, and friction is properly determined, go to Step 5.

(b) For each and every element not in the proper state, change  $\tilde{c}_e$  and  $\Delta f_e$  to the proper state with aid of Equations 7-24 through 7-29, then return to Step 2.

5. Advance the load step, and go to Step 1. After all load steps are applied, the problem is completed.



## CHAPTER 8

### PIPE MODELS AND DESIGN LOGIC

Pipe models refer to the stress-strain relationship or constitutive model employed to characterize the material behavior of the pipes. Design logic entails the methodology of sizing the pipe wall geometry to achieve desired safety factors. In later sections of this chapter, the pipe model and design logic for each pipe-type (steel, aluminum, concrete, and plastic) will be discussed individually. For now a general overview of the assumptions and developments common to all pipe types is presented.

The analytical characterization of an entire pipe is treated somewhat differently for the two basic solution methods. That is, the elasticity solution (Level 1) treats the pipe as a thin, uniform cylindrical shell, whereas the finite element solution (Levels 2 and 3) approximates the pipe with a connected series of plane-strain, beam-column elements. In either case, however, the mathematical representation of the pipe wall sectional and material properties is the same for all solution levels and is identified as follows:

- E = Young's modulus
- $\nu$  = Poisson's ratio
- I = moment of inertia of pipe wall per unit length
- A = area of pipe wall per unit length

In the above  $E$  and  $\nu$  are engineering material properties, while  $I$  and  $A$  are the standard geometric properties of the pipe wall section.

During a solution process these parameters are modified or updated to reflect material nonlinearities and/or to achieve a candidate design. This methodology is contained in modularized subroutines and are the key control areas of CANDE. Each pipe subroutine contains its own constitutive model and design criteria representative of the nonlinear behavior and potential failure modes of the pipe type.

The pipe subroutines perform four fundamental operations common to all pipe types and solution levels. These operations are denoted in Figure 8-1 and provide a convenient format for discussion.

## 8.1 PIPE SUBROUTINES

### 8.1.1 Data Specification

Data specification (refer to Figure 8-1) is dependent on the execution mode. In the analysis mode  $E$ ,  $\nu$ ,  $I$ , and  $A$  are prescribed for the unloaded pipe along with nonlinear properties (to be discussed next). In the design mode  $E$  and  $\nu$  are prescribed as above; however,  $I$  and  $A$  are unknown section properties and are the object of the design solution. In place of the section properties, desired safety factors  $\overline{SF}_1$  for potential modes of failure are prescribed to provide a basis

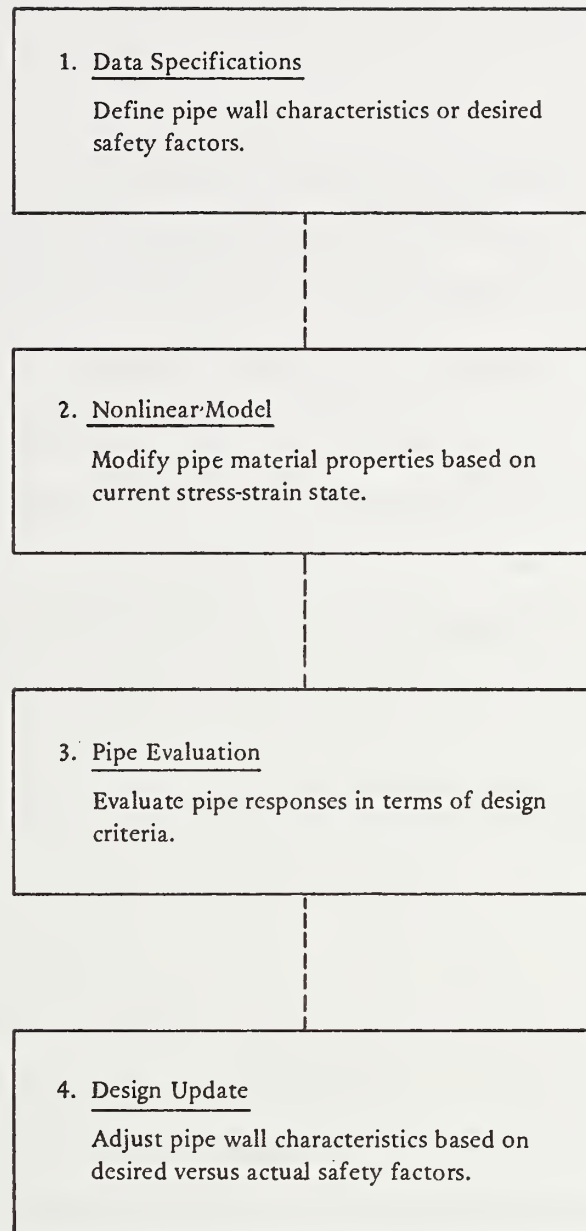


Figure 8-1. The four operations of pipe subroutines.

for design. Whenever feasible, all input specifications are supplied with recommended default values to minimize data preparation.

#### 8.1.2 Nonlinear Model

It is well known that most pipe culverts undergo some type of nonlinear behavior, such as outer fiber yielding or tensile cracking, under design loading. To account for this behavior a general nonlinear stress-strain model is presented. The model accounts for the interaction of thrust and moment by determining the axis of bending in a consistent manner. The assumptions common to all pipe types are as follows:

(1) Transverse strains and stresses through the pipe wall are negligible.

(2) Shear strains are negligible, i.e., shear deformation is not included.

(3) Circumferential strains are linear through the pipe wall section. Furthermore, these strains are decomposed into constant (thrust) and flexural (moment) contributions, as illustrated in Figure 8-2 and expressed in Equations 8-1 and 8-2

$$\epsilon = \epsilon_N + \epsilon_M \quad (8-1)$$

$$\epsilon_M = \phi(\bar{y} - y) \quad (8-2)$$

where  $\epsilon$  = circumferential strain  
 $\epsilon_N$  = uniform thrust strain  
 $\epsilon_M$  = linear flexural strain  
 $\phi$  = curvature of section (i.e., derivative of slope)  
 $\bar{y}$  = distance to bending axis,  $\epsilon_M = 0$   
 $y$  = spatial coordinate measuring depth of section

For linear materials  $\bar{y}$  is independent of the stress state and coincides with the geometric axis for minimum moment of inertia. However, for the nonlinear case  $\bar{y}$  must be determined as a function of the nonlinear stress-strain law as developed in the following.

A general incremental stress-strain law is introduced below and is shown graphically in Figure 8-3.

$$\Delta\sigma = E'(\epsilon) \Delta\epsilon \quad (8-3)$$

$$E'(\epsilon) = E_e [1 - \alpha(\epsilon)] \quad (8-4)$$

where  $\Delta\sigma$  = increment of stress (circumferential)  
 $\Delta\epsilon$  = increment of strain (circumferential)  
 $E'(\epsilon)$  = tangent modulus (or chord modulus)  
 $E_e$  = initial linear modulus  
 $\alpha(\epsilon)$  = dimensionless function of strain

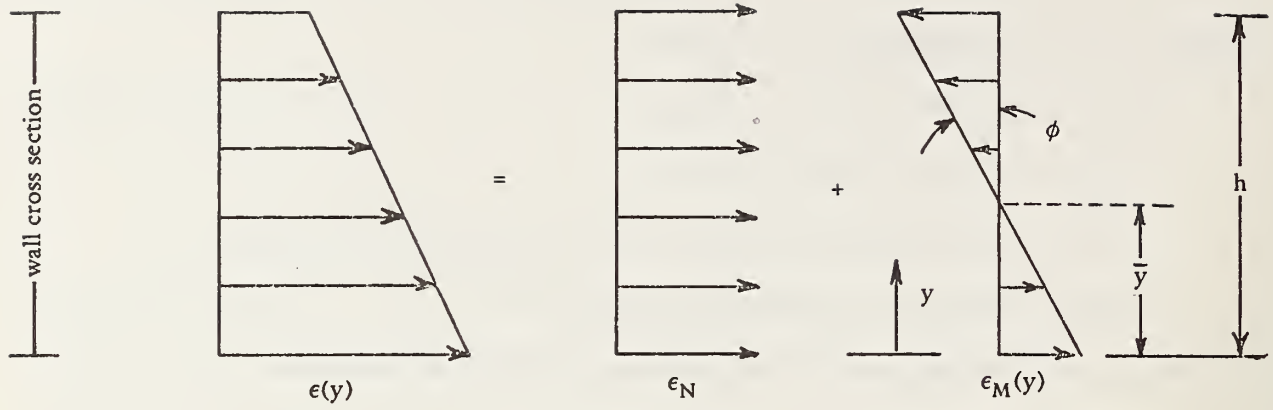


Figure 8-2. Linear strain components.

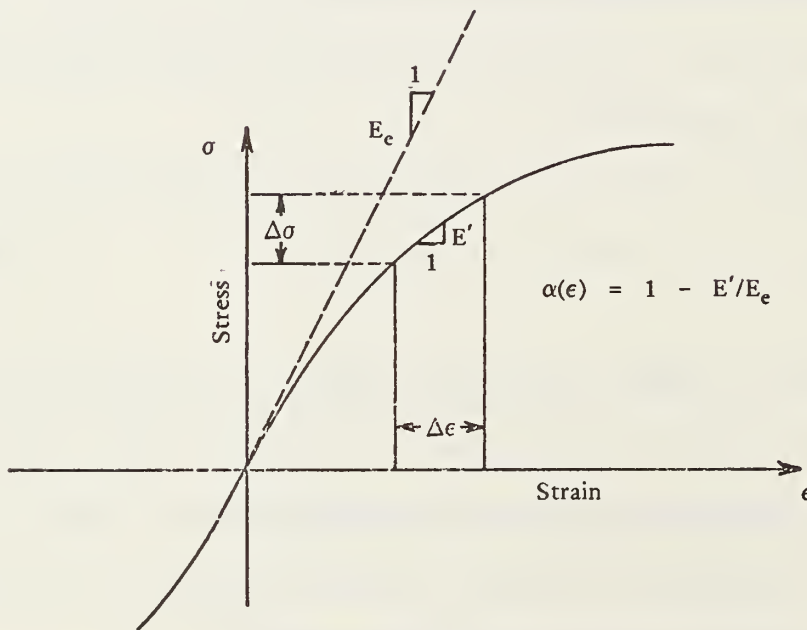


Figure 8-3. Incremental stress-strain law.



Equation 8-3 is a nonlinear, incremental, tangent modulus model for relating stress and strain increments. The tangent modulus function,  $E'(\epsilon)$ , is described in Equation 8-4 by a constant initial modulus  $E_e$  (note,  $E_e = E/(1 - \nu^2)$  for plane strain) and a dimensionless strain function,  $\alpha(\epsilon)$ , ranging in value from 0 to 1. If  $\alpha(\epsilon) = 0$ , a linear elastic law results, whereas, on the other extreme, if  $\alpha(\epsilon) = 1$ , a perfectly plastic relationship exists. The choice of  $E_e$  and  $\alpha(\epsilon)$  distinguishes one pipe model from another. The specific descriptions of  $E_e$  and  $\alpha(\epsilon)$  are given in later sections for each pipe-material; here the concern is with the general development.

By replacing  $\Delta\epsilon$  of Equation 8-3 with Equation 8-1 the circumferential stress increment can be defined as the summation of thrust and flexural contributions, i.e.,

$$\Delta\sigma = \Delta\sigma_N + \Delta\sigma_M \quad (8-4)$$

$$\Delta\sigma_N = E'(\epsilon) \Delta\epsilon_N \quad (8-5)$$

$$\Delta\sigma_M = E'(\epsilon) \Delta\epsilon_M \quad (8-6)$$

where  $\Delta\sigma_N$  = thrust stress increment

$\Delta\sigma_M$  = flexural stress increment

Since  $E'(\epsilon) = E_e [1 - \alpha(\epsilon)]$  and  $\Delta\epsilon_M = \Delta\phi(\bar{y} - y)$ , Equations 8-5 and 8-6 can be rewritten as:

$$\Delta\sigma_N = E_e [1 - \alpha(\epsilon)] \Delta\epsilon_N \quad (8-7)$$

$$\Delta\sigma_M = E_e [1 - \alpha(\epsilon)] \Delta\phi(\bar{y} - y) \quad (8-8)$$

By definition thrust and moment increments are given by:

$$\Delta N = \int_A \Delta\sigma \, dA = \int_A (\Delta\sigma_N + \Delta\sigma_M) dA \quad (8-9)$$

$$\Delta M = \int_A \Delta\sigma(\bar{y} - y) dA = \int_A (\Delta\sigma_N + \Delta\sigma_M)(\bar{y} - y) dA \quad (8-10)$$

Here  $\Delta N$  and  $\Delta M$  are the resultant thrust and moment increments after integrating the total stress,  $(\Delta\sigma_N + \Delta\sigma_M)$ , over the cross section. As yet the location of  $\bar{y}$  (bending axis) is still unspecified. To determine its location it is required that the thrust resultant,  $\Delta N$ , not contribute to the moment resultant,  $\Delta M$ , and vice-versa. In other words,  $\int_A \Delta\sigma_M dA$  and  $\int_A \Delta\sigma_N(\bar{y} - y) dA$  must equal zero. Upon replacing  $\Delta\sigma_M$  and  $\Delta\sigma_N$  with Equations 8-7 and 8-8 and noting  $\Delta\epsilon_N$  and  $\Delta\phi$  are constant over any cross section, both of the above requirements produce the same result for  $\bar{y}$ , namely:

$$\bar{y} = \frac{\int_A E_e [1 - \alpha(\epsilon)] y \, dA}{\int_A E_e [1 - \alpha(\epsilon)] \, dA} \quad (8-11)$$

If the material is homogeneous over the section, the elastic modulus,  $E_e$ , is constant and will cancel out of the above integration. For composite materials,  $E_e$  of the dominant material can be factored out of the integral, leaving dimensionless ratios in the integral for the remaining composite materials.

With the above understanding, Equations 8-9, 8-10 and 8-11 can be compactly expressed as:

$$\Delta N = \Delta \epsilon_N E_e A^* \quad (8-12)$$

$$\Delta M = \Delta \phi E_e I^* \quad (8-13)$$

$$\bar{y} = \int_A [1 - \alpha(\epsilon)] y \, dA / A^* \quad (8-14)$$

$$\text{where } A^* = \int_A [1 - \alpha(\epsilon)] \, dA \quad (8-15)$$

$$I^* = \int_A [1 - \alpha(\epsilon)] (\bar{y} - y)^2 \, dA \quad (8-16)$$

The above relationships for  $\Delta N$  and  $\Delta M$  have the same form as the familiar linear equations for thrust-extension and moment-curvature, where  $A^*$  and  $I^*$  represent the effective area and moment of inertia. Accordingly, a linear formulation can be adopted, providing the proper values of  $A^*$ ,  $\bar{y}$ , and  $I^*$  can be determined. Since these quantities are dependent upon the total strain during a given load step, an iterative technique is required.

The procedure adopted in CANDE is outlined below, wherein it is assumed the pipe is in equilibrium at step  $i$ , and one is preparing to add the load increment from  $i$  to  $i+1$ . Then for each discrete point (element) around the pipe, the procedure is:

1. Estimate  $A^*$ ,  $\bar{y}$ , and  $I^*$  based on the known strain distribution at load step  $i$ .

2. Apply load increment  $i$  to  $i+1$ , and obtain a trial solution for  $\Delta M$  and  $\Delta N$  (Solution Levels 1, 2, or 3).

3. Determine a new estimate of the strain distribution at load step  $i+1$  as follows:

$$\Delta \phi = \Delta M / E_e I^*$$

$$\Delta \epsilon_N = \Delta N / E_e A^*$$

$$\epsilon_{i+1} = \epsilon_i + \Delta\epsilon_N + \Delta\phi(\bar{y} - y)$$

4. Redetermine  $A^*$ ,  $\bar{y}$ , and  $I^*$  based on current strain distribution

$\epsilon_{i+1}$ , i.e.,

$$A^* = \int_A [1 - \alpha(\epsilon_{i+1})] dA$$

$$\bar{y} = \left\{ \int_A [1 - \alpha(\epsilon_{i+1})] y dA \right\} / A^*$$

$$I^* = \int_A [1 - \alpha(\epsilon_{i+1})] (\bar{y} - y)^2 dA$$

5. Check inner loop (Steps 3-5) convergence: If successive estimates of  $A^*$ ,  $\bar{y}$ , and/or  $I^*$  are sufficiently close, go to Step 6; otherwise, return to Step 3 for an improved estimate of strains.

6. Check outer loop (Steps 2-6) convergence: If successive values of  $A^*$ ,  $\bar{y}$ , and  $I^*$  used in Step 2 are sufficiently close, go to Step 7; otherwise, return to Step 2, and repeat load step to obtain new values of  $\Delta M$  and  $\Delta N$ .

7. Sum incremental responses to totals, advance the load step, and return to Step 1.

The heart of the above algorithm is the calculation  $A^*$ ,  $\bar{y}$ , and  $I^*$  in Step 4. This calculation is the distinguishing feature between pipe materials and will be discussed in the appropriate sections of this chapter.

During the solution phase, Step 2, the values of  $A^*$  and  $I^*$  are estimated at discrete points around the pipe periphery. For the case of the elasticity solution (Level 1), a smeared average of these values are used to obtain the responses  $\Delta M$ ,  $\Delta N$ , and displacements. Stresses and strains, however, are obtained by using the calculated  $A^*$  and  $I^*$  at the discrete points. Naturally, the finite element solution (Levels 2 and 3) does not suffer this inconsistency, since each element is assigned the corresponding value of  $I^*$  and  $A^*$ .

The above averaging process for the Level 1 treatment of pipe nonlinearities proves to be adequate for many situations; however, when bending strains are large (i.e., more than 50% of the section has yielded), the yield hinge theory correction provides a better Level 1 solution. (The yield hinge theory was discussed in Chapter 5 and developed in Appendix G. It is a correctional solution added to the elasticity solution to account for plastic hinging at the quarter points of the pipe.)

In the next section, the third operation in Figure 8-1 is discussed.

### 8.1.3 Pipe Evaluation

Once a converged solution is obtained, the pipe responses are



evaluated in terms of design criteria. This is a most significant operation, since design criteria presuppose the knowledge of what constitutes unacceptable responses of the pipe. As discussed in Chapter 3 the design criteria are for the most part based on commonly accepted measures of pipe failure.

The evaluation of pipe can be given in terms of safety factors (or safety ratios), defined as

$$SF_i = \frac{\text{measure causing failure (design criteria)}_i}{\text{observed measure (from CANDE)}_i} \quad (8-17)$$

where  $i = 1, 2, \dots$  number of design criteria. Hence, if  $SF_i \gg 1.0$  for all  $i$ , the pipe is safe for the anticipated loading.

In addition to safety factors, a pipe can also be evaluated by performance factors,  $PF_i$ . Performance factors are defined as the response ratio of a preselected standard norm to the corresponding actual value, i.e.,

$$PF_i = \frac{(\text{standard norm value})_i}{(\text{calculated value})_i} \quad (8-18)$$

where  $i = 1, 2, \dots$  number of performance factors.

Prime examples of performance factors are the handling requirements set down in Chapter 3. Other performance factors will be introduced for specific pipes later. Unlike the safety factors, performance factors

can be equal to 1.0 (and sometimes less than 1.0) without serious consequences.

If CANDE is operating in a design mode, then the last operation, Design Update, is undertaken; otherwise, the analysis is finished following the pipe evaluation.

#### 8.1.4 Design Update

The objective of design update is to size the wall dimensions so that the actual safety ratios,  $SF_i$ , are in agreement with the specified factors,  $\overline{SF}_i$ . This is accomplished by a trial and error process, wherein the first attempt is the minimum allowable wall dimensions based on handling or other minimum requirements. For subsequent attempts the wall dimensions are scaled up or down (but never less than the original minimum requirements) by the controlling ratio (or ratios):

$$R = \text{maximum of } (\overline{SF}_i / SF_i) \quad (8-19)$$

where  $i = 1, 2, \dots$  number design criteria.

The process is repeated until the ratio  $R$  is acceptably close to 1. Note that only the lowest  $SF_i$  will be in agreement with the corresponding  $\overline{SF}_i$ ; other  $SF_i$  will be on the conservative side. The above concepts will become clear by considering the specific design criteria for each pipe.

## 8.2 SPECIFIC DESIGN CRITERIA

### 8.2.1 Corrugated Steel

The design logic and pipe model for corrugated steel-pipe culverts are presented in a format paralleling Figure 8-1. The development is applicable to all standard wall corrugation and gage sizes. The shape and dimensions of the pipe are arbitrary; however, it is assumed the corrugation and gage size is constant around the periphery of the pipe.

8.2.1.1 Data Specifications. Prescribed parameters for the corrugated steel pipe model are listed below for reference; typical parametric values are noted in parentheses:

- D = diameter of pipe, or shape definition
- $E_1$  = Young's modulus ( $30 \times 10^6$  psi)
- $E_2$  = modulus in yield zone (0.0 psi)
- $\nu$  = Poisson's ratio (0.3)
- $\sigma_y$  = yield stress (33,000 psi)

In the analysis mode the following additional wall properties are defined:

A = area of wall section per unit length

I = moment of inertia per unit length

S = section modulus per unit length

Alternatively, in the design mode the additional parameters are:

$\overline{SF}_{\text{thrust}}$  = desired safety factor against wall yielding due  
to thrust stress (3.0)

$\overline{SF}_{\text{disp}}$  = desired safety factor against excessive deflection  
(4.0)

$\overline{SF}_{\text{buckling}}$  = desired safety factor against elastic buckling (2.0)

To complete the model description, the pipe behavior is specified as: elastic, or yield hinge, or bilinear stress-strain curve. Since most steel culverts exhibit yielding due to bending stresses, the bilinear stress-strain model provides the best representation of actual pipe behavior; however, for Level 1 solutions the yield hinge theory (Appendix G) may be preferable when excessive yielding occurs (i.e., more than 50% of the wall section).

8.2.1.2 Nonlinear Model. The stress-strain relationship for steel is approximated by a bilinear curve, as shown in Figure 8-4. Normally, the upper curve modulus,  $E_2$ , is zero for structural steel; however, for generality an arbitrary value will be assumed so that the following

developments will be applicable to a wide range of corrugated materials, including corrugated aluminum.

Within the framework of the general nonlinear model already presented, the objective is to determine the integral quantities  $A^*$ ,  $\bar{y}$ , and  $I^*$  given by Equations 8-14, 8-15, and 8-16. To accomplish this the function  $\alpha(\epsilon)$  must be defined in accordance with the bilinear assumption, and, secondly, the area of integration must be defined.

With regard to the latter, a manageable integration area can be obtained by approximating the actual corrugation geometry by a sawtooth pattern, such that the same area  $A$  and depth of section  $h$  is preserved, as shown in Figure 8-5. Then the differential area element becomes  $dA = A/h \, dy$ , so that the integral quantities can be written as:

$$A^* = \frac{A}{h} \int_0^h [1 - \alpha(\epsilon)] dy \quad (8-20)$$

$$\bar{y} = \frac{A}{hA^*} \int_0^h [1 - \alpha(\epsilon)] y \, dy \quad (8-21)$$

$$I^* = \frac{A}{h} \int_0^h [1 - \alpha(\epsilon)] (\bar{y} - y)^2 \, dy \quad (8-22)$$

The error of the sawtooth approximation can be assessed by considering the elastic case,  $\alpha(\epsilon) = 0$ . Integrating the above equations gives:

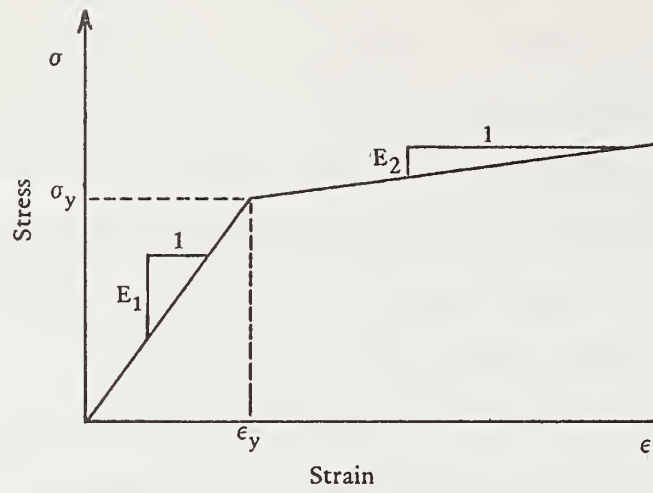


Figure 8-4. General bilinear stress-strain curve.

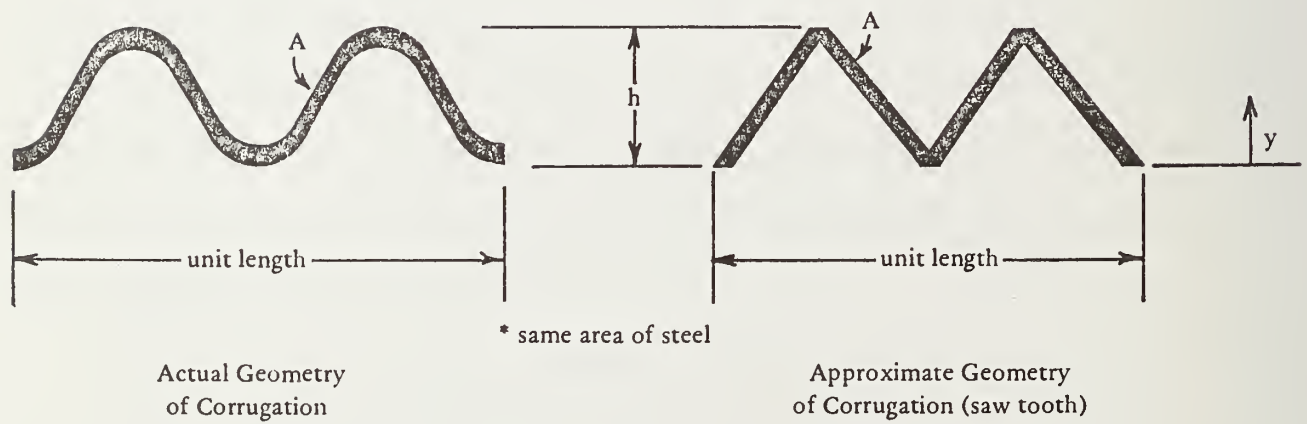


Figure 8-5. Geometry approximation of corrugated sections.



$A^* = A$ ,  $\bar{y} = h/2$ , and  $I^* = Ah^2/12$ . Both  $A^*$  and  $y$  are identically correct, while  $I^*$  is an approximation of  $I$ . By inspecting sectional properties of standard corrugation tables, it is observed that  $I^*$  is generally less than 10% lower than the reported value of  $I$ . Thus, the sawtooth approximation appears satisfactory, erring on the conservative side. Of course, if the steel is not yielding, the above integrations need not be undertaken, and the actual value of  $I$  can be used.

To prescribe  $\alpha(\epsilon)$  consistent with the bilinear approximation three distinct zones are identifiable as functions of the strain at the beginning and end of the load step. To clarify this, recall the incremental stress-strain relationship has the form  $\Delta\sigma = E_e [1 - \alpha(\epsilon)] \Delta\epsilon$ , where  $E_e = E_1/(1-\nu^2)$ , and consider three increments of loading at a particular point in the pipe wall such that the stress-strain path is as shown in Figure 8-6. In the first load increment the material remains elastic,  $\alpha(\epsilon) = 0$ , so that  $E_e [1 - \alpha(\epsilon)] = E_e$ . For the second increment there is a transition from the initial elastic modulus to the modulus of the upper curve. The effective modulus during this transition is  $E_e [1 - \alpha(\epsilon)] = E_e [\epsilon_1 - \epsilon_y + r(\epsilon_2 - \epsilon_y)]/\Delta\epsilon_2$ , where  $r = E_2/E_1$  (the modulus ratio) and  $\epsilon_y = \sigma_y/E_e$  (the yield strain). For the last increment, the response is entirely on the upper curve so that  $E_e [1 - \alpha(\epsilon)] = rE_e$ .

With the above insight,  $\alpha(\epsilon)$  can be specified for an arbitrary strain increment  $\epsilon_n$  to  $\epsilon_{n+1}$  as follows.

$$\text{elastic: } \alpha(\epsilon) = 0, \quad \text{if } |\epsilon_{n+1}| < \epsilon_y \text{ (load or unload) (8-23a)}$$

$$\text{transition: } \alpha(\epsilon) = \frac{1 - [\epsilon_y - |\epsilon_n| - r(|\epsilon_{n+1}| - \epsilon_y)]}{|\epsilon_{n+1} - \epsilon_n|} \quad \text{if } |\epsilon_{n+1}| > \epsilon_y > |\epsilon_n| \quad (8-23b)$$

$$\text{yield: } \alpha(\epsilon) = 1 - r, \quad \text{if } |\epsilon_{n+1}| > |\epsilon_n| > \epsilon_y \quad (8-23c)$$

The use of absolute values in the above equations implies the material behaves identically in compression and tension.

The foregoing has considered the stress-strain relationship at a point. To obtain  $A^*$ ,  $\bar{y}$ , and  $I^*$ , the stress-strain relationship must be defined over the cross-sectional area. Figure 8-7 illustrates typical strain distributions from load step  $n$  to  $n+1$ . Notice the depth of the section is divided into the regions: elastic, transition, and yield. The elastic region is that portion which remains totally elastic during the load step. The transition region is the zone that begins elastic and becomes plastic during the load step. And finally, the yield region signifies the zone where the material remains plastic.

Knowing the strain distribution at step  $n$  and having obtained a trial strain distribution at step  $n+1$ , it is a simple matter to locate the boundaries of the elastic, transition, and yield zones by straight-line equations. The function  $\alpha(\epsilon)$  can be specified within each zone in accordance with Equations 8-23a, b, and c. In the elastic and yield zones,  $\alpha(\epsilon)$  is constant with respect to  $y$ , whereas in the transition zone it is variable. To simplify the integrations of  $\alpha(\epsilon)$  in the transition zone, an average value is determined from Equation 8-23b, where

$\epsilon_n$  and  $\epsilon_{n+1}$  are the strains in the center of the transition zone.

This average value is assumed constant and is denoted as  $\bar{\alpha}$ .

With the above assumptions and using  $h_e$  and  $h_t$  (see Figure 8-7) as the distances to the top of the elastic and transition zones, the integrations for  $A^*$ ,  $\bar{y}$ , and  $I^*$  can be evaluated as:

$$A^* = \frac{A}{h} [h_e + (1 - \bar{\alpha})(h_t - h_e) + r(h - h_t)] \quad (8-24)$$

$$\bar{y} = \frac{A}{2hA^*} [h_e^2 + (1 - \bar{\alpha})(h_t^2 - h_e^2) + r(h^2 - h_t^2)] \quad (8-25)$$

$$I^* = \frac{A}{3h} \left\{ (h_e - \bar{y})^3 + \bar{y}^3 + (1 - \bar{\alpha})[(h_t - \bar{y})^3 - (h_e - \bar{y})^3] \right. \\ \left. + r[(h - \bar{y})^3 - (h_t - \bar{y})^3] \right\} \quad (8-26)$$

The above equations only apply to the case where the upper portion of the section is yielding. For the cases where the bottom is yielding or both top and bottom are yielding, the procedure is identical to that outlined above and simply requires more bookkeeping.

In summary, Equations 8-24, 8-25, and 8-26 are applicable to corrugated metal pipe and are representative of the calculations required in Step 4 of the general nonlinear algorithm presented previously. When a converged solution is obtained, the pipe is evaluated for safety and performance as discussed next.

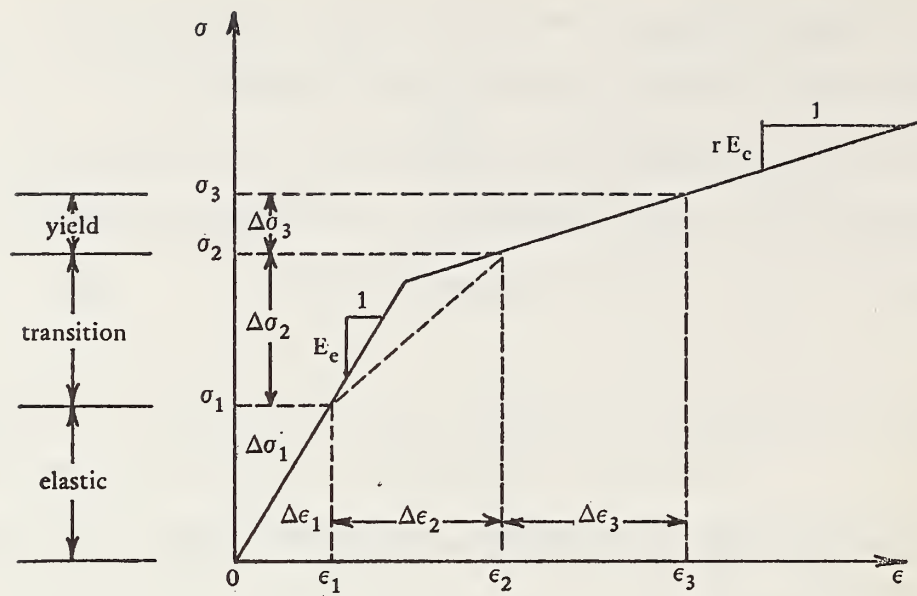


Figure 8-6. Incremental stress-strain path.

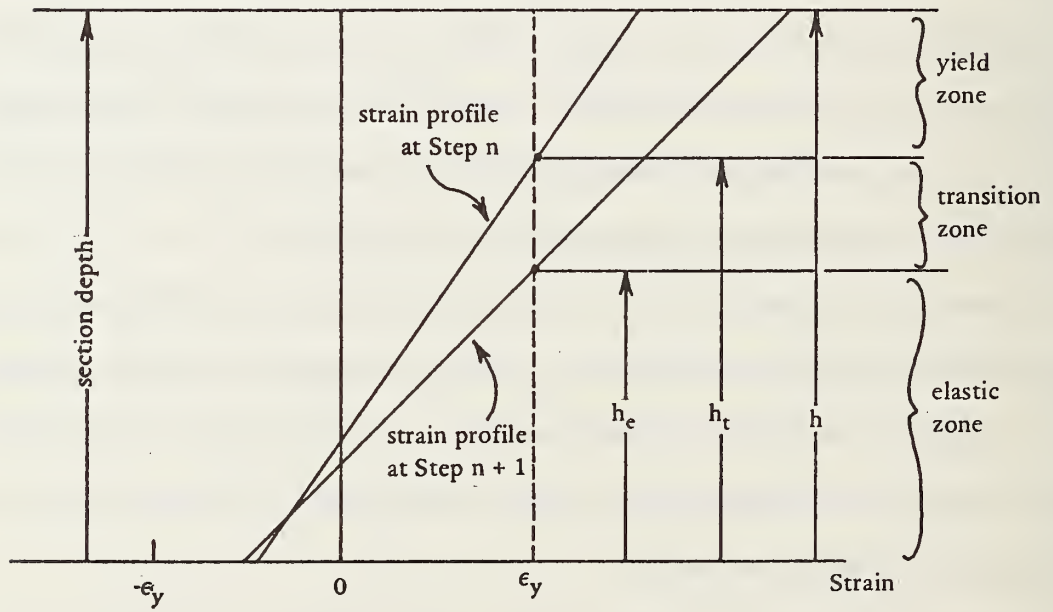


Figure 8-7. Typical strain profiles and zone descriptions.

8.2.1.3 Pipe Evaluation. Three potential modes of failure are considered for corrugated steel pipe: thrust stress above yielding, excessive deflection, and critical buckling pressure.

Thrust stress is the average stress over a particular cross section. If this value exceeds the yield strength or seam strength, the pipe is said to be unsafe. There is no concern, however, with regard to bending stresses. That is, plastic hinging of steel pipes is allowed in safe culvert designs, because steel exhibits a long ductile range and strain hardening phase prior to metal rupture.

The deflection limit considered tantamount to failure is 20% of the diameter (or average diameter). Finally, the critical buckling pressure for a pipe-soil system is predicted by the approximate buckling equation (presented in Chapter 5) as compared to the average soil pressure experienced by the pipe.

With the above in mind, the pipe can be evaluated with predicted safety factors as follows:

$$SF_{\text{thrust}} = \text{yield stress}/\text{maximum predicted thrust stress}$$

$$SF_{\text{disp}} = 20\% \text{ of diameter}/\text{maximum diameter change}$$

$$SF_{\text{buckling}} = \text{critical buckling pressure}/\text{average pipe pressure}$$

Clearly, the higher the safety factors the safer the pipe-soil system. A discussion of safety factors is given in Chapter 3.

In addition to safety factors, two performance factors also aid



in evaluating the pipe. The handling consideration (presented in Chapter 3) is one, and the maximum outer fiber strain is the other. The handling performance factor is a measure of the pipe's bending rigidity to withstand handling loads during transport, etc., while maximum strain is a measure of the severity of thrust and bending on the pipe from in-service conditions. These performance factors are defined as:

$$PF_{\text{handling}} = \text{flexibility factor}/(D^2/EI)$$

$$PF_{\text{strain}} = \text{yield strain}/\text{maximum strain}$$

For steel the flexibility factor, FF, is generally 0.0433 or FF = 0.02 for 6 x 2-inch corrugations (see Chapter 3). The  $PF_{\text{handling}}$  should be greater than 1.0 to conform to accepted practice. On the other hand,  $PF_{\text{strain}}$  can be substantially less than 1.0 with no serious consequences, i.e., acceptable plastic hinging.

In addition to safety and performance factors, the pipe can be evaluated by considering the structural responses around the pipe, including displacement, stresses, strains, moments, thrusts, and soil pressures on the pipe periphery.

8.2.1.4 Design Update. The objective of design update is to determine the most economical (least weight) corrugation and gage that will meet the specified safety factors,  $\overline{SF}_{\text{thrust}}$ ,  $\overline{SF}_{\text{disp}}$ , and  $\overline{SF}_{\text{buckling}}$ , for a specified pipe-soil system. To achieve this the geometric section



properties,  $I$  and  $A$ , are selectively varied until the specified safety factors are in agreement with the actual safety factors. During this process the section depth,  $h$ , is estimated from the sawtooth approximation,  $h = \sqrt{12 I/A}$ .

Specifically, the design procedure is initiated by computing a minimum required  $I$  to produce a handling performance factor of 1, and specifying a minimum  $A$  corresponding to 20-gage-thick metal. Next, an analytical solution (Levels 1, 2, or 3) is obtained for this initial guess, and the structural responses are evaluated for actual safety factors  $SF_{\text{thrust}}$ ,  $SF_{\text{disp}}$ , and  $SF_{\text{buckling}}$ . At this point, the section properties are scaled up or down (but never less than the original minimum) by the ratio of desired-to-actual safety factors as follows:

$$A_{\text{new}} = R_A A_{\text{old}}$$

$$I_{\text{new}} = R_I I_{\text{old}}$$

where  $R_A = \overline{SF}_{\text{thrust}} / SF_{\text{thrust}}$

$$R_I = \text{larger of } \begin{cases} \overline{SF}_{\text{disp}} / SF_{\text{disp}} \\ \overline{SF}_{\text{buckling}} / SF_{\text{buckling}} \end{cases}$$

Implicit in the above operations are the assumptions that thrust stress can be effectively reduced by increasing thrust area, and that displacements and/or buckling can be reduced by increasing moment

of inertia. These concepts are supported by analytical investigations and, indeed, seem intuitively obvious.

The  $I$  and  $A$  are repeatedly modified after each new solution until the ratios,  $R_A$  and  $R_I$ , are acceptably close to 1, say plus or minus five percent. When convergence has been achieved, the required section properties are printed out.

Next, standard steel corrugation tables are searched to find sections that most closely satisfy the design requirement. In particular, a list of satisfactory gages for the corrugation sizes  $1\text{-}1/2 \times 1/4$ ,  $2 \times 1/2$ ,  $2\text{-}2/3 \times 1/2$ ,  $3 \times 1$ , and  $6 \times 2$  inches is determined. From this list the corrugation with minimum  $A$ , and, hence, minimum weight, is selected for a final analysis.

Thereafter, the mode of the program is shifted from design to analysis, and the selected configuration is analyzed under the design loading schedule. Lastly, final evaluation of the selected pipe is printed out along with the pipe responses.

#### 8.2.2 Corrugated Aluminum

The following development is applicable to all standard aluminum wall corrugation and gage sizes. Shape and size of the pipe are arbitrary; however, it is assumed the corrugation and gage thickness is constant around the periphery of the pipe. The design logic and pipe modeling assumptions closely parallel the methodology for corrugated steel of

the previous section. As before, this presentation will follow the format of Figure 8-1; however, whenever pertinent, the reader will be referred to corrugated steel development for analytical details and elaboration.

8.2.2.1 Data Specifications. Input parameters for corrugated aluminum pipe are listed below for reference; typical parametric values are noted in parentheses:

- D = diameter of pipe, or shape definition
- $E_1$  = Young's modulus ( $10.2 \times 10^6$  psi)
- $E_2$  = modulus in yield zone ( $0.6 \times 10^6$  psi)
- $\nu$  = Poisson's ratio (0.33)
- $\sigma_y$  = yield stress (24,000 psi)
- $\epsilon_r$  = strain at ultimate rupture (0.05 in./in.)

For analysis problems, the following wall properties are also specified:

- A = area of wall section per unit length
- I = moment of inertia per unit length
- S = section modulus per unit length

Alternatively, for design problems the following safety factors are specified:

- $\overline{SF}_{\text{thrust}}$  = desired safety factor against wall yielding due to thrust stress (3.0)
- $\overline{SF}_{\text{disp}}$  = desired safety factor against excessive deflection (4.0)
- $\overline{SF}_{\text{buckling}}$  = desired safety factor against elastic buckling (2.0)
- $\overline{SF}_{\text{rupture}}$  = desired safety factor against outer fiber rupture (2.0)

The above parameter list is identical to that of corrugated steel, except this list includes an additional parameter,  $\epsilon_r$ , for rupture strain and a corresponding safety factor,  $\overline{SF}_{\text{rupture}}$ . The concept of rupture strain is the only difference between the treatment of corrugated steel and aluminum and will be discussed in subsequent sections.

8.2.2.2 Nonlinear Model. The assumed stress-strain relationship for aluminum is depicted in Figure 8-8, wherein a bilinear curve is defined by the moduli  $E_1$  and  $E_2$  and yield stress  $\sigma_y$ . Since this is identical to the parametric description of the steel relationship, the reader is referred to the development in Section 8.2.1.2 for the nonlinear model development. Of course, the actual values of  $E_1$ ,  $E_2$ , and  $\sigma_y$  differ between steel and aluminum, but the model development, assumptions, and solution methodology are identical.

8.2.2.3 Pipe Evaluation. Like corrugated steel, potential failure modes for corrugated aluminum include thrust stress above yield, excessive deflection, and elastic buckling. However, unlike steel pipes, unrestrained flexural strain (plastic hinging) is not allowed to become excessive in

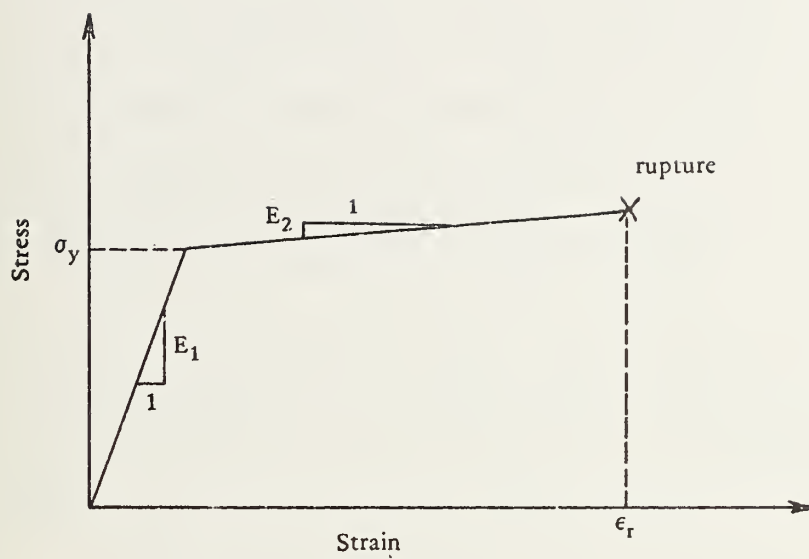


Figure 8-8. Idealized stress-strain relationship for aluminum.

aluminum pipe, because aluminum is less ductile, which allows metal rupture at a strain value,  $\epsilon_r$ , as indicated in Figure 8-8. Accordingly, excessive outer fiber strain of aluminum pipe is added to the list of potential failure modes.

From the above, aluminum pipe structural behavior can be evaluated with the following predicted safety factors:

$SF_{\text{thrust}} = \text{yield stress}/\text{maximum thrust stress}$

$SF_{\text{disp}} = 20\% \text{ of diameter}/\text{maximum diameter change}$

$SF_{\text{buckling}} = \text{critical buckling pressure}/\text{average pipe pressure}$

$SF_{\text{rupture}} = \text{ultimate rupture strain}/\text{maximum outer fiber strain}$

The only performance factor considered for aluminum, i.e., handling, is given by:

$$PF_{\text{handling}} = \text{flexibility factor}/(D^2/EI)$$

The concept of handling is exactly as described for steel (and in Chapter 3); however, the flexibility factor, FF, for aluminum is generally taken as  $FF = 0.09$ .

8.2.2.4 Design Update. The methodology for aluminum design is exactly as presented in Section 8.2.1.4 for corrugated steel with one notable exception. The scaling factor,  $R_I$ , which is used to scale the moment of inertia,  $I$ , up or down, is now defined as:



$$R_I = \text{larger of } \begin{cases} \overline{SF}_{\text{disp}} / SF_{\text{disp}} \\ \overline{SF}_{\text{buckling}} / SF_{\text{buckling}} \\ \overline{SF}_{\text{rupture}} / SF_{\text{rupture}} \end{cases}$$

Outside of the above relationship, the starting, iteration, and terminating procedures for finding the required wall properties, I and A, are as previously presented.

Once the required I and A are determined, a list of standard corrugation sizes is searched to determine (and print out) what gage thickness for each corrugation size is required. The corrugation sizes considered are: 2-2/3 x 1/2, 3 x 1, 6 x 1, 6 x 2, and 9 x 2-1/2 inches. From the list of candidate corrugation-gage sizes, the corrugation-gage with the least weight is selected for a final analysis. Thus, the final design includes an evaluation of pipe along with structural responses.

### 8.2.3 Reinforced Concrete

As before, Figure 8-1 depicts the general format for presenting pipe model and design logic for reinforced concrete pipe. The ensuing development is applicable to all standard wall designs and pipe shapes. The reinforcing steel cages may be circular, elliptical, or of arbitrary shapes; however, the concrete wall thickness is assumed to be prismatic around the periphery of the pipe.

8.2.3.1 Data Specification. Input parameters for reinforced concrete analysis and design methodology are listed below for reference (typical values are noted in parentheses):

$D$  = inside diameter of pipe, or shape definition  
 $f'_c$  = unconfined compressive strength of concrete (4,000 psi)  
 $E_1$  = Young's modulus for linear concrete ( $33 \gamma_w^{3/2} \sqrt{f'_c}$  psi)  
 $\nu_c$  = Poisson's ratio for concrete (0.17)  
 $\gamma_w$  = unit weight of concrete (150 pcf)  
 $f_y$  = yield stress of steel (40,000 psi)  
 $E_s$  = Young's modulus of steel ( $29 \times 10^6$  psi)  
 $\nu_s$  = Poisson's ratio of steel (0.3)  
 $\epsilon_t$  = concrete strain at tensile cracking ( $0^+$  in./in.)  
 $\epsilon_y$  = concrete strain at elastic limit ( $1/2 f'_c/E_1$ )  
 $\epsilon'_c$  = concrete strain at ultimate (0.002 in./in.)

In addition, the analysis mode requires the specification of:

$h$  = wall thickness of concrete  
 $A_{s_i}$  = steel area of inner cage per unit pipe length  
 $A_{s_o}$  = steel area of outer cage per unit pipe length  
 $c_i$  = concrete cover depth on inner cage (1.25 in.)  
 $c_o$  = concrete cover depth on outer cage (1.25 in.)

If desired, reinforcement properties can be specified at each point around the pipe.

In the design mode, the following safety and performance factors are specified in lieu of section properties.

$\overline{SF}_{\text{steel}}$  = desired safety factor against reinforcement yielding  
(2.0)

$\overline{SF}_{\text{crush}}$  = desired safety factor against concrete crushing (2.0)

$\overline{SF}_{\text{shear}}$  = desired safety factor against shear stress, i.e.,  
diagonal cracking (2.0)

$\overline{PF}_{\text{crack}}$  = desired "safety factor" (or performance factor) against  
0.01-inch flexural crack width (1.0)

There is no agreement among investigators with regard to the crack width criterion,  $\overline{PF}_{\text{crack}}$ . Ostensibly, the 0.01-inch crack width represents a threshold beyond which the reinforcing steel is subject to attack by corrosion. However, this is more conjecture than actual observation. In any event, until the crack width criterion is validated or rejected, it will be retained in CANDE as an option.

Another option in the design methodology is the treatment of the wall thickness. As one option, the wall can be considered of "fixed" thickness, in which case only the area of reinforcing steel is determined. Alternatively, the wall can be specified as "standard" or "arbitrary," wherein both wall thickness and reinforcing steel area are determined

in the design search. "Standard" implies the Standard Wall A, B, and C dimensions from ASTM C-76 are used for wall thickness designs, whereas "arbitrary" implies the wall thickness dimensions are varied continuously until the design requirements are satisfied.

For all of the above design options, the shape of the reinforcing steel cages can be considered as "circular" or "elliptical." Here "circular" implies the cages run parallel to the interior and exterior of the pipe wall regardless of the overall shape of the culvert. "Elliptical" implies the cage traverses the pipe wall from interior wall positions at the crown and invert to exterior wall positions at the springlines.

In the analysis mode any shape reinforcement cage can be specified.

8.2.3.2 Nonlinear Model. Unlike homogeneous ductile metals, reinforced concrete poses a difficult modeling problem, because (1) it is a composite of steel and concrete, and (2) concrete has minimal tensile strength and exhibits cracking. The most significant form of concrete cracking is the radial hairline cracking occurring at the inner and outer portions of the pipe wall in locations of high flexural stress. This form of cracking is expected and is the reason for incorporating steel reinforcement cages in the concrete wall. This, of course, is the same principle used in the design of reinforced concrete beams. However, unlike beams, concrete pipes invariably experience substantial compressive thrust stress that interacts with the flexural stresses and tends to limit the extent of cracking. In short, the interaction of thrust and moment

strongly influences the structural behavior of reinforced concrete with regard to both radial cracking and concrete crushing. Consequently, any mathematical model of reinforced concrete must give due regard to this interaction.

In addition to radial cracking, reinforced concrete pipe can also experience (1) diagonal cracking from excessive shear stress, and (2) separation of the tensile reinforcing steel from the concrete web because the curved steel cage tends to "straighten out" in regions of excessive flexural stress. This phenomenon is often referred to as "bowstringing." Both diagonal cracking and bowstringing are undesirable forms of cracking and represent potential modes of failure. Accordingly, proper designs should exclude or minimize these forms of cracking with either sufficient concrete tensile strength or secondary reinforcements, such as stirrups. These concepts are discussed in subsequent sections.

Based on the above discussion, the general nonlinear model developed in Section 8.1.2 is considered suitable for modeling concrete pipe behavior, wherein radial cracking, concrete yielding, and the interaction of thrust and moment are all considered.

To begin with, the assumed stress-strain relationship for concrete is shown in Figure 8-9, where cracking is noted by a small tensile strain limit,  $\epsilon_t$  (usually zero for design). In compression the concrete is approximated by a trilinear curve representing elastic, initial yielding, and crushing behavior. The zones on the trilinear curve are separated by specified strain values,  $\epsilon_t$ ,  $\epsilon_y$ ,  $\epsilon'_c$ , and  $\epsilon_u$ , representative of concrete behavior.



Figure 8-10 illustrates the idealization for the stress-strain model of reinforcing steel. The steel is assumed elastic-perfectly plastic and is identical in tension and compression.

The objective is to determine the integral quantities  $A^*$ ,  $\bar{y}$ , and  $I^*$  (Equations 8-14, 8-15, and 8-16) consistent with the assumed stress-strain relationships for steel and concrete. By assuming continuity of strain between concrete and steel, the integrations can be expressed as the sum of individual contributions from steel and concrete as shown below, where subscripts c and s denote concrete and steel:

$$A^* = A_c^* + A_s^* \quad (8-27)$$

$$\bar{y} = \bar{y}_c + \bar{y}_s \quad (8-28)$$

$$I^* = I_c^* + I_s^* \quad (8-29)$$

or in expanded form:

$$A^* = \int_{\text{concrete area}} [1 - \alpha_c(\epsilon)] dA + n \int_{\text{steel area}} [1 - \alpha_s(\epsilon)] dA \quad (8-30)$$

$$\bar{y} = \frac{\int_{\text{concrete area}} [1 - \alpha_c(\epsilon)] y dA + n \int_{\text{steel area}} [1 - \alpha_s(\epsilon)] y dA}{A^*} \quad (8-31)$$



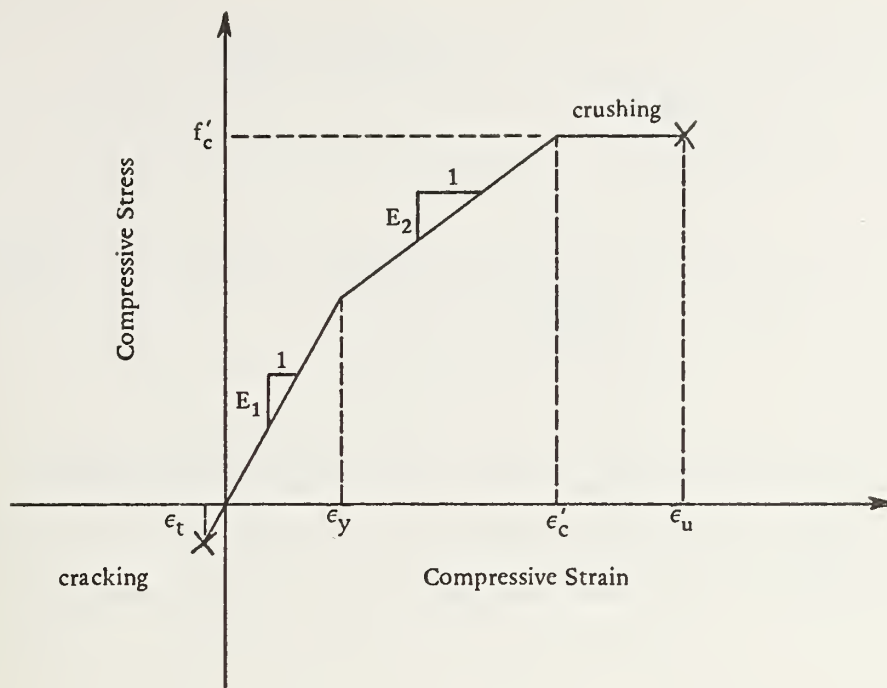


Figure 8-9. Idealized stress-strain model of concrete.

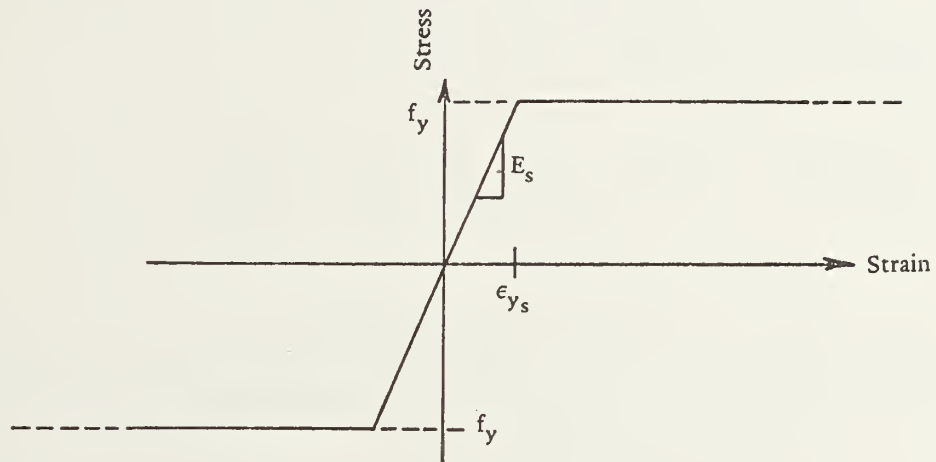


Figure 8-10. Idealized stress-strain model for reinforcing steel.

$$\begin{aligned}
I^* = & \int_{\substack{\text{concrete} \\ \text{area}}} [1 - \alpha_c(\epsilon)] (\bar{y} - y)^2 dA \\
& + n \int_{\substack{\text{steel} \\ \text{area}}} [1 - \alpha_s(\epsilon)] (\bar{y} - y)^2 dA \quad (8-32)
\end{aligned}$$

In the above  $n$  is the plane-strain modular ratio of steel-to-concrete, i.e.,  $n = [E_s / (1 - \nu_s^2)] \div [E_c / (1 - \nu_c^2)]$ , and  $\alpha_c(\epsilon)$  and  $\alpha_s(\epsilon)$  are the descriptions of the assumed stress-strain relationship for concrete and steel, respectively.

Recall that the general constitutive relationship has the incremental form  $\Delta\sigma = E_e [1 - \alpha(\epsilon)] \Delta\epsilon$ , so that  $\alpha(\epsilon)$  is dependent on the strain at the beginning and end of any load step. Specifically, the description for  $\alpha_s(\epsilon)$  consistent with Figure 8-10 and any arbitrary strain increment,  $\epsilon_n$  to  $\epsilon_{n+1}$ , is as follows:

$$\text{elastic: } \alpha_s(\epsilon) = 0, \quad \text{if } |\epsilon_{n+1}| < \epsilon_{y_s} \quad (8-33a)$$

$$\text{transition: } \alpha_s(\epsilon) = \frac{1 - (\epsilon_{y_s} - |\epsilon_n|)}{|\epsilon_{n+1} - \epsilon_n|} \quad \text{if } |\epsilon_{n+1}| > \epsilon_{y_s} > |\epsilon_n| \quad (8-33b)$$

$$\text{yield: } \alpha_s(\epsilon) = 1, \quad \text{if } |\epsilon_{n+1}| > |\epsilon_n| > \epsilon_{y_s} \quad (8-33c)$$

The absolute value signs indicate the material behaves identically in tension and compression. If the above expressions seem to be vague, the reader is referred back to the corrugated steel section for a more detailed discussion.

In a similar manner the description of  $\alpha_c(\epsilon)$  for the concrete model shown in Figure 8-9 is: (compression positive)

$$\text{cracking: } \alpha_c(\epsilon) = 1, \quad \text{if } \epsilon_{n+1} < \epsilon_t \quad (8-34a)$$

$$\text{elastic: } \alpha_c(\epsilon) = 0, \quad \text{if } \epsilon_t < \epsilon_{n+1} < \epsilon_y \quad (8-34b)$$

$$\begin{aligned} \text{transition: } \alpha_c(\epsilon) = 1 - \frac{[\epsilon_y - \epsilon_n - (E_2/E_1)(\epsilon_{n+1} - \epsilon_y)]}{\epsilon_{n+1} - \epsilon_n} \\ \text{if } \epsilon_t < \epsilon_n < \epsilon_y < \epsilon_{n+1} \quad (8-34c) \end{aligned}$$

$$\text{yield: } \alpha_c(\epsilon) = 1 - \frac{E_2}{E_1}, \quad \text{if } \epsilon_y < \epsilon_n < \epsilon_{n+1} < \epsilon'_c \quad (8-34d)$$

The description of  $\alpha_c(\epsilon)$  terminates at the initiation of the crushing zone, because the extent of interest in this study is the onset of crushing as opposed to the mechanism of crushing itself. A second notable point is the absence of any transition zone between cracking and elastic strains. This is not an oversight, but rather

a deliberate attempt to capture the abrupt nature of cracking. That is, cracking is a binary operation; either it does or does not occur. When it does occur, circumferential concrete stresses cannot be transmitted across the crack. Thus, regardless of the original strain state, when a strain increment produces a net tensile strain greater than the tensile limit, the effective modulus is zero or, equivalently,  $\alpha_c(\epsilon) = 1$ . Moreover, any previously existing stress must be removed and allowed to redistribute.

The above descriptions of  $\alpha_s(\epsilon)$  and  $\alpha_c(\epsilon)$  are valid for any particular point in the pipe wall; however, in order to integrate  $A^*$ ,  $\bar{y}$ , and  $I^*$  (Equations 8-30, 8-31, and 8-32), it is necessary to establish zone boundaries in the concrete wall for an arbitrary strain increment,  $\epsilon_n$  to  $\epsilon_{n+1}$ . To clarify this, consider the typical wall section shown in Figure 8-11 along with the strain profiles,  $\epsilon_n$  and  $\epsilon_{n+1}$ . Notice the concrete wall is divided into the zones: cracking, elastic, transition, and yielding. The cracked region is that portion of the wall, 0 to  $h_k$ , where the tensile strain profile,  $\epsilon_{n+1}$ , exceeds the tensile limit,  $\epsilon_t$ . The elastic region,  $h_k$  to  $h_e$ , is the material that remains elastic during the load step. The transition zone,  $h_e$  to  $h_t$ , is the material that was initially elastic, but entered the yield stage during the load step. And finally, the yield zone,  $h_t$  to  $h$ , is material that remained in the yield zone in a loading condition. Knowing the strain profiles  $\epsilon_n$  and  $\epsilon_{n+1}$ , it is a simple matter to compute the zone boundaries,  $h_k$ ,  $h_e$ , and  $h_t$ , by straight line equations.

The function  $\alpha_c(\epsilon)$  can now be specified for each zone in accordance with Equations 8-34a, b, c, and d. Note,  $\alpha_c(\epsilon)$  is a constant in each

zone except for the transition zone. To simplify the integration of  $\alpha_c(\epsilon)$  in the transition zone, an average value of  $\alpha_c(\epsilon)$  is determined by Equation 8-34c, where  $\epsilon_n$  and  $\epsilon_{n+1}$  are taken as the strains at the center of the transition zone. This average value is assumed constant and is denoted as  $\bar{\alpha}_c$ .

With the above assumptions the concrete portion of the integral quantities,  $A_c^*$ ,  $\bar{y}_c$ ,  $I_c^*$ , can be integrated to give:

$$A_c^* = (h_e - h_k) + (1 - \bar{\alpha}_c)(h_t - h_e) + \frac{E_2}{E_1}(h - h_t) \quad (8-35)$$

$$\bar{y}_c = \frac{1}{2A^*} \left[ (h_e^2 - h_k^2) + (1 - \bar{\alpha}_c)(h_t^2 - h_e^2) + \frac{E_2}{E_1}(h^2 - h_t^2) \right] \quad (8-36)$$

$$I_c^* = \frac{1}{3} \left\{ (h_e - \bar{y})^3 - (h_k - \bar{y})^3 + (1 - \bar{\alpha}_c)[(h_t - \bar{y})^3 - (h_e - \bar{y})^3] \right. \\ \left. + \frac{E_2}{E_1} [(h - \bar{y})^3 - (h_t - \bar{y})^3] \right\} \quad (8-37)$$

In a similar manner, the steel contributions,  $A_s^*$ ,  $\bar{y}_s$ , and  $I_s^*$ , can be determined. In this case, however, the integrations are trivial, because the steel reinforcement areas are assumed to be localized at discrete levels, as demonstrated in Figure 8-11. Accordingly,  $\alpha_s(\epsilon)$  can be evaluated directly at the steel levels for the current strain increment. Thus, the steel contributions are:

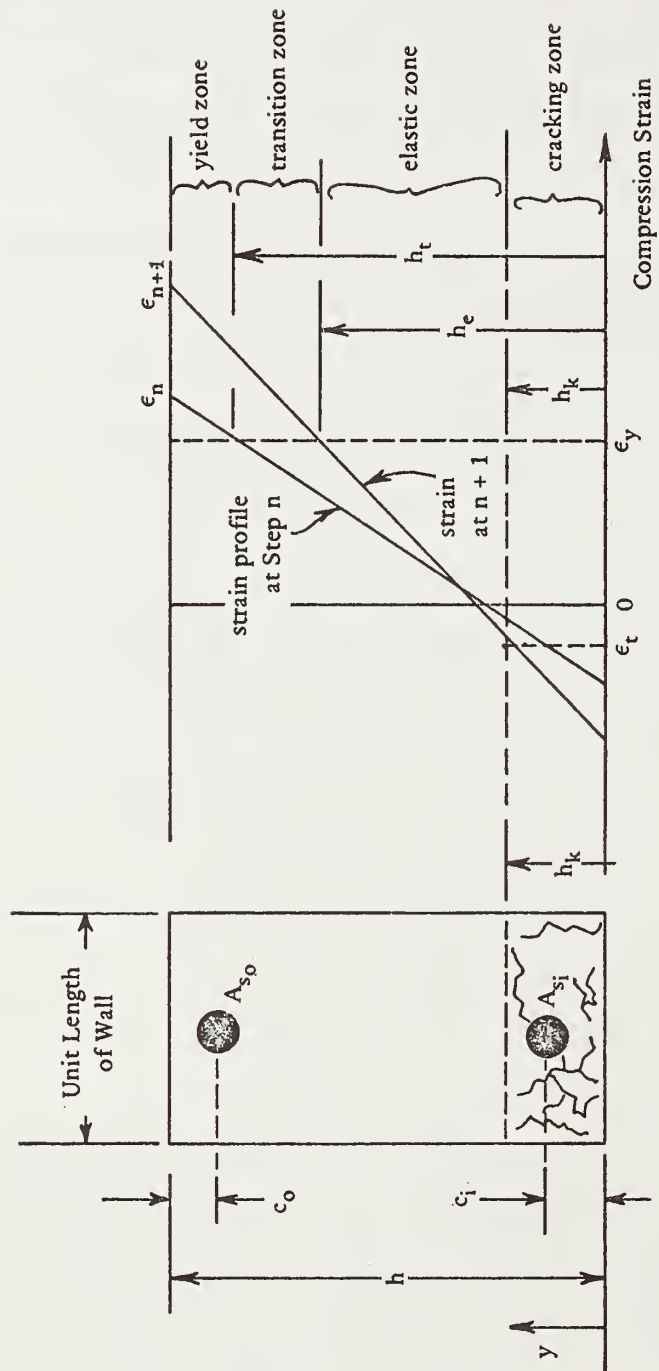


Figure 8-11. Typical strain profile and zone description for concrete.



$$A_s^* = n[(1 - \alpha_{s_i}) A_{s_i} + (1 - \alpha_{s_o}) A_{s_o}] \quad (8-38)$$

$$\bar{y}_s = \frac{n}{A^*} [(1 - \alpha_{s_i}) A_{s_i} c_i + (1 - \alpha_{s_o}) A_{s_o} (h - c_o)] \quad (8-39)$$

$$I_s^* = n[(1 - \alpha_{s_i}) A_{s_i} (\bar{y} - c_i)^2 + (1 - \alpha_{s_o}) A_{s_o} (\bar{y} - h + c_o)^2] \quad (8-40)$$

where  $n$  = steel-to-concrete modulus ratio

$A_{s_i}, A_{s_o}$  = steel area of inner and outer cages per unit length

$c_i, c_o$  = cover depths to steel centers of inner and outer cages

$\alpha_{s_i}, \alpha_{s_o}$  = current value of  $\alpha_s(\epsilon)$  at inner and outer cage locations

Combining Equations 8-35 through 8-40, the resulting values for  $A^*, \bar{y}$ , and  $I^*$  are obtained. These values are used in Step 4 of the general nonlinear algorithm previously presented. The process is repeated until a converged solution is found.

Upon convergence, the model provides the following information at each discrete section around the pipe: resultants for moment, thrust, and shear (i.e.,  $M, N$ , and  $V$ ) and, more importantly, stresses in the reinforcing steel, and stress distributions for circumferential and shear stress in the uncracked concrete wall.

The calculation of circumferential stresses is achieved quite simply from the circumferential strain profile obtained from the converged

solution together with the stress-strain relationships.

Shear stress distribution is a little more difficult and requires the use of equilibrium equations for curved members. Consider a small section of a curved member with radius of curvature  $R_o$  and angle variable  $\theta$ , as shown in Figure 8-12. The shear stress,  $v$ , at any depth,  $h_v$ , in the wall can be determined by equilibrium in the circumferential direction as:

$$v = \frac{1}{R_o} \int_{h_v}^h \frac{\partial \sigma}{\partial \theta} dy \quad (8-41)$$

Furthermore, equilibrium of the entire section requires that  $\partial M / \partial \theta = R_o V$  and  $\partial N / \partial \theta = V$ . Now, recalling Equations 8-12 and 8-13 together with the stress-strain relationships, circumferential stress can be expressed as  $\sigma = [1 - \alpha(\epsilon)][N/A^* + M(\bar{y} - y)/I^*]$ . Taking the partial derivative,  $\partial \sigma / \partial \theta$ , and assuming  $\alpha(\epsilon)$ ,  $A^*$ , and  $I^*$  are relatively constant over a short segment of pipe, one has upon substitution for  $\partial M / \partial \theta$  and  $\partial N / \partial \theta$ :  $\partial \sigma / \partial \theta = [1 - \alpha(\epsilon)]V[1/A^* + (\bar{y} - y)R_o/I^*]$ . Inserting this expression in Equation 8-41 and noting the term  $(1/R_o A^*) \int_{h_v}^h [1 - \alpha(\epsilon)] dy$  is small compared to  $(1/I^*) \int_{h_v}^h [1 - \alpha(\epsilon)](\bar{y} - y) dy$ , shear stress can be expressed in the familiar form:

$$v = V \frac{Q^*}{I^*} \quad (8-42)$$

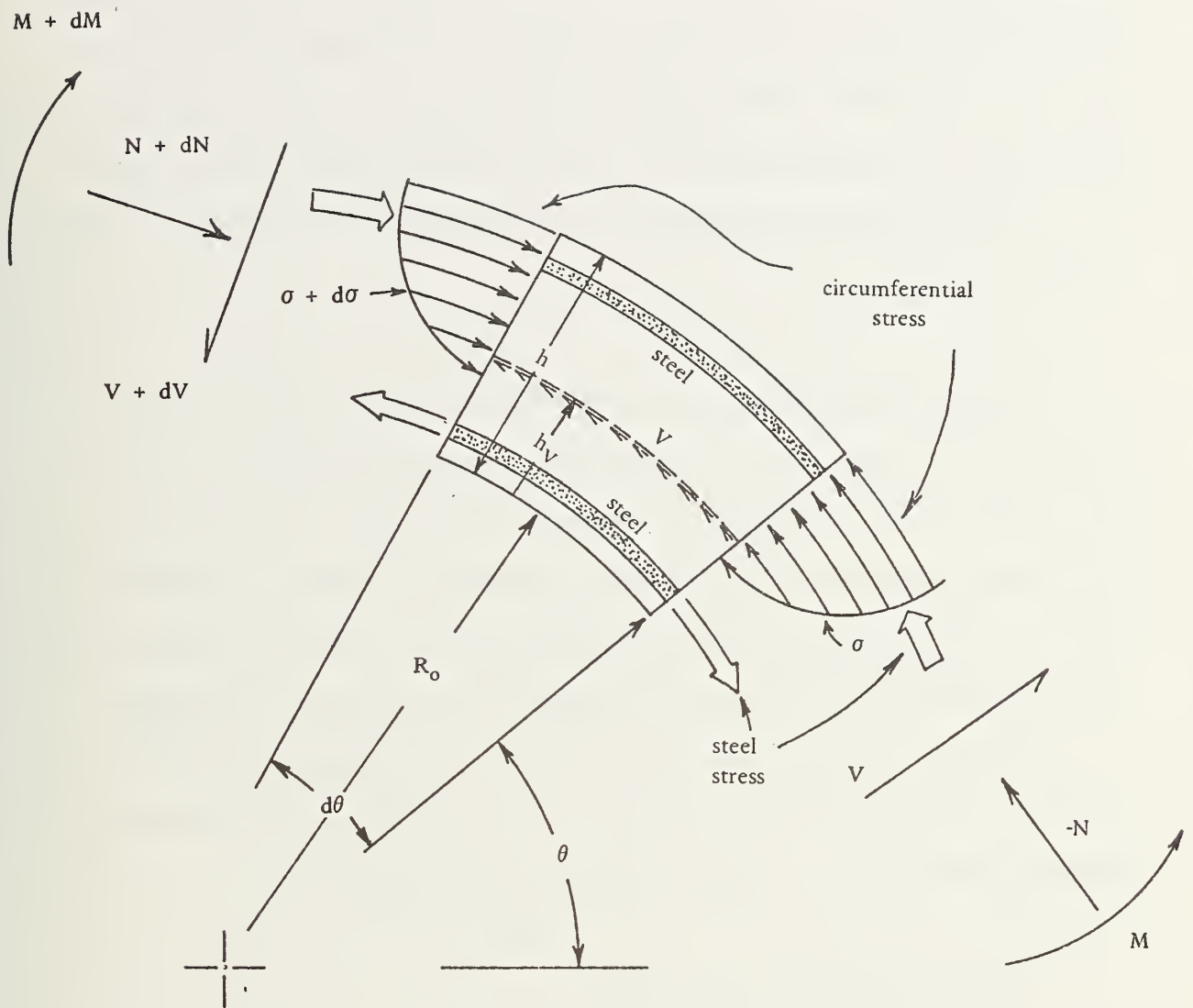


Figure 8-12. Stresses and resultants on a curved segment.

$$\text{where } Q^* = \int_{h_v}^h [1 - \alpha(\epsilon)] (\bar{y} - y) dy \quad (8-43)$$

Maximum shear stress occurs at the depth,  $h_v = \bar{y}$ ; when resolved to principal stresses, a tensile stress exists on an inclined plane and can cause diagonal cracking if it exceeds the tensile concrete strength.

Having determined stresses in concrete and steel the pipe is ready to be evaluated.

8.2.3.3 Pipe Evaluation. To evaluate the safety and performance of reinforced concrete pipe, the following modes of potential distress are considered: (1) yielding of reinforcement steel, (2) crushing of concrete, (3) shear stress producing diagonal cracking, (4) tolerable vertical deflection, (5) tolerable flexural crack widths (0.01 inch), and (6) separation of concrete and tension steel due to bowstringing.

The first four criteria can be evaluated directly by comparing predicted responses from the concrete pipe model with the following specified measures:

- (1) Yield stress of steel ( $f_y$ )
- (2) Compressive strength of concrete ( $f'_c$ )
- (3) Tensile strength of concrete ( $f'_t$ )
- (4) Allowable deflection limit ( $d_L$ )

In this study the tensile strength of concrete for shear resistance is taken as  $f'_t = 5 \sqrt{f'_c}$  (psi units), and the allowable deflection limit is taken from Lum [8-1] as  $d_L = D^2/(1200h)$ , where D is the pipe diameter and h is the wall thickness.

The last two criteria, crack width and bowstringing, require auxiliary developments for prediction as follows.

Crack width prediction is at best an art form and requires a semi-empirical approach. It should be noted that the concrete model offers a prediction for crack depth but not crack width. Actually, the model assumes an infinitude of infinitesimal crack widths in zones of tensile flexural stress. However, it is well known cracks occur in countable numbers at random locations within tensile zones. From experimental measurements it is observed crack width is strongly correlated with tensile steel stress and to a much lesser degree is influenced by steel area and spacing. The crack width predictions in this investigation are a modified form of the ACI recommendations for beams and plane-strain slabs [8-2] and is given as:

$$c_w = \frac{0.000135(f_s/1000.0 - 5.0)}{A_s^{1/3}} \quad (8-44)$$

where  $c_w$  = crack width (in.)

$f_s$  = tensile steel stress at crack location (psi)

$A_s$  = area of tensile steel (in.<sup>2</sup>/in.)

In a later chapter, it will be shown that crack width prediction based on Equation 8-44 correlates well with observed reinforced pipe performance.

Bowstringing is a complex phenomenon and deserves an intensive research effort to study the problem both experimentally and analytically. In this presentation, a simplified theory is offered which can be refined as more information becomes available.

Recall bowstringing occurs on the inner wall in zones of excessive tensile stress (e.g., invert and crown), wherein the curved reinforcement tends to straighten out by forcing the concrete to crack along the reinforcement. Referring to Figure 8-13a, consider a small segment of pipe in a zone of potential bowstringing (maximum moment, no shear) and assume the reinforcing steel is smeared over the length of the pipe as if it were a metal sheet rather than a set of discrete steel bars. Since only circumferential stresses exist in this zone (no shear), the reinforcing steel experiences a uniform circumferential stress,  $f_s$ , as shown in Figure 8-13a. In order for the reinforcement to retain its shape with radius of curvature  $R_o$ , a tensile radial stress,  $f_b$ , must exist over the interface of steel and concrete. Simple membrane equilibrium requires  $f_b$  to be:

$$f_b = \frac{f_s A_s}{R_o} \quad (8-45)$$



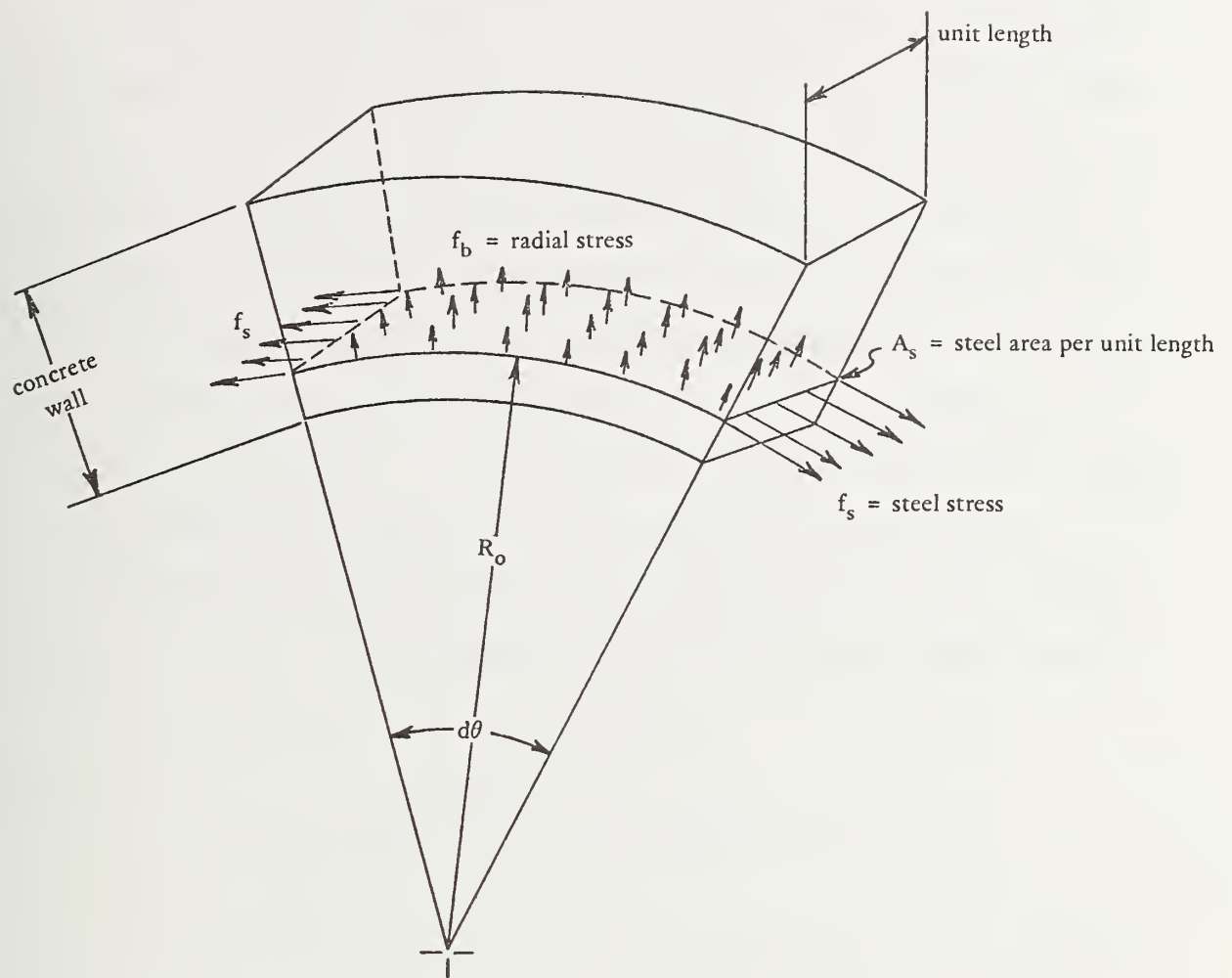


Figure 8-13a. Idealized stress distributions for continuous steel.

Therefore, to preclude circumferential cracking without radial reinforcement (stirrups) the concrete must be able to sustain the tensile stress  $f_b$ .

The shortcoming of the above development is the assumption that  $f_b$  is uniform over a unit length of pipe. In reality, the steel reinforcement is composed of discrete bars so that the actual stress distribution of  $f_b$  has a periodic wave form as suggested in Figure 8-13b, where the peak stress is given by a stress concentration factor,  $f_{b \max} = \beta f_b$ . The concentration factor  $\beta$  is primarily a function of bar spacing and requires further research for proper identification. However, if bar spacing conforms to ASTM-C76 requirements, engineering judgments suggest  $\beta = 10$  may be a conservative estimate.

Based on the above discussion, it is proposed to estimate the maximum tensile radial stress in the concrete immediately adjacent to the reinforcing steel by the relationship:

$$f_{b \max} = \beta \frac{f_s A_s}{R_o} \quad (8-46)$$

where  $A_s$  = inner cage steel area per unit length

$R_o$  = radius of steel curvature

$f_s$  = computed steel stress

$\beta$  = stress amplification factor (assumed to be 10)

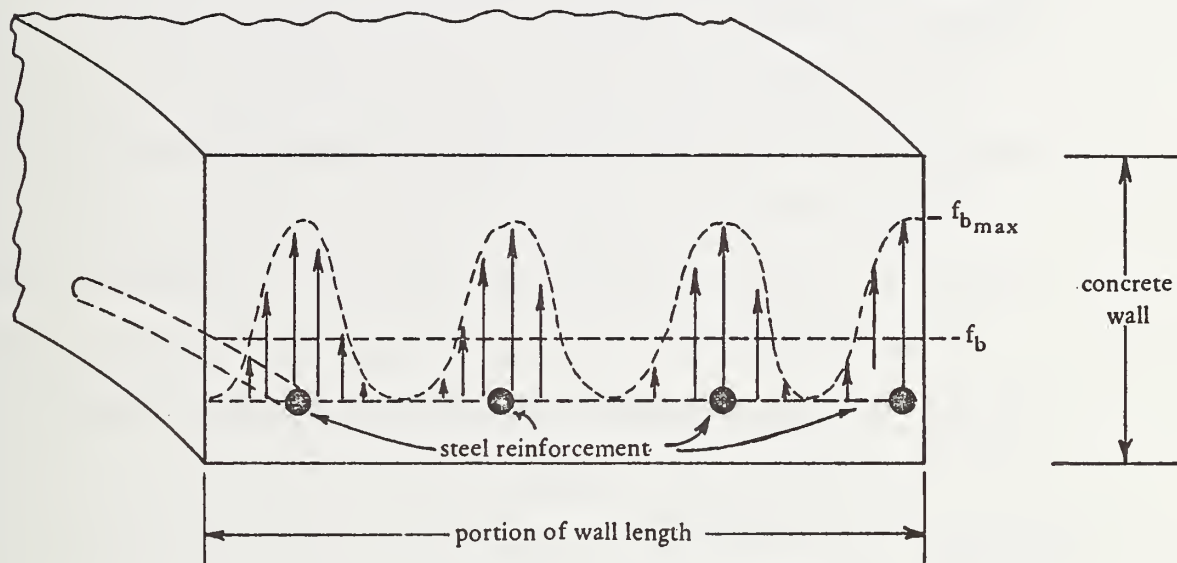


Figure 8-13b. Radial stress distribution for discrete steel reinforcement.

If  $f_{b_{max}}$  exceeds the tensile strength of concrete,  $f'_t$ , then circumferential cracking and bowstringing can occur, if no secondary reinforcement is used.

To summarize, the evaluation of reinforced concrete pipe can be assessed by the following safety and performance factors:

$SF_{steel}$  = steel yield stress/maximum predicted steel stress

$SF_{crush}$  = concrete compressive strength/maximum predicted concrete stress

$SF_{shear}$  = concrete tensile strength/maximum predicted shear stress

$PF_{disp}$  = allowable displacement limit/maximum predicted displacement

$PF_{crack}$  = allowable crack width (0.01 inch)/maximum predicted crack width

$PF_{bowstring}$  = concrete tensile strength/maximum predicted radial stress

Suggested values for desirable safety factors are given in Chapter

3. Note the bowstringing criterion is classed as a performance factor due to the conservatism in the prediction of  $f_{b_{max}}$  ( $\beta = 10$ ). For safe designs the above performance factors should not be less than 1.0.

8.2.3.4 Design Update. The objective of design update is to determine the required wall thickness (if applicable) and area of reinforcing

steel per unit length so that the specified safety factors,  $\overline{SF}_{\text{steel}}$ ,  $\overline{SF}_{\text{crush}}$ ,  $\overline{SF}_{\text{shear}}$  and  $\overline{PF}_{\text{crack}}$ , are satisfied. This is achieved by selectively modifying steel area and wall thickness (if applicable) in a sequence of analyses.

To start the design process, minimum acceptable values for wall thickness and steel area are determined and used for the first trial design. Minimum wall thickness is dependent on the design specification: arbitrary, standard, or fixed. For arbitrary wall designs the minimum wall thickness is taken as 5% of pipe diameter. For standard designs the ASTM C-76 wall A thickness corresponding to the pipe diameter is taken as minimum. Lastly, for fixed wall designs the specified wall thickness is minimum.

Minimum required steel area is determined from the maximum of three conditions: (1) steel area required to satisfy the deflection limit for handling loads developed in Chapter 3, (2) steel area required for temperature considerations, i.e.,  $A_s = 0.0014h$  (in.<sup>2</sup>/in.), where  $h$  is wall thickness, and (3) minimum practical reinforcement, i.e.,  $A_s = 0.0058$  in.<sup>2</sup>/in. Generally, condition (2) controls the establishment of minimum required steel area.

For doubly reinforced cages the steel area is proportioned to the inner and outer cages in a specified outer-to-inner ratio. In keeping with ASTM C-76 practices this ratio is normally taken as 0.75.

After an initial solution (Levels 1, 2, or 3) is determined for the minimum section, the pipe is evaluated for actual safety factors.

Next the steel area,  $A_s$ , and the concrete thickness,  $h$ , are scaled up or down (but never less than minimum requirements) by ratios of specified-to-actual safety factors as follows:

$$h_{\text{new}} = R_h h_{\text{old}}$$

$$A_{s_{\text{new}}} = R_s A_{s_{\text{old}}}$$

$$\text{where } R_h = \text{larger of } \begin{cases} \overline{SF}_{\text{crush}}/SF_{\text{crush}} \\ \overline{SF}_{\text{shear}}/SF_{\text{shear}} \end{cases}$$

$$R_s = \text{larger of } \begin{cases} \overline{SF}_{\text{steel}}/SF_{\text{steel}} \\ \overline{PF}_{\text{crack}}/PF_{\text{crack}} \end{cases}$$

For fixed wall designs,  $h_{(\text{new})}$  is held constant (i.e.,  $R_h = 1.0$ ). For standard wall designs,  $h_{(\text{new})}$  is used as the basis for finding the closest standard wall size on the conservative side. Lastly, arbitrary wall designs use  $h_{(\text{new})}$  directly.

For doubly reinforced cages the ratio  $R_s$  is applied to both inner and outer cages so that they remain in constant proportions during the design process.

The entire procedure is repeated until successive values of  $R_h$  and  $R_s$  are acceptably close to 1, say 5%.

Implied in the above design methodology is the concept that steel yielding and concrete flexural cracking are controlled by increasing



steel area, while concrete crushing and diagonal cracking are controlled by increasing concrete wall thickness. The rationale for this supposition is based largely on experimentation with different design strategies. The above technique provided the most efficient convergence scheme.

#### 8.2.4 Plastic Pipe

The generic name "plastic" pipe includes a broad range of pipe material and manufacturing processes; thus, the term is somewhat misleading for the restricted class of "plastic" pipes considered in this study. Here the term "plastic pipe" refers to a smooth-wall pipe with a homogeneous cross section and uniform thickness around the periphery of the pipe (however, the pipe may be an arbitrary size and shape). Furthermore, the "plastic" is assumed to be of a brittle nature and exhibit no time-dependent effects.

Although the above restrictions exclude many "plastic" pipe materials and cross sections, it is applicable to several commonly used plastic pipe products. Moreover, the following design/analysis methodology is also applicable to other brittle pipe materials, such as clay and cast iron which are linear up to brittle fracture.

The "plastic" pipe design/analysis methodology is presented in the format of Figure 8-1.

8.2.4.1 Data Specification. Prescribed parameters for plastic pipe are listed below for reference. Typical values for a fiberglass reinforced plastic pipe (Techite) are shown in parentheses:

$D$  = diameter of pipe, or shape definition  
 $E$  = Young's modulus ( $1.6 \times 10^6$  psi)  
 $\nu$  = Poisson's ratio (0.35)  
 $\sigma_u$  = ultimate stress at brittle failure (25,000 psi)

In the analysis mode, the wall thickness,  $h$ , is specified. Alternatively, in the design mode the desired safety factors are specified:

$\overline{SF}_{disp}$  = desired safety factor against 0.2D relative displacement (4.0)  
 $\overline{SF}_{stress}$  = desired safety factor against ultimate stress in outer fibers (3)  
 $\overline{SF}_{buckling}$  = desired safety factor against elastic buckling (3)

8.2.4.2 Stress-Strain Model. The material is assumed elastic up to brittle failure, as shown in Figure 8-14. Tension and compression are treated identically so that no material nonlinearity is considered. Accordingly,  $\alpha(\epsilon) = 0$ , and no iteration is required for analyzing the pipe.

8.2.4.3 Pipe Evaluation. The adequacy and performance of plastic pipe are evaluated by considering three potential modes of distress: (1) excessive deflection (20% of diameter considered failure), (2) outer fiber rupture due to stresses exceeding ultimate stress, and

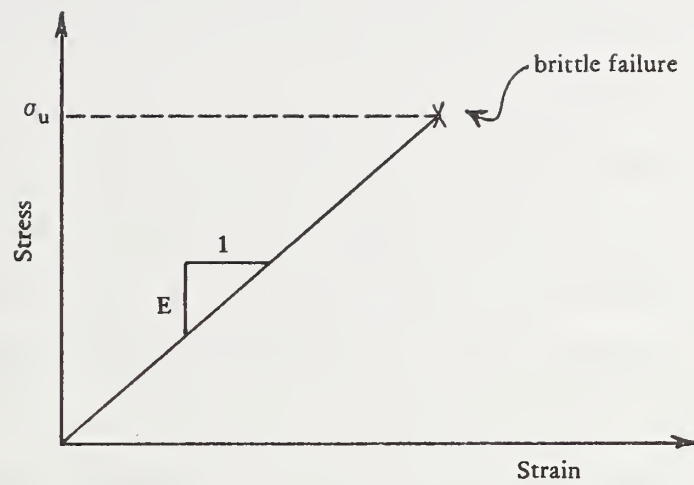


Figure 8-14. Assumed material behavior for plastic.

(3) elastic buckling due to the average soil pressure on the pipe exceeding the critical buckling pressure approximation presented in Chapter 5.

These measures of evaluation are quantified by the following actual safety factors:

$$SF_{\text{disp}} = 20\% \text{ diameter/maximum predicted displacement}$$

$$SF_{\text{stress}} = \text{ultimate stress/maximum predicted stress}$$

$$SF_{\text{buckling}} = \text{critical buckling pressure/average pressure on pipe}$$

Suggested safety factors are given in Chapter 3. It should be noted that smooth-wall pipes are much more susceptible to buckling than walls stiffened by corrugation. Thus, due to the approximate method for determining critical buckling pressure,  $SF_{\text{buckling}}$  should be higher for smooth walls than corrugated walls.

The handling criterion for plastic pipe developed in Chapter 3 also aids in evaluation of the pipe performance. Specifically the handling performance factor is:

$$PF_{\text{handling}} = \frac{FF}{D^2/(Eh^3/12)}$$

where FF is the flexibility factor for plastic (FF = 0.33 for fiberglass).

For proper design  $PF_{\text{handling}}$  should be greater than or equal to 1.

8.2.4.4 Design Update. The objective is to determine the required wall thickness,  $h$ , so that the specified safety factors,  $\overline{SF}_{disp}$ ,  $\overline{SF}_{stress}$ , and  $\overline{SF}_{buckling}$ , are satisfied.

The process is initiated by determining a minimum required thickness so that  $PF_{handling} = 1$ . With this trial section a solution is obtained (Levels 1, 2, or 3) and the thickness is scaled up or down (but never less than minimum) by the controlling ratio of specified-to-actual safety factors, i.e.:

$$h_{new} = R_h h_{old}$$

where

$$R_h = \text{larger of } \begin{cases} \overline{SF}_{disp}/SF_{disp} \\ \overline{SF}_{stress}/SF_{stress} \\ \overline{SF}_{buckling}/SF_{buckling} \end{cases}$$

The process is repeated until the value of  $R_h$  is acceptably close to 1.

It is evident from the above design logic that the strategy is to increase wall thickness whenever the controlling safety factor is too low. Generally, this method works quite well; however, situations have been observed where increased wall thickness resulted in increased bending stress. Upon further increases of wall thickness this trend reversed, and wall stresses were lessened. This example illustrates the nonlinear nature of design even for a linear system.

### 8.2.5 Basic Pipe

The basic pipe model is intended only for the analysis mode. No assumptions are made with regard to type of pipe; consequently, there is no evaluation in terms of safety or performance factors. The stress-strain law is assumed linear elastic. Unlike the previous pipe models, the basic model allows arbitrary specification of pipe properties around the pipe periphery so that built-up or tapered wall construction can be analyzed.

Specifically, the properties  $E$ ,  $I$ ,  $\nu$ , and  $A$  are defined at each point (element) around the pipe. Output includes distributions for displacement, moment, thrust, shear, and pressure on pipe. Naturally, nonprismatic wall properties are best treated by Solution Levels 2 or 3. Solution Level 1 will provide a smeared approximation.

Lastly, the basic model offers a convenient format for incorporating new pipe models into the CANDE program.



## A TECHNICAL SUMMARY AND RECOMMENDATIONS

The philosophy and analytical developments of the CANDE methodology have been presented in preceding chapters. Before discussing the results of CANDE, it is well to summarize the analytical features and limitations, and provide recommendations for modeling assumptions.

## 9.1 TECHNICAL SUMMARY

CANDE is provided with three levels of design or analysis capability to permit matching the degree of analytical power to the problem at hand. Level 1 is the enhanced elastic theory option; Level 2 features preprogrammed finite element meshes while Level 3 permits the full finite element versatility for plane-strain geometry.

Automated design logic and nonlinear stress-strain models are developed for standard culvert materials, including corrugated steel, corrugated aluminum, reinforced concrete (with flexural cracking), and plastic pipe. Other features are: incremental construction and loading, nonlinear soil models, and nonlinear interface models. Table 9-1 provides a box score summary of the analytical capabilities available with each solution level for both analysis and design.

Table 9-1. Analytical Capability of Each Solution Level

Solution Level	Pipe Models		Soil Models		Construction Model		Load Types		Interfaces*
	Pipe Shape	Pipe Material Character	Soil Material Zone	Soil Material Character	Symmetry Constraint	Construction Technique	Live Loads	Dead Loads	
Level 1 (Elasticity)	Round	Linear Plastic hinge Quazi-nonlinear	Homogeneous	Linear Overburden dependent	Quartic symmetric	Single lift (only)	Approximation	Overburden	A B
Level 2 (F. E. with auto mesh)	Round V. Ellipse H. Ellipse	Linear Plastic hinge Nonlinear	In-situ Backfill Bedding Packing	Linear Anisotropic Overburden dependent Nonlinear	Semi- symmetric Trench and embankment	Ten lifts (max), predefined lifts	Compaction on lifts Equipment on pipe Surface loads	Overburden Pipe weight	A B C D
Level 3 (Standard F. E.)	Round V. Ellipse H. Ellipse Pipe-arch Arbitrary	Linear Plastic hinge Nonlinear Composite	In-situ Backfill Bedding Packing Inclusions Other	Linear Anisotropic Overburden dependent Nonlinear	Arbitrary boundary conditions	Ten lifts (max) user defined lifts	Compaction on lifts Equipment on pipe Surface	Overburden Pipe weight	A B C D E

\*Pipe-soil interface symbol description:

- A = bonded
- B = frictionless slip
- C = Coulomb friction
- D = tensile separation and rebond
- E = applies to any interface.

## 9.2 LIMITATIONS AND DEFICIENCIES

Limitations inherent in the CANDE methodology mostly stem from the global assumptions and constraints in the theories employed. Other practical limitations are imposed by the lack of conformity between design specifications and actual field installations.

The more significant limitations and deficiencies include:

- (1) Small displacement theory is assumed, limiting the treatment of buckling for flexible culverts. The CANDE buckling prediction is external to the solution levels and is based on simplifying assumptions.
- (2) Time-dependent material responses are not directly considered. As an indirect approach, long-time material moduli can be used to assess long-term effects.
- (3) Out-of-plane effects, such as longitudinal bending, must be investigated external to the design methodology. See Appendix C for recommendations.

(4) Durability is not considered in the structural design.

See Appendix A for recommendations.

(5) Dynamic considerations, such as earthquakes and shock, are absent.

In spite of these limitations, CANDE provides a powerful design, analysis, and investigative tool for treating culverts.

### 9.3 MODELING RECOMMENDATIONS

CANDE invites a host of parametric design and analysis studies. Also, new design concepts can be tested in a feedback loop to optimize new configurations.

Applying CANDE to such studies often evokes modeling questions, such as: what solution level to use, what soil and/or pipe model is proper, and how are live loads handled. There is no clear cut answer to these questions because each problem is unique and modeling assumptions that are good for one case may not be good for another.

When several options are open, the best approach is to try them all. In some cases, the differences may be inconsequential, or, on the other hand, some modeling assumptions may substantially alter

the structural behavior. In all cases, useful information and insight are obtained that permit more intelligent advances in culvert design concepts.

#### 9.3.1 Selection of Solution Level

A good rule of thumb is to use the solution level that permits description of everything known about the pipe-soil system. For many common design problems Level 1 is often commensurate with system knowledge; however, for shallow burial depths, i.e., less than one radius of cover, Level 1 should not be used. Level 2 is intended to be the workhorse and is applicable to most design and analysis problems. When using Level 2 design operations, it is good practice to also obtain a Level 1 design for comparison and insight. Level 3 is a last resort because of the input tedium. However, for box, arch, or open culvert shapes, Level 3 is required unless Level 2 can be modified appropriately.

#### 9.3.2 Selection of Pipe and Soil Model

If the type of pipe is not pre-specified, a logical design approach is to obtain CANDE solutions for each pipe type and compare economics.

For corrugated metal pipes two nonlinear options are offered: (1) yield-hinge-theory, or (2) general nonlinear stress-strain model. The latter is recommended for general use; however, for Level 1 operations when nonlinear straining becomes excessive (say more than 50% of section yielded), the yield-hinge-theory is recommended.

A particularly sensitive reinforced concrete parameter is the concrete tensile strain limit,  $\epsilon_t$ . For design, a conservative recommendation is, to set  $\epsilon_t$  equal to 0.0, whereas for experimental verification,  $\epsilon_t$  should be the actual tensile strain limit.

Soil model forms are: (1) linear, (2) overburden dependent, and (3) fully nonlinear (Extended-Hardin). The last form only applies to Levels 2 and 3 and is not recommended for design operations, unless triaxial test data are available. In most design problems the overburden dependent model is adequate. Chapter 6 provides suggested Young's secant modulus values as a function of soil type, compaction, and overburden pressure.

### 9.3.3 Load Representation

Four fundamental load distributions for pipe-soil systems are: (1) uniform pressure load, (2) gravity load, (3) strip load, and (4) concentrated load. These distributions are illustrated in Figure 9-1.



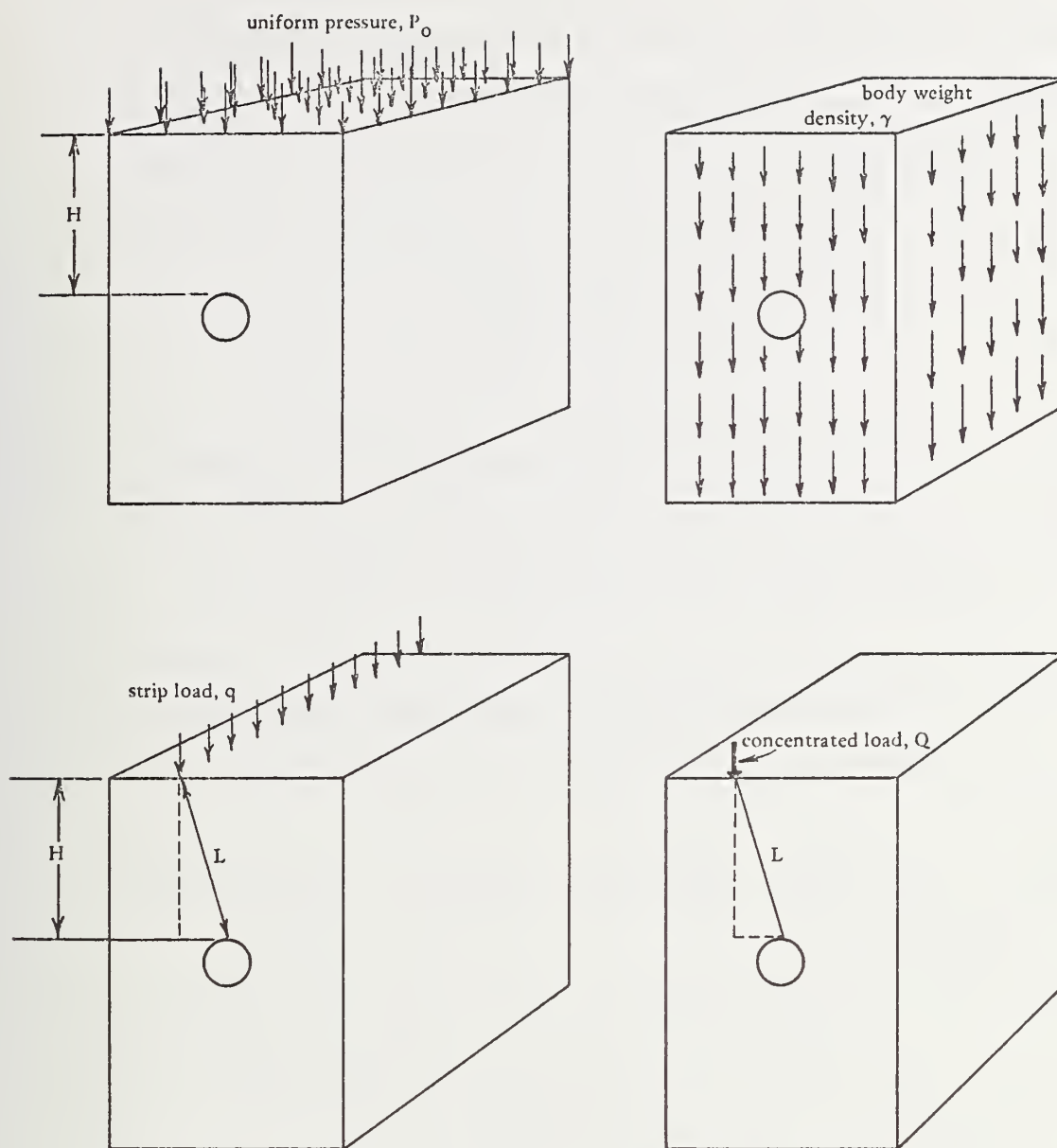


Figure 9-1. Four basic load conditions.

For deeply buried pipe (say  $H > 5$  feet), gravity stresses on the pipe generally overshadow the contributions from concentrated or strip loads. To assess the influence of a concentrated load,  $Q$ , consider the free-field (no pipe) vertical stress at the location of the pipe crown given by:

$$p_Q = \frac{3}{2} \frac{Q}{\pi} \left( \frac{H^3}{L^5} \right) \quad (9-1)$$

where  $p_Q$  = vertical stress due to concentrated load (Boussenesq)

$H$  = vertical height of cover to pipe crown

$L$  = distance from load to pipe crown

If  $p_Q$  is small (say 5% or less) compared to the free-field gravity stress,  $p_g = \gamma H$  (where  $\gamma$  is soil density), then concentrated loads may be ignored.

Similarly, for a strip load of line intensity  $q$ , the free-field vertical stress is:

$$p_q = \frac{2}{\pi} q \left( \frac{H^3}{L^4} \right) \quad (9-2)$$

Again if  $p_q$  is small compared to  $p_g$ , strip loads may be ignored.

In Level 1 operations, gravity loads are simulated by an equivalent overburden pressure,  $p_o$ , computed as  $p_o = \gamma H$ . This simulation is adequate provided  $H > R$  ( $H > 3R$  is preferable), where  $R$  is the pipe radius. Since Level 1 is formulated strictly for overburden pressure, concentrated and strip loads must be converted to "equivalent" overburden pressure by Equations 9-1 and 9-2 to give:

$$p_o = p_g + p_Q + p_q \quad (9-3)$$

where  $p_q$  and  $p_Q$  are the superposition of all live loads.

The finite element method, Levels 2 and 3, is capable of handling gravity, overburden pressure, and strip loads without additional approximation; however, a concentrated load must be expressed as an "equivalent" strip load by equating  $p_q = p_Q$  to give:

$$q_Q = \frac{3}{4} \left( \frac{Q}{L} \right) \quad (9-4)$$

where  $q_Q$  is the equivalent strip load for a concentrated load  $Q$  at a distance  $L$  from the pipe crown.

#### 9.4 EXTENSIONS OF CANDE

The modular architecture of CANDE permits new pipe types and soil models to be incorporated with relative ease. Eventually it may be practical to expand CANDE into a program for the complete system optimization of culverts, including hydraulics, durability, etc. However, this is not recommended until CANDE has been proven thoroughly in use.

CANDE is also useful for soil-structure problems other than culverts, such as underground storage facilities, retaining walls, open excavations, and tunnels. The interface model permits consideration of jointed rocks and other contact surfaces.

Future enhancements of CANDE should include large deformation theory for buckling and viscoplastic constitutive laws for soil representation.

## Chapter 10

### APPLICATIONS OF CANDE

In this chapter results from applying CANDE are presented in three parts: (1) parametric investigations, (2) design comparisons, and (3) experimental comparisons. The parametric studies demonstrate the influence of selected modeling assumptions on the structural behavior of the pipe-soil system. Design comparisons illustrate CANDE design solutions compared with traditional design solutions. Lastly, experimental comparisons illustrate the validity of CANDE.

For each of the above studies the intent is to lay ground work for future investigations. Accordingly, simple systems and basic modeling techniques are emphasized to illustrate the fundamentals of soil-structure interaction.

#### 10.1 PARAMETRIC STUDIES

The following parametric studies are presented in a progressive order beginning with a fundamental linear system composed of a smooth-wall pipe in a homogeneous medium. Subsequent variations of the system consider the influence of: pipe wall corrugations, pipe material nonlinearity, interface effects, bedding configurations, imperfect trench studies, and other modifications. The progression of studies begins with Level 1

solutions and advances to Levels 2 and 3 solutions. The interface study includes a comparison between the elasticity solution (Level 1) and the finite element solution (Levels 2 and 3).

#### 10.1.1 Basic Soil-Structure Interaction for Simple Systems

Consider the fundamental pipe-soil model defined by a round conduit of radius  $R$  with uniform wall thickness  $t$ , and a linear modulus,  $E_e$ , ( $E_e = E/(1-\nu^2)$ ). Further, the pipe is assumed deeply buried in a homogeneous elastic medium with a confined modulus,  $M_s$ , a Poisson's ratio,  $\nu_s$ , and an overburden pressure,  $p$ .

Utilizing the elasticity solution (Level 1), the responses of the above system can be presented in nondimensional graphs by appropriately combining the input parameters:  $R$ ,  $t$ ,  $E_e$ ,  $M_s$ ,  $\nu_s$ , and  $p$ , as indicated in Chapter 5.

Specifically, the radius-to-thickness ratio is investigated for the range  $5 < R/t < 500$ ; normalized responses for deflection, thrust, pressure, and moment at specified locations are shown in Figures 10-1 through 10-4. Within each figure, parametric families are plotted for soil-to-pipe moduli ratios of  $M_s/E_e = 0.1$ ,  $0.001$ , and  $0.00001$ . Each family is repeated for two soil Poisson's ratios;  $\nu_s = 0.333$  and  $0.444$ .

Listed below are some fundamental soil-structural interaction concepts illustrated by these graphs and other companion results. Note, moduli ratios for typical culvert installations are in the range  $0.001 < M_s/E_e < 0.00001$ .



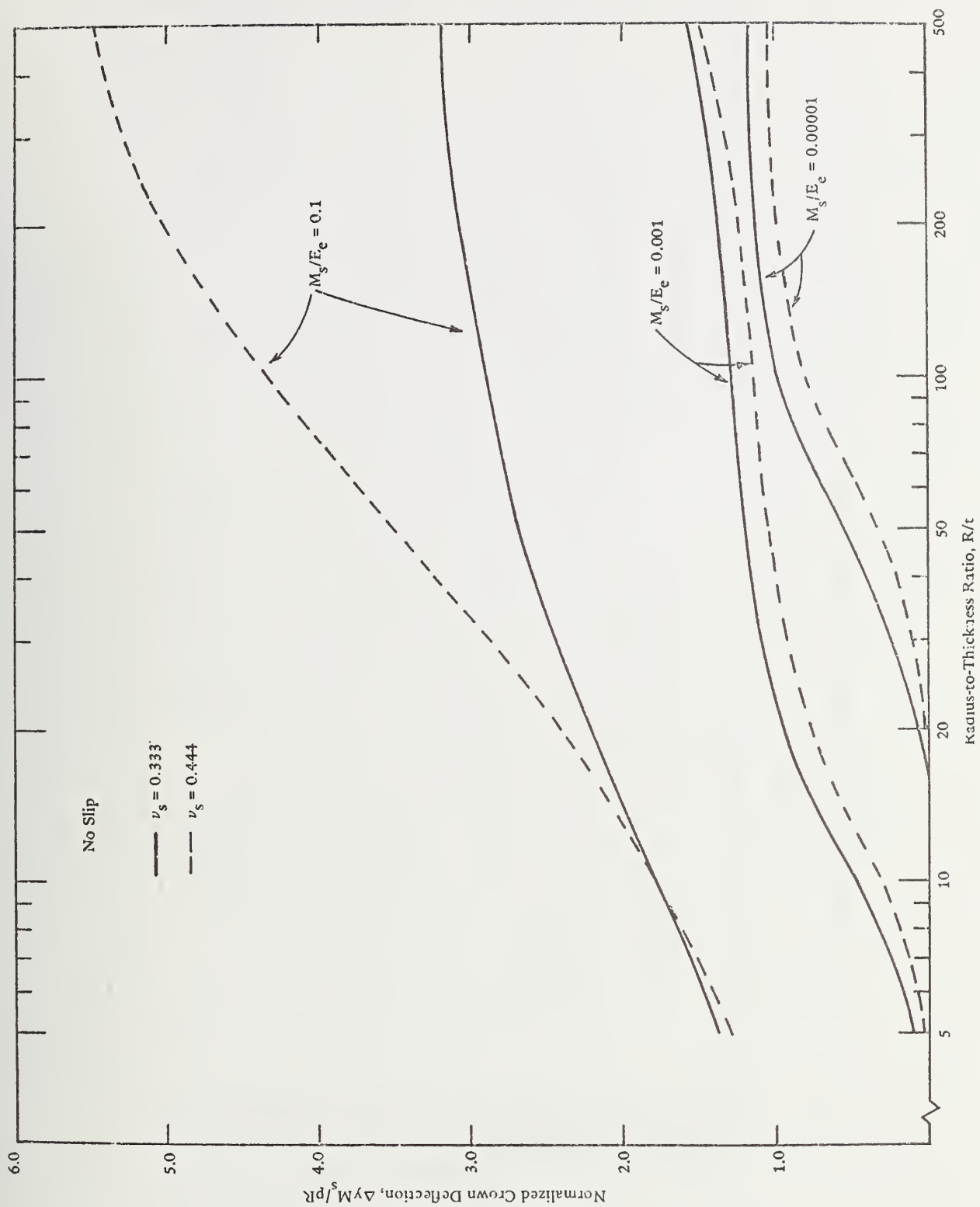


Figure 10-1. Normalized crown deflection versus radius-to-thickness ratio.

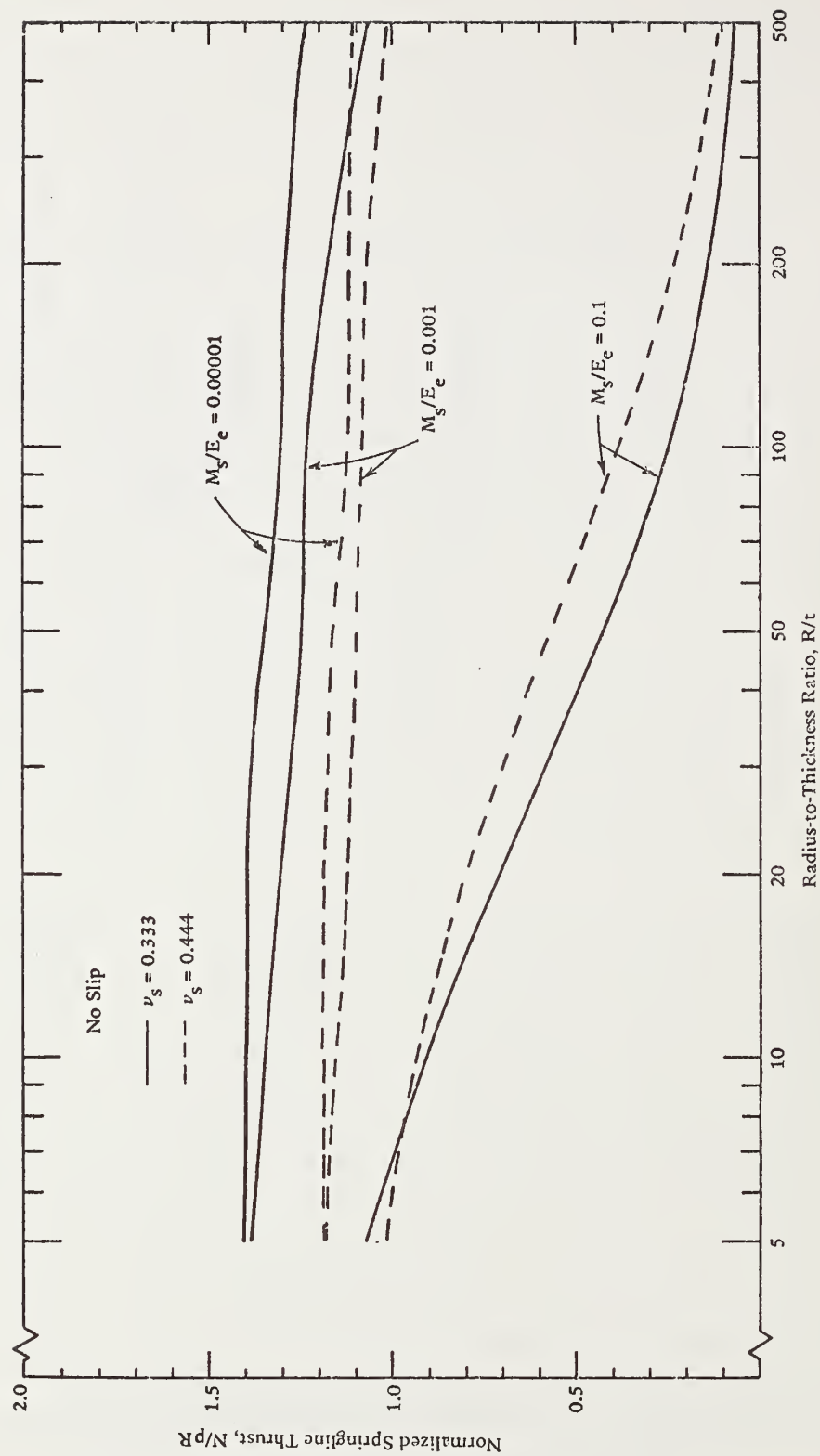


Figure 10-2. Normalized springline thrust versus radius-to-thickness ratio.

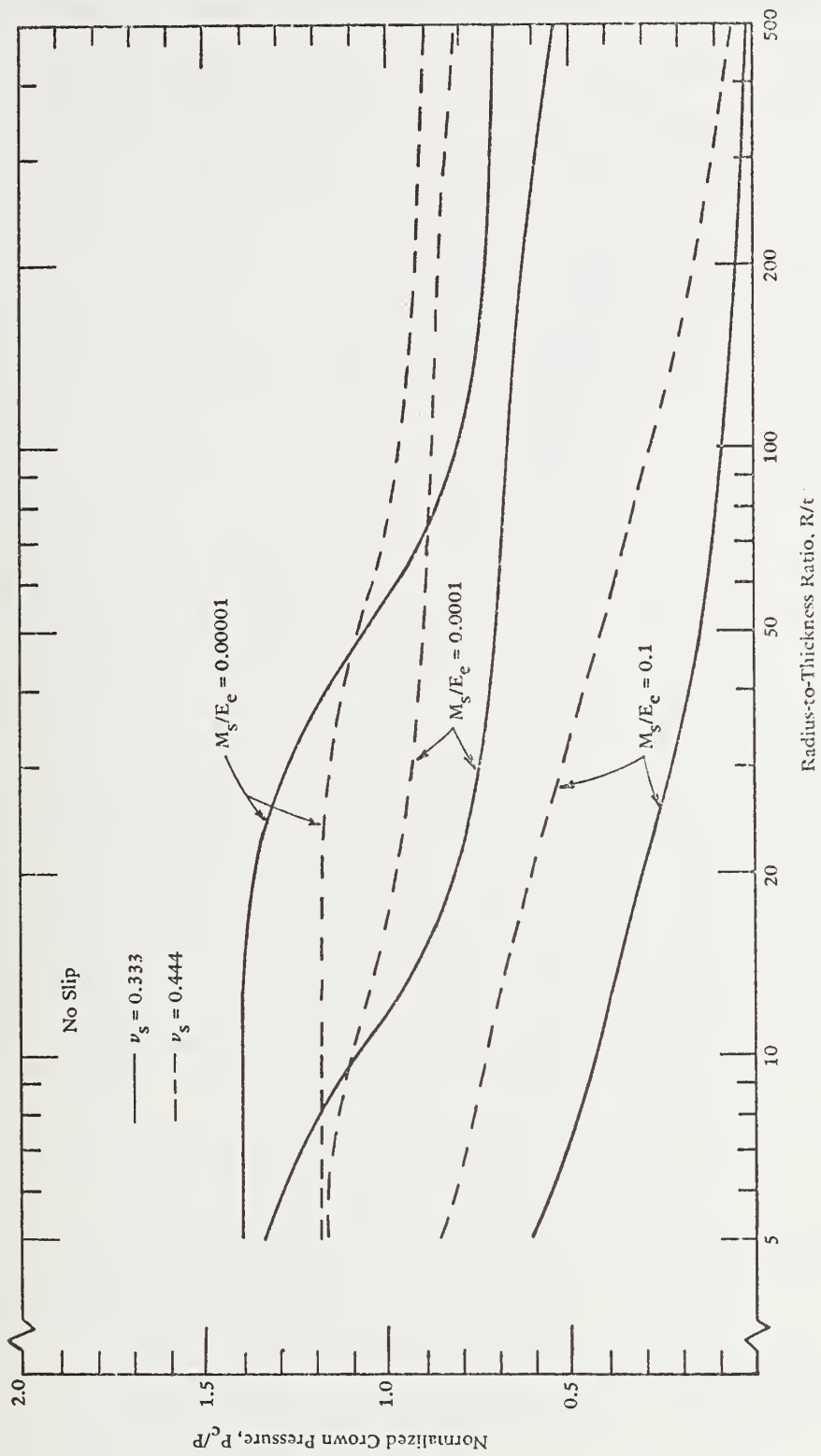


Figure 10-3. Normalized crown pressure versus radius-to-thickness ratio.

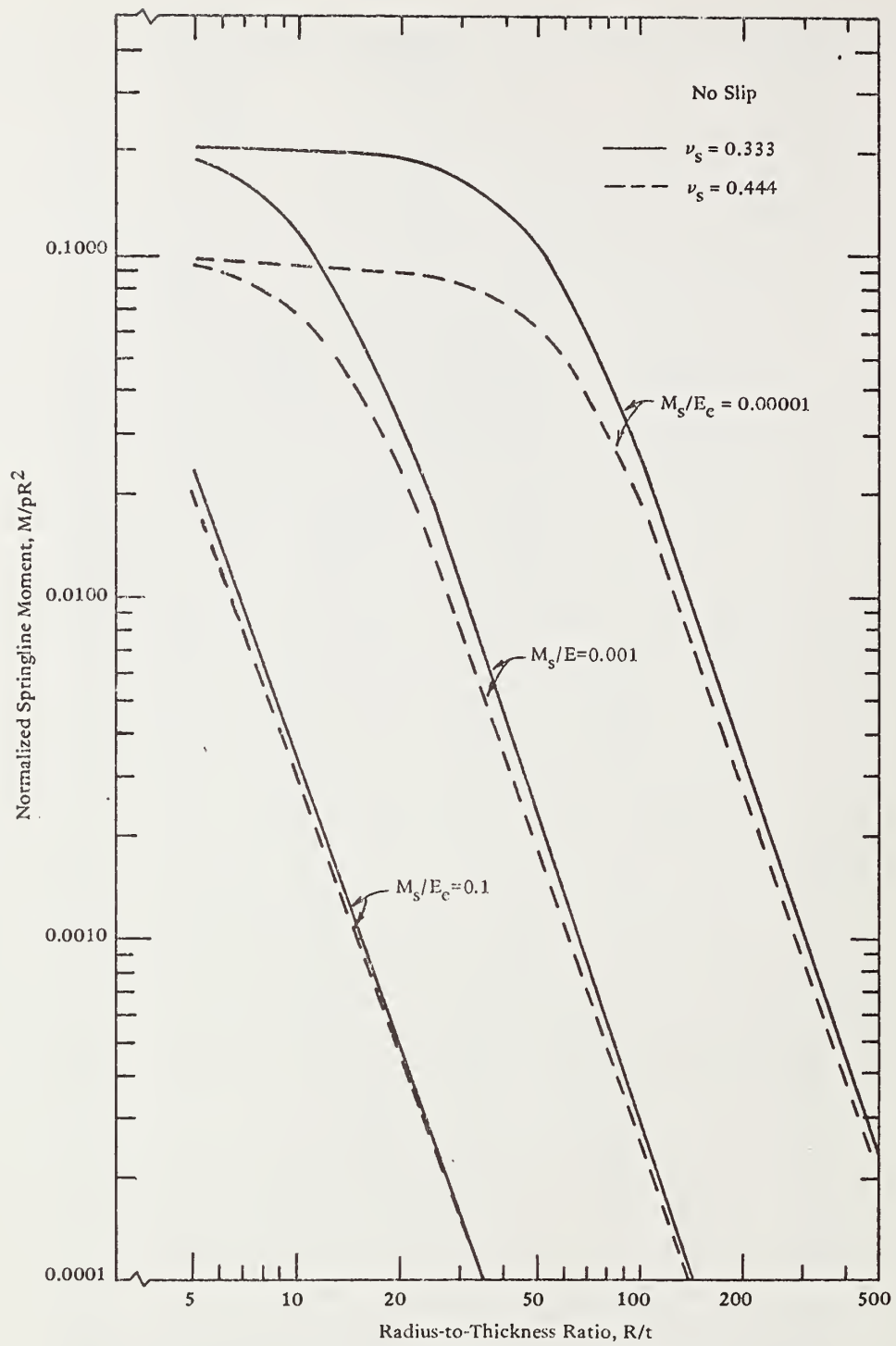


Figure 10-4. Normalized springline moment versus radius-to-thickness ratio.

(1) Maximum diametrical deflection occurs at the pipe crown relative to invert and is normalized in Figure 10-1 by dividing the crown deflection by the equivalent free-field deflection,  $pR/M_s$ . Accordingly, a value greater than 1.0 implies the pipe-soil system is "softer" in deflection resistance than a homogeneous soil field. Normalized deflections increase with  $R/t$  and  $M_s/E_e$ , indicating a relatively softer system. (Note, actual deflections, not normalized, decrease with increasing  $M_s$ ).

From companion results, horizontal elongation (not shown) is nearly equal to vertical flattening for values of  $M_s/E_L < 0.001$ ; however, for values of  $M_s/E_L > 0.1$ , horizontal elongation is substantially less and becomes negative (contraction) as  $R/t$  increases.

(2) Thrust is maximum at the springline and is normalized in Figure 10-2 by dividing it by the soil column weight,  $pR$ . The normalized springline thrust remains relatively constant between 1.1 and 1.4 for the typical range of moduli ratios,  $0.001 < M_s/E_L < 0.00001$ , indicating the pipe is drawing load in excess of the soil column weight (negative arching).

(3) The location of maximum radial pressure shifts from the crown to the springline as  $R/t$  increases. Figure 10-3 illustrates that normalized crown pressure decreases with increasing  $R/t$  and  $M_s/E_e$ . Normalized values less than 1.0 imply the crown pressure is less than the free-field pressure.

The graphs for  $M_s/E_e = 0.001$  in Figures 10-2 and 10-3 illustrate a common pitfall in interpreting experimental observations. To wit, an observed normalized crown pressure less than 1.0 does not automatically imply a corresponding normalized springline thrust less than 1.0. On the contrary, normalized thrust typically remains above 1.0, even though the normalized crown pressure may be as low as 0.5. This apparent anomaly is due to the distribution of radial pressure, which increases from the crown to the springline, and to the clockwise shear drag of the soil on the pipe shoulder.

(4) Moments are maximum at the springline and are normalized in Figure 10-4 by the quantity  $pR^2$ . It is observed that normalized moments decrease several orders of magnitude with increasing  $R/t$  and  $M_s/E_e$ .

The moment distributions are characterized by an inflection point approximately midway between the springline and crown. The crown moment is nearly equal in magnitude, but opposite in sign, to the springline moment.

(5) Overall it is observed that increases in the soil modulus,  $M_s$ , decrease the peak values of deflection and moment in the pipe as do increases in Poisson's ratio,  $\nu_s$ , provided  $M_s/E_e < 0.001$ . Increases in soil modulus do not appreciably reduce thrust unless  $M_s/E_e > 0.001$ .



### 10.1.2 Effects of Wall Corrugations

For the case of the smooth-wall pipe just considered, the pipe wall area per unit length,  $A$ , and the moment of inertia per unit length,  $I$ , were dependent on the wall thickness (i.e.,  $A = t$  and  $I = t^3/12$ ). However, for corrugated pipe walls,  $A$  and  $I$  represent independent quantities controlled by the pitch, depth, and gage of the corrugation. Accordingly, it is of practical interest to independently vary  $A$  and  $I$  and ascertain their influence on the structural responses.

To this end, a reference pipe-soil system is defined in the insert of Figure 10-5 that has a section area  $A_R = 0.1 \text{ in}^2/\text{in}$  and a moment of inertia  $I_R = 0.01 \text{ in}^4/\text{in}$ , which represent average values of standardly manufactured corrugation sizes. Manufactured wall areas typically range from  $1/5 A_R$  to  $5 A_R$ , while moments of inertia typically range from  $1/10 I_R$  to  $10 I_R$ .

Figure 10-5 shows the vertical diametrical deflection as a function of  $I$  for three families of  $A$ . In a similar manner, Figure 10-6 illustrates the springline thrust stress (i.e., thrust/ $A$ ) and bending stress (moment/ $S$ ), where the section modulus  $S$  is based on the sawtooth approximation (Chapter 8) given by  $S = \sqrt{AI/3}$ .

Upon inspecting Figures 10-5 and 10-6, the following observations are noted over the range of  $I$  and  $A$  considered.

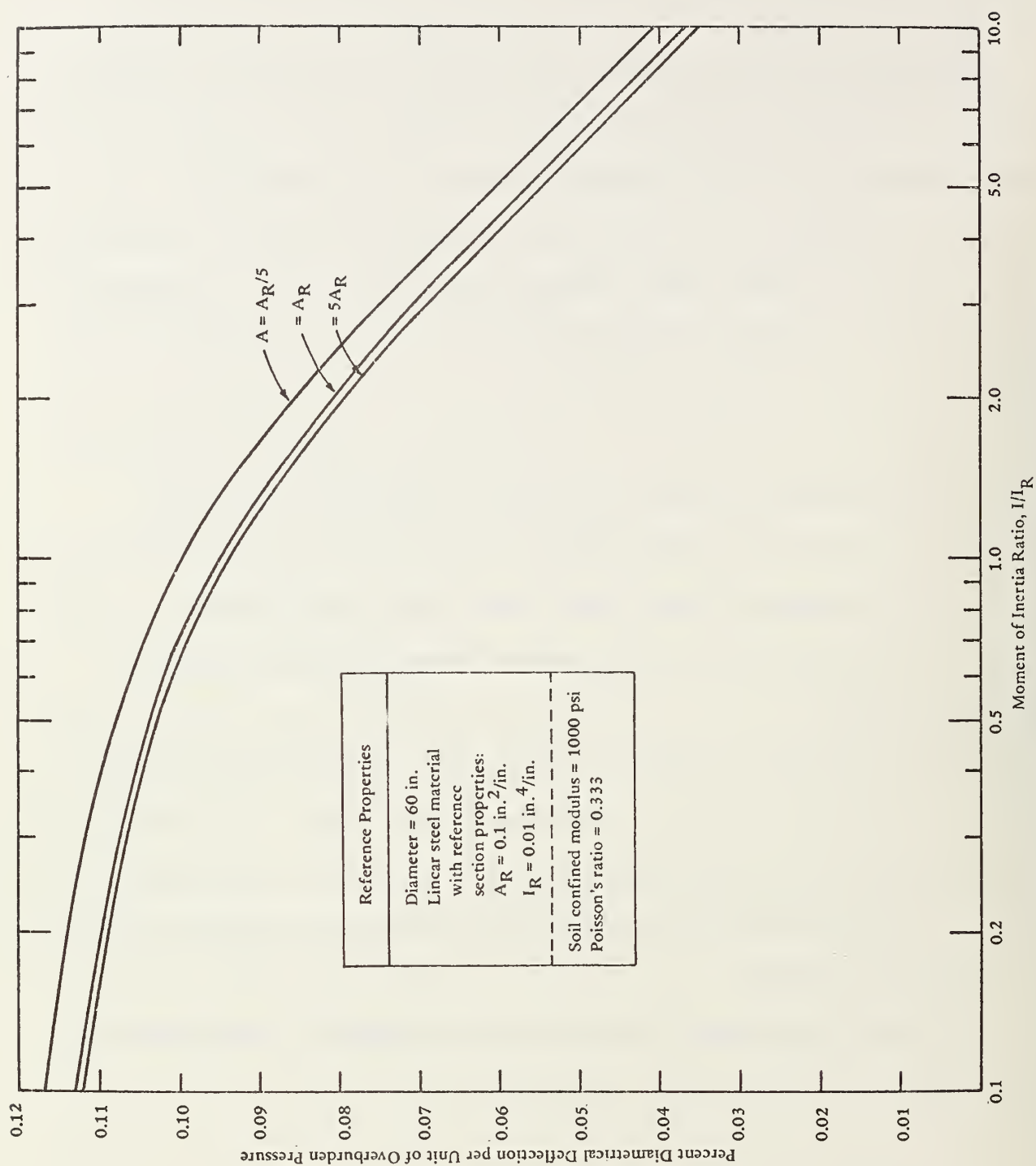


Figure 10-5. Percent deflection versus moment of inertia for three areas.

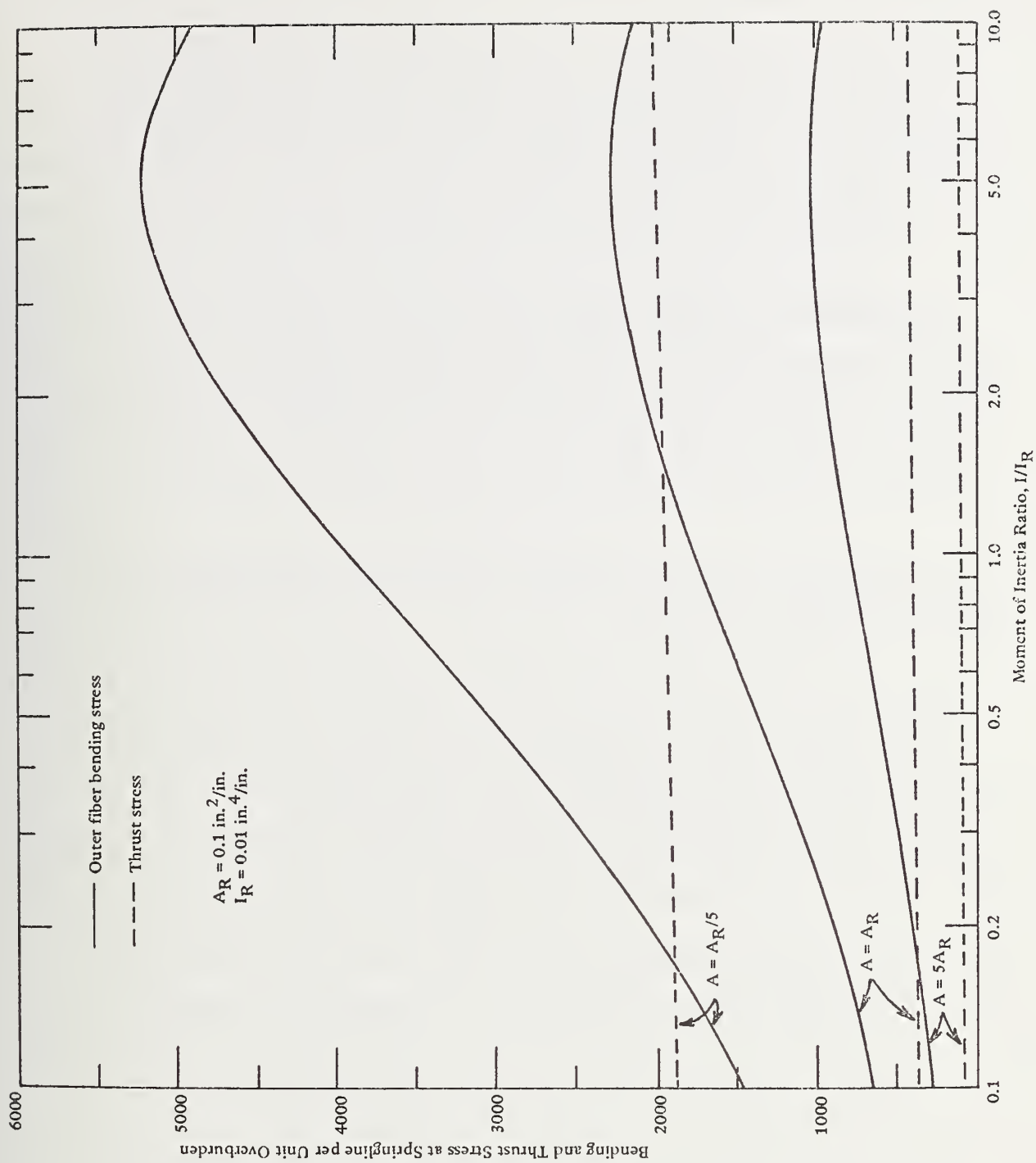


Figure 10-6. Bending and thrust stress versus moment of inertia for three areas.

(1) Deflections are practically independent of A, but are substantially reduced with increased I.

(2) Thrust stress is relatively unaffected by I and is inversely proportional to A. Since thrust stress = thrust/A, thrust is near constant over the range of I and A.

(3) Remarkably, bending stress increases substantially with increasing I up to a peak value and then decreases slightly. Bending stress is inversely proportional to the square root of A. Moments are insensitive to A but increase markedly with I.

(4) For a given area A, bending stress by and large exceeds thrust stress by a factor of 2 to 10.

The last observation indicates that corrugated metal culverts will generally experience outer fiber yielding under design loads. That is, assuming the sectional area A is selected such that thrust stress = yield stress/safety factor where the safety factor = 2 to 4 then the bending stress will be 2 to 10 times greater. Since outer fiber stress is the sum of thrust and bending, yield stress will generally be exceeded.

### 10.1.3 Effects of Pipe Nonlinearity

The influence of pipe nonlinearity is examined for corrugated metal pipes and reinforced concrete pipes. In the former case nonlinear behavior is characterized by plastic yielding, and in the latter case by concrete cracking, nonlinear behavior in compression, and steel reinforcement yielding (see Chapter 8).

For both pipe types, the following system parameters are assumed constant: confined soil modulus,  $M_s = 1,000$  psi; Poisson ratio,  $\nu_s = 0.333$ ; and a nominal pipe diameter,  $D = 60$  inches. All solutions are obtained with Level 1 nonlinear approximations, which were discussed in Chapters 5 and 8.

For the corrugated metal pipes, three 12-gage steel corrugation sizes are investigated;  $2\frac{2}{3} \times \frac{1}{2}$ ,  $3 \times 1$ , and  $6 \times 2$  inches. Section properties are noted in Figure 10-7. Similarly for the concrete pipes, three amounts of circular steel reinforcement are investigated for a constant 6-inch wall thickness. The combined inner and outer reinforcement steel areas are 0.5, 1.0, and 1.5% of the concrete area. Additional concrete and steel properties are noted in Figure 10-8.

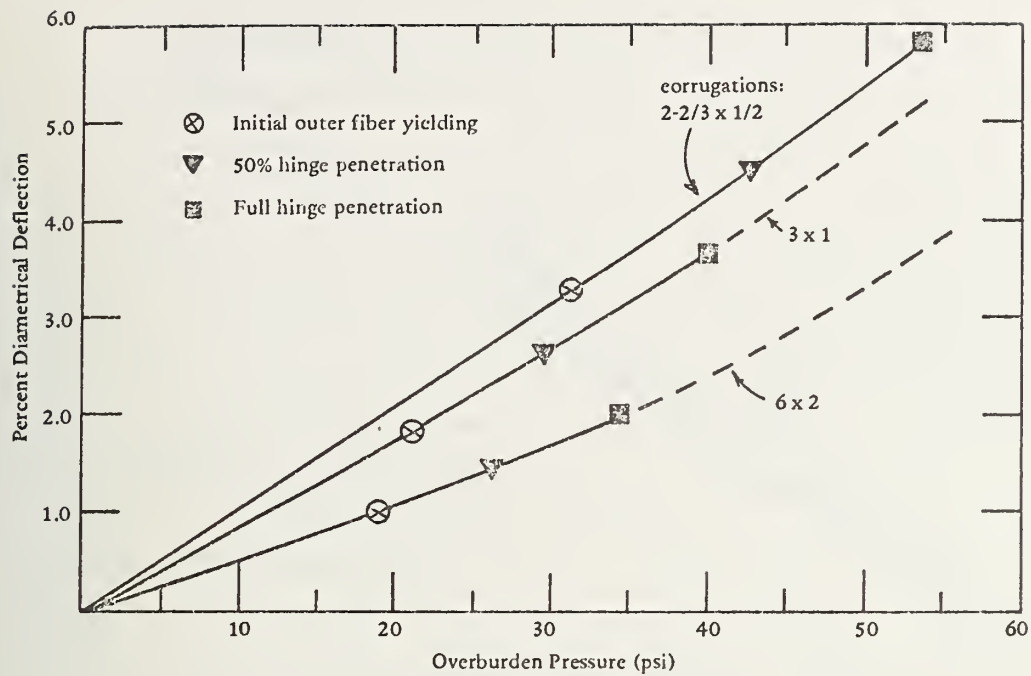
Vertical diametrical deflections versus overburden pressure are plotted in Figures 10-7 and 10-8 for corrugated steel and reinforced concrete pipes, respectively. The following observations are made:

(1) In Figure 10-7 it is seen that larger corrugations reduce deflections; however, initial outer fiber yielding and full hinge penetration occur in the larger corrugations at significantly lower loads than in the smaller corrugations. This observation is in accord with the previous section, wherein it was noted deflections decreased but bending stresses increased with I. Deviation from a linear deflection path starts to become observable when hinge penetration exceeds 50%.

(2) In Figure 10-8 it is observed that initial concrete cracking introduces an abrupt change in the deflection slope (initial cracking occurs on the inner wall at crown and invert, and on the outer wall at the springlines). Increased percentages of steel area reduce deflections; however, more significantly, increases of steel substantially increase the pipes ultimate capacity against concrete crushing.

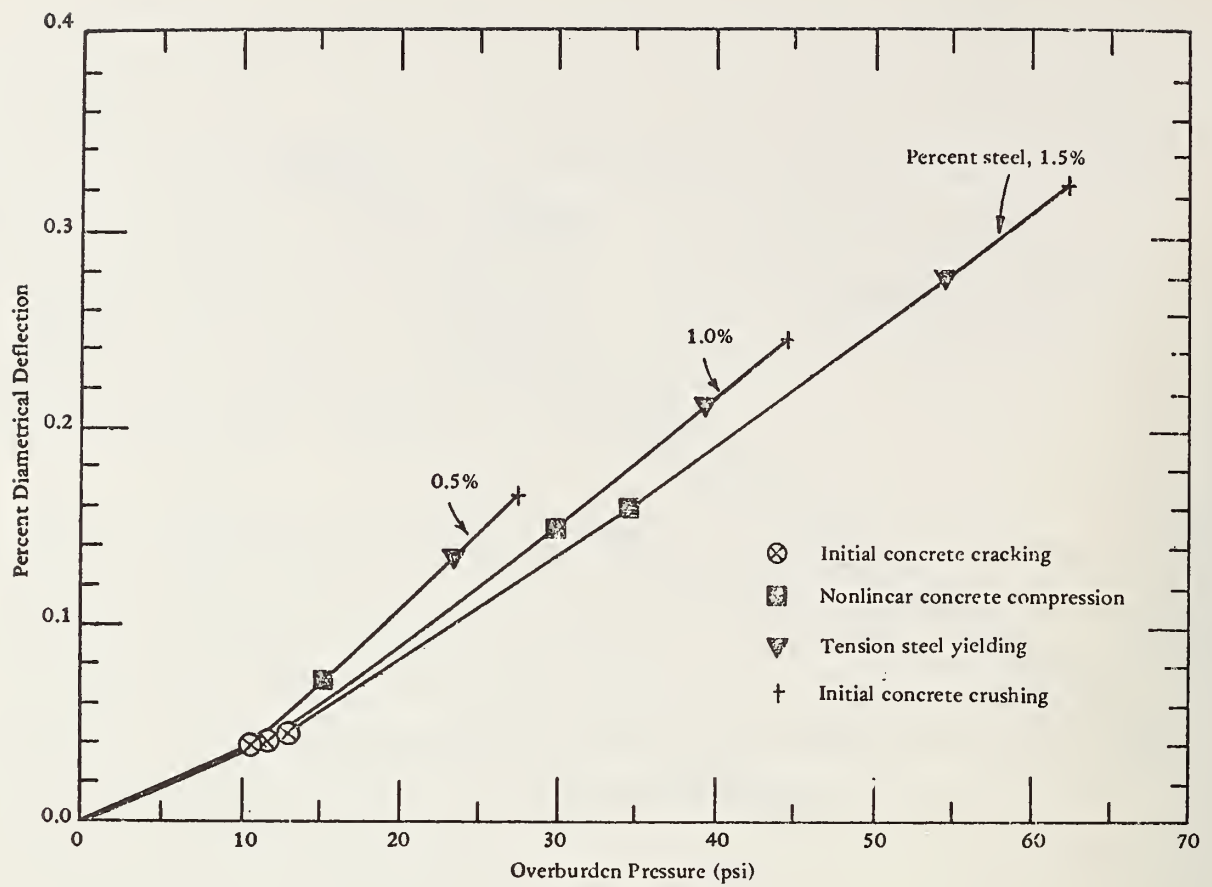
(3) Comparing the performance of corrugated steel to reinforced concrete pipes, it is clear that for the same overburden, the steel pipe deflections are an order of magnitude greater than concrete pipe deflections. As discussed in Chapter 8, full hinge penetration for corrugated metal pipes does not necessarily imply the capacity of the pipe is reached; however, for concrete pipe, yielding of the reinforcement steel is to be avoided to safeguard against concrete crushing and excessive crack widths.





12-gage steel corrugations, yield stress = 33,000 psi			
Corrugation Size (in.)	A (in. <sup>2</sup> /in.)	I (in. <sup>4</sup> /in.)	S (in. <sup>3</sup> /in.)
2-2/3 x 1/2	0.1130	0.00342	0.01133
3 x 1	0.1300	0.01545	0.02798
6 x 2	0.1296	0.06041	0.05741

Figure 10-7. Vertical deflections of corrugated pipe as a function of overburden for three corrugation sizes.



Concrete Wall	Steel Cages
Wall thickness = 6.0 in.	Outer-to-inner ratio = 0.75
Compressive strength = 4,000 psi	Yield strength = 40,000 psi
Cracking strain = 0.00008 in./in.	Total steel area = 0.03, 0.06, and 0.09 in. <sup>2</sup> /in.
Yield strain = 0.0005 in./in.	
Crushing strain = 0.002 in./in.	

Figure 10-8. Concrete deflection as a function of overburden for three steel areas.

#### 10.1.4 Effects of Friction on Pipe-Soil Interface

The results presented thus far have assumed the pipe and soil are completely bonded at the interface (i.e., sufficient friction to prevent relative slipping). As discussed in Chapters 5 and 7, both the elasticity formulation (Level 1) and the finite element formulation (Levels 2 and 3) permit consideration of frictionless interfaces. In addition, the finite element formulation permits consideration of intermediate values of friction as well as separation and rebonding during the loading schedule.

Three values of Coulomb friction at the pipe-soil interface will be considered;  $\mu = \infty$ , 0.25, and 0.0. The Coulomb friction hypothesis implies the interface remains bonded wherever the interface shear traction is less than the maximum frictional resistance defined by the product of normal traction and friction coefficient. Thus,  $\mu = 0$  allows free relative movement along the interface.

The friction study is applied to the following linear system: confined modulus,  $M_s = 4,000$  psi, Poisson's ratio,  $\nu_s = 0.333$ ; and a 66-inch-diameter pipe with 3 x 1-inch corrugation of 12-gage steel. For the cases  $\mu = 0.0$  and  $\mu = \infty$  both the elasticity solution and the finite element solutions are presented, thereby permitting a comparison of solution methods. For all finite element solutions the Level 2 mesh topology is used.

Figure 10-9 shows normal and shear interface pressure distributions over one pipe quadrant per unit of overburden pressure for each friction value. In a similar manner, Figures 10-10 and 10-11 illustrate thrust

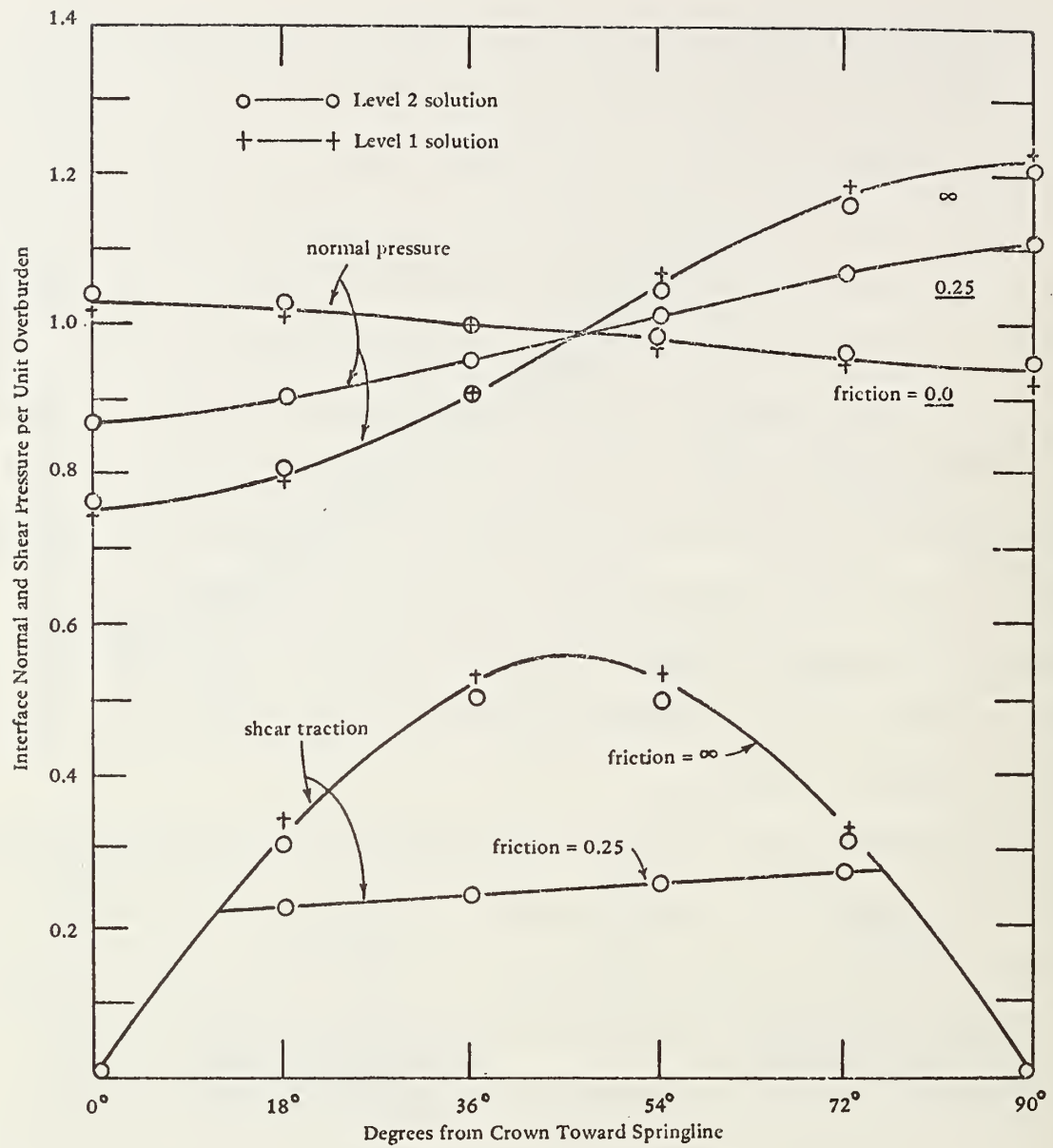


Figure 10-9. Normal and shear soil pressures on pipe for three interface friction values.

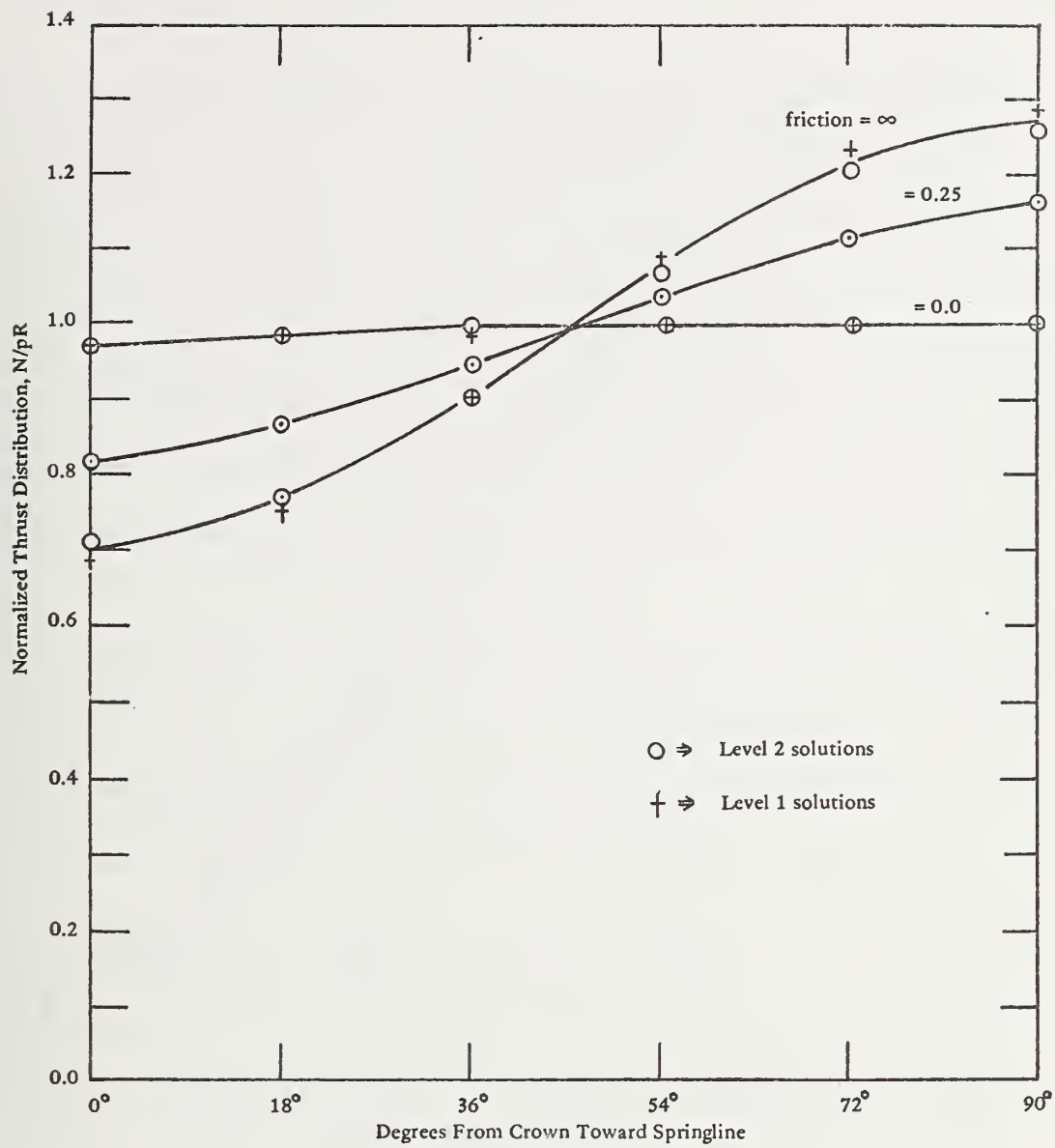


Figure 10-10. Normalized thrust distribution in pipe wall for three interface friction values.

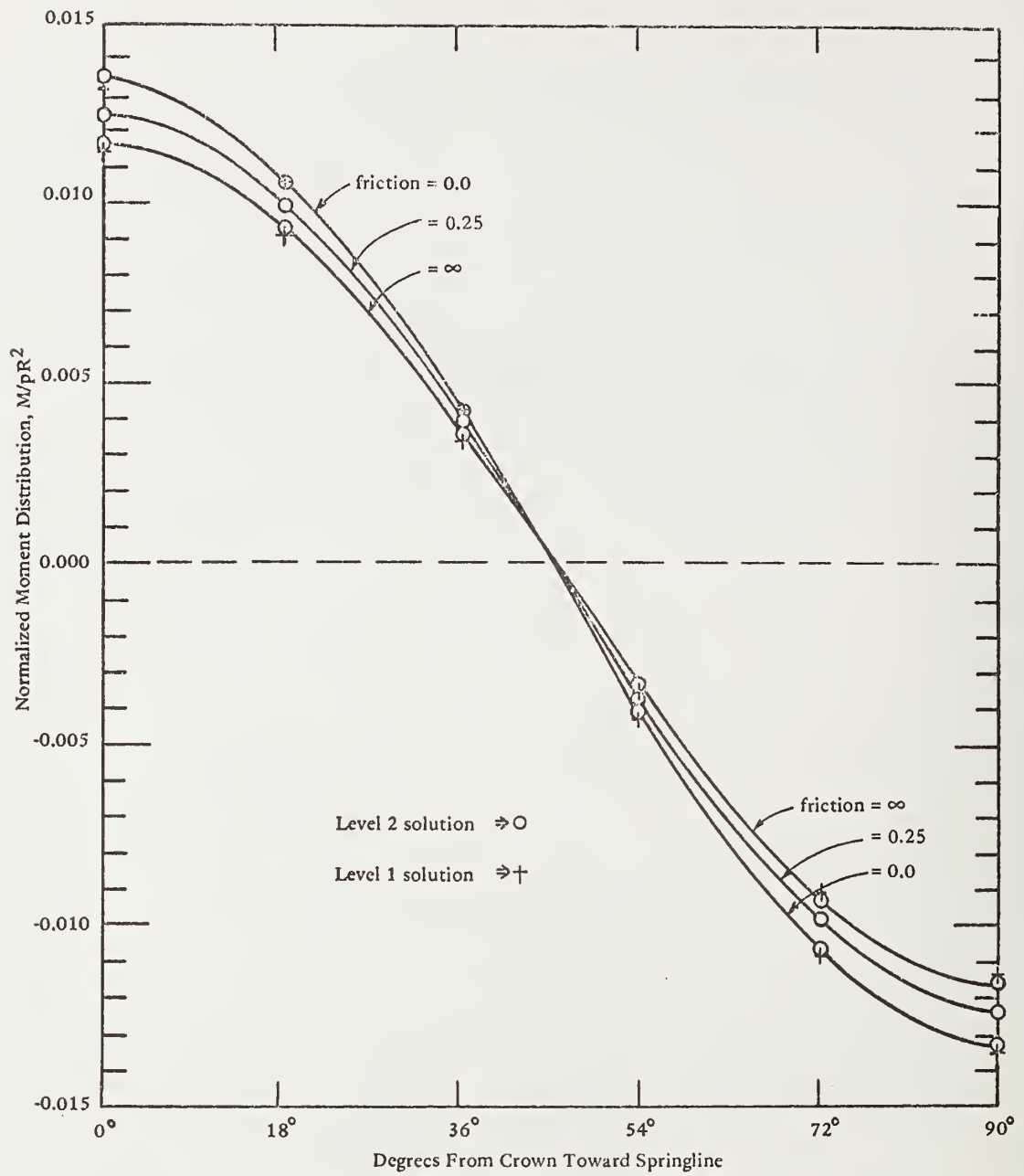


Figure 10-11. Normalized moment distribution in pipe wall for three interface friction values.



and moment distributions, respectively. The following observations are made:

(1) The normal pressure distribution shown in Figure 10-9 becomes more hydrostatic as friction decreases. Shear traction shifts from a smooth parabolic distribution to a "truncated" parabola for intermediate friction values. The truncated shear region shown,  $12^{\circ} < \theta < 76^{\circ}$ , denotes the portion of the pipe where frictional resistance is exceeded for the case  $\mu = 0.25$ . Comparing normal and shear pressure distributions, it is seen friction values greater than 0.6 will restrain any frictional movement for this system.

(2) Thrust distributions (Figure 10-10) become more uniform with decreased friction as would be expected in view of the near hydrostatic normal pressure distribution. For  $\mu = 0$ , peak thrust values are reduced by 25% for this system.

(3) Unlike thrust, moment distributions (Figure 10-11) increase in amplitude with decreasing friction; however, the maximum change is only 17%. The fact that high moment values remain in the near-hydrostatic pressure condition ( $\mu = 0$ ) demonstrates the importance of properly assessing the load distribution on the pipe. That is, a perfect hydrostatic pressure condition would result with zero moments. However, here it is seen that a small variation in hydrostatic pressure produces significant

bending moments. Clearly, analytical and design approaches that assume the load distribution on the pipe are questionable.

(4) For the cases  $\mu = 0$  and  $\mu = \infty$ , the elasticity solutions and the finite element solutions are everywhere in excellent agreement with an average discrepancy less than 1% and a maximum discrepancy of 5%.

#### 10.1.5. Influence of Bedding Parameters

The influence of bedding geometry and bedding stiffness on the structural behavior of corrugated metal and reinforced concrete pipe is examined for a linear soil system. For both pipe types the following system parameters are assumed constant: confined soil modulus  $M_s = 4,000$  psi; Poisson's ratio,  $\nu_s = 0.333$ ; (note: Young's modulus is  $E_s = 2667$  psi); and a nominal pipe diameter,  $D = 66$  inches. The corrugated metal wall is a 3 x 1-inch corrugation of 12-gage steel, and the reinforced concrete wall thickness is 6.5 inches with inner and outer circular reinforcement steel area percentages of 0.88% and 0.67%, respectively. Material behavior of both pipes is specified as linear except concrete cracking is permitted with no tension resistance. Therefore, all responses are proportional to load magnitude.

The bedding study is based on 28 finite element solutions (Level 3), wherein variations of bedding height, bedding width, and bedding stiffness are accommodated with a mesh topology similar to the Level 2 mesh, except

35 additional soil elements are used to define material boundaries. Unless otherwise noted, the bedding modulus is  $E_b = 10 E_s$  with Poisson's ratio  $\nu_b = 0.333$ . Figures 10-12, 10-13, and 10-14 illustrate the bedding configuration for each parameter study along with graphs of selected response ratios; i.e., the value of a key pipe response from the system with bedding divided by the corresponding response from a homogeneous system (no bedding). For the corrugated steel pipe, response ratios for maximum wall thrust and diametrical deflection are shown with solid lines, while the reinforced concrete pipe response ratios for maximum reinforcement stress and maximum compressive concrete stress are shown with dashed lines. In all cases response ratios less than 1.0 imply the bedding parameter is beneficial in relieving pipe distress, whereas response ratios greater than 1.0 imply the bedding parameter aggravates pipe distress.

Examining Figures 10-12 through 10-14, the following trends are observed:

(1) Increasing the bedding height from zero up to the springline (Figure 10-12) initially aggravates the concrete pipe response values; however, for larger encasement heights, the response values are near unity. For the corrugated steel pipe, thrust stress is increased, while displacements are decreased with increasing bedding encasement.

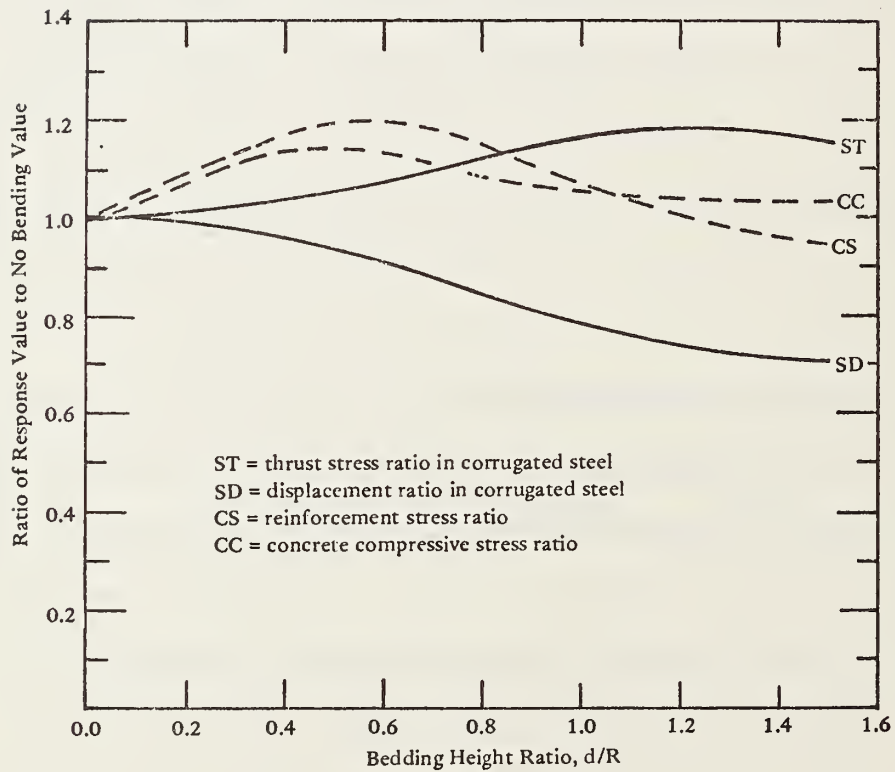
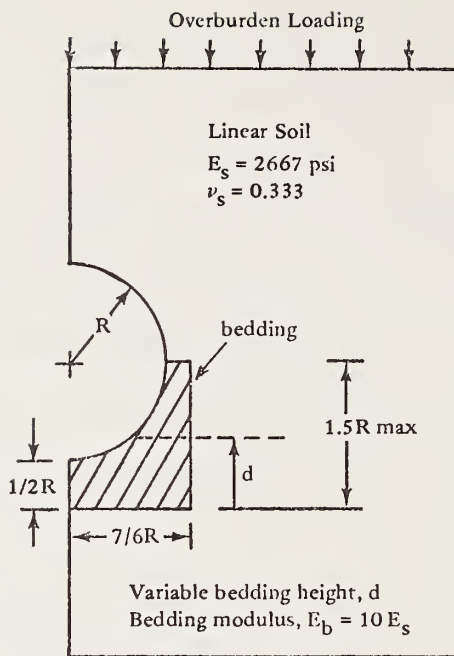


Figure 10-12. Influence of bedding height.

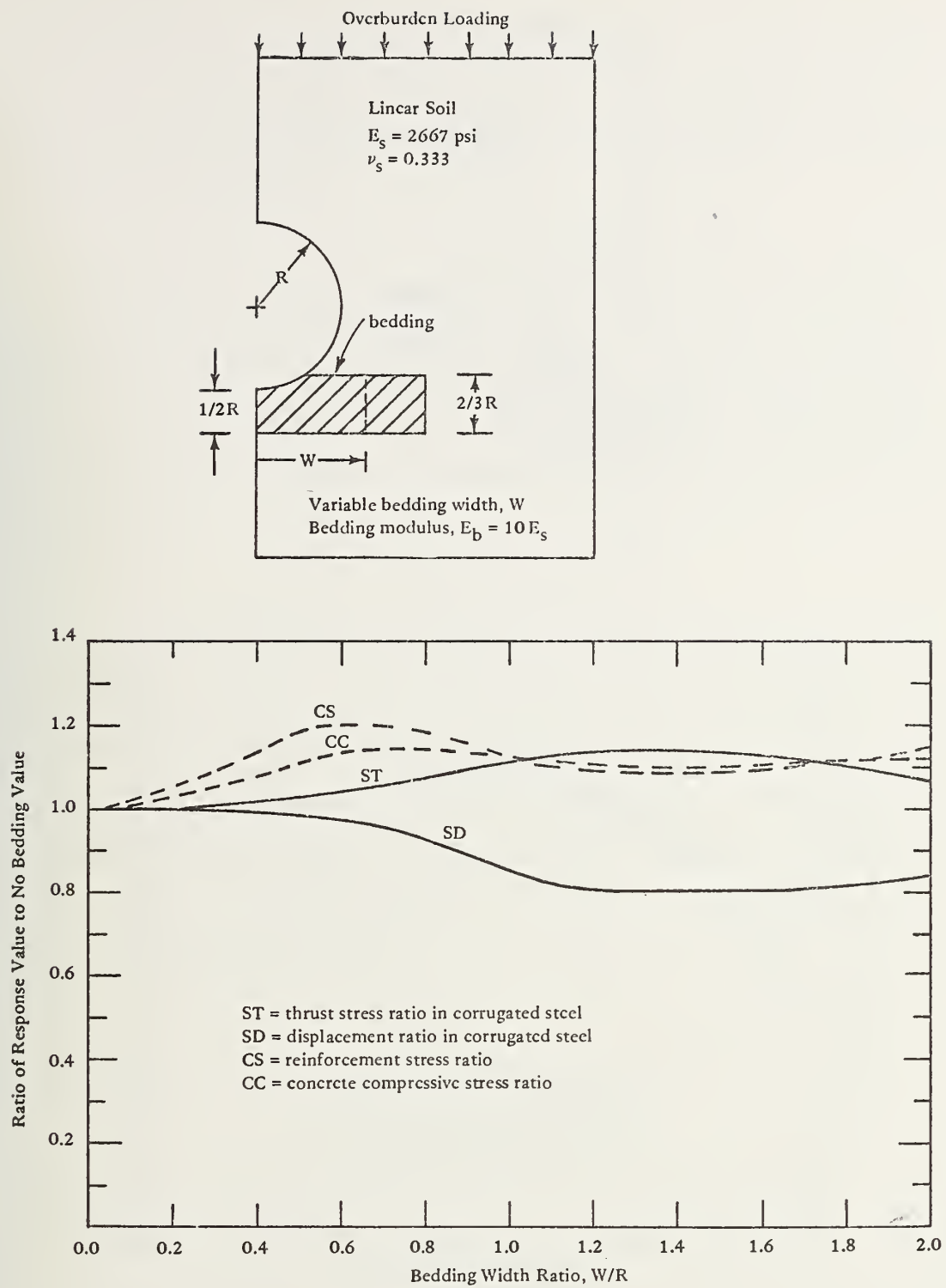


Figure 10-13. Influence of bedding width.

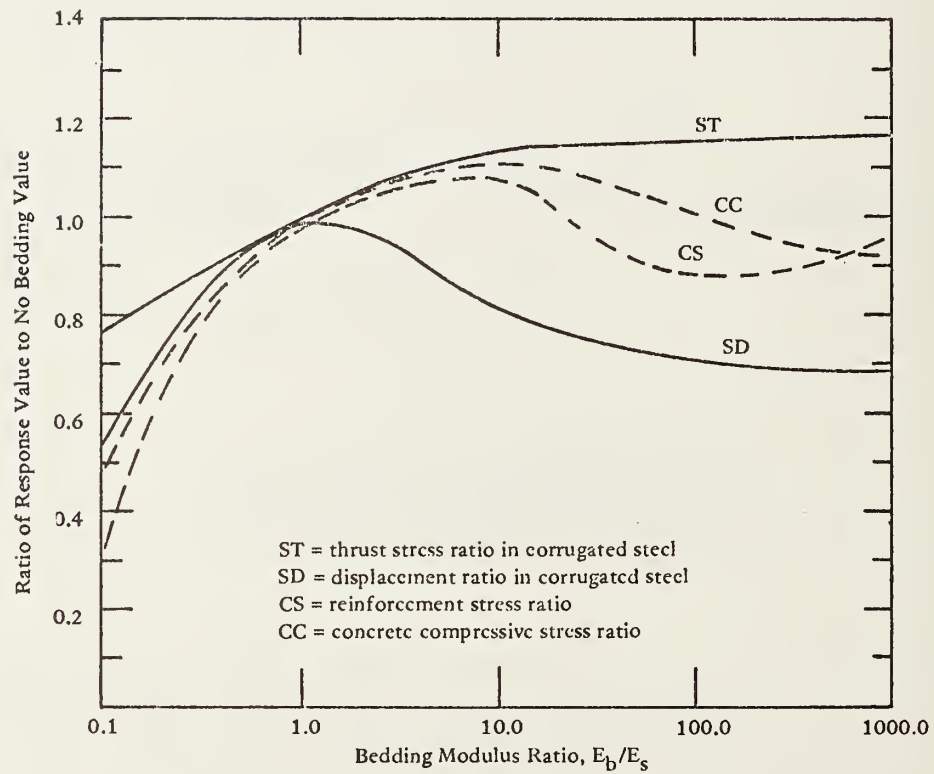
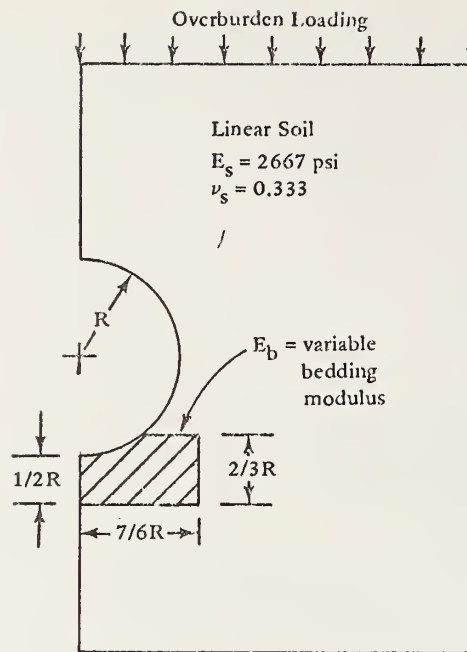


Figure 10-14. Influence of bedding stiffness.



(2) Extending the bedding width from zero to  $2R$  shows trends similar to the above. However, the response ratios remain relatively constant beyond  $1.2R$ , indicating bedding beyond  $1.2R$  has negligible influence on the pipe's performance.

(3) Changing the bedding modulus while maintaining a constant configuration (Figure 10-14) produces significant reductions in the response ratios when the bedding is softer than the surrounding soil. However for stiff beddings, the response ratios follow the same patterns noted above.

(4) In reviewing these figures it is observed that on the whole stiff beddings aggravate, rather than benefit, in-plane structural responses of culverts. Recall this finding was advertised in Chapter 2 with the concept of negative and positive arching. Contrary to the above, it is recognized stiff beddings are beneficial with respect to longitudinal bending, alignment, and joint control. However, this study has been restricted to in-plane deformations.

#### 10.1.6 Influence of Imperfect Trench Parameters

The purpose of an imperfect trench is to develop positive arching by introducing soft material into a portion of the trench above the pipe as discussed in Chapter 2. In this section the influence of imperfect

trench height, width, and material stiffness is examined in a manner identical with the previous bedding study. The same linear soil system is assumed (no bedding) together with the same 66-inch-diameter corrugated steel and reinforced concrete pipes previously described.

The imperfect trench parameter study is based on 18 finite element solutions by selectively varying the material boundaries and properties of the imperfect trench zone for both pipes. Unless otherwise noted, the modulus of the imperfect trench material is  $E_t = 1/5 E_s$  with Poisson's ratio  $\nu_t = 0.333$ . Figures 10-15, 10-16, and 10-17 describe the imperfect trench zone for each parameter study, wherein the finite element mesh topology (Level 3) is as described in the bedding study.

Along with trench zone descriptions, each of the above figures display graphs of selected response ratios for corrugated steel (solid lines) and reinforced concrete (dashed lines). These are the same response ratios defined in the bedding study and are the response from the imperfect trench system divided by the corresponding response from a homogeneous system. Accordingly, response ratios less than 1.0 indicate the degree that pipe distress is being relieved by the imperfect trench parameter.

Examining Figures 10-15 through 10-17 reveal the following trends:

(1) Increasing the imperfect trench material height (Figure 10-15) from zero to 2R substantially reduces maximum concrete compression and maximum reinforcement stress by ratios of 0.61 and 0.42, respectively. For corrugated steel pipe, the diametrical deflection is also substantially

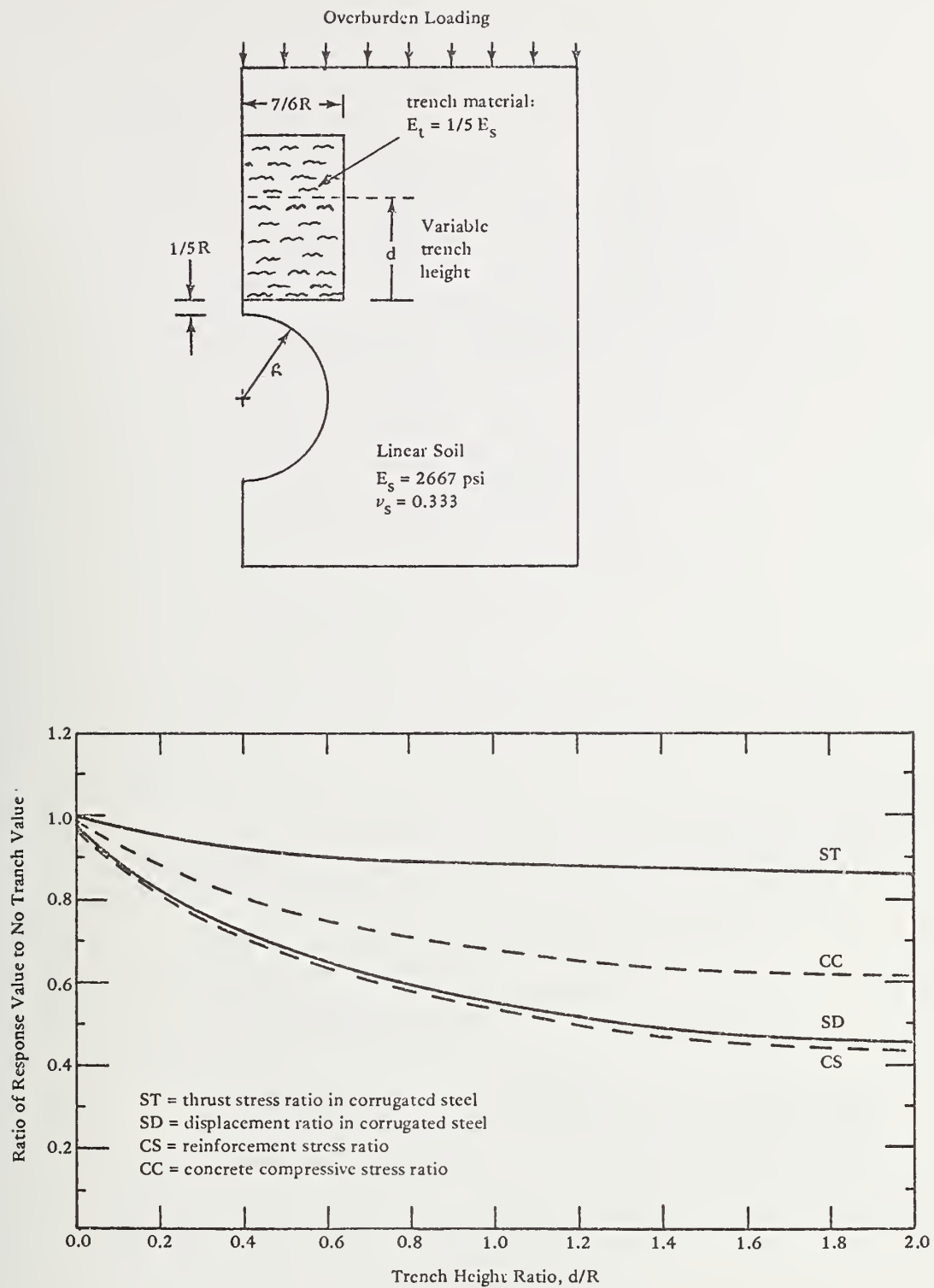


Figure 10-15. Influence of imperfect trench height.

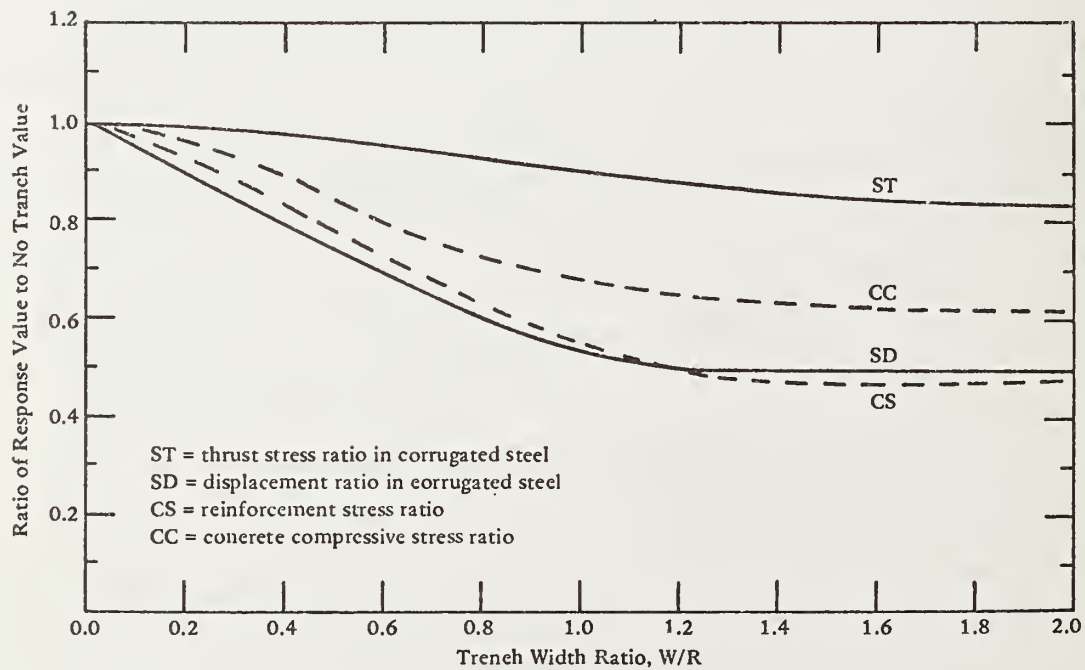
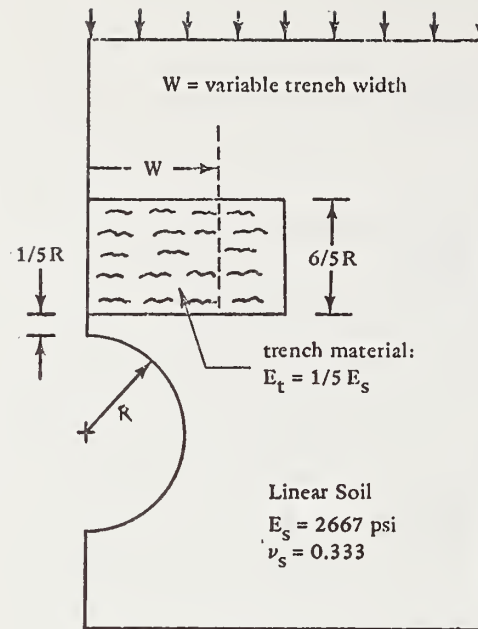


Figure 10-16. Influence of imperfect trench width.

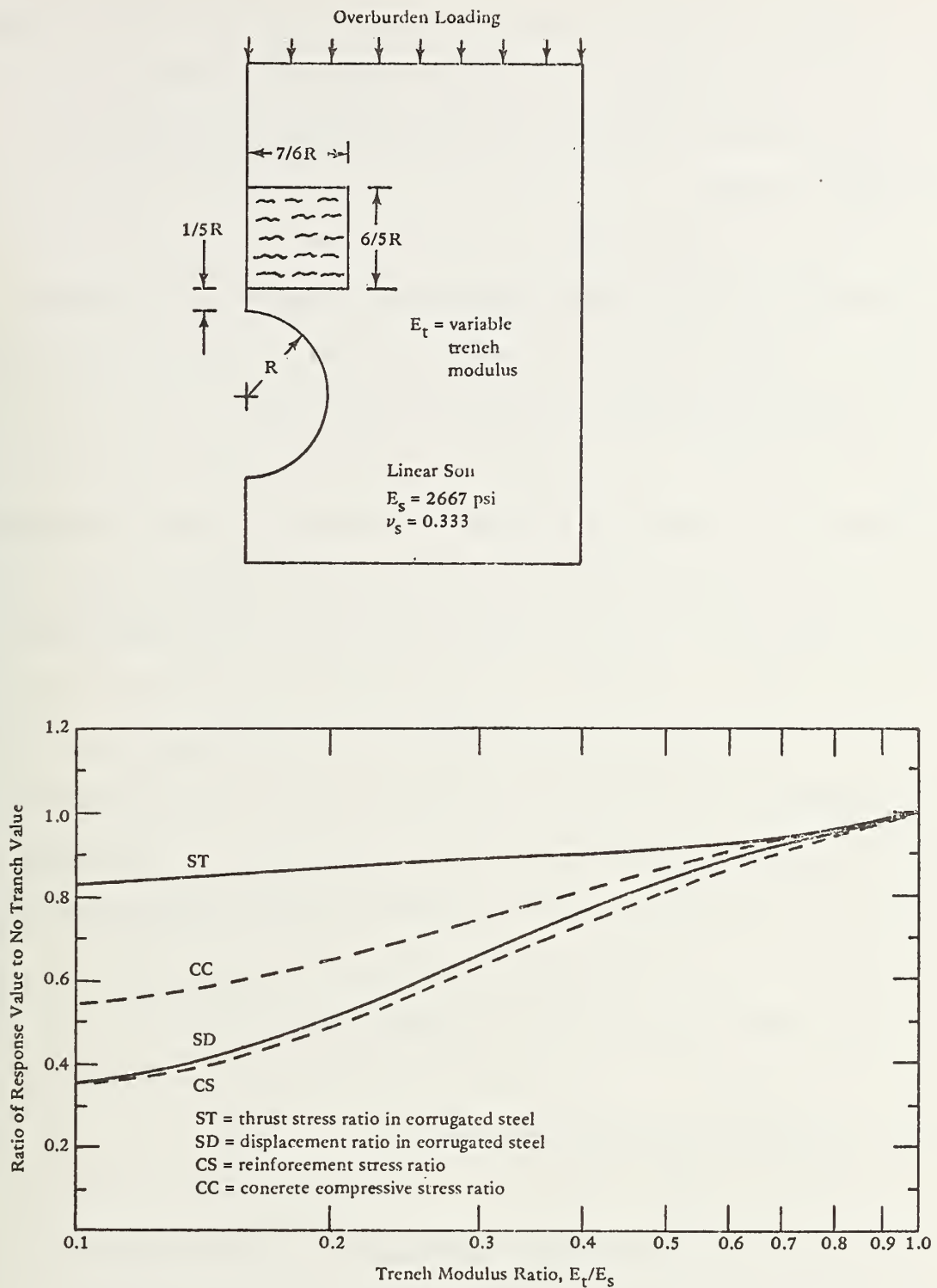


Figure 10-17. Influence of imperfect trench stiffness.

reduced by a ratio 0.44; however, thrust stress is only reduced by a ratio of 0.86. In all cases a point of diminishing returns is reached at a trench height of approximately  $1.2R$ . Beyond this height the response ratios are not appreciably reduced.

(2) Extending the trench width symmetrically from zero to  $2R$  (Figure 10-16) produces results similar to those above. Again a point of diminishing returns is observed at a symmetric trench width of  $1.2R$ .

(3) Lowering the modulus of the imperfect trench material with respect to the surrounding soil enhances the reduction of all response ratios. Practical considerations limit achieving trench modulus ratios much below 0.1.

(4) In overview, it is observed that the imperfect trench technique, if properly employed, can reduce peak concrete pipe responses by 50% and peak corrugated metal pipe responses by 20% for the system considered. Optimum trench size is 1.2 pipe radii deep and 1.2 pipe radii wide from the centerline. Larger sizes yield diminishing returns.

#### 10.1.7 Influence of Various System Parameters

In this section the parametric investigation is concluded with the comparison of the following system variations: gravity loading versus



overburden loading, multilift versus single-lift, nonlinear soil versus linear soil, elliptical pipe shapes versus round pipe, and backpacking ring inclusions versus no backpacking ring. All comparisons are based on a nominal 66-inch-diameter, 3 x 1-inch-corrugation, 12-gage linear steel culvert. Except where noted otherwise, a linear homogeneous soil system is assumed with a confined modulus  $M_s = 4,000$  psi and a Poisson's ratio  $\nu_s = 0.333$ .

All solutions are obtained from the finite element method using Level 2 mesh topology with overburden loading except as noted for gravity loads. Table 10-1 displays key response ratios at the crown and springline for diametrical deflection, radial pressure, thrust, and moment. Response ratios are determined by dividing the responses from the "varied" system by the corresponding responses of the "reference" system. Thus, ratios less than 1.0 indicate the "varied" system reduces pipe distress. Comments at the bottom of Table 10-1 describe the parameter variations of each comparison.

The following observations are noted:

(1) The response ratios of a pipe-soil system loaded with gravity versus the reference system loaded with "equivalent" overburden pressure (i.e., fill soil above crown times soil density; column A, Table 10-1) increases springline thrust by the ratio 1.09 and decreases crown deflection by the ratio 0.80. These results are based on a cover height of three radii above the crown. As cover height increases the discrepancy between gravity and overburden loading decrease.

Table 10-1. Response Ratios of System Variations for 66 inch CMP

Response Ratios	A	B	C	D	E	F	G
	Gravity Load to Overburden Load	Multilift to Single Lift	Nonlinear Soil to Linear Soil	Vertical Ellipse to Round Pipe	Horizontal Ellipse to Round Pipe	Soft Backpacking to No Backpacking	Stiff Backpacking to No Backpacking
<u>Ratios at Springline</u>							
Horizontal deflection	0.86	1.16	0.84	0.78	1.18	1.45	0.60
Lateral pressure	0.93	0.82	0.97	0.87	1.12	0.49	1.29
Thrust	1.09	0.86	0.88	1.00	1.00	0.52	1.27
Moment	1.17	1.22	0.07	0.67	1.38	1.41	0.61
<u>Ratios at Crown</u>							
Vertical deflection	0.80	1.31	1.10	0.75	1.32	1.43	0.61
Crown pressure	1.34	0.91	0.89	1.20	0.84	0.75	0.60
Thrust	0.77	0.86	0.88	1.02	0.97	0.68	0.60
Moment	0.63	1.62	1.38	0.87	1.09	1.57	0.58
Comments	Single-lift gravity versus single-lift overburden	Fives lifts of gravity load versus one large gravity load	Hardin Mixed: $v_{min} = 0.1$ $v_{max} = 0.49$ $q = 0.26$	Vertical ellipse by 10%, Same average diameter	Horizontal ellipse by 10%, Same average diameter	Backpacking: $t = 8.25$ in. $E = 266.7$ psi $\nu = 0.333$	Backpacking $t = 8.25$ in. $E = 26667.0$ psi $\nu = 0.333$

(2) Response ratios of gravity load applied in five construction lifts beginning from invert and ending 3 radii above the crown produce increases in deflection and decreases in thrust compared to the same system with a monolift gravity loading (column B).

(3) In column C the fully nonlinear Extended-Hardin soil model (Chapter 6) for a mixed soil under 50-psi overburden pressure is compared with a linear reference soil, wherein the reference soil properties are based on the Hardin soil model prediction for a free-field condition with 50-psi overburden (i.e.,  $M_s = 9,200$  psi,  $\nu_s = 0.31$ ). On the whole, response ratios do not deviate significantly from unity with the notable exception of springline moment, which is drastically reduced by the ratio 0.07. This is attributed to the stiffening of the soil model near the springline.

(4) Columns D and E depict response ratios for a 10% vertical and a 10% horizontal elliptical pipe compared to a round pipe with the same average diameter of 66 inches. Deflections are reduced in the vertical ellipse but are increased in the horizontal ellipse. However, thrust is not affected by either pipe shape. Therefore, from a design viewpoint, the elliptical shapes do not change design steel area requirements.

(5) Lastly, columns F and G show the influence of a soft and stiff backpacking ring completely around the culvert (see Chapter 2). The soft backpacking modulus is one-tenth of the soil modulus and reduces springline thrust by approximately one-half. On the other hand, the stiff backpacking modulus is ten times the soil stiffness and increases springline thrust by the ratio 1.27. Thus, soft backpacking reduces design requirements for steel area while stiff backpacking increases them. However, stiff backpacking limits deflections. Backpacking is investigated further with respect to design in the next sections.

## 10.2 DESIGN COMPARISONS

Perhaps the most basic question to be answered is, how do CANDE design solutions compare with traditional design solutions. In this section this question is explored for reinforced concrete and corrugated steel pipe. However, it must be appreciated that direct comparisons are difficult because traditional design methods use lumped empirical parameters for soil, bedding, etc., which are not well correlated with the rational engineering material properties used by CANDE (see Chapters 1-3). To reduce these discrepancies simplistic problems are considered where a linear homogeneous soil is assumed with overburden loading. Further, a range of soil parameters are input for both design methods to facilitate comparison of results.

### 10.2.1 Reinforced Concrete

CANDE designs are compared with the ACPA design method [10-1] for reinforced concrete pipe. The design problems posed are to determine the required reinforcing steel areas (specified wall thicknesses) for each of the following conditions:

(1) 30-inch pipe diameter with two circular cages of steel in a 3.5-inch-thick wall for a range of fill heights.

(2) 60-inch pipe diameter with two circular cages of steel in a 6.0-inch-thick wall for a range of fill heights.

(3) 90-inch pipe diameter with two circular cages of steel in a 8.5-inch-thick wall for a range of fill heights.

(4) 60-inch pipe diameter with one elliptical cage of steel in a 6.0-inch-thick wall for a range of fill heights.

(5) 60-inch pipe diameter with two circular cages of steel in a 6.0-inch-thick wall for 30 feet of fill with a range of bedding stiffnesses.



Figures 10-18 through 10-22 further identify each of the above design problems and show the total required steel area predicted by CANDE and the ACPA design method. In the first four design problems the corresponding figures show design envelopes reflecting reasonable ranges of soil parameters for the two methods. The ACPA envelopes reflect the influence of varying the so-called settlement ratio from 0.3 to 1.0 for a class C bedding and a 0.01-inch D-load crack design. The CANDE design envelopes are based on Level 1 solutions, wherein Young's modulus for soil is taken as 333.0 and 3333.0 psi. In all cases the 0.01-inch crack width was the controlling design criterion.

Inspection of Figures 10-18, 10-19, 10-20, and 10-21 reveals that CANDE predicts a substantial savings of reinforcement steel for the cases considered. Or equivalently, CANDE indicates the pipe can be buried deeper for a given steel area than allowed by ACPA. This finding supports the contention that traditional concrete pipe designs are overconservative. This will be discussed further in the last part of this chapter.

Figure 10-22 illustrates the influence of bedding stiffness (or class) on required steel area for the 60-inch pipe under 30 feet of fill. ACPA designs allow a substantial reduction in reinforcing steel for improved bedding classes D, C, B, and A. On the other hand, CANDE predicts that a stiffer bedding material does not appreciably alter the steel requirements. In this case, CANDE design predictions employed Solution Level 2 with a fixed bedding configuration, and only the bedding modulus



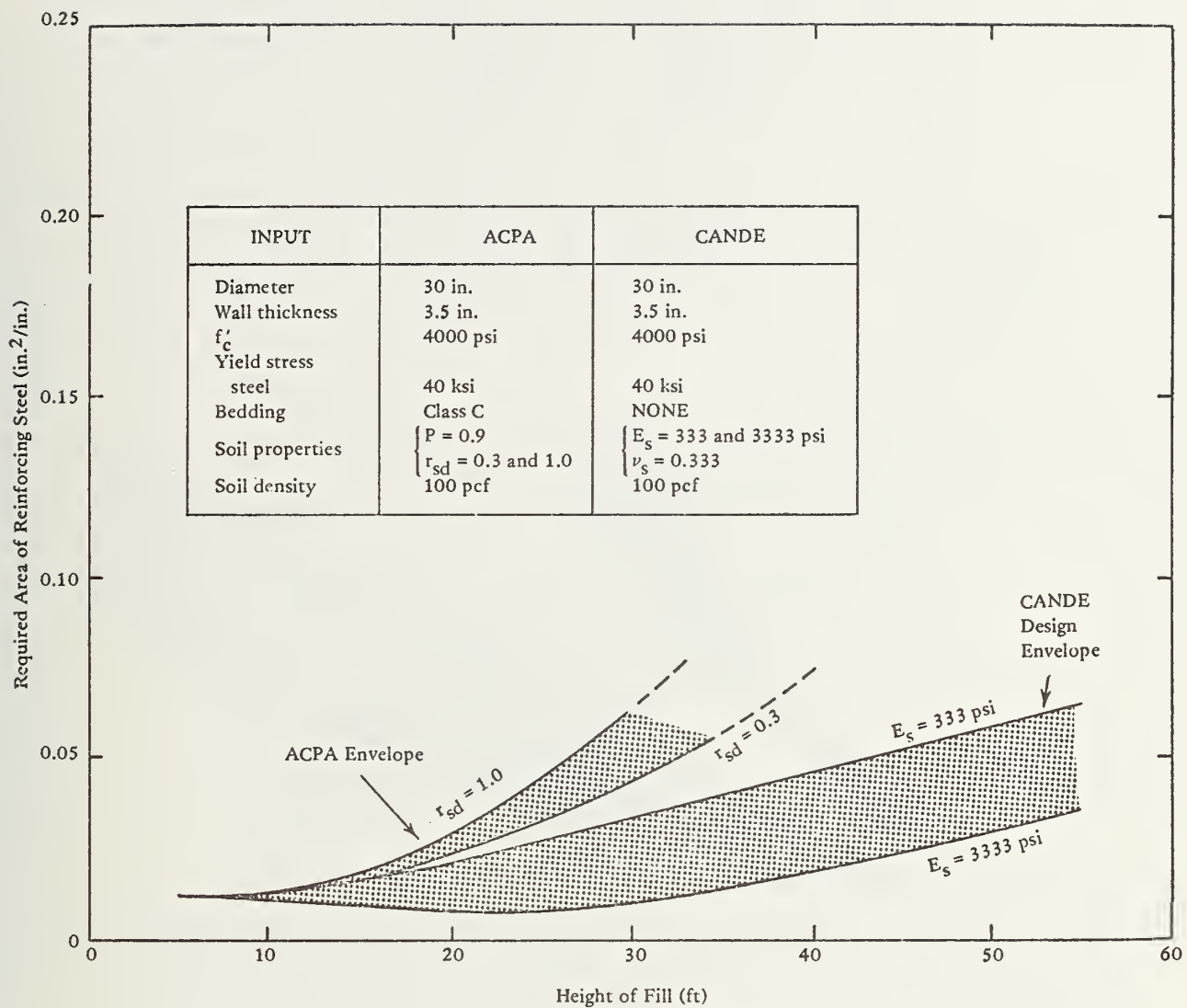


Figure 10-18. Double cage steel area designs for 30-inch pipe.

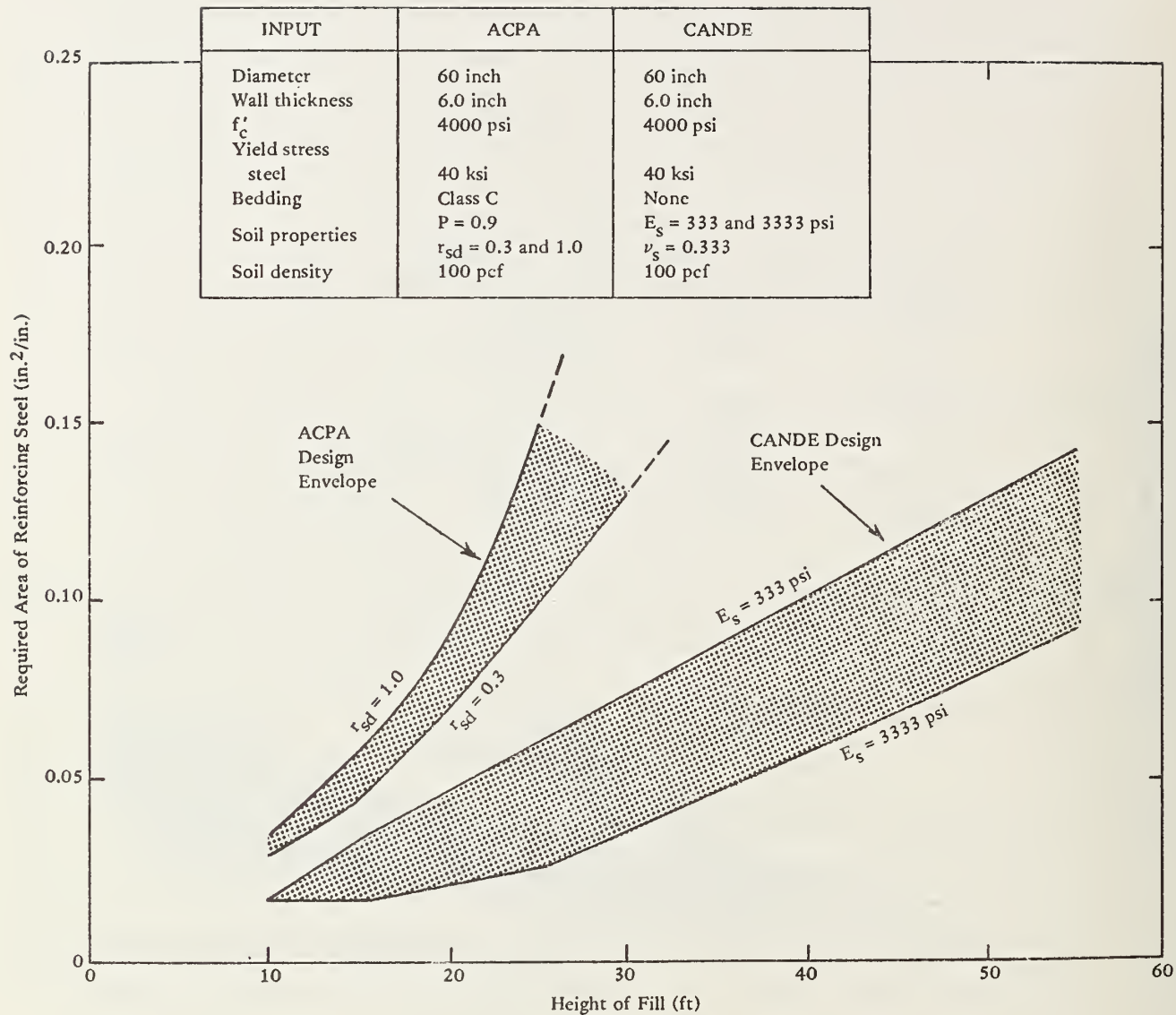


Figure 10-19. Double cage steel area designs for 60-inch pipe.

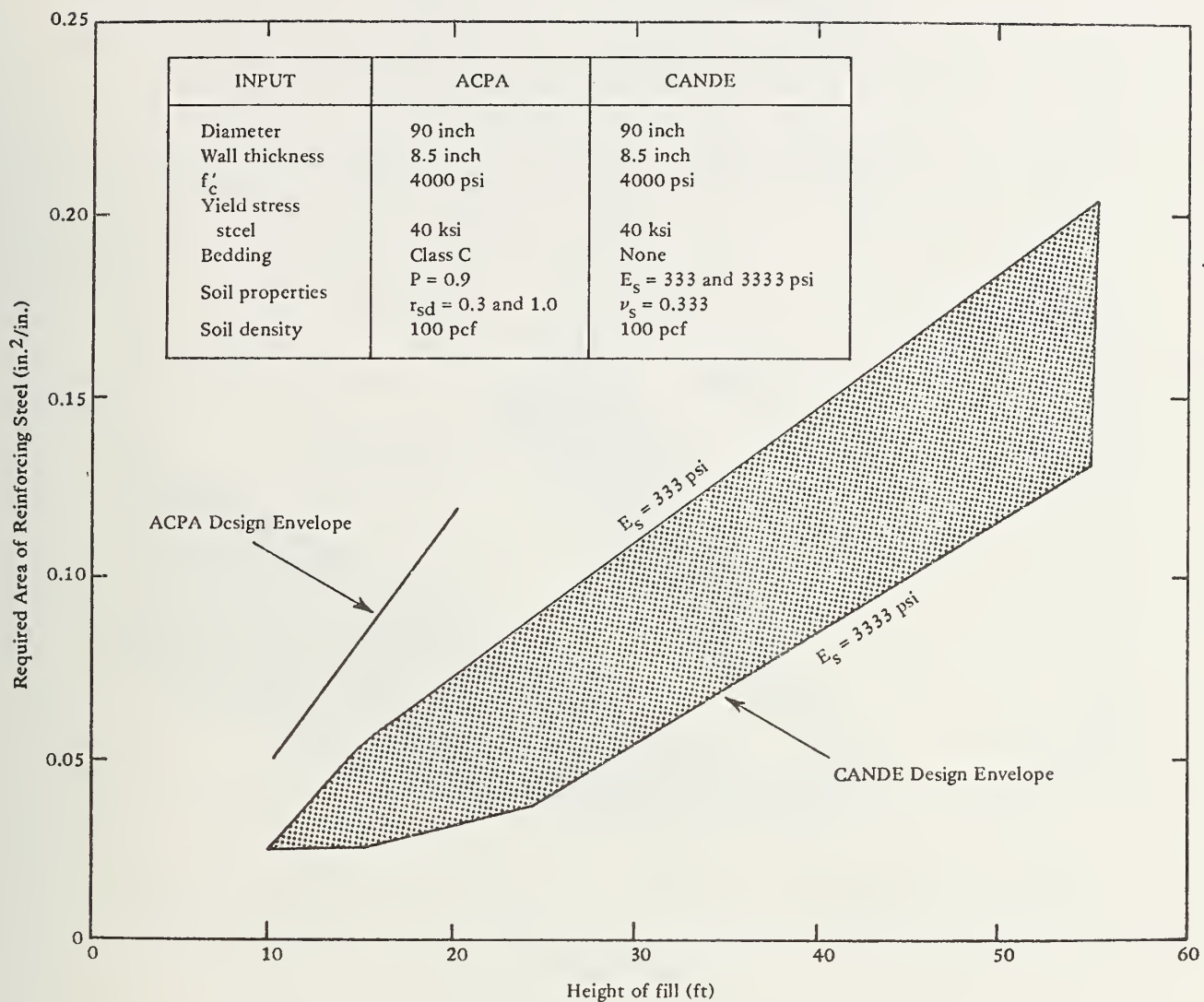


Figure 10-20. Double cage steel area designs for 90-inch pipe.

INPUT	ACPA	CANDE
Diameter	60 inch	60 inch
Wall thickness	6.0 inch	6.0 inch
Steel yield	40 ksi	40 ksi
Bedding	Class C	None
Soil properties	$P = 0.9$	$E_s = 333 \text{ to } 3333 \text{ psi}$
	$r_{sd} = 0.3 \text{ to } 1.0$	$\nu_s = 0.333$
Soil density	100 pcf	100 pcf

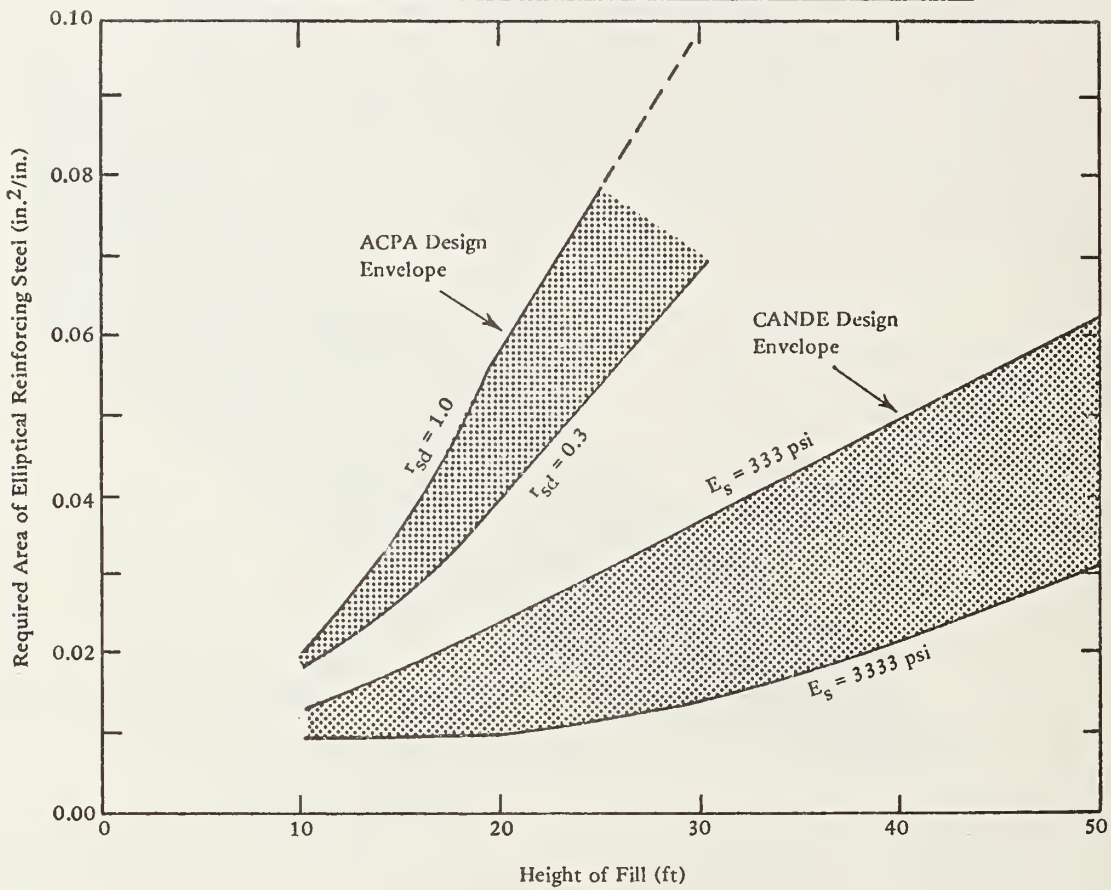


Figure 10-21. Elliptical steel area designs for 60-inch pipe.

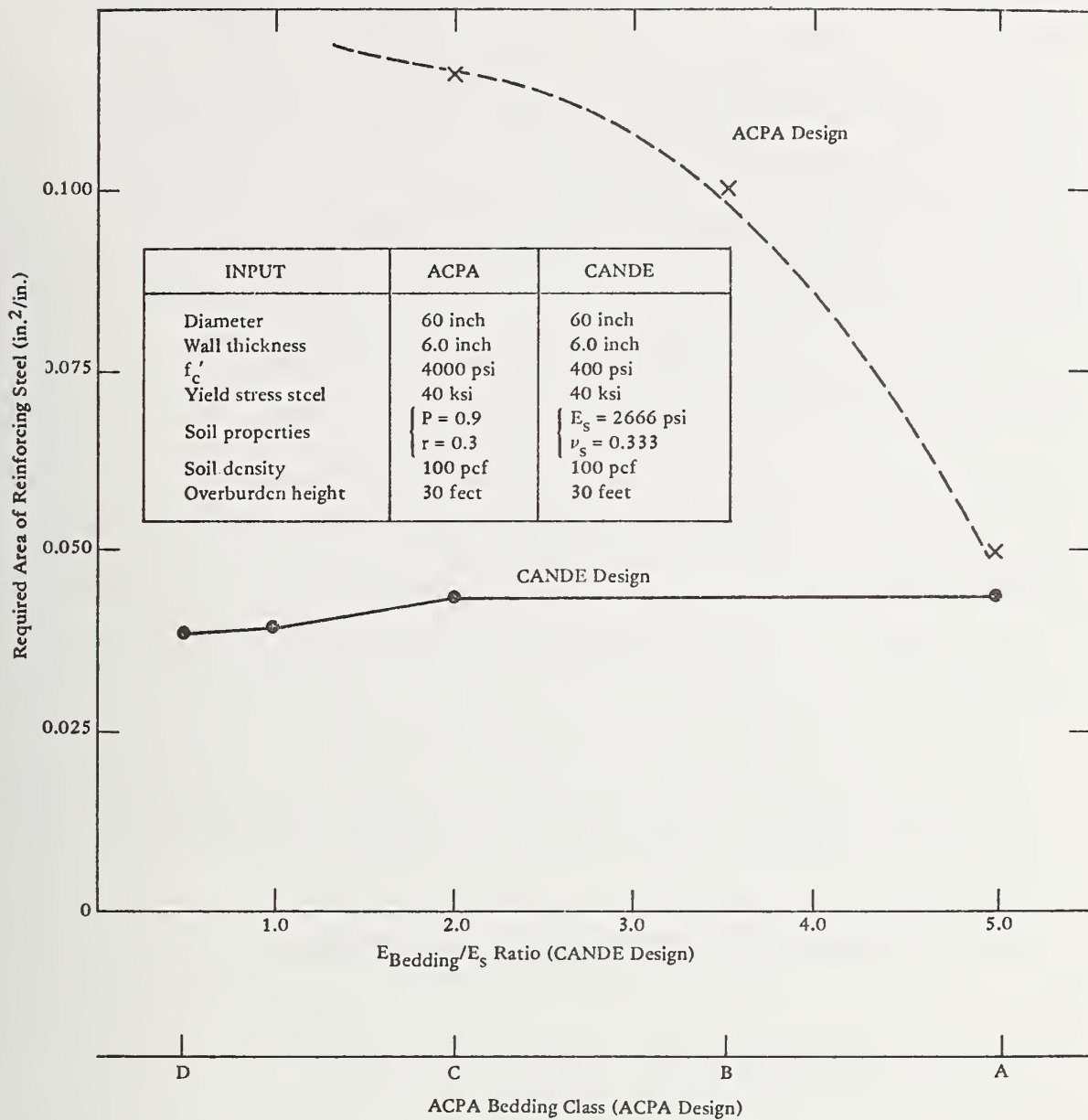


Figure 10-22. Influence of bedding on double cage steel area designs.

was varied. It must be noted the bedding configuration of Level 2 is not identical to ACPA bedding classes and, thus, inhibits a direct comparison. Nonetheless, in view of the previous bedding parameter study, CANDE results indicate stiff beddings are not beneficial in reducing steel area requirements from in-plane loading. However, it is recognized beddings are useful for maintaining uniformity and relieving distress in the longitudinal direction.

#### 10.2.2 Corrugated Steel

CANDE designs are compared with the AASHTO [10-2] design method for corrugated steel culverts. The design problems posed are to determine the least weight of corrugated steel area from standard available sizes for the following conditions:

- (1) 36-inch-nominal-diameter pipe for a range of fill heights.
- (2) 66-inch-nominal-diameter pipe for a range of fill heights.
- (3) 96-inch-nominal-diameter pipe for a range of fill heights.
- (4) 66-inch-nominal-diameter pipe under 30 feet of fill for a range of bedding stiffness.



(5) 66-inch-nominal-diameter pipe under 30 feet of fill for a range of backpacking stiffness.

Figure 10-23 shows the results of the first three design problems and further identifies the input parameters. The CANDE predictions for the first three designs are based on the Level 1 solution where, as in the concrete design study, the soil modulus is taken as 333.0 and 3333.0 psi. In this case however, the "envelopes" degenerate to single curves because thrust stress (safety factor = 3) governs the design steel area, and thrust stress is practically insensitive to this range of soil moduli. Likewise, the AASHTO steel area designs are governed by ring compression thrust (safety factor = 4) as opposed to buckling or deflection; thus, steel areas are insensitive to soil moduli.

It is evident that the results of the two design methods are remarkably close for the three diameters considered. However, it is noted the specified thrust stress safety factors differed by 30% in accordance with recommendations of each design procedure. If identical safety factors were used CANDE designs would be more conservative than the traditional method.

The influence of bedding stiffness on corrugated steel designs is illustrated in Figure 10-24 for a 66-inch-diameter pipe under 30 feet of fill. The standard Level 2 bedding configuration is used for bedding moduli ranging from 1.0 to 5.0 times the soil modulus. As before, the bedding is shown to have little influence on the required steel area and

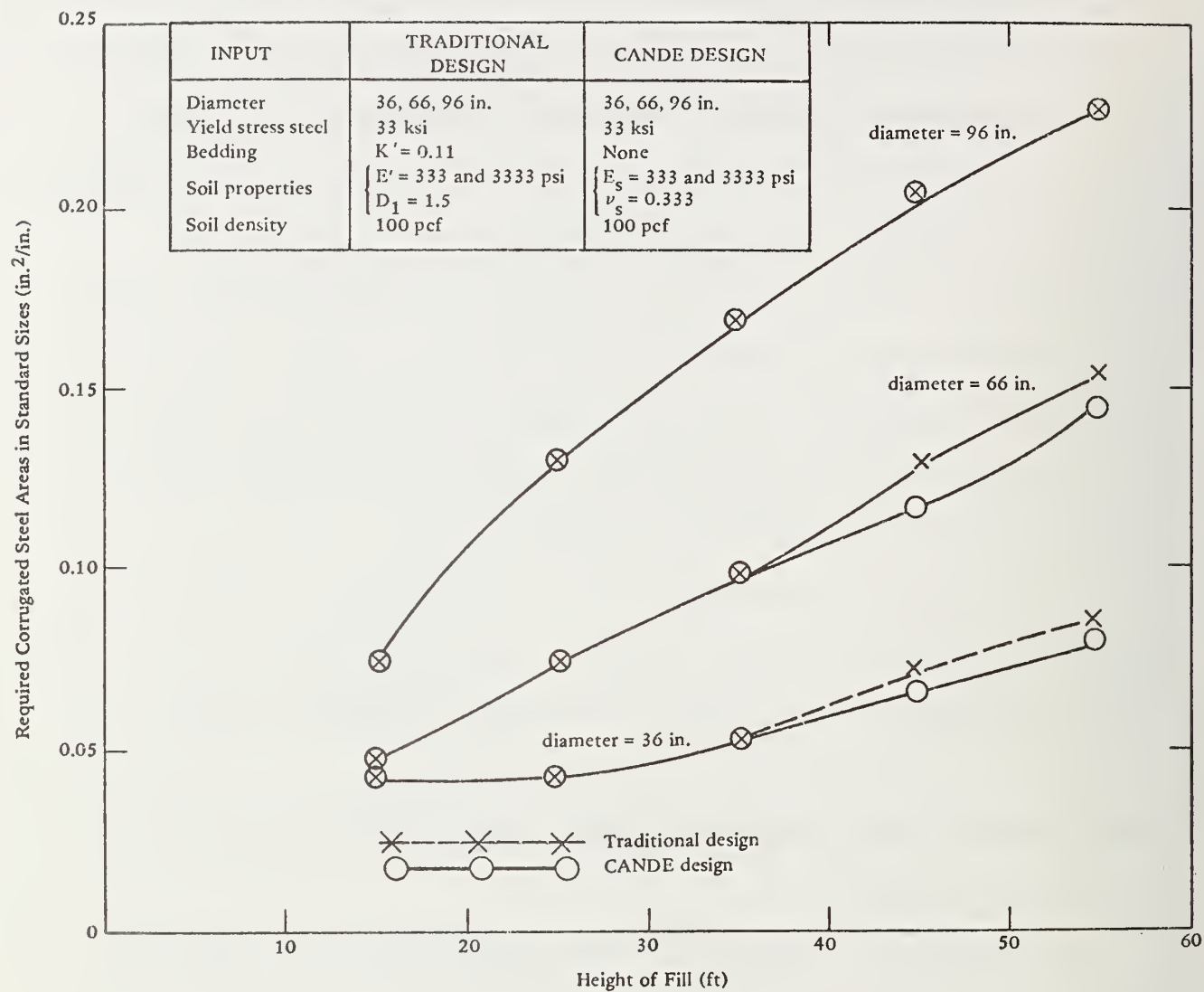


Figure 10-23. Corrugated steel area designs for 36-, 66-, and 96-inch pipes.

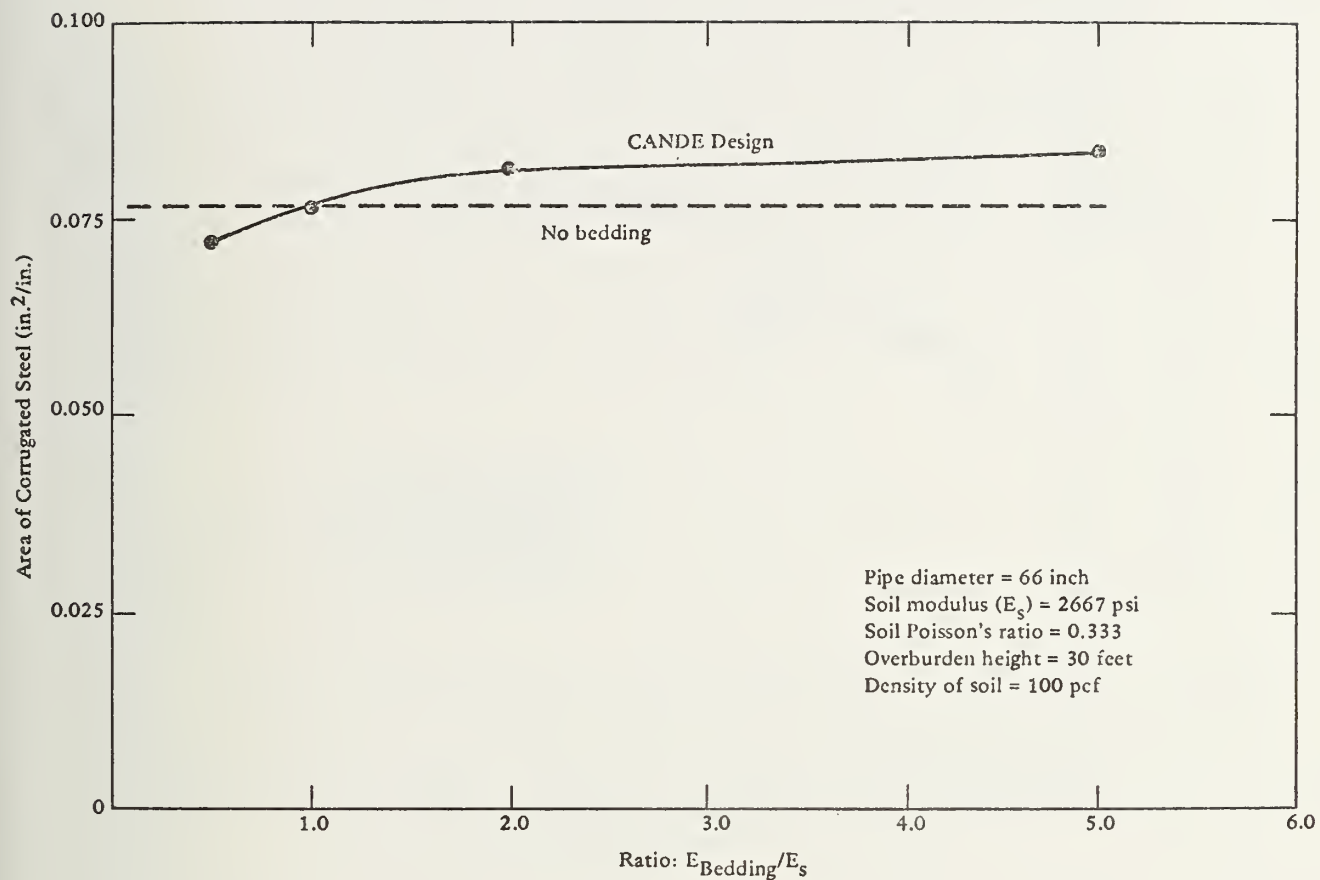


Figure 10-24. Corrugated steel area designs for increased bedding stiffness.

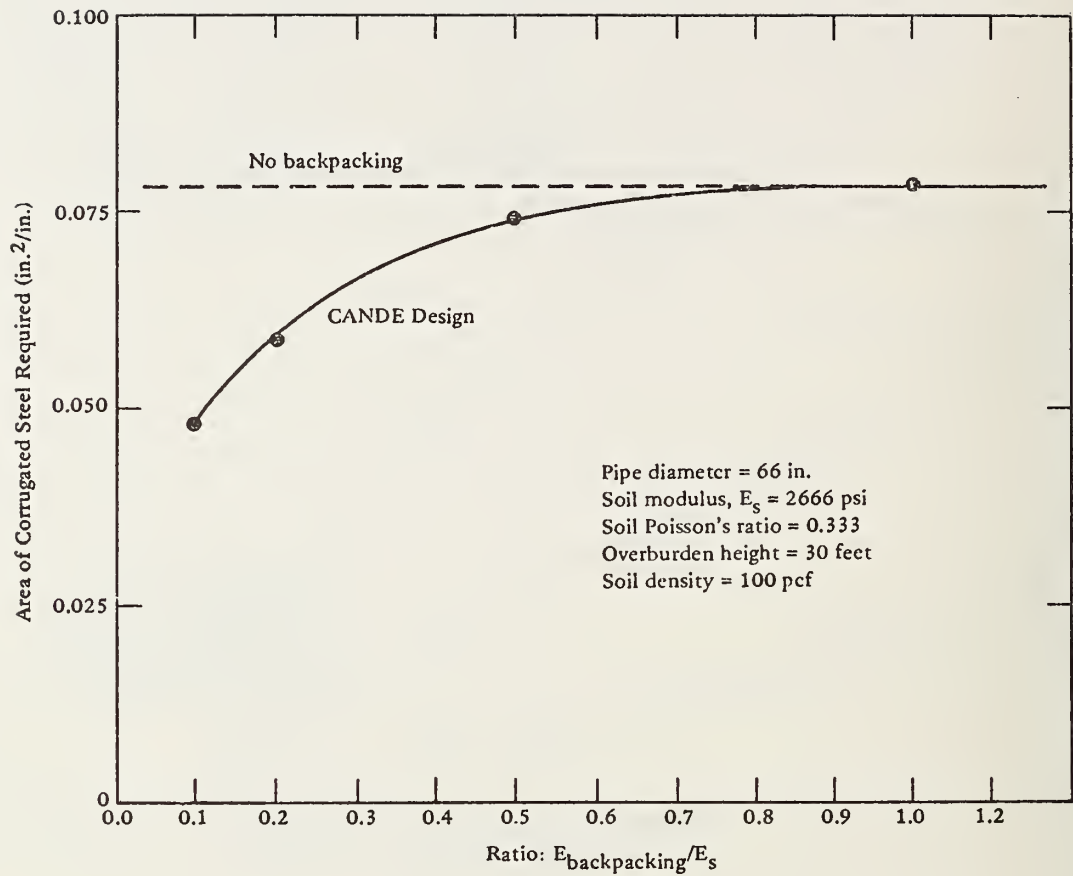


Figure 10-25. Corrugated steel area designs for a range of backpacking stiffness.

actually has a slight adverse effect with increased bedding stiffness. The AASHTO designs do not exhibit any influence of bedding when ring compression controls the design.

Lastly, the influence of backpacking modulus on required corrugated steel area is shown in Figure 10-25 for 66-inch-diameter pipe under 30 feet of fill. The design predictions are based on Level 2 solutions of a 5-inch backpacking ring completely surrounding the pipe. Backpacking modulus is varied from 0.1 to 1.0 times the soil modulus with the results that soft backpacking can substantially reduce the required steel area. Note, backpacking designs are outside the scope of traditional design methods. To test and evaluate new design concepts is a primary objective of CANDE.

### 10.3 EXPERIMENTAL COMPARISONS

Results from CANDE models are compared with ASTM D-load strengths for reinforced concrete pipe, followed by comparisons with prototype test culvert data obtained from California Department of Transportation [10-3].

#### 10.3.1 CANDE and D-Load Comparisons

The concrete design comparisons of the previous section demonstrate a significant difference of required reinforcing steel area (or allowable

fill height) between CANDE and ACPA design methods. Accordingly, it is of practical interest to compare CANDE predictions of reinforced concrete pipe behavior with D-load test results to ascertain the validity of the concrete pipe model independently of the soil system. To this end, the ASTM C-76 D-load tables constitute a set of data from three-edge bearing tests such that, for a given pipe diameter, up to five strength classes are defined by successively higher D-load ratings for both the cracking load,  $D_{0.01}$ , and the ultimate load,  $D_{ult}$ . Within each strength class, up to three wall designs are declared equivalent and are called wall A, B, and C. Wall A has less concrete but more steel than wall B, as does wall B with respect to wall C.

Since the ASTM D-load ratings are known to be conservatively low values, the corresponding CANDE model of each concrete pipe is conservatively assigned zero tensile strength for concrete cracking as was done for design comparisons. It was previously noted that pipe performance is sensitive to tensile strength (e.g., predicted loads to produce a 0.01-inch crack may increase 50% or more when full tension resistance is specified).

With the above understanding, Level 3 of CANDE is used to model three-edge bearing test, and predictions for D-loads causing 0.01-inch crack widths, initial steel yielding, and ultimate load are calculated for each specified ASTM C-76 wall designation for a 60-inch-and 90-inch-diameter pipe with circular reinforcement cages. Figures 10-26 and 10-27 show the comparison of CANDE D-load predictions with the



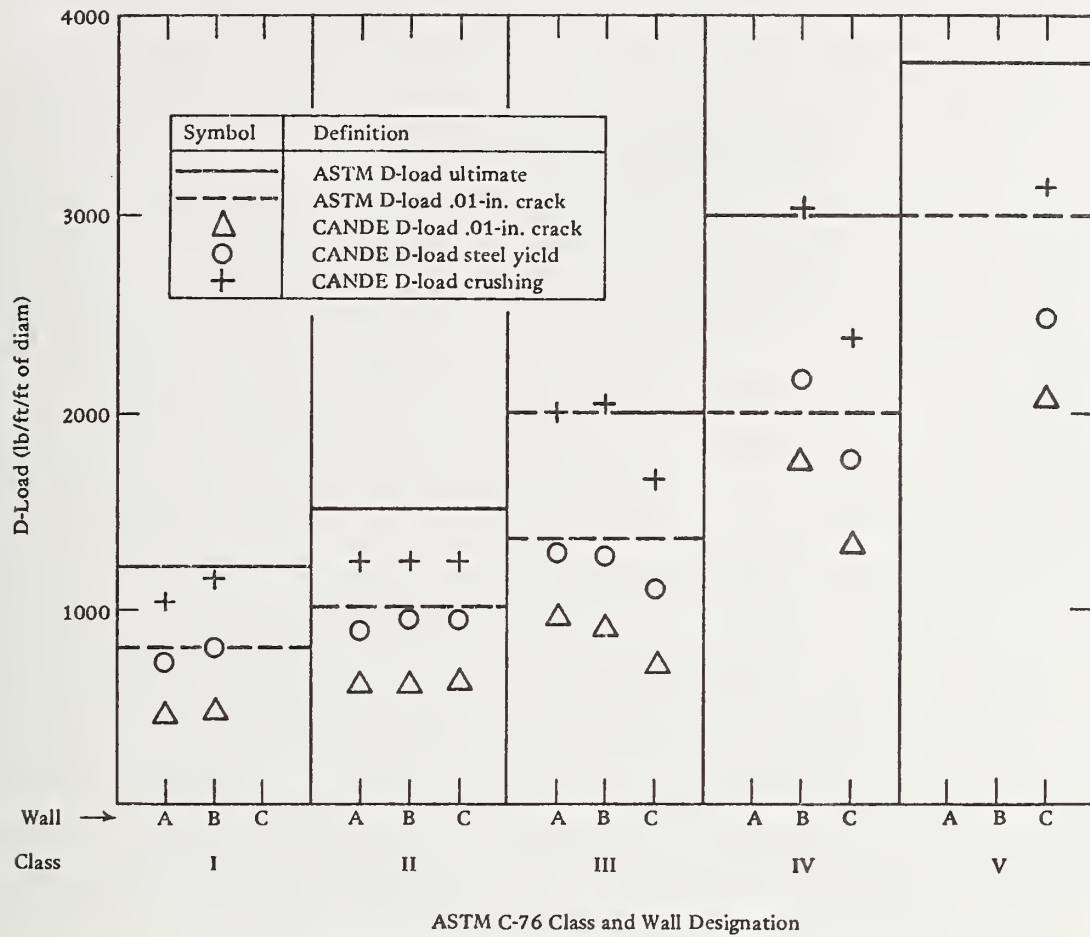


Figure 10-26. D-load comparisons for 60-inch pipe.

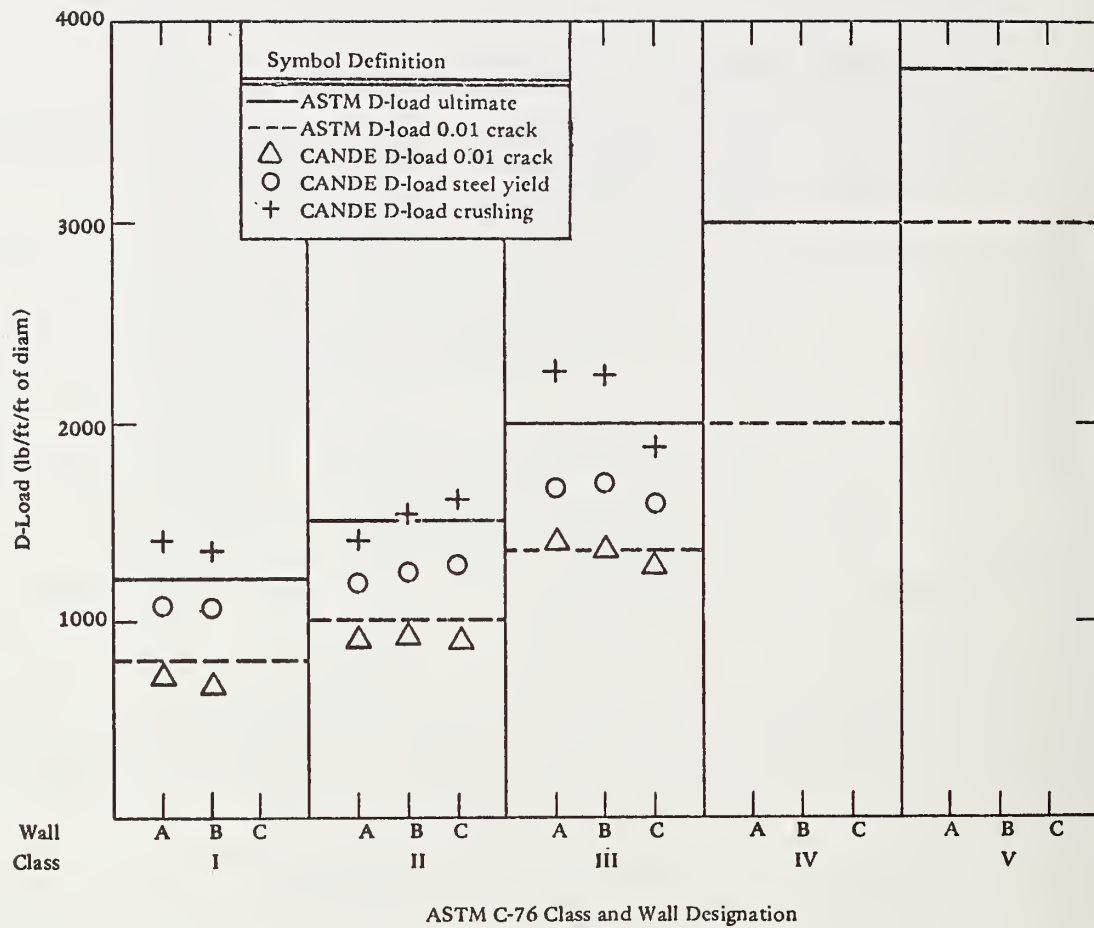


Figure 10-27. D-load comparisons for 90-inch pipe.

corresponding ASTM D-load strength classifications for both pipe diameters, respectively. Within each strength class, the dashed line denotes the ASTM D-load for cracking and the solid line is the ASTM D-load for ultimate. CANDE predictions are denoted by discrete symbols for each individual wall type specified in the ASTM tables (absent symbols implies no ASTM wall design is specified).

It is observed that the CANDE predictions for D-load cracking using zero tensile strength are consistently on the conservative side of the corresponding ASTM rating, more so for the 60-inch pipe than the 90-inch pipe. Comparisons between ASTM ultimate D-loads and CANDE D-loads for concrete crushing correlate quite well on the average. The significant observations to be kept in mind is that CANDE results follow the trends of the ASTM ratings, but are on the conservative side, particularly with respect to D-load cracking.

The above observation indicates that the reduced reinforcing steel requirements predicted by CANDE in the previous section are not due to CANDE's reinforced concrete pipe model, because CANDE D-load results are below ASTM ratings. Rather, the difference between traditional and CANDE design predictions must be attributed to the treatment of soil-structure interaction. It has been emphasized throughout this writing that the shortcoming of traditional methods is the lack of proper representation of soil-structure interaction. Consequently, it is contended in this report that the traditional ACPA design method is too conservative in assessing the increased strength characteristics of buried pipe. This contention is supported in the next section.

### 10.3.2 California Experimental Test Culverts

The current California culvert research program, called the Cross Canyon Project, is an extraordinarily well-conceived and well-executed experimental culvert test program. The scope of the project includes investigation of corrugated steel and reinforced concrete test culverts that are divided into different testing zones. For each zone various installation configurations are examined, including: embankment, trench, imperfect trench, polystyrene backpacking, and a host of bedding parameters. The reinforced concrete culvert is an 84-inch inside diameter pipe with an 8-inch wall thickness designed with four D-load strength classes. The corrugated steel culvert is a 120-inch nominal diameter pipe constructed with 12-gage, 6 x 2-inch corrugated structural plate. Final fill heights for both test culverts range from approximately 150 to 190 feet.

In addition to these test culverts, a functional 96-inch-diameter prestressed concrete pipe is included in the experimental investigation with a maximum fill height of approximately 200 feet.

Strain gages and special soil pressure gages are located on the pipe periphery to measure both normal and shear traction. Pipe displacements, soil settlements, and rigid body rotations are also measured. Laboratory tests include stress-strain measurements of all culvert materials and inclusions, as well as, triaxial and other standard soil tests for each soil zone.

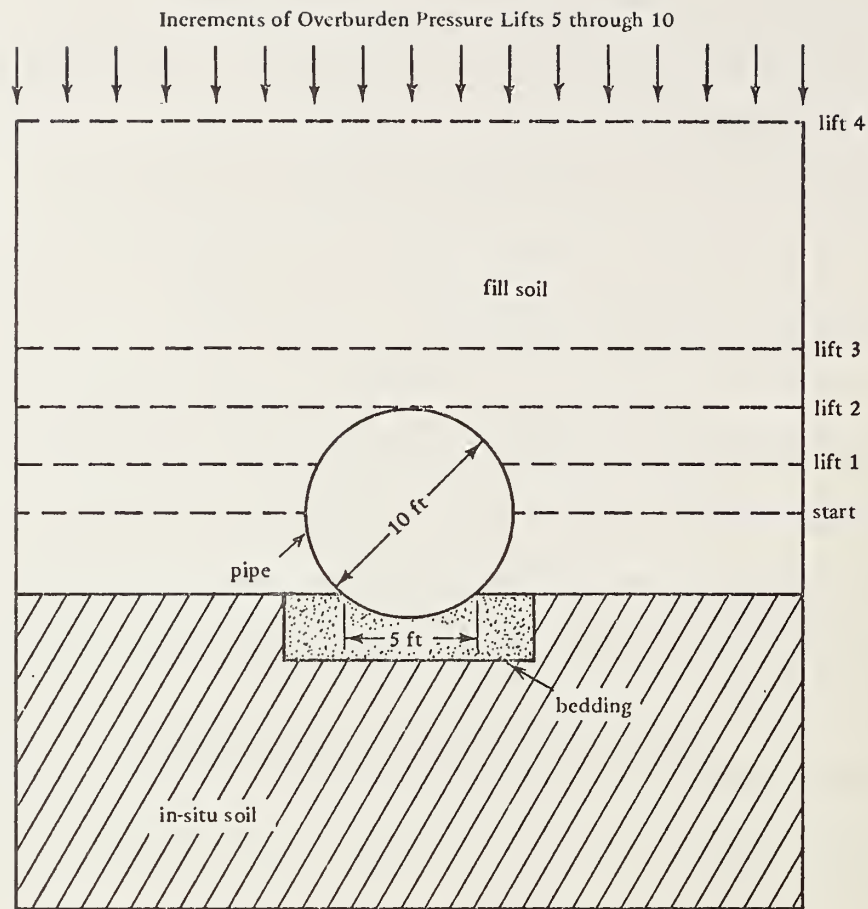
At the time of this writing, much of the experimental data was not yet reduced; only pipe displacement data are currently available along with some soil data. The available data are used in this study for comparison with CANDE predictions. To this end, zone 4 of both test culverts are investigated and are described in the next section.

### 10.3.3 CANDE Model of Test Culverts

Since experimental data are currently limited, the approach adopted herein is to simplify the CANDE model commensurate with available data. Accordingly, the objective is to determine if CANDE can predict the trend of the pipe displacements without the aid of sophisticated modeling techniques, such as, slipping interfaces or the Extended-Hardin soil model. Further, the Level 2 finite element mesh configuration is employed with minor modifications to approximate soil zone boundaries and loading schedules.

Figure 10-28 illustrates the embankment configuration of zone 4 for the corrugated metal test culvert along with wall properties of the steel pipe. Similarly, Figure 10-29 illustrates the positive projecting trench condition of zone 4 for the reinforced concrete culvert along with reported wall properties.

Tensile concrete cracking strain is taken at  $1/3$  of the value determined from concrete tensile tests because of the numerous temperature cracks in the pipe prior to loading.



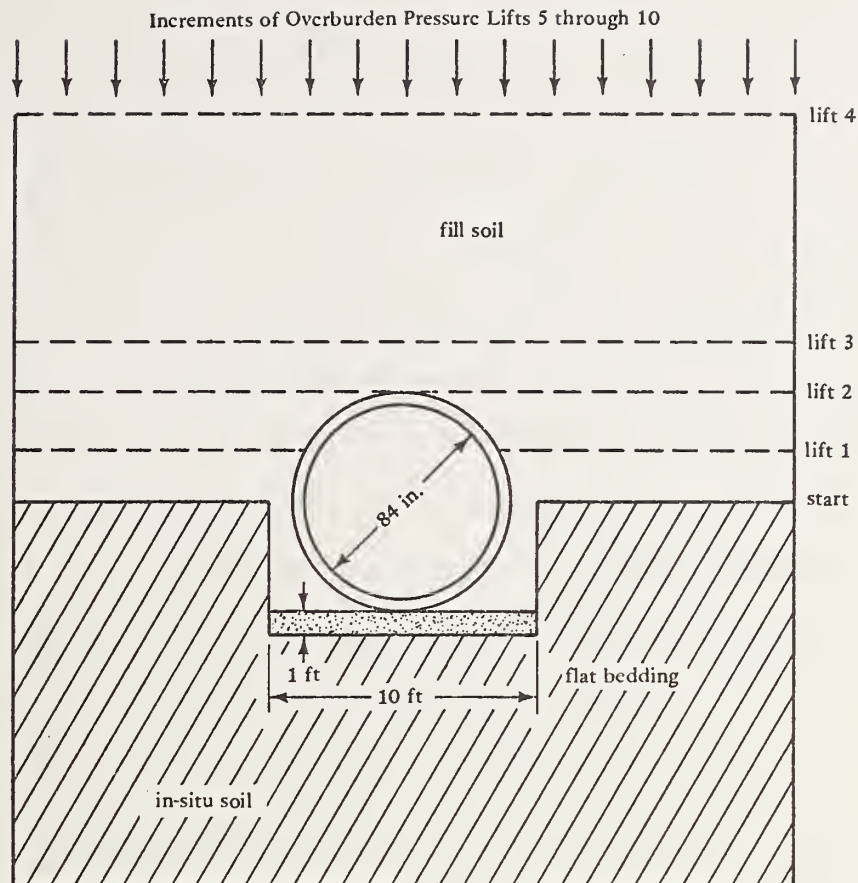
Steel pipe, \* 12 gage, 6 x 2-inch corrugation:

Thrust area =  $0.1296 \text{ in.}^2/\text{in.}$   
 Moment inertia =  $0.0604 \text{ in.}^4/\text{in.}$   
 Section modulus =  $0.0574 \text{ in.}^3/\text{in.}$   
 Young's modulus =  $30 \times 10^6 \text{ psi}$   
 Poisson's ratio = 0.3  
 Yield stress = 33000 psi

\* Modeled with bilinear stress-strain curve.

Figure 10-28. Representation of zone 4 for corrugated steel test culvert.





Circularly Reinforced Concrete Pipe, 84-Inch Diameter	
Concrete Wall	Steel Cages
Wall thickness = 8.0 inch Compressive strength = 5700 psi Cracking strain = 0.00004 in./in. Yielding strain = 0.00072 in./in. Crushing strain = 0.002 in./in. Young's modulus = $3.85 \times 10^6$ psi Poisson's ratio = 0.17	Inner steel area = 0.0283 in. <sup>2</sup> /in. Outer steel area = 0.0225 in. <sup>2</sup> /in. Cover depth = 1.1 in. Yield stress = 60000 psi Young's modulus = $29 \times 10^6$ psi Poisson's ratio = 0.30

Figure 10-29. Representation of zone 4 for reinforced concrete test culvert.

For both test culverts the initial configuration for starting the analysis is with fill soil up to the springline. Thereafter, the loading schedule is as shown by the dashed lines. That is, lift 1 is one-fourth diameter above springline, lift 2 is one-half diameter, lift 3 is three-fourths diameter, and lift 4 is two diameters. Subsequent loading is applied in equivalent increments of overburden pressure. In addition to the gravity loads, temporary 5-psi surcharge pressures are applied to the surface of each lift between springline and crown to account for loads from compaction equipment. As each new lift is added into the system, the temporary surcharge pressure on the previous lift is removed by applying the opposite pressure. This process promotes inward horizontal movement of the pipe through lateral pressure due to the Poisson effect.

The in-situ soil zones for both the concrete and metal test culverts are assumed linear elastic with a Young's modulus of 2,000 psi and a Poisson's ratio of 0.4. This assumption is based on engineering judgment as no in-situ soil data are currently available. However, for the fill soil surrounding the pipes and the bedding materials, triaxial test data are available. Inspection of these data reveals that the behavior of all soil zones is similar. Therefore, in keeping with the simple modeling concept, a single overburden dependent soil model (see Chapter 5) is used to characterize all soil zones except the in-situ soil. To determine the overburden-dependent curve shape for Young's modulus, Poisson's ratio is taken as 0.4, and triaxial data are used as follows. Tangent values of Young's modulus are computed by dividing the axial stress increment by

the axial strain increment for all stress states representative of confined compression, such that the ratio of the axial pressure-to-lateral pressure is approximately 1.5 (i.e., consistent with Poisson's ratio = 0.4). Figure 10-30 shows the tangent moduli values calculated from triaxial data at four confining pressures for each material zone. Scatter of data is apparent, and no clear trend between individual soil zones is observed. However, viewed as a whole, the data illustrate a rather well-defined overburden-dependent curve shape. In particular, the solid line represents a lower bound data fit and forms the basis of the overburden-dependent model used herein. Lower-bound fits of controlled laboratory tests are usually more representative of actual field performance than are curve fits of average values because of quality control.

Table 10-2 presents discrete tangent modulus values from the curve fit and the corresponding secant modulus for specified ranges of overburden pressure. Soil density for the fill soil is 130 pcf. The above modeling assumptions and data constitute the CANDE model.

#### 10.3.4 CANDE Predictions and Experimental Data

Measured horizontal and vertical diametrical deflections for the corrugated metal culvert are shown in Figure 10-31 along with corresponding predictions from CANDE. The deflections are shown as a function of fill height above the springline. Accordingly all experimental data [10-3] are

Table 10-2. Soil data<sup>a</sup> for CANDE Models of Test Culverts

(Overburden dependent modulus values for all zones except in-situ soil.)

Overburden Pressure Range (psi)	Young's Tangent Modulus (psi)	Young's Secant Modulus (psi)
0 - 2	750	750
2 - 5	950	860
5 - 10	1,200	1,000
10 - 20	1,800	1,280
20 - 30	2,300	1,500
30 - 40	2,800	1,700
40 - 60	3,200	2,000
60 - 80	3,800	2,300
80 - 100	4,200	2,500

<sup>a</sup>Soil density for all soil above springline = 130 pcf

Poisson's ratio for all zones = 0.4

Young's elastic modulus for In-situ soil = 2,000 psi

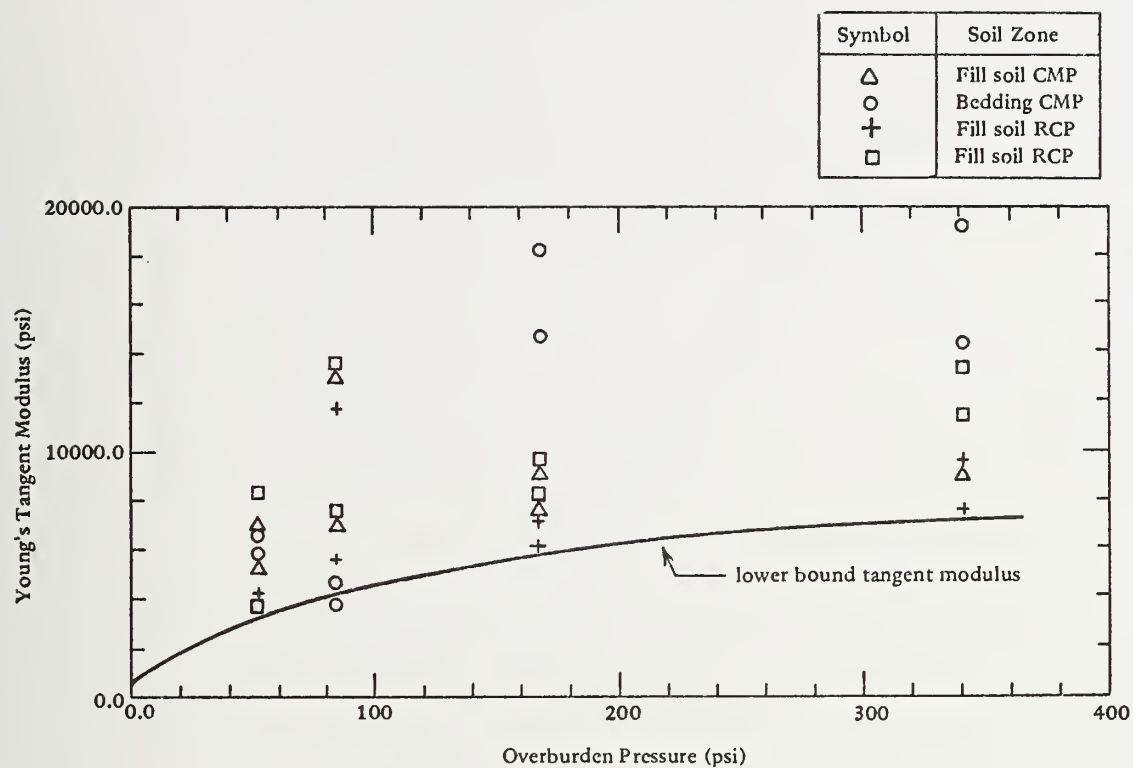


Figure 10-30. Young's tangent modulus from triaxial test.

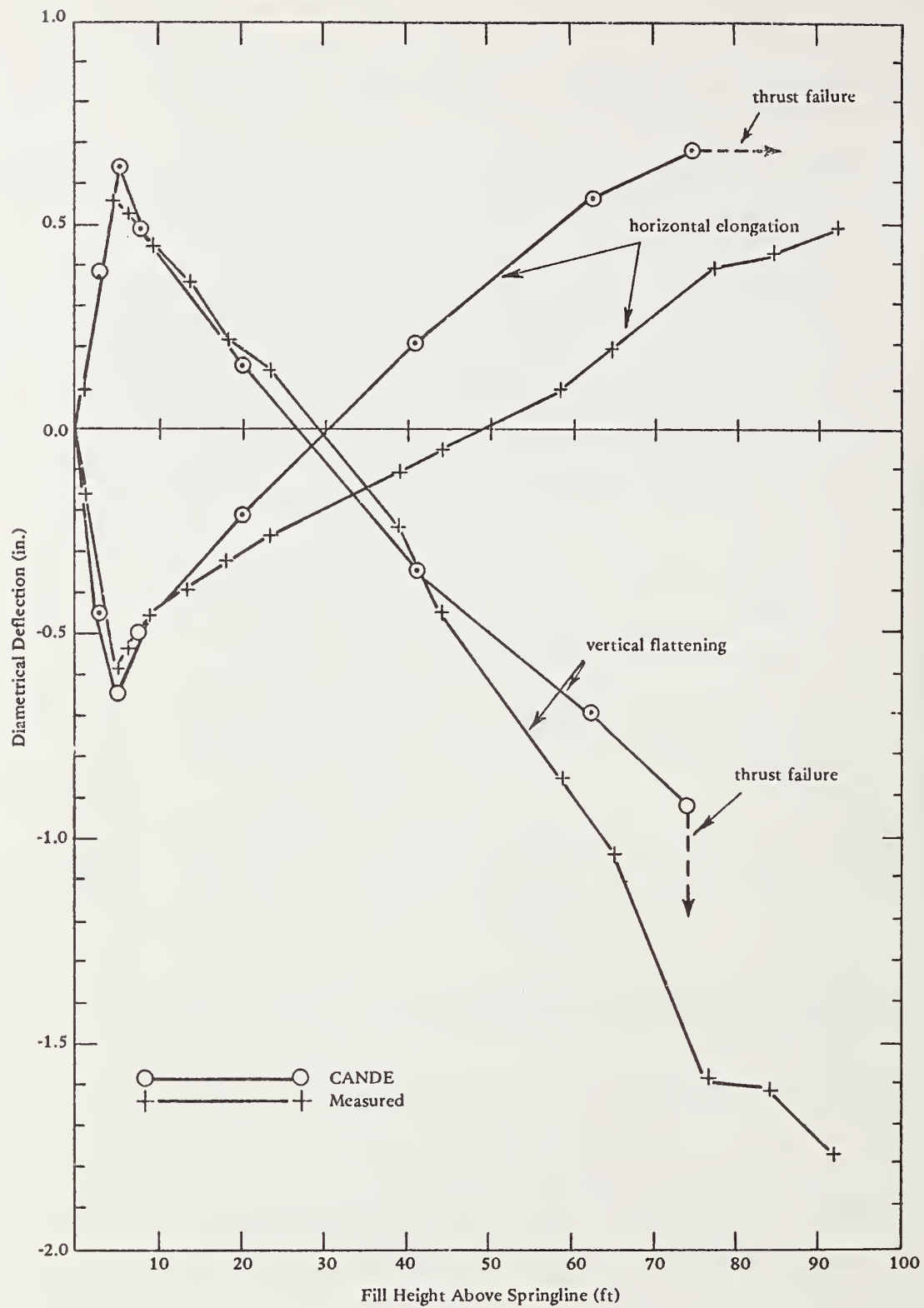


Figure 10-31. Horizontal and vertical diametrical deflections for corrugated steel test zone 4.



referenced with respect to the springline (i.e., the initial displacements due to fill up to the springline are subtracted).

During the first 5 feet of fill above the springline, the pipe moves horizontally inward and elongates vertically. Thereafter, the shape change reverses direction, resulting in horizontal elongation and vertical flattening. The CANDE predictions mimic these trends with remarkably close agreement in view of all the modeling simplifications. At about 20 feet of fill the CANDE predictions for horizontal deflection begin to diverge from observed values. The reason for this discrepancy is because the overburden-dependent soil model is insensitive to lateral pressures developing at the springline. That is, as horizontal movement reverses direction, lateral springline soil pressure builds up and exceeds the springline vertical soil pressure. However, the overburden-dependent model is strictly a function of vertical pressure and is unaware of increased lateral confining pressure. Consequently, the soil model in the vicinity of the springline does not stiffen sufficiently to retard the horizontal movement at the same pace as is actually observed. Apparently, if a soil model sensitive to confining pressure had been employed (e.g., Extended-Hardin soil model), the predicted horizontal displacements would have been reduced.

Perhaps the most significant observation of the experimental data is the abrupt increase in the vertical deflection between 65 and 75 feet of fill, suggesting initial wall compression failure. Indeed, at 88 feet of fill, tearing of the bolted springline seam was clearly visible to the

inspection team. In excellent correlation with these data, CANDE predicts initial thrust compression yielding at the springline at 74 feet of overfill (indicated by the dashed lines in Figure 10-31). It must be noted, however, that after substantial tearing and separation of the springline seam, the test culvert withstood the full fill height (more than 150 feet) without collapse.

Figure 10-32 displays experimental and predicted diametrical deflections for the reinforced concrete pipe in the same fashion discussed above. Experimental data and CANDE predictions are in extraordinarily good agreement over the entire fill height range. Due to the relative stiffness of the concrete pipe, lateral soil pressures at the springline do not exceed the vertical gravity pressures; consequently, the overburden-dependent soil model is more representative of soil behavior than is the case of the corrugated metal pipe.

The first observed 0.01-inch crack (1 foot in length) occurs at the invert with 45 feet of fill above springline. CANDE also predicts the first 0.01-inch crack to occur at the invert with 53 feet of fill, clearly a satisfactory correlation in view of the random nature of crack propagation.

At approximately 125 feet of fill, spalling of concrete was observed at the invert; however, the pipe continued to carry the entire fill load of approximately 190 feet without collapse. CANDE results predict initial steel yielding to occur at the invert at 100 feet of fill, at which time the safety factor against concrete crushing is 1.6.

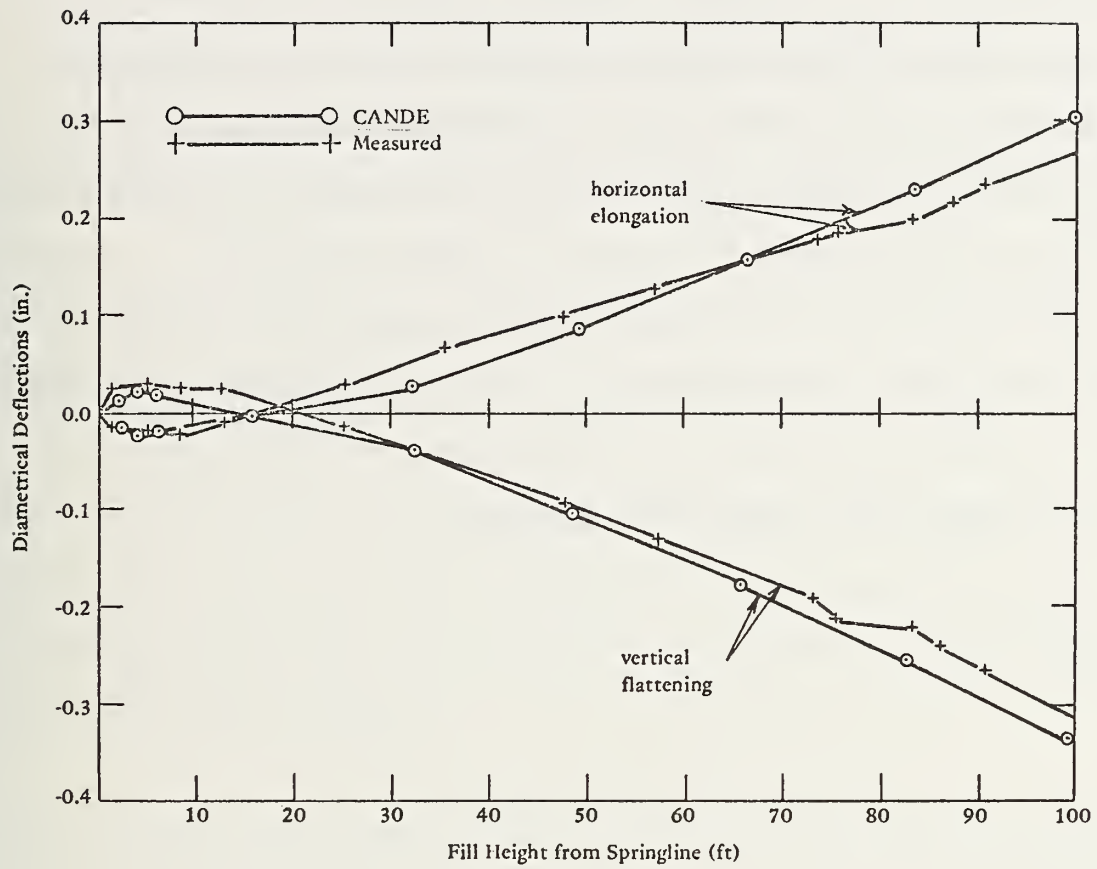


Figure 10-32. Horizontal and vertical diametrical deflections for reinforced concrete test zone 4.

It is interesting to note the traditional design fill height for the reinforced concrete culvert based on allowable 0.01-inch crack (Class I, wall B) is less than 16 feet of overfill. However, the actual fill height for 0.01-inch cracking is almost triple this amount. This finding supports the contention that traditional concrete designs are often overly conservative.

In summary, CANDE predictions demonstrate good agreement with the horizontal and vertical deflections for both the corrugated metal and reinforced concrete test culvert sections. Furthermore, observed measures of wall distress correlated well with the CANDE predictions.

The foregoing illustrates the potential of the CANDE program to adequately predict culvert behavior. It is hoped that further validation of the program will continue in the future with all Cross Canyon test data and other data as they become available.

FINDINGS AND CONCLUSIONS

In Chapter 9 the theoretical developments and limitations of CANDE were summarized along with recommendations for use and future extensions. In this Chapter the results and findings of CANDE applications are summarized.

Based on the investigation reported herein, the following findings and conclusions appear valid:

1. The elasticity solution (Level 1) and the finite element solution (Levels 2 or 3) are in excellent agreement for corresponding homogeneous linear systems. For nonlinear systems correlation is good to fair depending on the degree of nonlinearity.
2. Soil pressure acting on the crown of a corrugated metal pipe is generally less than corresponding soil column pressure, and conversely for reinforced concrete pipe. However, a crown soil pressure less than the column pressure does not imply the springline thrust force is less than the column weight. On the contrary, because of shear traction and pressure distributions,

springline thrust generally exceeds soil column weight; however, it is less so for corrugated metal culverts than for concrete culverts.

3. Thrust at the springline is relatively insensitive to soil modulus, pipe modulus, and pipe section properties within the practical range of these parameters. However, a ring of backpacking material around the pipe whose stiffness is one-tenth of the surrounding soil can reduce thrust by 50%.

4. For corrugated metal culverts, outer-fiber yielding due to bending stress is to be expected under design loading. Increasing the corrugation size (moment of inertia) limits deflections but generally increases bending stress.

5. For reinforced concrete pipe, crack width and pipe performance is sensitive to the tensile strength of concrete. Increasing percentages of reinforcing steel increases the structural capacity almost proportionally.

6. Decreasing the friction between the pipe-soil interface shifts the normal pressure distribution on the pipe so that it appears close to hydrostatic. However, the maximum moments increase slightly due to loss of interface shear traction.

7. Increases in bedding height, width, and stiffness do not appreciably improve the plane-strain structural capacity of the culvert system for



either reinforced concrete or corrugated metal pipes. In most cases stiff bedding configurations adversely affect the structural performance. Soft beddings produce significant decreases in peak structural responses. However, it is recognized that bedding plays an important role in longitudinal effects.

8. Imperfect trench configurations significantly improve the structural capacity of both reinforced concrete and corrugated metal culverts with a greater influence on concrete. Optimum size of the imperfect trench appears to be 1.2 pipe-radii deep and 2.4 pipe-radii wide filled with a soft modulus material one-tenth as stiff as the surrounding soil.

9. Varying the initial shape of a corrugated metal culvert from a 10% horizontal ellipse to a 10% vertical ellipse significantly reduces moments and displacements but has negligible affect on thrust.

10. Design comparisons between CANDE and traditional methods for reinforced concrete pipe with Class C bedding reveal that CANDE permits substantially deeper fill heights (or, alternatively, reduced steel area requirements) prior to 0.01-inch cracking. For Class A beddings, the traditional method allows for a substantial reduction in reinforcing steel. Accordingly, for this case, design results are similar between CANDE and traditional methods.

11. Design comparisons between CANDE and the AASHTO design method for corrugated steel pipe display close agreement for required corrugated steel area. Thrust stress controls the design of both methods for the systems investigated. Increasing the bedding stiffness does not appreciably alter the design requirements of either method. However, inclusion of a soft backpacking ring in the CANDE design reduces steel area requirements by nearly one-half.

12. Results from CANDE models of reinforced concrete pipe D-load tests follow the same trends as the D-load ratings from ASTM C-76 tables. CANDE D-load predictions for 0.01-inch cracking are generally on the conservative side of ASTM ratings, because zero tensile strength is specified. Based on these results, it is concluded that the difference between the concrete design results of CANDE and the traditional method is attributed to the treatment of soil-structure interaction and not the treatment of the concrete pipe itself.

13. CANDE predictions for vertical and horizontal diametrical deflection paths are in good general agreement with experimental data for a 10-foot-diameter corrugated steel culvert. Initial wall compression yielding is apparent between 65 to 76 feet of fill, and CANDE predicts thrust yielding at 74 feet of fill.

14. Experimental results and CANDE predictions are in excellent correlation for horizontal and vertical diametrical deflection paths for an 84-inch reinforced concrete pipe culvert. Initial 0.01-inch cracking of 1-foot length occurs at the invert with 45 feet of fill. Likewise, CANDE predicts the first 0.01-inch crack to occur at the invert at 53 feet of fill, whereas the traditional design method implies a 0.01-inch crack occurs with less than 16 feet of fill. This finding supports the contention that traditional concrete design procedures are sometimes overly conservative.



## Appendix A

### DURABILITY (CORROSION AND ABRASION)

The purpose of this appendix is to cite recent key studies on corrosion and abrasion in culverts and to provide suggestions for corrective measures. Good summaries of the basic aspects of corrosion are given in References A-1 and A-2. Hence, such background need not be repeated here. Principal deductions and conclusions therefrom are as follows:

- (1) The culvert durability problem is a complex one that has not yet been completely solved.
- (2) Corrosion damage is usually most severe at the invert intrados.
- (3) Efforts to find a correlation between corrosion and measurable properties of water and soil have been generally unsuccessful.
- (4) The only well-defined corrosion correlation is with pH. Below a pH of approximately 4 a high rate of metal loss will occur with most metals; above a pH of 4 metal loss may or may not occur.

(5) A statistical average corrosion rate technique [A-2] appears to hold the most promise for near-term use.

(6) There is little variation in the corrosion rate of mild steel for pH values between 4 and 9.5 if the temperature and oxygen concentration stay constant.

Guidelines for taking corrosion losses into account are recommended in NCHRP-116 [A-1] as follows:

(1) Determine the pH at the site under normal flow conditions.

(2) Determine the flow velocity through the culvert at peak design flow.

(3) For  $\text{pH} < 4.5$ , use a protective coating or reinforced concrete culvert.

(4) For  $\text{pH} > 4.5$  and galvanized steel, add an allowance for metal loss using the New York Method [A-1,A-2].

(5) For  $\text{pH} > 9$ , do not use aluminum pipe.

(6) For peak flow velocities  $> 8$  fps, pave the invert.



Several additional studies have been published since the printing of NCHRP-116, including two on steel pipe [A-3, A-4] and one on aluminum pipe [A-5]. In the latter study it is recommended that "...bare aluminum alloy pipe be allowed in areas where the pH of the soil or water is between 4.5 and 9 and where soil resistivity is greater than 1000 ohm-cm."

Resistivity is largely a measure of salt concentration, as pH is a measure of hydrogen ion concentration. Neither of these are sensitive to oxygen concentration and other factors influencing corrosion. It follows that a corrosion criteria based on pH or on pH and resistivity may be inadequate. Other factors that may influence corrosion include:

#### On Soil-Side

- (1) Ions other than hydrogen - sulfides, sulfates, etc. - influenced by unstable groundwater conditions.
- (2) Soil bacteria (aerobic and anerobic) - particularly sulfate-reducing bacteria.
- (3) Oxygen content of soil - influenced by grain size, porosity, etc.

- (4) Difference in oxygen and water content.
- (5) Water content and quality.
- (6) Stray currents.

On Inside

- (1) Water hardness and acidity.
- (2) Dissolved oxygen content.
- (3) Flow velocity.
- (4) Temperature.

Inside corrosion may also be influenced by accompanying abrasion.

Reportedly, sand is transported at stream velocities of 4 to 6 fps, while cobbles require 20 to 30 fps. Naturally, the character of the upstream bed in conjunction with the flow velocity and duration will largely govern whether or not abrasion damage occurs. A reasonable relationship for defining abrasion might be

$$A_b = K_{bn} f v_f^2 T_b$$

where  $A_b$  = rate of abrasion

$f$  = upstream bed fineness

$v_f$  = average flow velocity through culvert

$T_b$  = duration of flow per time period

$K_{bn}$  = empirical constant for given pipe type,  $n$

Good suggestions for minimizing abrasion are given in Reference A-6.

They include:

- (1) Design the culvert entrance to reduce rock flow.
- (2) Reduce the velocity of approach wherever possible.
- (3) Use deep corrugations to slow rock flow.
- (4) Increase the metal gage in the region of the invert.
- (5) Use oversize pipe where necessary to further reduce flow velocities.

Reinforced concrete pipe is subject to abrasion and corrosion damage as is metal pipe, although the processes are somewhat different. Ionic corrosion on the intrados is usually insignificant in concrete pipe, providing freeze-thaw damage is precluded. Discussions of corrosion in concrete pipe may be found in Reference A-1.

Quantifying the above cited corrosion and abrasion factors into a criteria that is usable in a quantitative design presents a challenge that has not yet been achieved. Perhaps the closest anyone has come to this is the New York method employing a durability index [A-2, A-7]. The durability index is a number composed of the sum of numerical ratings assigned to the four categories: surface water corrosiveness, abrasiveness, flow, and service importances. Unfortunately, the ratings are based largely on judgment rather than measured quantities. Hopefully, a more completely quantified durability index will be forthcoming.

An effort to gather together all available information on durability has been initiated under the National Cooperative Highway Research Program (NCHRP) Synthesis Project 20-5, Topic 5-09: Durability Drainage Study.

## Appendix B

### EMBANKMENT CONSIDERATIONS

#### CRITERIA

Culverts should be thought of as components of embankments; it is the embankment that envelopes the culvert and provides the support needed to maintain the opening. Clearly, if the embankment performance or that of its foundation is faulty, it will adversely affect culvert performance.

It is not the purpose here to offer a dissertation on embankment design, construction, and performance; that has been accomplished elsewhere, e.g., References B-1, B-2, and B-3. Rather, the purpose is to cite and discuss embankment criteria, particularly those dealing with soil characteristics, that influence culvert criteria, design, and behavior.

An embankment must meet general criteria as follows:

- (1) The slopes must be stable during construction and under load - including earthquakes.
- (2) Design and construction must be such as to avoid excessive stresses in the foundation or undue settlement thereof.

- (3) Seepage, fluid flow from consolidations, and other ground water must be controlled to avoid internal erosion and excessive settlement.
- (4) The slopes must be protected against erosion.
- (5) Materials and design stresses should be selected to avoid excessive creep and to assure long-term stability.

#### PROBLEM AREAS

Culvert designers should consider the quality of the embankment construction with the same care as the fabrication and quality of the pipe. Admittedly, control over the embankment materials and construction is difficult; nonetheless, with diligent inspection and courage to reject unacceptable materials or workmanship, proper embankment structures can be erected.

Some of the factors which should be considered in embankment and culvert backfill design are:

- (1) There is considerable variation in the behavior of soils at small strains (in the  $< 10$ -psi stress regime).



- (2) Uniform round rock backfill may act like ball bearings and cause grave problems (lack of interlocking impairs shear strength). Problems stem from an inability to adequately compact uniformly sized particles.
- (3) Moisture content is a serious and continuing problem with silty soils and swelling clays.
- (4) Soft foundation soils may cause large lateral displacements, excessive settlement, and gross differential movements in embankments.
- (5) Accumulation of water within an embankment increases the tendency for sliding.
- (6) In cuts, newly exposed material tends to expand because of removal of the overburden and moisture variations at the surface.
- (7) Serious structural deficiencies can arise from attempting to either compact partially frozen soil or to add water to freezing or frozen soils.

- (8) Capillary rise or moisture from lower levels may cause significant changes in load, soil strength, and stiffness.
- (9) Creep of the soil skeleton or long term consolidations, where original soil is heavily overloaded, may result in large culvert deformations.
- (10) Prediction of the field strength of cohesive soils based upon laboratory tests is considerably more complicated than for cohesionless materials. It is not presently possible to compact cohesive soil in the laboratory so that it will behave the same as the same soil compacted in the field.
- (11) The materials used in an embankment may vary from layer to layer due to the character of natural deposits.
- (12) Reliance on density criteria alone may result in serious over or underdesigns.
- (13) Poisson's ratio increases with increasing relative density. Values of  $\nu$  vary widely depending on the compaction density and water content.

(14) Poisson's ratio is also quite sensitive to confining stress level and shear stress (or strain level).

(15) In regions subject to occasional or seasonal seepage flows, additional soil stresses may be incurred due to the seepage pressures (equal to  $i\gamma_w$ , where  $i$  is the hydraulic gradient and  $\gamma_w$  is the weight of water).

In summary, it is important to integrate design, construction, and soil control aspects to be complimentary factors for successful embankment-culvert installations.



## Appendix C

### LONGITUDINAL BENDING

The purpose of this appendix is to summarize the literature on longitudinal bending of buried pipes and to assess therefrom the consequent effects on culvert design. Longitudinal bending may stem from a variety of causes, including embankment foundation consolidation, a variable stiffness sub-base profile, and geodynamic deformations.

A method for approximating foundation consolidation based on Buisman's Law and an empirical relationship between the compressibility factor and the initial void ratio of the sub-base is given in NCHRP-116 [C-1]. The solution is based on an idealized cross section that consists of a compacted fill embankment over a compressible layer resting on a relatively incompressible basement media. Settlement is determined from the relationship

$$S = F L D \quad (C-1)$$

where  $S$  = settlement

$D$  = thickness of the compressible layer (CL)

$L = \log[(p_o + \Delta p)/p_o]$

$F = 0.156 e_o + 0.0107$

$p_o$  = natural overburden pressure

$\Delta p$  = applied load

$e_o = G_s (\gamma_w / \gamma_d) - 1$

$G_s$  = specific gravity of the CL particles

$\gamma_d$  = dry density of the CL

$\gamma_w$  = density of water

Equation C-1 does not account for shear; however, it should provide adequate predetermination of pipe camber where no preconsolidation stress exists.

Longitudinal bending due to foundations with a stiffness that varies along the pipe length (from large boulders or other causes) can be estimated by drawing on experience with footings. Footings only 20 feet apart are known to experience differential settlements as much as 50% of their total settlements.

As an alternate to Equation C-1, pipe settlement can be estimated from foundation theory by considering the pipe as a long footing, or it can be determined from the theory of beams on elastic foundations [C-2]. In either case, deflections of 50% of the calculated settlement should be presumed to act over a wavelength of 20 feet. For a worst-case condition, stresses from this "local" flexing should be superimposed on the bending attributable to load-settlement. Under this combined stress condition, as in actual practice [C-3], yielding in the longitudinal direction is not an uncommon experience.



Longitudinal bending stresses can be evaluated by several approaches, including that of Tschebotarioff [C-4]. This method (which is widely used in Europe) employs the basic flexure expressions:

$$M_L = \frac{E_L I_L}{\rho} \quad (C-2)$$

and

$$\sigma_{L_{\max}} = \frac{M_L}{I_L} \left( \frac{D}{2} \right) \quad (C-3)$$

with  $\rho$  approximated as,

$$\rho = L^2/8S \quad (C-4)$$

where  $M_L$  = bending moment in the longitudinal direction

$E_L I_L$  = pipe stiffness (longitudinal)

$\rho$  = bending radius of curvature, maximum

$\sigma_{L_{\max}}$  = maximum bending stress

$D$  = pipe diameter

$L$  = pipe length of concern

$S$  = settlement corresponding to  $L$

Combining the immediately preceding relationships one can obtain the maximum stress due to longitudinal bending in terms of the settlement as

$$\sigma_{L_{\max}} = \frac{4 S E_L D}{L^2} \quad (C-5)$$

Superposition may be employed to account for both the general and localized settlement; however, induced stresses from embankment caused settlement will usually be small compared to those from local settlements (wherein  $S_L = 0.5S$  and  $L = 20$  feet).

Longitudinal bending stresses will be reduced where pipe lengths are appreciably less than the settlement wavelength. Also, circumferential corrugations will tend to deter the development of longitudinal stresses and flattening deformations by virtue of their "bellows" type action. Severe ogee-shaped deflection occurred along a 20-foot length of a 20-foot-diameter multiplate culvert on the Peace River in Canada without failing the pipe. Cause of the longitudinal deformation was development of a slip plane in the embankment.

Vertical deflection (flattening) of a pipe from longitudinal bending can be estimated from the relationship

$$\frac{\Delta y_L}{D} = \frac{(1 - \nu^2)}{16(t_e/D)^2 (\rho/D)^2} \quad (C-6)$$

where  $\Delta y_L$  = vertical (flattening) deflection attributable to longitudinal bending

$\nu$  = Poisson's ratio of the pipe material

$t_e$  = effective wall thickness

$\rho$  = bending radius =  $E_L I_L / M_L = E_L D / 2\sigma_{L_{\max}}$

$\sigma_{L_{\max}}$  can be calculated from Equation C-5. If care is taken in achieving

a good foundation and bedding, distress from longitudinal bending effects will be avoided.



## Appendix D

### REVIEW OF STATE HIGHWAY DEPARTMENT PRACTICES

This appendix contains data on culvert backfilling and bedding practices used in various states and the Commonwealth of Puerto Rico. The purpose of assembling the data was to summarize the differences and similarities of present practices and to obtain input for parametric studies of these practices. The most frequently encountered configurations are evaluated with the analytical options of the CANDE program. The ultimate goal is to use the results of these evaluations as a basis for recommending improvements in current practices.

The data assembled here were obtained from 39 state highway departments and the Commonwealth of Puerto Rico, who responded to a form letter sent to every state highway department. This summary is based almost entirely on data provided in response to the letters sent to the various highway departments. In a few cases, data were verified or clarified by follow-up telephone conversations.

The data contained herein are related to bedding and backfilling materials and configurations with respect to circular pipe culverts. Placement conditions of positive and negative projecting embankment sites, trench installations, and induced-trench installations are also considered. Because use of other types of pipe is limited,

only reinforced concrete (RCP) and corrugated metal pipe (CMP) were considered.

Several placement conditions that are mentioned in this appendix will now be defined:

- (1) The "embankment condition" exists when the finished highway grade is above the original ground elevation. Within the embankment a culvert may be placed above, on, or below the original ground surface.
- (2) Positive projecting culverts are installations in which the outside top of the culvert is above the undisturbed soil surface.
- (3) A negative projecting culvert is one in which the outside top of the pipe is below the undisturbed soil surface.
- (4) The "trench condition" exists when the highway grade is at or below the original ground line; thus, the culvert is surrounded by undisturbed soil.



- (5) The imperfect or incomplete trench is a placement method that creates potentially beneficial loading conditions on a pipe by use of soft inclusions to promote arching. Additional discussion is given elsewhere in this appendix.

Each of the foregoing placement conditions is illustrated in Figure D-1. Although quantitative data, such as the projection ratio, may be associated with these placement conditions, the basic definitions will be adequate for qualitative descriptions of placement.

## BEDDING

For the purpose of this discussion, bedding shall be defined as that material on which a pipe culvert is placed and any extension of that same material to the sides or along the outer circumference. Bedding has a significant influence on the longitudinal stress distribution of the pipe. State culvert specifications, thus, provide specific guidelines on what bedding types are permitted and which are recommended. The bedding practices, configurations, and materials used by the various state highway departments will be reviewed and summarized in this section.

A review of the data indicates that most highway specifications generally treat bedding as a separate entity which is independent of

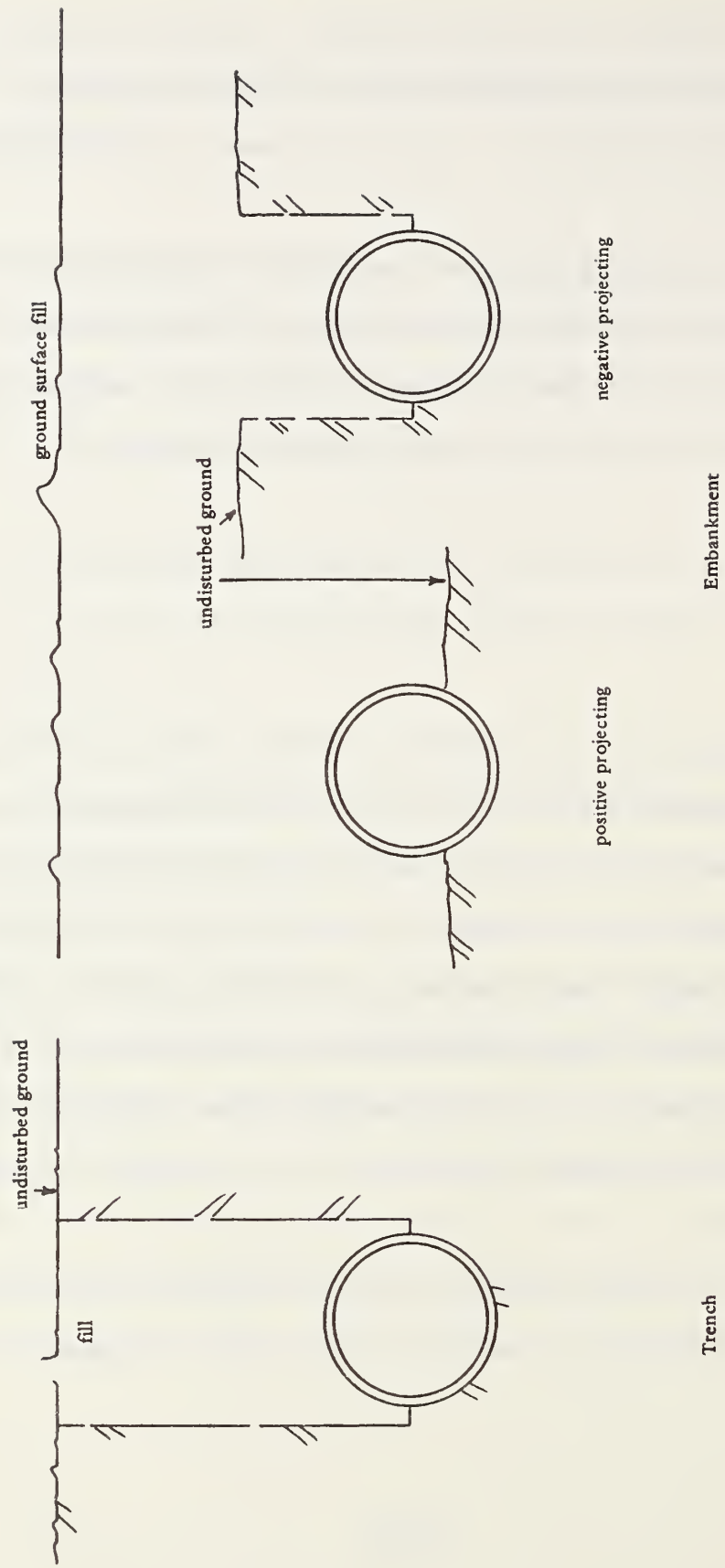


Figure D-1. Placement conditions.

pipe type or placement condition. The exceptions to this trend are Arkansas, New Mexico, North Carolina, and Washington, where thin layers of loose, granular material are placed under corrugated metal pipes to insure intimate contact with the corrugations. Colorado requires the material to be hand-tamped under the haunches of CMP, but does not make such a requirement for RCP. In all other states surveyed the pipe type did not influence the bedding requirements. All states surveyed used the same bedding practices for positive projecting, negative projecting, trench, and induced-trench installations.

The states surveyed provided only qualitative guidance for culverts that must be placed on poor in-situ soil. They require the removal of the soil to a depth specified by the site engineer and the replacement of that soil with a specified bedding material. In situations where rock or other hard material is encountered at the culvert grade, the states provide specific instructions on the amounts of material to be removed and replaced. These requirements are independent of pipe type for all states, except Missouri and New Mexico. These states require specific amounts of material to be removed beneath CMP, but specify the removal of amounts proportional to the fill height for RCP.

Despite the foregoing exceptions, bedding geometrics and materials are generally independent of pipe type, and will be treated as such in this section.

All of the states surveyed utilized the variation of the standard bedding types recommended by the American Concrete Pipe Association. Variations of the Class C bedding are used as the 'normal' bedding in all states, except Colorado, Connecticut, Illinois, and Washington. These states use Class B for all installations. Class A or concrete cradle bedding is generally permitted as an alternative. Configurations used by the various states for normal, rock foundation, and concrete cradle bedding are summarized in Table D-1.

Data from the bedding material specifications are summarized in Table D-2. Bedding materials most commonly used were sand or granular materials. In several states, the bedding is simply carved out of the undisturbed soil underlying the pipe. These states are indicated in Table D-2 as in-situ soil bedding. Most states did not have quantitative specifications for the placement and compaction of these materials. This finding indicates the need for greater specificity in the statement of bedding requirements.

## BACKFILL

For the purpose of this discussion, backfill shall be defined as that material immediately adjacent to and over the culvert. This section will summarize and discuss state highway practices and specifications for culvert backfill based on the above definition.

Table D-1. Bedding Geometry

State	Normal Bedding			Rock Foundation			Concrete Cradle		
	d <sub>1</sub>	d <sub>2</sub>	w	d <sub>2</sub>	d <sub>2</sub> <sub>min</sub> /d <sub>2</sub> <sub>max</sub>	w	d <sub>1</sub>	d <sub>2</sub>	w
Alabama	0.1 OD	0	OD + 3 ft	H/24	12 in./24 in.	OD + 1 ft	—	—	—
Alaska	—	0	—	H/24	12 in./0.75 OD	—	—	—	—
Arizona	0.5 OD	0.5 OD	OD + 3 ft	—	12 in./0.75 OD	OD + 1 ft	OD + 5 in.	4 in.	OD + 8 in.
Arkansas	0.1 OD	6 in.	OD + 2 ft	H/24	— /0.75 OD	OD + 2 ft	0.25 OD	0.25 ID	OD + 8 in.
California	0.07 OD	0	OD + 2 ft	H/24	12 in./60 in.	—	—	—	—
Colorado	0	3 in.	OD + 3 ft	12 in.	—	ID + 3 ft	—	—	—
Connecticut	0.1 OD	4 in.	OD + 1 ft	12 in.	—	ID + 3 ft	—	—	—
Delaware	0.15 OD	0	—	H/24	8 in./—	OD + 2 ft	0.25 ID	0.25 ID	OD + 8 in.
Florida	0.1 OD	0	—	H/24	12 in./0.75 OD	—	0.25 ID	0.25 ID	OD + 8 in.
Georgia	0.15 OD	0	—	6 in.	—	—	—	—	—
Hawaii	0.1 OD	0	—	H/24	12 in./0.75 OD	OD + 2 ft	0.25 OD	0.25 ID	OD + 8 in.
Idaho	0.25 ID	0	—	H/24	8 in./0.8 ID	ID + 4 ft	—	—	—
Illinois	0.5 OD	0	OD + 3 ft	H/24	12 in./—	OD + 2 ID	—	—	—
Indiana	0.1 OD	0	1.6 OD	12 in.	—	—	0.25 OD	0.25 ID	OD + 20 in.
Iowa	0.1 OD	0	—	12 in.	—	—	—	—	—
Kansas	0.1 OD	0	—	12 in.	—	—	—	—	—
Kentucky	0.15 OD	0	5 OD	H/24	12 in./0.75 OD	OD + 2 ft	—	—	—
Louisiana	0.1 OD	3 in.	—	H/24	8 in./—	—	—	—	—
Maine	—	—	—	—	—	—	—	—	—
Maryland	0.1 OD	0	2 OD	H/24	8 in./—	2 OD	—	—	—
Massachusetts	0.5 OD	0	—	—	—	—	—	—	—
Michigan	0.1 OD	0	—	H/24	8 in./—	OD + 0.5	0.25 OD	0.25 ID	OD 3 8 in.
Minnesota	0.15 OD	6 in.	—	12 in.	—	—	—	—	—
Mississippi	—	—	—	—	—	—	—	—	—
Missouri	0.1 OD	0	—	H/24	6 in./0.75 OD	OD + 1 ft	0.25 OD	0.25 ID	OD + 8 in.
Montana	—	—	—	—	—	—	—	—	—
Nebraska	0.07 OD	0	1.25 OD	—	6 in./0.75 OD	—	0.25 OD	0.25 ID	OD + 8 in.
Nevada	0	0	OD + 3 ft	12 in.	—	OD + 3 ft	0.25 OD	0.25 ID	OD + 8 in.
New Hampshire	0.5 ID	12 in.	—	—	—	—	—	—	—
New Jersey	0	0	—	12 in.	—	OD + 2 ft	—	—	—



Table D-1. (Continued)

State	Normal Bedding			Rock Foundation			Concrete Cradle		
	$d_1$	$d_2$	w	$d_2$	$d_2/d_1$	$d_2$	$d_1$	$d_2$	w
New Mexico	0.1 OD	0	-	H/24	6 in./0.75 OD	OD + 1 ft	0.25 OD	0.25 ID	OD + 8 in.
New York	-	-	-	-	-	-	-	-	-
North Carolina	0.1 OD	0	-	H/24	8 in./18 in.	OD + 2 ft	-	-	-
North Dakota	-	-	-	-	-	-	-	-	-
Ohio	-	-	-	-	-	-	-	-	-
Oklahoma	0.1 OD	4 in.	-	-	6 in./-	OD + 8 ft	-	-	-
Oregon	0.1 OD	0	-	H/24	8 in./0.75	2 OD	0.25 0 OD	0.25 ID	OD + 8 in.
Pennsylvania	0.15 OD	0	-	H/24	12 in./24 in.	OD + 2.5 ft	0.25 0 OD	0.24 ID	OD + 8 in.
Rhode Island	-	-	-	-	-	-	-	-	-
South Carolina	-	-	-	-	-	-	-	-	-
South Dakota	-	-	-	-	-	-	-	-	-
Tennessee	0.5 OD	6 in.	-	6 in.	-	OD + 3 ft	-	-	-
Texas	0.1 OD	0	-	H/24	8 in./0.75 OD	OD + 1 ft	0.25 OD	0.25 ID	OD + 8 in.
Utah	-	-	-	-	-	-	-	-	-
Vermont	0	12 in.	OD + 6 ft	-	12 in./24 in.	-	-	-	-
Virginia	0.1 OD	4 in.	-	H/24	8 in./-	OD + 3 ft	-	-	-
Washington	0.15 OD	8 in.	OD + 4 ft	8 in.	-	OD + 4 ft	-	-	-
West Virginia	0.15 OD	12 in.	OD + 3 ft	H/24	12 in./24 in.	OD + 3 ft	-	-	-
Wisconsin	0.1 OD	0	OD + 3 ft	H/24	8 in./-	OD + 3 ft	-	-	-
Wyoming	-	-	-	-	-	-	-	-	-
Puerto Rico	0.1 OD	2.5 in.	-	2.5 in.	-	OD + 3 ft	-	-	-

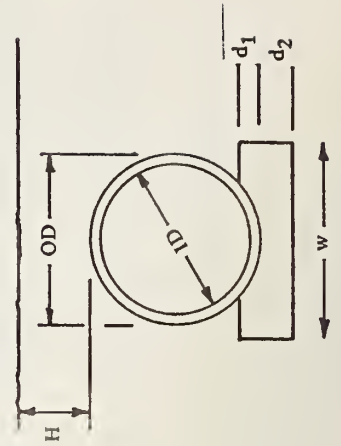




Table D-2. Bedding Materials

State	Soil	Density (%)	AASHTO Specification	Concrete Cradle, $f'_c$ (psi)
Alabama	loan	—	—	—
Alaska	—	95	T-180	—
Arizona	silty sand	95	—	3,000
Arkansas	silty sand	—	—	2,100
California	sand	95	—	—
Colorado	sand	95	T-180	—
Connecticut	sand	95	T-180	—
Delaware	in-situ	—	—	2,000
Florida	in-situ	—	—	2,200
Georgia	—	—	—	—
Hawaii	in-situ	—	—	—
Idaho	sand	95	T-99	—
Illinois	sand	90	T-99	—
Indiana	sand	—	—	3,000
Iowa	sand	—	—	—
Kansas	in-situ	—	—	—
Kentucky	sand	—	—	—
Louisiana	loose	—	—	—
	in-situ	—	—	—
Maine	—	—	—	—
Maryland	in-situ	—	—	—
Massachusetts	—	—	—	—
Michigan	in-situ	—	—	3,000
Minnesota	—	—	—	—
Mississippi	—	—	—	—
Missouri	in-situ	—	—	2,500
Montana	—	—	—	—
Nebraska	sand	—	—	2,000
Nevada	in-situ	—	—	3,000
New Hampshire	sand	—	—	—
New Jersey	sand	—	—	—
New Mexico	in-situ	—	—	—
New York	—	—	—	—
North Carolina	in-situ	—	—	—
North Dakota	—	—	—	—
Ohio	—	—	—	—

Table D-2. (Continued)

State	Soil	Density (%)	AASHTO Specification	Concrete Cradle, f' <sub>c</sub> (psi)
Oklahoma	sand	-	-	-
Oregon	in-situ	-	-	-
Pennsylvania	in-situ	-	-	3,000
Rhode Island	-	-	-	-
South Carolina	-	-	-	-
South Dakota	-	-	-	-
Tennessee	sand	-	-	3,000
Texas	in-situ	-	-	3,000
Utah	-	-	-	-
Vermont	granular	-	-	-
Virginia	sand	-	-	-
Washington	gravel	-	-	-
West Virginia	sand	-	-	-
Wisconsin	in-situ	-	-	-
Wyoming	-	-	-	-
Puerto Rico	sand	-	-	-

Alternate practices for different pipe types and placement conditions, such as embankment or trench, will be discussed. The various requirements specifying the extent of the culvert backfill and material properties will also be summarized.

Backfilling practices and specifications for most states are independent of pipe type. Exceptions exist in some states where special care is required for backfilling corrugated metal pipe. These exceptions are generally in the form of qualitative statements to insure that the backfill is brought up evenly on both sides of the culvert to prevent lateral distortions. New Mexico is one state that provides specific quantitative differences in backfilling requirements for reinforced concrete and corrugated metal pipe. The differences do not appear to be significant, but a detailed analysis might indicate beneficial effects that are not obvious.

Most states do not have significantly different backfill requirements for the various placement conditions of trench, positive-projecting embankment, or negative-projecting embankment. Michigan is an exception in that it requires granular backfill to within one trench width of the ground surface for trench installations, but granular backfill is required for only 24 inches over the crown of embankment pipe.

All states from which data were obtained specify that backfill for negative-projecting embankment installations shall be the same as for trench installations.

The various state backfilling practices include a variety of configurations and placement techniques. The configuration elements that can be quantified are the height,  $h$ , above the top of the pipe to which special backfill is required, and the width,  $w$ , of the area of special backfill. The primary backfilling technique that can be quantified is the required lift thickness,  $\ell$ , of the material. This quantity is generally specified as a maximum loose thickness, but several states specify a maximum compacted thickness.

Backfill configurations used by the various states are summarized in Table D-3. The table shows that the most commonly used practice for embankment culverts is to fill to a level above the culvert crown, and then cut a trench in which the culvert is placed. In these cases the extent of the special culvert backfill is defined by the dimensions of the trench. In states where embankment culverts are backfilled before the main embankment, the dimension,  $w$ , in Table D-3 indicates the extent over which special backfilling techniques are used.

A coherent quantitative description of backfill material properties was difficult to obtain. Generally sand or silty sand is preferred for backfill, but such materials are often unavailable or not economically available. Most states specify a required backfill density based on maximum density of the soil determined by AAHSTO T-99 or T-180. Specifically, most of the states having relative density requirements fall into three categories: (1) 95% of T-99,

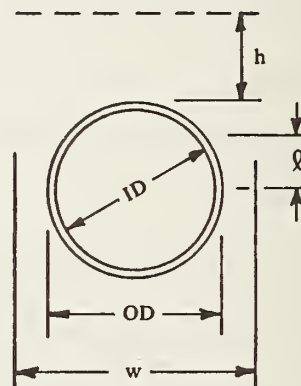
Table D-3. Backfill Practices

State	Lift Height,* l	Height, h	Width, w
Alabama	6 in. L	—	—
Alaska	6 in.	—	—
Arizona	8 in. L	—	—
Arkansas	—	—	—
California	8 in. L	6 in.	—
Colorado	6 in. L	—	—
Connecticut	6 in. L	—	—
Delaware	8 in. L	—	—
Florida	6 in. C	12 in.	3 OD
Georgia	6 in. L	—	—
Hawaii	8 in. L	—	—
Idaho	8 in. L	12 in.	ID + 8'
Illinois	4 in. L	12 in.	—
Indiana	6 in. L	—	—
Iowa	8 in. L	12 in.	OD
Kansas	8 in. L	0	3 OD
Kentucky	6 in. L	24 in.	—
Louisiana	6 in. C	12 in.	3 OD
Maine	—	—	—
Maryland	6 in. L	9 in.	2 OD
Massachusetts	6 in. L	24 in.	—
Michigan	6 in. C	24 in.	3 OD
Minnesota	—	12 in.	OD + 3'
Mississippi	—	—	—
Missouri	6 in. L	0	3 OD
Montana	—	—	—
Nebraska	6 in. L	0.5 OD	OD + 4'
Nevada	8 in. L	—	—
New Hampshire	—	—	—
New Jersey	6 in. L	24 in.	—
New Mexico	12 in. L	12 in.	5 ID
New York	—	—	—
North Carolina	6 in. L	0	3 OD
North Dakota	—	—	—
Ohio	—	—	—

Table D-3. (Continued)

State	Lift Height,* $\ell$	Height, $h$	Width, $w$
Oklahoma	8 in. L	12 in.	OD + 11'
Oregon	6 in. L	6 in.	5 OD
Pennsylvania	—	—	OD + 2.5'
Rhode Island	—	—	—
South Carolina	—	—	—
South Dakota	—	—	—
Tennessee	6 in. L	12 in.	—
Texas	6 in. L	—	—
Utah	—	—	—
Vermont	6 in. L	—	—
Virginia	6 in. L	0	3 OD
Washington	6 in. L	0	OD + 3'
West Virginia	6 in. L	0	—
Wisconsin	6 in. L	0	—
Wyoming	—	—	—
Puerto Rico	6 in. L	12 in.	5 OD

\*L is loose measure, C is compacted measure.





(2) 90% of T-99, (3) 90% of T-180 maximum density.. Case 1 was most frequently encountered. Cases 2 and 3 were about equally common, but to a lesser degree than case 1. The various state requirements for culvert backfill compaction are summarized in Table D-4.

#### IMPERFECT TRENCH PRACTICES

The imperfect or incomplete trench method is used in several states for embankment conditions in which the usual placement methods would result in calculated loads that are greater than the estimated strength of the culverts. Some states specify a minimum height of fill in which the method may be utilized. The usual method employed is to backfill over the culvert in the normal way to a depth of one diameter plus one foot above the top of the pipe. Soft organic material, such as straw, hay, cornstalks, leaves, brush or wood shavings, is placed in the lower one-fourth to one-third of the trench. The remainder of the trench is filled with a loose backfill material before the embankment backfilling is continued. A variation on this method is to place the embankment to a depth of one diameter plus one foot above the planned top of the pipe and to excavate a trench and place the pipe in the trench. The pipe is backfilled to one foot over the crown and the soft material and loose backfill are placed in the remainder of the trench in the

Table D-4. Backfill Property Specifications

State	Density (%)	Method	Case*
Alabama	95	T-99	1
Alaska	95	T-180	3
Arizona	95	T-99	1
Arkansas	—	—	—
California	95	Other	—
Colorado	95	T-180	3
Connecticut	95	T-180	3
Delaware	95	T-99	1
Florida	100	T-99	—
Georgia	100	Other	—
Hawaii	95	T-180	3
Idaho	95	T-99	1
Illinois	90	T-99	2
Indiana	—	—	—
Iowa	—	—	—
Kansas	90	—	—
Kentucky	—	—	—
Louisiana	95	—	—
Maine	—	—	—
Maryland	92	T-180	—
Massachusetts	—	—	—
Michigan	95	T-99	1
Minnesota	100	—	—
Mississippi	—	—	—
Missouri	90	T-99	2
Montana	—	—	—
Nebraska	90	T-99	2
Nevada	95	Other	—
New Hampshire	—	—	—
New Jersey	—	—	—
New Mexico	95	T-99	1
New York	—	—	—
North Carolina	—	—	—
North Dakota	—	—	—
Ohio	—	—	—

Table D-4. (Continued)

State	Density (%)	Method	Case*
Oklahoma	95	T-99	1
Oregon	-	-	-
Pennsylvania	-	-	-
Rhode Island	-	-	-
South Carolina	-	-	-
South Dakota	-	-	-
Tennessee	95	-	-
Texas	-	-	-
Utah	-	-	-
Vermont	90	T-99	2
Virginia	-	-	-
Washington	95	Other	-
West Virginia	95	T-99	1
Wisconsin	90	T-99	2
Wyoming	-	-	-
Puerto Rico	95	-	-

\*Case 1: 95% of T-99  
Case 2: 90% of T-99  
Case 3: 95% of T-180

same manner as for the previous method. Figure D-2 illustrates the former method.

The purpose of imperfect trench placement is to artificially create a partial trench condition in an embankment. The intended objective is to permit the soft material to compress and, thus, activate shear in the soil prism above the culvert (i.e., arching).

It is interesting to note that, of the states using the imperfect trench method, most apply it only to reinforced concrete pipe, but several states imply that it can be used for both reinforced concrete and corrugated metal pipe. Although the use of a relatively flexible pipe would seem to eliminate the need for the load redistribution provided by the imperfect trench, the latter application might be beneficial in some installations.

Table D-5 is a summary of imperfect trench practices used by the state highway departments. Only three states specifically mentioned that they did not use the imperfect trench technique; however, twelve states did not mention the technique in their replies. Only three of the highway departments that replied (Arizona, Nevada, and Puerto Rico) used the second technique described. These departments are evident in the table, because the specified trench width is greater than the pipe outside diameter.

The foregoing discussion summarizes the practices used by state highway departments. For the most part each state establishes its own structural design codes and regulations; however, they are

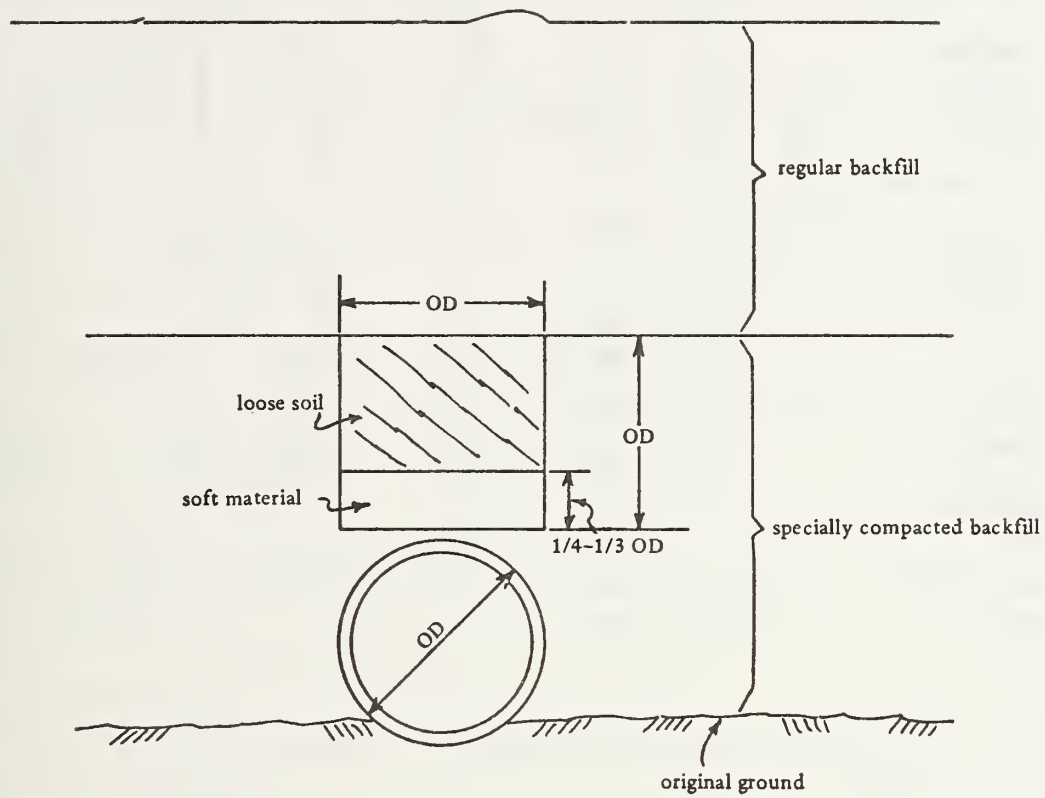


Figure D-2. Imperfect trench installation.

Table D-5. Imperfect Trench Practices

State	Gap, g	Trench Width, w	Soft Material (case <sup>b</sup> )	Minimum Fill Height	Use <sup>c</sup>
Alabama	1 ft	OD	1	30 ft	RCP/CMP
Alaska	NU <sup>a</sup>	NU	NU	NU	NU
Arizona	1 ft	1.5 OD	2	23 ft	RCP
Arkansas	1 ft	OD	2	—	RCP
California	—	—	—	—	—
Colorado	1 ft	OD	1	—	RCP
Connecticut	—	—	—	—	—
Delaware	—	—	—	—	—
Florida	1 ft	OD	1	—	RCP/CMP
Georgia	1 ft	OD	2	20 ft	RCP
Hawaii	6 in	OD	1	—	RCP
Idaho	—	—	—	—	—
Illinois	1 ft	OD	2	—	RCP
Indiana	—	—	—	—	—
Iowa	1 ft	OD	1	—	RCP
Kansas	0	OD	2	27.5 ft	RCP
Kentucky	1 ft	OD	1	27 ft	RCP
Louisiana	—	—	—	—	—
Maine	—	—	—	—	—
Maryland	—	—	—	—	—
Massachusetts	—	—	—	—	—
Michigan	1 ft	OD	1	—	RCP
Minnesota	1 ft	OD	2	—	RCP/CMP
Mississippi	—	—	—	—	—
Missouri	1 ft	OD	2	—	RCP
Montana	—	—	—	—	—
Nebraska	NU	NU	NU	NU	NU
Nevada	1 ft	OD + 3 ft	1	—	RCP
New Hampshire	—	—	—	—	—
New Jersey	—	—	—	—	—
New Mexico	—	—	—	—	—
New York	—	—	—	—	—
North Carolina	0	OD	1	30 ft	RCP/CMP
North Dakota	—	—	—	—	—
Ohio	—	—	—	—	—



Table D-5. (Continued)

State	Gap, g	Trench Width, w	Soft Material (case <sup>b</sup> )	Minimum Fill Height	Use <sup>c</sup>
Oklahoma	1 ft	OD	1	—	RCP
Oregon	1 ft	OD	1	—	RCP
Pennsylvania	1 ft	OD	2	13 ft	RCP
Rhode Island	—	—	—	—	—
South Carolina	—	—	—	—	—
South Dakota	—	—	—	—	—
Tennessee	1 ft	OD	1	—	RCP
Texas	—	—	—	—	—
Utah	—	—	—	—	—
Vermont	NU	NU	NU	NU	NU
Virginia	0	OD	2	30 ft	RCP/CMP
Washington	6 in.	OD	1	—	RCP
West Virginia	1 ft	OD	1	—	RCP
Wisconsin	—	—	—	—	—
Wyoming	—	—	—	—	—
Puerto Rico	0	OD + 1.2 ft	1	—	RCP/CMP

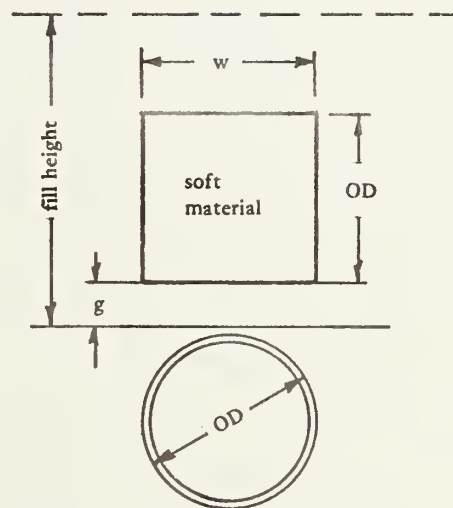
<sup>a</sup> NU = Not Used.

<sup>b</sup> Case 1: 1/4 to 1/3 OD filled with organic material, the remainder with loose soil.

Case 2: loose soil.

<sup>c</sup> RCP = reinforced concrete pipe.

CMP = corrugated control pipe.



generally based on recommendations of national organizations, such as shown in Table D-6. Common practices and general culvert criteria are shown in Table D-7.

Table D-6. Current Structural Design Methods<sup>a)</sup>

Agency	Culvert Type		Reference
	Flexible	Stiff	
Federal Highway Administration (FHWA)	X	X	D-1
American Association of State Highway and Transportation Official (AASHTO)	X		D-2
American Iron and Steel Institute (AISI)	X		D-3
National Clay Pipe Institute		X	D-4
Manufacturers of Aluminum Pipe (Example)	X		D-5
Manufacturers of Plastic Pipe (Example)	X		D-6
American Concrete Pipe Association (ACPA)		X	D-7
States (Example)	X	X	D-8

<sup>a)</sup> Adapted from a compilation by G. W. Ring, III, FHWA.

Table D-7. General Culvert Criteria

Design Life<sup>a</sup> (FHWA)

Interstate roads . . . . .	50 years
Other roads. . . . .	25 years

Minimum cover,  $d_o$  (FHWA)

1-in. to 95-in. pipe . . . . .	12 in.
96-in. to 192-in. pipe . . . . .	24 in.
193-in. to 252-in. pipe. . . . .	36 in.

Deflection Lag,  $D_L$  (FHWA)

Good fill (85% standard Proctor density) . . .	1.5
Excellent fill (95% standard Proctor density) . . . . .	1.25

Impact factor for trucks<sup>b</sup> (AASHTO upper bound). . .  $1.4 - d_o/120$

Soil Compaction . . . . . 85% AASHTO T-99

<sup>a</sup>Period of service without major repairs.

<sup>b</sup> $d_o$  is in inches.

Appendix E  
RECENT CULVERT TECHNOLOGY

INTRODUCTION

This appendix contains a review of relatively recently developed culvert pipes and installation methods. The data presented were obtained from manufacturers, trade associations, and others. The material summarized is that which is considered to be most pertinent to the present research.

RECENT INNOVATIONS IN PIPE DESIGN

Corrugated Metal Pipe

Helical Corrugated Metal Pipe. Helical corrugated metal pipe is a relatively new product that has several design and manufacturing advantages over riveted circumferential corrugated pipe [E-1]. In the manufacturing process, flat sheet metal from a large coil is fed into a device that forms the corrugations and rolls the deformed sheet into a helix to form the pipe. Seams are automatically welded or "locked" as the pipe is formed.

Primary advantages of the helical method are that it is a continuous process and requires only a single operator. Thus, production rates are high and labor costs are low. Of course, capital equipment costs for such pipe are high, and a relatively long time is required to change pipe sizes or gages.

In the past, the structural design of helical corrugated metal pipe has been the same as for pipe with annular corrugations, although this does not seem rational. In the first place, the gage of the helical pipe is based on the same seam strength as annular corrugated pipe. The latter has longitudinal seams, and the former has seams which approach circumferential orientation for larger sizes. Also, seams for helical pipe are parallel to the axis of the corrugations. The stress transfer and the resulting strength of the seams may be significantly different for the two corrugation orientations. A benefit of helical corrugated pipe is that it has better hydraulic characteristics than circumferentially corrugated pipe. Tests have shown that the value of Manning's "n" decreases for higher helix angles [E-2], at least for small diameter pipe.

The main disadvantages of helical corrugated pipe is that helical corrugations have slightly less resistance to diametral deflections than their annular counterparts, and tight connections between pipe sections are difficult to obtain.



Smooth-Lined Pipe. This product has a double-wall with a corrugated outer wall and a smooth inner wall. The walls are attached at helical lock seams at spacings not greater than 30 inches. The primary advantage of smooth-lined pipe is its low friction factor and high abrasion resistance. Manning's "n" is equal to 0.02 or more for most corrugated pipe, but is only 0.01 for smooth-wall pipe. In some cases, the improved hydraulic characteristics may permit the use of a smaller diameter pipe with consequent cost savings. Smooth-wall pipe contains approximately the same total metal area per unit length as standard corrugated pipe of the same nominal diameter. Furthermore, the strength of smooth-wall pipe is approximately the same as for standard pipe. Figure E-1 shows a typical cross section of a smooth-lined pipe wall. These pipes can be fabricated of either aluminum or steel.

Coatings. A relatively new corrugated metal pipe process, which improves hydraulic flow characteristics and improves abrasion resistance, is coating of the invert. The coatings consist of asphalts or polyesters, depending on economics or other requirements. Coatings may effect the structural performance of pipe culverts, where they limit the long-term reduction in section due to abrasion and/or corrosion.

Exterior coatings for corrugated metal pipe are being used more frequently as a method of reducing corrosion of the pipe. Both

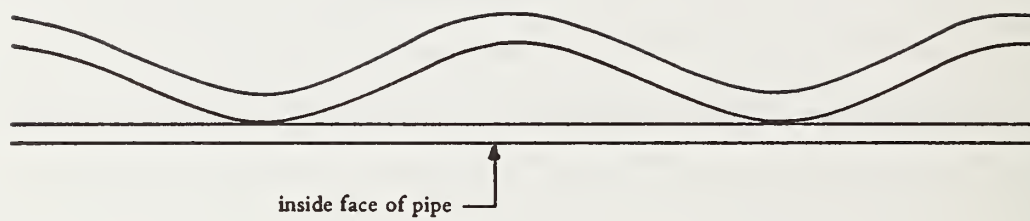


Figure E-1. Smooth-lined steel pipe wall section.

asphaltics and plastic coatings are used for this purpose. In addition to corrosion resistance, a proper choice of exterior coating could contribute to a slight load reduction on the pipe. Analyses have indicated that some load reduction may be achieved by reducing the interface friction at the soil-pipe interface; thus, a low friction coating could provide a modest structural improvement.

Aluminum Pipe. Despite higher unit costs for materials, aluminum corrugated pipe has several advantages that sometimes make it competitive with steel pipe. Aluminum's lightweight permits relatively easy and inexpensive installation. This is a particular advantage for large-diameter multiplate culverts where individual plates can be placed without heavy equipment. The natural corrosion resistance of aluminum is a second advantage. Plating or coating is generally not required.

Manufacturers of corrugated aluminum plates tend to use large corrugations even for relatively small-diameter pipe. These large corrugations provide greater bending stiffness for wall sections to compensate for the lower strength and modulus of aluminum compared to steel.

Multiple Plate Pipe and Arch Culverts. These structures are generally used for long-span applications where the culvert is

basically a substitute for a bridge. These elements are generally field assembled because of their large size. Specialized arch designs have been developed in addition to standard pipe culvert designs.

Super-span arch culverts have been developed in Canada [E-3]. They consist of multiple plates that form an arch which is longitudinally stiffened with concrete thrust beams. The thrust beams are located at the three-quarter-point of the arch, as shown in Figure E-2. Reportedly, part of the horizontal reaction of the arch is taken by the thrust beam. Thus, the top quadrant of the culvert acts as a laterally restrained arch.

A reinforced soil bridge [E-4] has been developed that consists of a corrugated steel arch with soil bins over the crown, as shown in Figure E-3. Advantages claimed for the bins are that they: (a) stiffen the arch against concentrated loads, (b) develop a keystone at the top of the arch, and (c) hold the arch shape during backfilling.

#### Concrete Pipe

Cast-in-Place Concrete Pipe. Cast-in-place pipe is not necessarily a new technique, but one concept utilizes a sufficiently different technique to warrant discussion. The method consists of cutting a trench with a width equal to the outside diameter of the pipe and

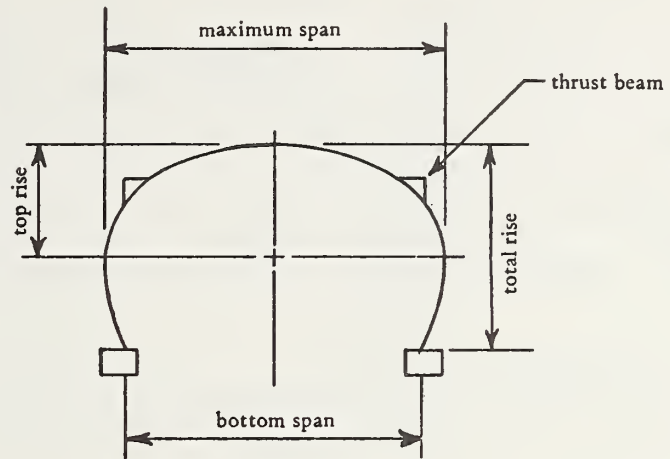


Figure E-2. Super-span arch culvert section.

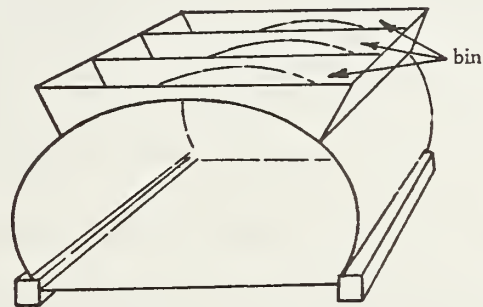


Figure E-3. Reinforced soil bridge section.

with a rounded bottom. Pipe is produced in a type of slip-form machine using the bottom and sides of the trench as stationary forms [E-5]. The inside diameter is shaped with temporary forms that are removed when the concrete sets. The conduit walls do not contain reinforcing steel; structural strength is derived from lateral soil confinement. Figure E-4 shows a typical cross section of such a conduit.

A new variation of the slip-formed cast-in-place pipe is a pre-cast reinforced concrete core around which concrete is poured [E-6]. The pre-cast core provides a reinforced section with carefully controlled properties and dimensions. The core contains reinforcing steel that conforms to steel area requirements specified for standard reinforced concrete pipe. The method has the same advantages as the slip-formed pipe.

Prestressed Concrete Pipe. Although prestressed pipe has been used extensively for pressure pipe, it is becoming practical and popular for large-diameter culvert applications. Circumferential prestressing of culvert pipes reduces tensile bending stresses induced by high fills, and provides more economical use of materials in some applications. Figure E-5 shows a typical wall section of a prestressed



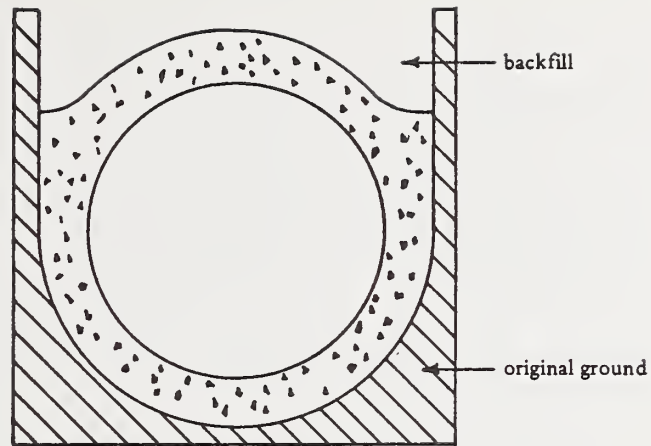


Figure E-4. Cast-in-place pipe cross section.

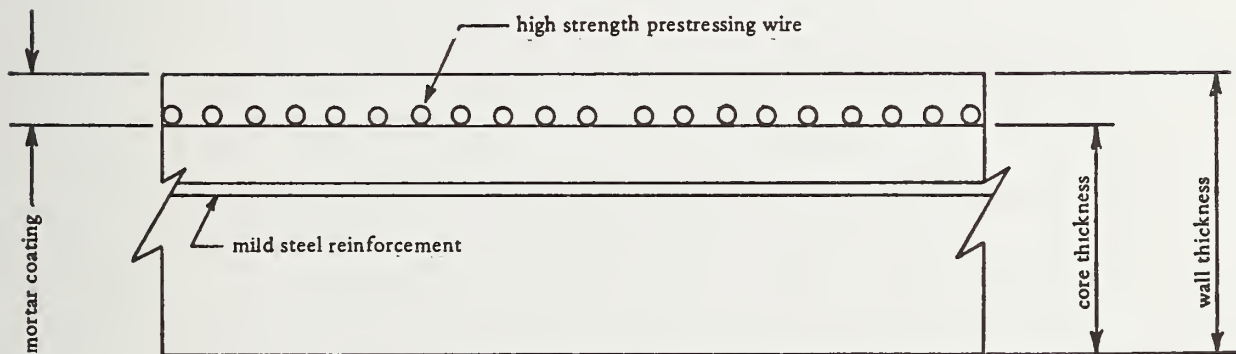


Figure E-5. Prestressed concrete pipe wall section.

culvert pipe. The following benefits are claimed for prestressed culvert pipe:

- (1) High strength steel and concrete.
- (2) Equal strength around the circumference.
- (3) Moment resistance without cracking.
- (4) Elastic behavior under overloads.
- (5) High shear resistance.
- (6) Proofloading during prestressing.

#### Other Pipe Materials

Asbestos-cement pipe is an alternate to some of the more commonly used pipes for culverts. Potential advantages of this pipe over concrete pipe are higher flow capacity for a given diameter and lower installation and excavation costs. Asbestos-cement pipe is generally limited to diameters less than 36 inches.

Cast iron and vitrified clay are two pipe materials that are also used for small-diameter culverts and under-drains. With the

exception of the development of ductile cast iron pipe, these types of pipe have experienced little development in recent years.

Plastic pipe is a relatively new, yet potentially useful, material for pipe culverts. There are at least three different concepts for such pipes. One consists of a fiberglass-reinforced wall with helically wound fibers [E-7]; another uses helical ribs to provide added bending stiffness [E-8]. An example of a wall section for the ribbed-wall type is shown in Figure E-6. A third type of plastic pipe is made from a thermosetting compound that is heated and formed in place [E-9]. The pipe is rolled-out flat on pre-formed bedding, and a heated mandrill is pulled through the pipe to rigidize the walls.

Although applications for plastic pipe have been primarily for sewage or corrosive chemical environments, the pipe has features that may permit its use for culverts. Favorable attributes include relatively light weight, corrosion resistance, and smooth inner walls. Compared to metal and concrete pipe of the same weight, plastic pipe has lower strengths and greater susceptibility to creep. A further problem is that plastics are temperature sensitive; they tend to become brittle at low temperatures and weak at high temperatures. Many plastics are also potentially flammable.

One composite pipe, the truss pipe [E-10], consists of inner and outer concentric plastic skins held apart with longitudinal plastic stiffeners. The approximately triangular spaces between these thin

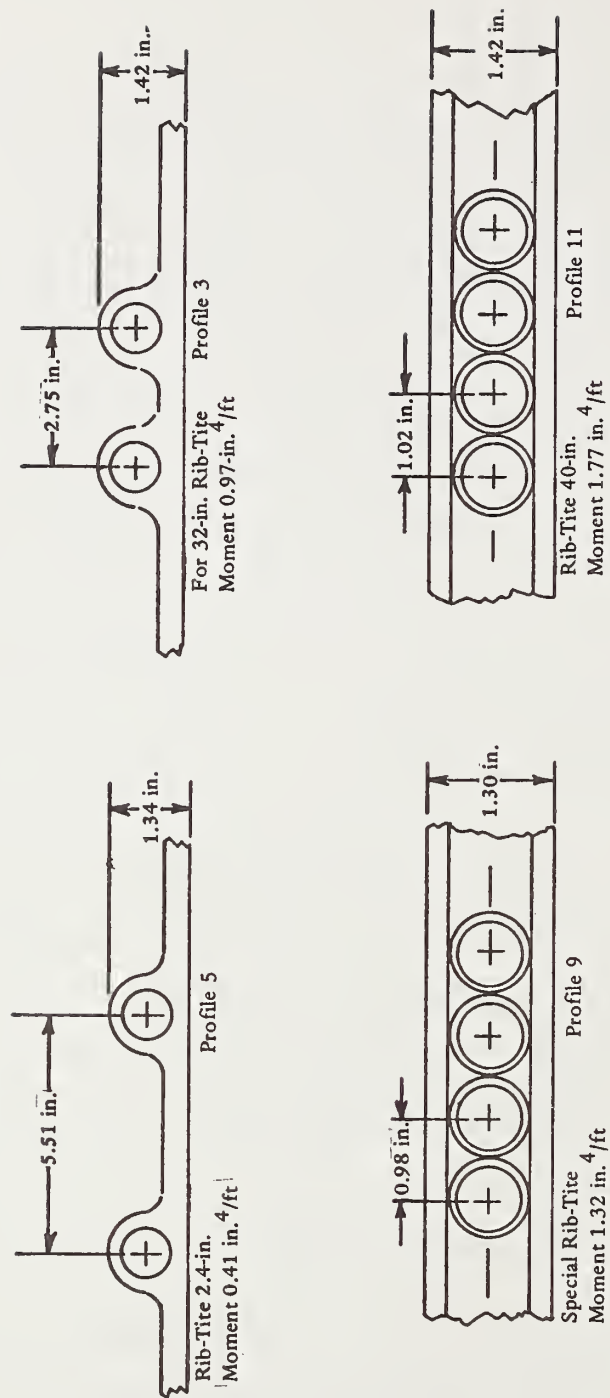


Figure E-6. Ribbed-wall plastic pipe wall sections.

plastic elements, Figure E-7, are filled with foamed cement to achieve stiffness and strength. These pipes are only made in diameters to 15 inches; however, manufacture of larger sizes is planned.

Among other materials that may be utilized for culverts are concrete polymer composites [E-11]. These are portland cement concretes with a monomer and resin that are added to the mix and subsequently polymerized. The resulting material has strengths that are greater than normal concrete by a factor of three or more. Use of these materials could reduce the weight and increase the strength of concrete pipe.

#### INNOVATIONS TO CULVERT ENVELOPMENTS

Recent innovations for treating the extrados of culverts include: backpacking, wrappings and coatings, modified soil stiffnesses, and other modifications to the enveloping media. These concepts are discussed below.

##### Backpacking

The term backpacking connotes a low modulus material (polyurethane foam, etc.) introduced into the confining medium near a pipe or liner to reduce or redistribute the interface pressure. Theoretically,

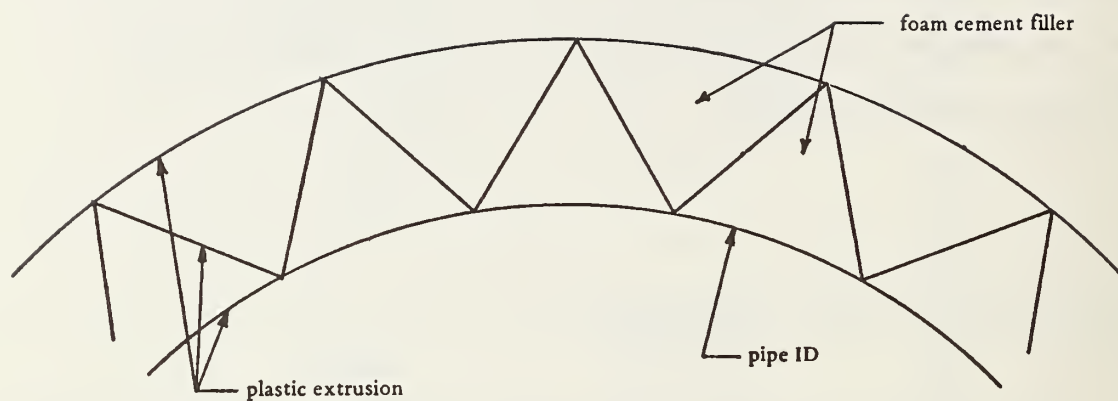


Figure E-7. Trussed pipe wall section.



interface pressures may be reduced by factors of up to 10 by proper use of backpacking. Factors of 2 or 3 are considered practicable for high fills or other large loadings.

Properly used, backpacking permits adjusting the relative stiffness of an inclusion (consisting of the cylinder and the backpacking) with respect to the stiffness of the soil. Improperly employed, serious imbalances in interface load, gross distortions of shape, or premature transitional buckling can result.

Key experimental research on backpacking was performed by Linger [E-12]. An approximate design theory was developed by Allgood [E-13], and a preliminary finite element study of different backpacking geometries was done by Takahashi [E-14]. Other laboratory, field tests, and applied theories have also provided useful information [E-15, E-16, E-17].

Findings from work accomplished to date indicate that for statically loaded, buried structures with backpacking:

- (1) Large reductions in interface pressure are possible.
- (2) Backpacking over the crown tends to result in initial upward crown deflections.
- (3) Backpacking is best used with angular, nonuniform granular backfill.

- (4) Large compressive strains (concomittant with crushing of the backpacking) are necessary to develop the arching associated with large reductions of interface pressure.
- (5) Backpacking completely around the perimeter gives a large, uniform reduction of interface pressure. The optimum backpacking configuration is dependent on pipe type, loading, and soil.
- (6) Use of a soft material as bedding for stiff pipe shows considerable promise.

Care should also be taken to assure that the backpacking is not initially crushed when fill is compacted around the pipe. Crushing should occur as the maximum fill height is approached.

Tests of culverts with backpacking are in progress under the sponsorship of the California Highway Department and the Federal Highway Administration. These tests and the planned investigation utilizing the CANDE finite element program should markedly improve knowledge of the use of backpacking.

## Wrappings and Coatings

A variety of wrappings and coatings is used on the pipe exterior in corrosive or otherwise severe environments. Such materials modify interface conditions and, thereby, alter the soil-structure interaction. An indication of the influence of interface shear may be observed by comparing the results of elastic theory solutions for the cases of no-slip and full-slip (CANDE). Such a comparison shows that, with respect to corresponding full-slip conditions, no-slip displacements, thrusts, and moments are respectively 15% less, 25% greater, and 15% less. These are approximate maximum differences for the practical range of pipe diameters and soil-to-pipe stiffnesses. Thus, if thrust stress controls the design, wrappings and coatings that promote slippage can be structurally beneficial.

## Other Modifications

A variety of modifications, both to pipes and their surroundings, has been tried to achieve improved performance. These include changing pipe shape, adding longitudinal or transverse stiffeners, and changing the stiffness of the soil in selected regions around the pipe. Longitudinal stiffeners are effective in maintaining straightness in large-diameter pipes and, if properly placed, serve to facilitate achievement of a dense soil "abutement."

Transverse (circumferential) stiffeners are used at the ends of pipes to provide additional section modulus for long-span pipe under high loads. There is also promise in the use of soil reinforcing anchors or reinforced earth in very long span (>50 feet) culverts, but this technique has not been exploited as yet.

Ironically, one of the first methods for modifying the enveloping soil was the imperfect trench proposed in the 1930s by Marston [E-18] and others. Modern applications of this technique are discussed in Appendix D and elsewhere [E-19].

Appendix F  
CULVERT FAILURES

In Part I of this appendix a cause-and-effect description is given for all potential failure modes and culvert hazards. In Part II this information is supplemented by the findings of an independent survey to document culvert failures experienced by state highway departments and other agencies.

PART I: CAUSES OF FAILURE

Known potential failure conditions of buried pipe are categorized and delineated in Table F-1. Some of these potential failure modes are evinced in the survey of known recent failures presented in Part II. Failure is generally used here to mean distress visible to the naked eye; however, a more precise definition is subsequently suggested for specific types of pipe. The failure modes of Table F-1 are discussed in the following paragraphs. Detailed treatment of nonstructural failure modes is beyond the scope of the present endeavor. Mention is made, however, of all known potential failure conditions with lengthier discussion and more detailed treatment given to the structural modes, which are of principal concern here.

Table F-1. Potential Failure Conditions

## Handling

Bending during transport . . . . .	Sp*
Collapse from own weight . . . . .	Cr**
Loads on pipe. . . . .	Cr
Dropping impact. . . . .	Sp

## Emplacement

Improper backfill. . . . .	Sp
Equipment on pipe. . . . .	Sp
Faulty bedding . . . . .	Sp
Improper bell holes. . . . .	Sp
Rock impact during backfill. . . . .	Sp
Improper positioning of pipe . . . . .	Sp
Inadequate joining . . . . .	Sp
Incorrect use of backpacking or imperfect trench . . . .	Cr and Sp

## Dead and Live Loading

Wall yielding or crushing. . . . .	Cr
Seam failure . . . . .	Sp
Excessive deflection . . . . .	Cr
Buckling . . . . .	Cr
Longitudinal bending, tension, and compression . . . . .	Sp

## Hydraulic Loading

Undermining. . . . .	Sp
Flotation. . . . .	Sp
Invert uplift. . . . .	Sp
Hydrostatic uplift of ends . . . . .	Sp
Saturation of backfill . . . . .	Sp
Inlet collapse . . . . .	Sp

## Other Potential Failure Conditions

Embankment failure . . . . .	Sp
Rodent damage. . . . .	Sp
Corrosion. . . . .	Sp
Abrasion . . . . .	Sp
Soil-induced failure . . . . .	Sp
Natural disasters. . . . .	Sp



Table F-1. Continued

Other Potential Failure Conditions (continued)

Effects from adjacent structures . . . . .	Sp
Excessive settlement . . . . .	Sp
Pipe twist . . . . .	Sp
Infiltration or exfiltration . . . . .	Sp
End-wall failure . . . . .	Sp
Freeze-thaw. . . . .	Sp
Creep. . . . .	Sp
Fire . . . . .	Sp
Caving of tunneled culverts. . . . .	Sp
Sediment closure . . . . .	Sp

\*Sp implies a specification for construction.

\*\*Cr implies a criteria for structural design.

Bending During Transport. Seemingly obvious mistakes are sometimes made in getting pipe to the site, unloading, and storing it. Errors include lack of adequate support on truck or rail beds, leaving too long a length extending beyond the bed, and dropping the pipe off the side to unload it quickly. Such practices should be prevented. Also, precast concrete and plastic products should be properly stored to avoid warpage. This is especially important for the larger pipe sizes and for the newer thin wall pipes.

Collapse From Own Weight. Large-diameter concrete pipe is susceptible to collapse from its own weight when it is green, unreinforced, or positioned incorrectly. Large-diameter pipe ( $D \geq 5$  feet) often has an "upside," marked by an arrow or other means. If the pipe is handled incorrectly, or emplaced wrongside down, failure may result.

Maximum moment, thrusts, and shears induced in a ring by its own weight are given in the literature [F-1,F-2,F-3].

Heger [F-4] gives plots of the moment, thrust, and shear distribution due to the weight of the pipe, among other loadings. He shows that there is little difference in the distribution of moments between cracked and uncracked pipe. Extensive tabulation of the internal forces from various external loads has been developed by Katoh [F-5].

Loads on Pipe. Most flexible pipes have relatively little load capacity until they are properly embedded. They should not, therefore, be used as temporary supports or subjected to any loading that might damage them.

A wheeled compactor is sometimes run along a pipe as a guideway while the soil at the sides is being compacted. This is an effective technique for preventing the crown from rising while the backfill is compacted. Care must be exercised, however, to assure that the pipe is not overstressed by this or other equipment loads.

Dropping Impact. Particular care should be exercised in handling concrete pipe to avoid dropping impact and subsequent difficult rubble removing jobs. A dynamic load factor of 2 should be used for impact.

#### Emplacement

Perhaps the largest number of culvert structural failures are attributable to faulty emplacement. It is during emplacement that stringent controls are needed. Such controls should be enforced by engineers and inspectors who thoroughly understand culvert behavior.

Improper Backfill. One of the more common errors in backfilling is raising the fill unevenly on the opposite sides of buried structures. For flexible pipes this may cause collapse or severe distortion from the

desired transverse section shape. Running construction equipment in an improper manner too close to partially emplaced culverts also causes difficulty as exemplified by recent failures of long-span arches.

Merely dumping soil around a pipe rather than building a soil structure around the pipe form counts as the number one deficiency in culvert construction. Such a deficiency may result in excessive deflection, bending strain, or in-plane buckling, in-plane distortion, or longitudinal twisting. No other single deficiency can cause so many potential failure conditions.

The engineer and the field construction crew must be educated to the fact that they are building a soil structure and that the pipe mainly serves as a form for the soil structure. Instilling this point-of-view in those concerned with culvert projects will result in improved culvert installations. It is an absolutely essential outlook for long-span culvert bridges.

Equipment on Pipe. During pipe laying operations contractors have been known to run four-wheeled compactors on top and down the length of the pipe as it is backfilled. The weight of the vehicle prevents the crown of the pipe from raising excessively as the sides are densely compacted. This excellent procedure may tempt other equipment operators to take a ride down the pipe - with disastrous results.

Backfilling over large-span culverts is an art that requires a skilled "cat" operator who has been carefully briefed as to the proper

procedures - particularly in the vicinity of the crown. The operator must lift his blade on approach to the structure to assure against imposing large lateral forces that might cause caving. As he drops his load, he must back-off quickly to avoid allowing time for appreciable deformations to occur. Under no circumstances should backfilling of large-span culverts be permitted unless the field engineer is on site.

Another cautionary note is that any attempt at strutting culverts should be approached with caution. Long-span culverts are more likely to be weakened than strengthened by strutting.

Carryalls or other heavy equipment passing over the pipe before sufficient backfill is in place can cause distortion or collapse. A recent event of this type involved a concrete truck pouring a partial head wall. The heavily laden truck caused a severe restriction in the end of the pipe.

Faulty Bedding. Bedding has an important influence on the behavior of stiff pipe and a lesser, but significant, influence on flexible pipe. Part of the present effort is to better assess the importance of bedding and to recommend the best bedding for each of the major pipe types.

California State Highway Department experiments reveal that concrete pipe performance varies inversely with the stiffness of the bedding [F-5]. This is contrary to present bedding practice (ACPA). Even so, existing bedding specifications are believed to be correct



in requiring uniform support and avoidance of rock bases in both the transverse and longitudinal directions.

If uniform support is not provided along the length, unacceptable local or longitudinal bending stresses may result. Also, excess settlement might develop that could damage a highway pavement.

Improper Bell Holes. If adequate excavation for pipe bells is not provided, the load of the pipe, the overburden, and the live loads will be transferred to the bell. Then the bell may fail, depending on the outcome of the contest between the resistance of the supporting medium and the resistance of the bell. The character of the bedding must be tailored to the type of installation being designed. In low-bearing pressure area, the soil may have to be drained and otherwise stabilized prior to emplacement of a culvert.

Rock Impact During Backfilling. Occasionally a large boulder is pushed against a pipe causing local damage. This, however, is more likely with trenches than in embankments.

Improper Positioning of Pipe. Failure may result from improper spacing between multiple culverts or by running a pipe over sink holes or other voids, through a slide region, or over a low-bearing area. Nielson has given interface pressure concentration factors for multiple culvert installations [F-6]. In general, radial pressure



concentration factors are small ( $<1.3$ ) for spacings of one diameter or more. Troublesome regions require careful design treatment that is often a job for a specialist.

Inadequate Joining. Faulty joints are a particular hazard in fine soils where infiltration or exfiltration may occur. Since most commercial pipes have good joining systems, this problem usually does not occur. Joining pipe sections on curves requires special care. Criteria and charts with maximum pipe lengths as a function of radii of curvature are given in pipe manufacturer's association manuals (e.g., ACPA, AISI).

Incorrect Use of Backpacking or Imperfect Trench. Large increases in load capacity are theoretically possible from using backpacking with culverts (See Appendix E). To the time of this writing, however, no properly designed functional culvert installation using backpacking has been built. Straw and other organic materials have been used over the crown, but this practice is strongly discouraged. Tests by the California Highway Department have demonstrated the deleterious behavior that can result from such practices [F-7].

Similarly, improper response can result from the use of the so-called imperfect trench method [F-8]. A soft medium above the pipe may result in excessive upward deflections of the crown.

The configuration, stiffness, yield stress, yield strain, confining soil, and construction procedure must be carefully selected and controlled to achieve successful backpacked installations. Otherwise, undesirable behavior and failures can be expected.

#### Dead and Live Loading

Wall Yielding or Crushing. Wall crushing has been noted in several buried R/C pipe tests, including the culvert experiment at Mountainhouse Creek [F-5]. A parallel phenomenon for metal culverts, characterized by a local crimping, has been observed in tests of metal pipe [F-9,F-10]. This type of failure usually occurs near the springline. For well-compacted soils wall yielding is the anticipated mode of failure for corrugated metal pipes with excessive soil load. On the other hand, loose compaction promotes buckling and bending.

Seam Failure. A few seam failures have been noted in lock-seam pipe and at the holes of large bolted corrugated metal pipes [F-9,F-10]. Such failures are rare and would not be expected to occur in practice.

Excessive Deflection. One of the major criteria for flexible culvert design has been that the horizontal diametral deflection shall not exceed 5% of the diameter. This is about one-fourth of the deflection to cause caving of the crown. For flexible culverts, deflection

is primarily dependent on the effective soil modulus; hence, excessive deflection will not occur if the backfill is densely compacted and if that compaction is maintained.

The Iowa Formula has been used as the principal relationships for predicting deflections. Recent studies have, however, cast doubt on the degree of its validity; mainly because the modulus used therein does not seem to be subject to determination from any standard laboratory soils test [F-11].

Adequate prediction of deflection depends upon correct determination of culvert deformation from backfilling. It is also highly dependent on correct evaluation of the effective soil modulus in the near vicinity of the interface.

Excessive upward deflection of the crown during backfill may occur on the larger pipes. Control is acquired simply by piling earth on the crown. It should be kept in mind that excessive deflection can develop long after the installation has been completed if the backfill and embankment soils exhibit creep.

Buckling. Buckling may be either elastic or inelastic and usually develops from a higher mode shape [F-12]. The buckling load depends on the soil modulus in addition to the stiffness of the pipe. As with most transitional phenomenon, buckling of buried pipes occurs very suddenly in a snap-through action.

As is illustrated in this report, many corrugated metal culverts experience yielding in their outer fibers at relatively low loads. It follows that inelastic buckling theory is applicable. No complete inelastic buckling theory is available for confined cylinders; however, some work has been done on the problem [F-13].

The inelastic buckling load can be conservatively approximated by using the effective moment of inertia of the section corresponding to any given loading in an elastic buckling theory.

Two factors alleviate this potentially difficult problem. First, corrugations in most pipe are sufficient to insure against buckling failure if the backfill is good. Second, variation of the inelastic buckling load from the elastic value is probably less than the variation due to the soil modulus. Nonetheless, if elastic buckling theories are used, a higher safety factor against buckling can and should be used to account for the acknowledged variations and uncertainty.

A dangerous buckling condition may occur for deeply laid pipes in poor soil with a high water table environment. As Molin has pointed out, for those circumstances and with cohesive soils, the soil modulus decreases as the load increases.

Metal pipes are corrugated to permit their efficient handling and to achieve good buckling and in-plane bending resistance. Still, the buckling load should be checked in the normal course of design. Even after buckling failure occurs, some pipes are still capable of resisting

substantially increased load prior to failure. This is possible because of arching developed in the soil.

Special care must be taken to avoid buckling if backpacking is used. The reason is that the backpacking may have a lower modulus than the soil, thereby reducing buckling resistance.

Longitudinal Bending, Tension, and Compression. Major causes of longitudinal bending are uneven settlement of the foundation due to underlying rock or other factors, and differential settlement from varying load (fill height) across the embankment. Various approaches to handling this problem are summarized in Appendix C.

Longitudinal bending is not a problem in embankments if the settlements are calculated in advance and the pipe is cambered accordingly.

Longitudinal tension or joint separation tends to occur as the soil moves toward the toe of embankments [F-7]. The outward displacement is caused by compaction and dead load from the upper layers. Such motion may be large if the original grade transverse to the length of the embankment is steep. Except in special circumstances, longitudinal compression failure would not be expected to be of concern in culverts; however, this mode of failure has occurred in drain tile. The circumstances involved compression of shallow buried tile by longitudinal interface shear from thermal expansion of the soil. Leaving space for expansion in the joints solved the problem.



The subject of hydraulic loading is beyond the scope of the present research except insofar as hydraulic loading causes structural failures. Comments here, therefore, will be restricted accordingly.

Undermining. Hydraulic undermining may be a long-term phenomenon, or it may occur surprisingly sudden. The first type of behavior involves infiltration or exfiltration of fluid or longitudinal flow along the extrados. A second type follows flotation uplift of the ends, which permits a torrent of water to rifle along the exterior of the pipe.

In the infiltration process, fine particles of soil are gradually transported into the pipe until the pipe confinement is debilitated. With exfiltration, the strength of the supporting soil is reduced by an increase in water content. These problems may be averted by a variety of techniques, the most obvious of which is assuring good joint seals. Diaphragm barriers may be used to prevent flow along the outside of the pipe, or sub-drains may be used where the cost is warranted. Stilling basin should be configured to avoid vortex action which could undermine the end of the pipe, the embankment, or both. Several good studies have been made on stilling basins [F-14, F-15].



Flotation. One technique for consolidating granular backfill in trench-type installations is by combined flooding and vibration. Unless care is exercised, the pipe will float out of the backfill. This unfortunate situation can be avoided by using the method only in free-draining soils, by not flooding too great a length at one time, and by employing alternate compaction methods above the springline.

Invert Uplift. According to manufacturers' representatives, large radii of curvature inverts in large-span or soil-arch culverts have been known to buckle upward under the pressure from groundwater in regions where streams do not flow year round. This is another condition which may be readily designed for if the designer is aware of the potential problem. Draining, venting, or using a smaller than normal invert radius are among the solutions to the problem.

Hydrostatic Uplift of Ends. Several failures have involved hydrostatic uplift of the ends. In these cases, the water level rose above the crown, and the bouyant force caused several diameters of pipe length near the end to bend vertically upward.

High water at the upstream end of the culvert is often attributable to debris blockage. This condition should be avoided, and good tie-down anchors should be provided at the ends.

Under high-water conditions, a vacuum may develop in the pipe near the upstream end. It has been hypothesized that this vacuum, in

conjunction with the external pressure, initiates collapse. Flow along the exterior length of the pipe completes the destruction.

Saturation of Backfill. Achieving quality backfill of other than granular materials requires control of water content. Heavy rains or other causes of change in soil water content during the construction period may cause appreciable changes in system stresses, as has been shown in field tests [F-6,F-7]. Reinforced plastic film can be used during construction to protect large culvert systems from significant changes in moisture content.

The possible occurrence of liquefaction should be considered in any soil system where free water is present, particularly in regions of high earthquake activity. Underlying saturated granular layers could, due in part to the increased pore pressure from the embankment load, be a location of failure [F-16].

Canyon walls and other areas where embankments are built may contain springs capable of saturating large areas if they are not properly drained. Such saturation could reduce the strength of the foundation or the backfill and produce a condition susceptible to liquefaction.

Although the probability of liquefaction failure is small, the possibility should be considered -- at least for the more expensive installations.

Inlet Collapse. Flash floods have been known to collapse inlets of metal culverts without headwalls [F-17]. The sides fold inward and the bottom folds upward at the inlet, thereby grossly restricting the flow. Such behavior has occurred with sufficient frequency that some states now require headwalls on all new installations other than small-diameter pipe.

#### Other Potential Failure Conditions

Embankment Failure. Embankment materials that will stabilize and provide the required confinement are of critical importance to culvert installations. Embankments and retaining walls have failed after several years of service due to creep or to water conditions [F-18]. Only in recent years have methods become available for learning whether or not a given soil will stabilize and roughly the rate at which the process will occur [F-19].

Culvert literature, written before the basic theory of creep in soils was developed, gives a variety of times for achieving stability. Now it is known that the time to stabilize depends on the thermo-chemical properties of the soil and on the state of stress. Stresses on a culvert remain essentially constant after completion of an embankment; however, deformation in time continue until the deflection is two or more times the initial values.

The above considerations are important for clayey environments,\* since estimates of creep are necessary to determine whether or not long-term failure will occur, and, if not, what the final deformed state will be. Such evaluations are, however, beyond the scope of the present program.

An even more serious concern with embankments than creep is water content. Use of excessively wet fill in embankments or intrusion of water into the embankment after its completion may result in failures. A general criteria for fill in embankments is that the moisture content must be less than 1.2 times the plastic limit. For high fills, a more stringent criteria would be justified. The water content, gradation, face slope, compaction, and other aspects of embankment criteria and design inevitably influence culvert performance, even when select materials are used in the near vicinity (one diameter) of the pipe. More on embankments is given in Appendix B.

Rodent Damage. Ground squirrels and other burrowing creatures can seriously degrade an embankment face, loosening the soil and producing paths for the intrusion of water. Saturation of the soil, thereby, can contribute to culvert failure.

---

\*Competent granular soils experience very little creep except under very high stress.



Special care should be taken with instrumented installations where long-term measurements are to be obtained. Scientific investigations show that gophers and ground squirrels cannot get their mouths open wide enough to chew cables over 1.5 inches in diameter. Smaller cables, pipe wrappings, or other succulent materials should be suitably protected near the embankment face in areas where rodent infestation exists.

Corrosion. Corrosion may occur from interaction of pipe materials with the atmosphere, the soil, or contacting fluids. The fluids may be in the earth or internally transported. Some corrosion problems can be extremely complex, requiring solution by experts. With most culverts, however, the wall thickness is increased or coated by a predetermined amount to account for the loss of materials from corrosion and abrasion over the design life.

A number of state highway departments have done work on the corrosion of culverts, including New York and Utah. The latter and certain other information on corrosion of culverts are reviewed in Appendix A.

Where severe corrosion environments are encountered, plastic pipe can be used. Many such pipes, however, are susceptible to creep and damage from fire. Other solutions include the use of bituminous, rubber, neoprene, or other suitable coatings, wrappings, or linings. Plastic-impregnated concrete also has a high resistance to corrosion.

Care should be taken to carefully assess the influence of linings and wrappings on the hydraulic and structural performance of a pipe. Abrasion may destroy interior liners, if they are not made of proper materials.

Abrasion. Most culvert abrasion is caused by water laden-granular particles acting against the pipe interior. Severe abrasion may be expected where there are continuously flowing, steep, granular stream beds. Additional information on abrasion is available in Appendix A.

Failure From Expansive Soils. According to a recent article, 20% of the area of the United States is affected by expansive soil movements [F-20]. Reportedly, the damage therefrom is more than twice that from other natural disasters. Thin-walled pipes near the surface are vulnerable to expanding soil; however, damage seldom will be experienced for burial depths greater than 20 feet. Shallow, large-diameter culverts are particularly vulnerable. Uplift of soil near the inlet or outlet of a deep embankment could cause uplift of the ends, although, such problems would usually be precluded in the normal course of embankment design.

Natural Disasters. Other natural disasters of concern in culvert design are floods and earthquakes. One instance of collapse from a flood is documented in Part II of this appendix. Drainage systems,



including culverts, are commonly designed for 50-year storms, and, occasionally, a more severe storm induces a failure. Such criteria recognize that it is not economically practical to design for the extreme flood condition any more than it is to design for the extreme earthquake.

Earthquakes pose several threats, yet there is no documentation of a single culvert failure attributable directly to earthquake effects. Potential failure conditions from earthquakes include slide initiation, pipe shear or elongation, and vibration settlement. Vibration settlement would only be expected in areas where there are granular soils, particularly sand. If the sand is saturated and loose, liquefaction could develop. Perhaps the reason that there are no known failures from earthquake-related effects is that they have been properly anticipated in design. Sink hole or subsurface excavation settlements or collapse are other possible, but unlikely, sources of problems.

Effects From Adjacent Structures. There is a trend toward using multiple culverts as alternatives to bridges. Properly done, great economy is achieved thereby. Interacting stress fields or displacements may be a source of difficulty; accordingly, careful analysis of such designs is warranted prior to their construction. In general, spacing of one-fourth of the width of the largest pipe will be adequate,

providing that width is sufficient for compaction equipment to pass between the structures.

Excessive Settlement. Surface deflection of a loaded pavement is related to crown deformation of shallow-buried culverts. Thus, stiffness is a prime consideration in the design of shallow culverts. For this reason, some highway design groups insist on using circumferentially corrugated pipe rather than the newer helical corrugated pipe, because, for a given diameter, gage and corrugation, the latter has a slightly lower stiffness than the former.

Pipe Twist. Some difficulty has been experienced with corrugated pipe twisting as it is backfilled along its length. This is most likely to occur where the fill is over a slope that varies along the length. No failures are known to have resulted from such action, and none need occur if engineers and constructors are made aware of the potential problem and they take steps to avoid it.

Infiltration or Exfiltration. As with tunnels, water passing into culverts from the surroundings is not necessarily bad, providing soil fines do not move with the water. Likewise, water leaking out of the pipe is not necessarily bad, if it does not reduce the strength of the confining soil. The infiltration-exfiltration problem is not nearly as severe as it is in sewers. Still, the designer must be alert to

this threat, and care must be taken in the field to assure proper joining to avoid destruction of the pipe confinement by water.

Endwall Failure. Difficulties may be expected in certain installations with endwalls due to differential settlements of the wall and the pipe and other problems common to retaining walls. Most reinforced concrete culvert endwalls are not very high, consequently, endwall problems after construction are usually minimal.

Freeze-Thaw. Some unusual problems have been encountered due to freezing. For example, pavement heave was experienced over a shallow-buried metal culvert under the Washington, D.C., Beltway. Freezing of the cover soil from above and from cold air in the pipe caused the uplift. Suspending a burlap cover over the ends of the pipe to prevent circulation of cold air solved the problem. The bottom of the burlap was fastened to a floating plank that raised and lowered with the water level.

Damage to concrete pipe from freeze-thaw cycles might be expected; however, the good quality of concrete that is used in most large concrete pipe minimizes this problem.

In designing and building culverts or culvert bridges for cold climates one should always be alert to the potential deleterious effects of freezing. Compacting ice blocks or frozen soil in the backfill is

probably the most common of this class of problems. As the ice melts, backfill stability is greatly reduced.

Creep. The characteristics of plastic pipe vary widely, depending on the manufacturer. All pipes creep, however, resulting in a reduced modulus with time. One design criterion is for a 50% reduction in modulus after 50 years. In granular soil environments, load will be transferred to the soil as creep takes place with no degradation in system performance (except where very high soil stresses exist). In clay soils essentially hydrostatic conditions will develop as creep takes place in the pipe and in the soil.

There are some advantages to the noted change in modulus with time. For instance, the pipe is relatively stiff during backfill (when the stiffness is needed), yet it becomes less stiff with respect to the soil (often improving the system performance) after the installation is completed.

The principal danger of creep is that the buckling resistance decreases as the modulus decreases. As a consequence, a larger safety factor against buckling is recommended for plastic pipe than for other common pipe types.

Fire. Culverts are common shelters for hobos and hippies and an intriguing, even though unauthorized, play area for children. Thus,

the possibility exists of a fire being built in the culvert. (Brush fires might also affect the ends of culverts.) For these reasons, plastic or other pipe used as a culvert should be fire-resistant.

Caving of Tunneled Culverts. Newly developed tunneling machines have enhanced the practicability of installing tunneled culverts in existing or new embankments. Considerable embankment construction time can be saved, if the culvert discontinuity is avoided. Tunneled culverts, however, entail most of the dangers and troubles of conventional tunneling, including surface settlement.

Potential failure modes for tunneled culverts should be thoroughly understood before undertaking to design or build such an installation.

Sediment Closure. Sediment sometimes fills a significant portion of culvert openings during periods of low flow. This is not as serious a problem as one might think, since the deposited silt is readily eroded away when large flows occur; the culvert becomes "re-opened" to accommodate the higher flows. Sediment blockage might cause difficulties in flash floods where time is not available for erosion of the sediment.

Soil-Induced Failure. Of the various soil types that might contribute to failure of a buried pipe, expansive soils is the most



likely [F-20]. The large pressures developed by expansive soils could easily crush a buried pipe, and steps should be taken to avoid any such failures, especially in locations of montmorillonite clay.

## PART II. A SURVEY OF CULVERT FAILURES

Early in this investigation it was found that relatively little quantitative information is available in the literature on culvert failures. Some failures are documented in NCHRP-116 [F-21] and in the Montana study report [F-17]; there is a modicum of failure data from tests [F-5,F-7]; and, in general, unpublished information is known on a few of the more dramatic recent failures. To help improve knowledge of failures, a contract was let to Utah State University under the direction of Reynold Watkins to accumulate the needed data. The next four sections of this appendix are from the Utah State University report; appendixes to that report are deleted for brevity.

### Objective

The objective was to compile data on important structural failures of reinforced concrete and corrugated metal pipe culverts. The



following information was considered essential to properly describe culvert failures:

- (1) A discussion of the estimated cause and mode of failure.
- (2) A complete description of the culvert including material properties, geometry, etc.
- (3) A complete description of the boundary value problem; i.e., the live loads, depth of cover, type of bedding, backpacking, construction method, etc.
- (4) A complete description of the backfill soil; e.g., soil type and classification, density, soil modulus, etc.
- (5) All data on measurements, such as pressure, stress, strain, or displacement of the culvert, taken before, during, or after the failure.

#### Survey Procedure

A letter and a questionnaire were sent to each Department of Highways in the fifty states and Puerto Rico, requesting the above information. In addition, known cases of failure in the private

sector of the industry were also investigated. The majority of all cases encountered was incompletely documented.

## Survey Results

Of the 51 highway departments contacted, 31 had responded by the time this report was written. Seventeen of these reported that they either had no structural failures or that they had no documentation of such failures. Three states reported that they had experienced failures due to secondary problems, such as corrosion, scour, settlement, and under-design (Tables F-2 through F-4).

Twelve states reported structural failures of culverts with the addition of limited information from other sources.

From available information, a number of similar causes of culvert failures are detectable. Table F-3 is a listing of the causes of failure reported.

In nearly every case, there was apparently more than one cause of failure. The information in Table F-3 cites the most likely, primary cause for each case. It should be remembered that there are contributing factors from other sources besides the primary cause.

Table F-2. Response to Questionnaire Sent  
to State Highway Departments

State	No. of Failures	Comments
Alabama	4	Corrosion problems
Arizona	0	No records
Arkansas	0	No records
Colorado	3	No records
Florida	0	No records
Georgia	0	No records
Hawaii	0	-
Idaho	0	Corrosion problems
Indiana	4	-
Kansas	0	No problems
Kentucky	15	Two cases documented
Michigan	1	-
Minnesota	19	Statewide survey conducted
Mississippi	0	Records not available
Missouri	0	Secondary problems
Nebraska	0	-
Nevada	3	-
New Hampshire	2	-
New Mexico	0	Under-design problems
North Carolina	2	-
Oklahoma	0	No problems
Oregon	1	-
Ohio	18	Culvert durability survey conducted
Pennsylvania	0	No records
Puerto Rico	0	Records not available
Rhode Island	0	No records
Tennessee	0	No records
Texas	0	No records
Vermont	2	-
Virginia	1	-
Washington	<u>3</u>	-
	78	

Table F-3. Failures Reported by Other Sources

Location	Failure Cause
Juneau, Alaska	Scour of outlet slopes
Black Mesa, Arizona	Poorly compacted fill
New Port, Kentucky	Poorly compacted and saturated fill
Wolf Creek, Montana	Logitudinal joint failure
Alleghany County, New York	Uplift of inlet by vortex
Dallas, Texas	Loose joint seals
Parley's Canyon, Utah	Construction accident

Table F-4. Causes of Failures

Cause	Source		
	States	Other	Total
Backfill			
Poorly compacted	4	2	6
Saturated material	4	0	4
Frozen material	1	0	1
Uplift of inlet	10	1	11
Insufficient bedding	2	0	2
Scour			
At inlet	1	0	1
At outlet	0	1	1
Settlement	1	0	1
Piping	2	0	2
Under-design			
Excessive dead load	4	0	4
Inadequate pipe	1	0	1
Inadequate reinforcement	1	0	1
Maintenance Problems			
Fire	2	0	2
Undercut inlet	1	0	1
Corrosion	12	0	12
Construction	5	2	7
Unknown	13	0	13

## Discussion of Results

Poor construction procedures were one of the main causes of failure. This included such things as distortion from allowing heavy equipment to pass over the installed culvert before sufficient fill had been placed, and failures due to poorly placed rivets or joint-protection gaskets. Only careful on-site supervision and inspection can forestall this type of problem.

Construction accidents were also cited as a failure cause. This included landslides caused by blasting or heavy rains.

Scour of the banks beneath the ends of culverts was another cause of failure. Scour usually occurs when insufficient slope protection has been provided, and the water dissipates its energy by eroding the slopes. Once sufficient erosion has taken place, the cantilevered end breaks away from the supported culvert sections. Scour may be prevented by installing a drop-structure and/or slope protection.

One very dramatic cause of failure was uplifting of the inlet end due to vortex action. When a culvert is unable to carry unusually high flows, such as those due to floods, the inlet becomes submerged, and a vortex is created at the inlet. The pressures inside the vortex, where there is no water, will be close to atmospheric; consequently, the downward pressure inside the pipe becomes less than the upward hydrostatic pressure on the extrados in the region of the invert.



Apparently it is this net uplift that raises the culvert's end, blocking the flow. This can be prevented by properly anchoring the mouth to its foundation with anchor bolts and/or straps; Minnesota rectifies the problem by requiring headwalls for metal pipes with diameters greater than 8 feet.

Another reported cause of failure was placing the backfill soil in a near-saturated condition. Upon compaction of or the addition of fill material, the soil tends to liquefy due to excessive pore pressures. These pore pressures can cause the sides of the culvert to deflect inward. As the deflection occurs, the liquid soil flows with it, maintaining pressure on the culvert sides. The result, as described in the Georgia response, was a culvert squeezed vertically until the sides nearly touched. This cause can be better controlled by placing backfill that is near its optimum moisture content and is not excessively wet.

Improperly compacted backfill was another failure cause. Thereafter, sidefill is unable to support the culvert laterally, and the culvert deflects downward as the weight of the fill material increases. A similar problem is that of placing backfill containing frozen material which can later thaw and produce settlement.

Still another cause was insufficient bedding, which can cause shear, joint separation, and cracking.



Of the failures reported, only four could be attributed to under-design. This indicates the conservative nature of most design procedures in use today.

There were six cases of failure attributed to maintenance problems. These included a fire started to clear a culvert of weeds, and an inlet that was undercut during cleaning and was subsequently eroded by water. Failure due to abrasion or to chemical corrosion was included under maintenance failures.

Table F-5 lists the types of culverts that failed.

#### Commentary

Principal observations from the survey are that:

- (1) The number of failures that have occurred is exceedingly small, considering the very large number of culvert installations.
- (2) Corrosion and uplift of inlet ends occurred with the greatest frequency, followed by faulty construction procedures.

(3) Most failures seem to stem from more than one cause; probably failure in one mode triggers failure in one or more other modes.

(4) Documentation is scanty. Complete documentation of future failures is strongly encouraged.

Table F-5. Failures by Culvert Type

Type	Number of Failures by Source		
	States	Other	Total
Structural plate pipe - Arch	11	0	11
Structural plate pipe - Circular	6	1	7
Corrugated metal pipe - Arch	3	0	3
Corrugated metal pipe - Circular	27	6	33
Reinforced concrete pipe	9	0	9
Reinforced concrete box culvert	1	0	1
Not specified	<u>6</u>	<u>0</u>	<u>6</u>
Total	63	7	70

## YIELD-HINGE THEORY

## DEVELOPMENT OF PLASTIC HINGING FOR CULVERTS

In this section a theory is formulated to account for symmetrical yielding at the quarter points of cylindrical shells embedded in a homogeneous, isotropic, elastic medium. The theory is primarily intended for use in conjunction with Burns' Elastic solution (Level 1, CANDE).

In Chapter 10 it is shown that Burns' solution gives maximum moments at the crown and springline. More importantly, these moments are approximately equal in magnitude and opposite in sign. Since Burns' theory is based on quartic symmetry, i.e., symmetry about the horizontal and vertical pipe axes, it follows that the quarter points (crown, invert, and horizontal diametral extremities) are regions where plastic yielding and hinging will occur. Accordingly, the hinging theory is based on quartic symmetry.

With the above in mind, consider the stages of deformation portrayed in Figure G-1. Starting from the undeformed position, (1), the pipe is assumed to deflect to the elastic position, (2), (predicted by Burns' theory), and it is fictitiously restrained from yielding. Now, as the yielding constraint is relaxed, yielding occurs in the outer fibers in the region of the crown and springline. This yielding

causes a plastic rotation at the hinges, (4), which in turn promotes additional deflection, (3). Next, as the pipe deflects, additional passive soil pressure is mobilized in the region of the springline, and soil pressure is reduced in the area of the crown. This change in pressure distribution corresponds to a reduction or a "correction" of the moment diagram to maintain equilibrium.

Figure G-2 depicts a typical elastic moment diagram,  $M_e$ , and a final moment diagram,  $M_f$ . The latter denotes the equilibrium position of the final deformed shape. Inherent in Figure G-2 is the "correctional" moment diagram,  $M_c$ , defined as:  $M_c = M_e - M_f$ . Thus, if the "correctional" solution were known, it would be a simple matter to determine the final solution by superposition. Thus, the problem can be resolved to finding the "correctional" solution.

If the plastic hinge rotations are assumed to occur equally at points of the crown and springline, then the correctional boundary value problem can be approximated by a "pinned" pipe segment embedded in a soil medium, as indicated in Figure G-3. The plastic rotations,  $\alpha_p$ , are the prescribed boundary conditions. The solution to this boundary value problem is detailed in a later section; for present purposes it is sufficient to know that a solution exists if the plastic rotations,  $\alpha_p$ , are known. However, they are not known. Therefore, an iterative procedure must be developed in which the rotations are "guessed," and the correctional boundary value problem is solved to determine a trial final moment diagram,  $M_f$ . Using  $M_f$  in plastic hinge

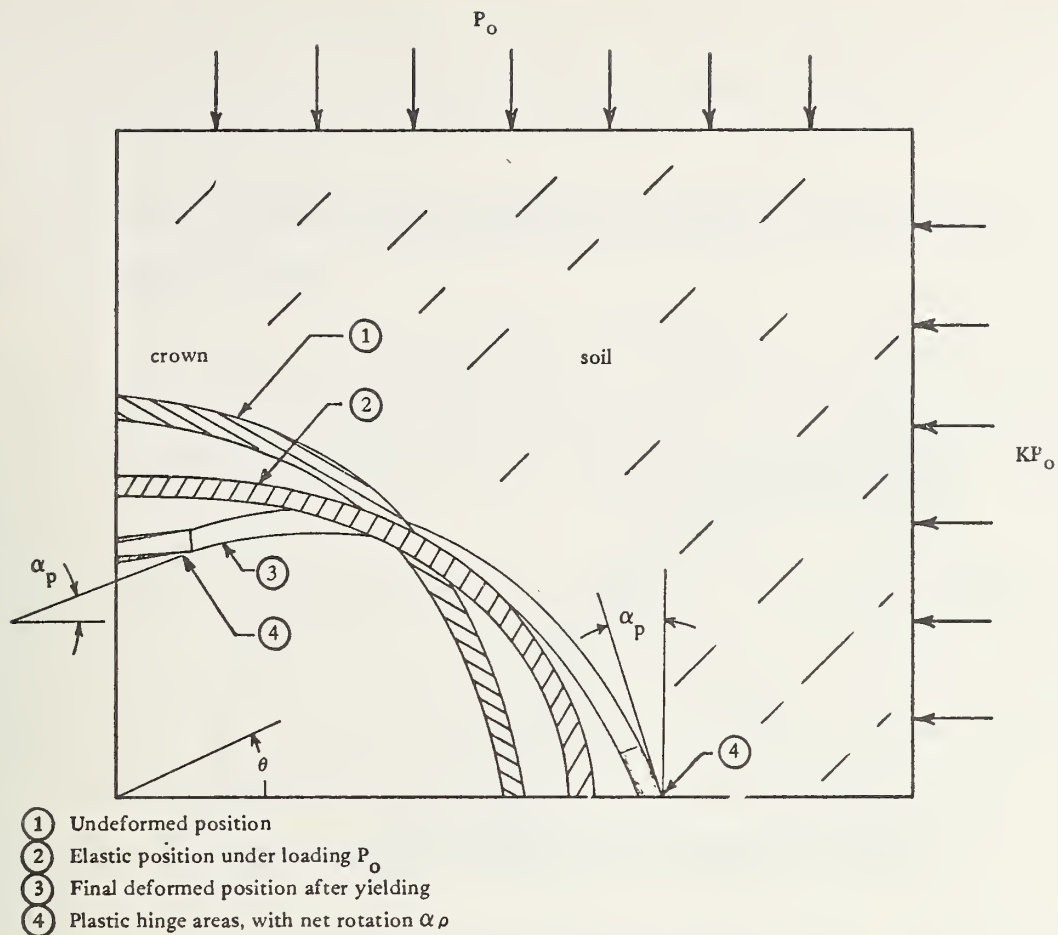


Figure G-1. Deformation stages of pipe segment.

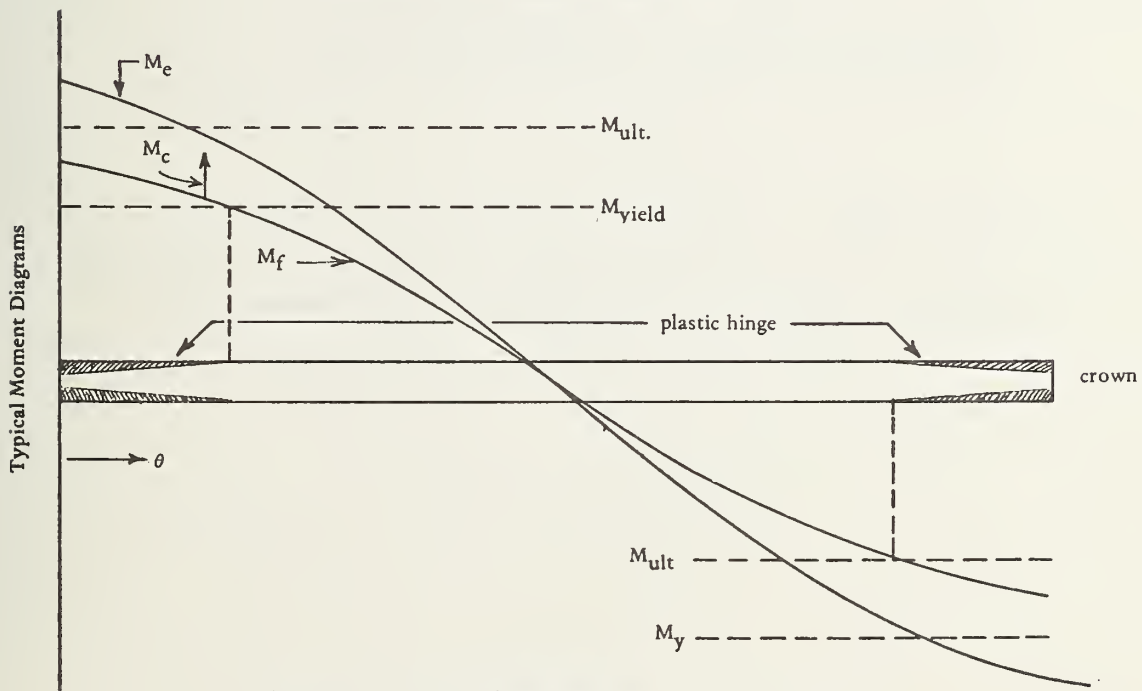


Figure G-2. Moment diagrams along quarter pipe segment.

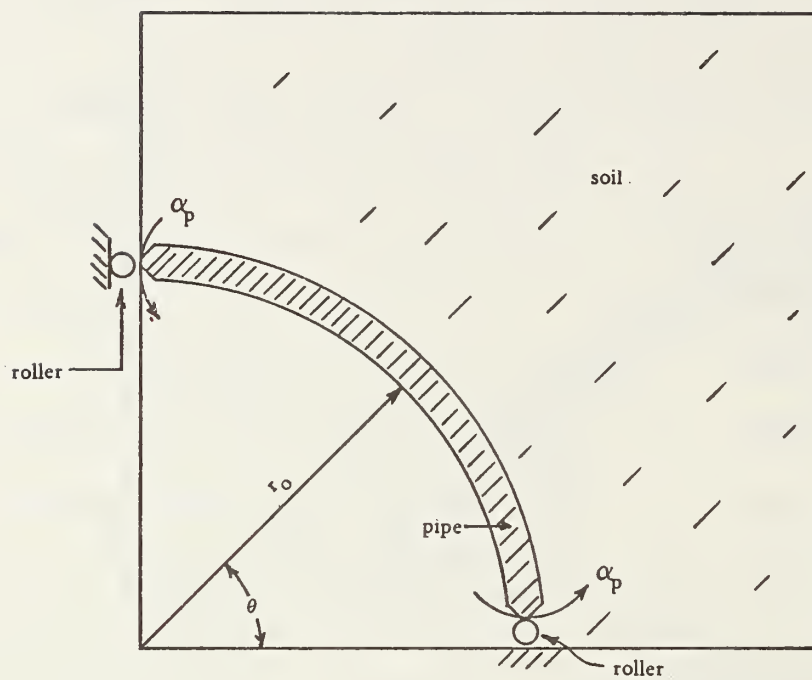


Figure G-3. Correctional boundary value problem.



theory, the corresponding plastic rotations can be computed and compared with the assumed values; then, they can be updated accordingly until convergence is achieved.

Specifically, the following steps are required in solving the plastic hinging problem:

- (1) Solve the elastic problem, and obtain the structural responses, including the elastic moment diagram,  $M_e$ .
- (2) Guess at an initial value for the end rotations,  $\hat{\alpha}_p$ .
- (3) Solve the "correctional" boundary value problem using  $\hat{\alpha}_p$  as the specified end rotations. Obtain the correctional structural responses, including the moment diagram,  $M_c$ .
- (4) Determine the assumed final moment distribution,  $M_f = M_e + M_c$ ; then use plastic hinge theory to calculate the plastic rotation,  $\alpha_p$ .
- (5) Compare the computed plastic rotation,  $\alpha_p$ , with the assumed end rotations,  $\hat{\alpha}_p$ . If they are in acceptable agreement, go

to Step (6). If they are not in agreement, return to Step (3) with a new end rotation given by:

$$\hat{\alpha}_{p2} = (\hat{\alpha}_{p1} + \alpha_p)/2$$

- (6) Having achieved the correctional solution, the final structural responses are determined by superimposing the elastic and correctional solutions.

In the following sections details and assumptions of solving the correctional boundary value problem are presented as well as the formulation for determining plastic rotations.

#### CORRECTIONAL BOUNDARY VALUE PROBLEM

In this development, the correctional boundary value problem, depicted in Figure G-3, is restricted to circular pipes deeply embedded in a homogeneous soil with equal rotations applied at the quarter points. The soil is assumed to offer resistance to radial displacement in the manner of an elastic foundation. Therefore, the radial pressure developed on the pipe during deformation is taken as:

$$p_r(\theta) = \frac{\bar{K}}{r_o} U_r(\theta) \quad (G-1)$$

where  $p_r(\theta)$  = radial pressure on pipe

$U_r(\theta)$  = radial displacement of pipe

$\bar{K}$  = soil foundation modulus

$r_o$  = radius of pipe

$\theta$  = angle from horizontal

The soil foundation modulus,  $\bar{K}$ , can be determined from the plane-strain solution of a cavity of radius  $r_o$  in an infinite, elastic medium subjected to internal pressure. By determining the radial displacement at the cavity wall for a unit of cavity pressure, and using Equation G-1, the soil foundation modulus is found as:

$$\bar{K} = M_s (1 - K)$$

where  $M_s$  = confined soil modulus

$K$  = coefficient of earth pressure

From thin-cylinder shell theory, the equilibrium equations for the correctional boundary value problem are:

$$\text{Radial equilibrium: } N(\theta) + Q'(\theta) = -\bar{K} U_r(\theta) \quad (G-2)$$

$$\text{Circumferential equilibrium: } -N'(\theta) + Q(\theta) = 0 \quad (G-3)$$

$$\text{Moment equilibrium: } M'(\theta) - r_o N'(\theta) = 0 \quad (G-4)$$

where  $N(\theta)$  = thrust per unit length of pipe  
 $M(\theta)$  = moment per unit length of pipe  
 $Q(\theta)$  = shear per unit length of pipe  
 $(\cdot)'$  = derivative with respect to  $\theta$ , and Roman numeral  
 superscripts denote higher order derivative

Equations G-2, G-3, and G-4 combine to give equilibrium as:

$$M^{III}(\theta) + M'(\theta) + r_o \bar{K} U_r'(\theta) = 0 \quad (G-5)$$

The kinematic assumption of planes remaining plane in bending provides the following relationship for circumferential displacement.

$$U_\theta(\theta, z) = U_{\theta a}(\theta) - U_r'(\theta) \frac{z}{r_o} \quad (G-6)$$

where  $U_\theta(\theta, z)$  = circumferential displacement  
 $U_{\theta a}(\theta)$  = circumferential displacement at neutral axis  
 $z$  = distance from neutral axis, positive outward

The polar strain-displacement relationship is:

$$\epsilon_{\theta\theta}(\theta, z) = \frac{1}{r_o} \left[ U_r(\theta) + U'_{\theta a}(\theta) - U_r^{II}(\theta) \frac{z}{r_o} \right] \quad (G-7)$$

where  $\epsilon_{\theta\theta}$  = circumferential strain and all other strains are assumed negligible.

The stress-strain relationship is:

$$\sigma_{\theta\theta} = E^* \epsilon_{\theta\theta} \quad (G-8)$$

where  $\sigma_{\theta\theta}$  = circumferential stress

$$E^* = E/(1 - \nu^2)$$

$E$  = Young's modulus of pipe

$\nu$  = Poisson's ratio of pipe

The moment and thrust resultants are determined from Equations G-6, G-7, and G-8 as:

$$M = - \int_A \sigma_{\theta\theta} z \, dA = \frac{E^* I}{r_o^2} U_r^{II} \quad (G-9)$$

$$N = \int_A \sigma_{\theta\theta} \, dA = \frac{E^* A}{r_o} (U_r + U'_{\theta a}) \quad (G-10)$$

where  $A$  = area per unit length of pipe

$I$  = moment of inertia per unit length of pipe

Lastly, inserting Equation G-9 into Equation G-5, the governing displacement equation of equilibrium is determined as:

$$U_r^V(\theta) + U_r^{III}(\theta) + \alpha U_r'(\theta) = 0 \quad (G-11)$$

where\*  $\alpha' = r_o^3 \bar{K}/E^* I$

The solution to Equation G-11 for  $\alpha > 1/4$  is:

$$\begin{aligned} U_r(\theta) = & e^{p\theta} (A_1 \cos q\theta + A_2 \sin q\theta) \\ & + e^{-p\theta} [A_3 \cos q\theta + A_4 \sin(q\theta)] + A_5 \end{aligned} \quad (G-12)$$

where  $p = 1/2 \sqrt{2\sqrt{\alpha} - 1}$

$q = 1/2 \sqrt{2\sqrt{\alpha} + 1}$

$A_i$  = undetermined coefficients,  $i = 1, 2, 3, 4, 5$

In order to determine the unknown coefficients,  $A_i$ , the boundary conditions must be expressed in terms of the radial displacements.

---

\*Note:  $\alpha = 1/4$  includes most practical problems.



From Equations G-2, G-3, G-4, G-9, and G-10, the following relationships are derived:

$$M = \frac{E^* I}{r_o^2} U_r^{II} \quad (G-13)$$

$$Q = \frac{E^* I}{r_o^3} U_r^{III} \quad (G-14)$$

$$N = - \left( \frac{E^* I}{r_o^3} U_r^{IV} + \bar{K} U_r \right) \quad (G-15)$$

$$U_{\theta a} = - \frac{I}{A r_o^2} U_r^{III} - \left( \frac{\bar{K} r_o}{E^* A} + 1 \right) \int_{\theta} U_r d\theta + A_6 \quad (G-16)$$

where  $A_6$  is yet another undetermined coefficient arising from the indefinite integration of the circumferential displacement. Fortunately, there are six boundary conditions to determine the six undetermined coefficients. They are:

$$\begin{aligned} Q(0) &= 0 \\ Q(\pi/2) &= 0 \\ U_r'(0) &= \hat{\alpha}_p \\ U_r'(\pi/2) &= -\hat{\alpha}_p \\ U_{\theta a}(0) &= 0 \\ U_{\theta a}(\pi/2) &= 0 \end{aligned} \quad (G-17)$$

Using Equations G-12, G-14, and G-16 in the above boundary conditions produces six simultaneous, linear equations that can be solved numerically to achieve the unknown coefficients and the final solution.

This completes the derivation of the correctional boundary value problem. Applications are given in the main body of this report.

## PLASTIC ROTATION

In this section a formulation for determining the plastic rotation at the quarter points of a cylindrical shell is presented. The basic assumptions are:

- (1) Bending stresses dominate circumferential stresses so that yielding is due only to bending.
- (2) The magnitude of the moments at the quarter points is equal; therefore, the plastic rotations are equal, but opposite in sign.
- (3) The shell material is elastic-perfectly plastic.
- (4) Planes remain planes in bending.

Referring to Figure G-4, the plastic hinge area is shown shaded in the region  $0 \leq \theta \leq \theta_h$ . Drawn above the pipe are portions of the elastic moment diagram,  $M_e$ , the final moment diagram,  $M_f$ , and the yield and ultimate moments,  $M_y$  and  $M_{ult}$ , respectively.

Assuming  $M_e$  and  $M_f$  are known, it is a simple matter to determine the hinge length by finding the angle,  $\theta_h$ , such that  $M_f(\theta_h) = M_y$ . Thus, the hinge length,  $H_1$ , is given by  $H_1 = r_o \theta_h$ .

Next, it is required to determine the distance,  $q(\theta)$ , from the neutral axis to the beginning of the hinge for each point in the region  $0 \leq \theta \leq \theta_h$ . Figure G-5 shows an elastic-plastic stress diagram for some  $\theta$  in the hinge region. Equating the moment of the stress diagram to the external moment,  $M_f$ , gives the relationship:

$$\frac{M_f(\theta)}{2} = \frac{1}{q(\theta)} \int_0^{q(\theta)} \sigma_y z^2 dz + \int_{q(\theta)}^c \sigma_y z dz \quad (G-18)$$

where  $\sigma_y$  = yield stress

$c$  = distance to outer fiber from neutral axis

$z$  = coordinate from neutral axis

In most cases, the integration requires knowledge of the sectional properties of the pipe. However, with regard to standard corrugated

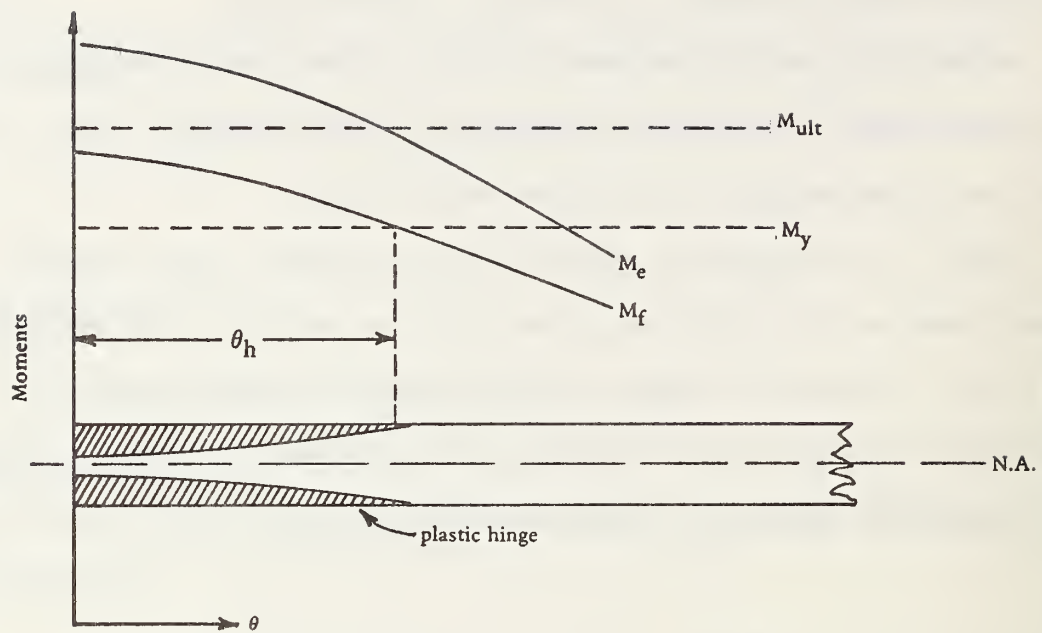


Figure G-4. Hinge area of shell.

sections, if the corrugations are approximated by a sawtooth pattern such that the same area and section depth are preserved (see Chapter 8), then the above integrals can be evaluated and  $q(\theta)$  can be determined as:

$$q(\theta) = c \sqrt{3[1 - M_f(\theta)/M_{ult}]} \quad (G-19)$$

where  $M_{ult} = (3/2)M_y$

$$M_y = \sigma_y I/c \quad (G-20)$$

Having determined  $q(\theta)$ , the strain profile corresponding to the stress distribution of Figure G-5 can be deduced. Referring to Figure G-6, strain is still linearly proportional to stress in the region  $|z| \leq q(\theta)$ . In particular, at the limit point  $z = q(\theta)$ , the strain,  $\epsilon_q$ , is:

$$\epsilon_q = \sigma_y/E \quad (G-21)$$

Making use of strain linearity, the strain in the outer fiber,  $\epsilon_f$ , is:

$$\epsilon_f = \frac{\sigma_y c}{E q(\theta)} \quad (G-22)$$

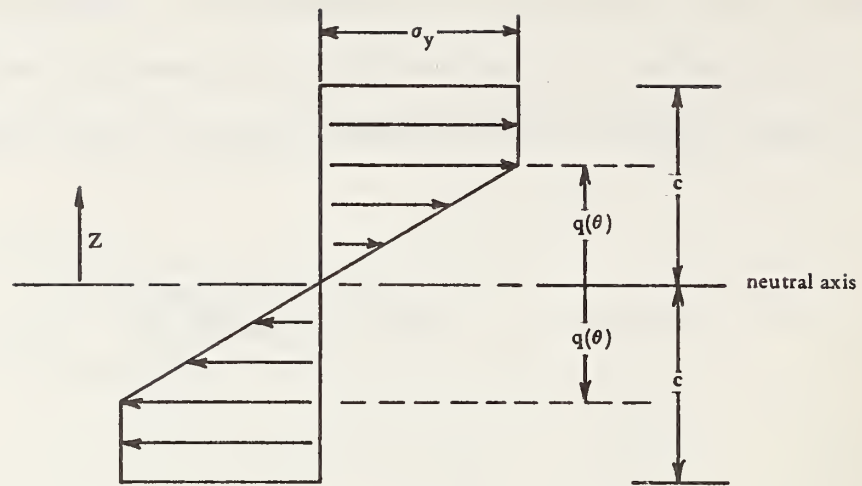
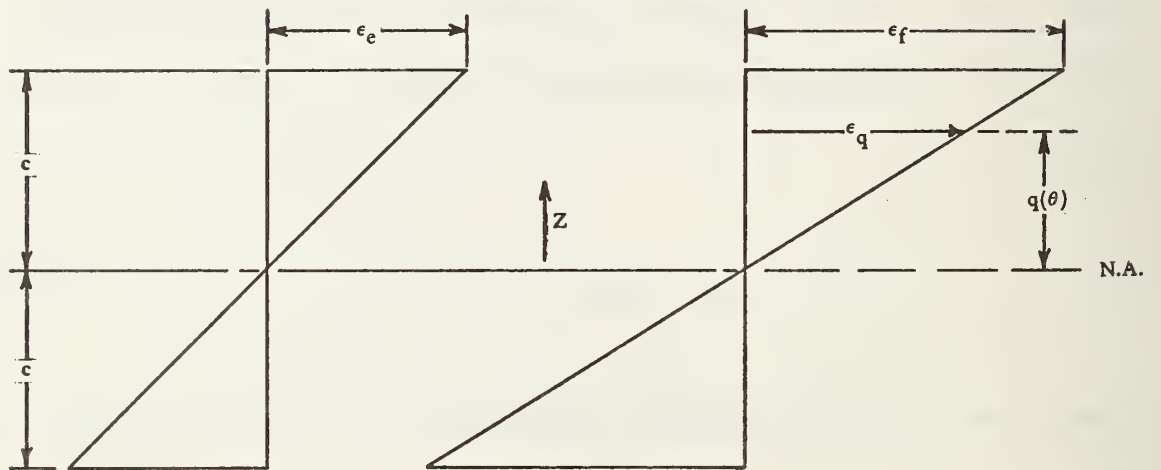


Figure G-5. Final stress distribution.



(a) Elastic strain profile

(b) Final strain profile

Figure G-6. Strain profiles.



or, replacing  $q(\theta)$ :

$$\epsilon_f = \frac{\sigma_y}{E} \frac{1}{\sqrt{3[1 - M_f(\theta)/M_{ult}]}} \quad (G-23)$$

Again referring to Figure G-6, the plastic strain in the outer fiber,  $\epsilon_p$ , is defined as the increase in strain from the elastic position to the final position, i.e.,

$$\epsilon_p = \epsilon_f - \epsilon_e \quad (G-24)$$

where  $\epsilon_e$  is the elastic strain given by:

$$\epsilon_e = \frac{M_e(\theta) c}{E I} \quad (G-25)$$

Combining Equations G-23 and G-25, the plastic strain in the outer fiber can be written as:

$$\epsilon_p = \frac{\sigma_y}{E} \left\{ \frac{1}{\sqrt{3[1 - M_f(\theta)/M_{ult}]}} - \frac{M_e(\theta)}{M_y} \right\} \quad (G-26)$$

Lastly, the plastic rotation,  $\alpha_p$ , can be obtained by integrating over the hinge length:

$$\alpha_p = \frac{r_o}{c} \int_0^{\theta_h} \epsilon_p d\theta \quad (G-27)$$

or

$$\alpha_p = \frac{\sigma_y r_o}{E c} \int_0^{\theta_h} \left\{ \frac{1}{\sqrt{3[1 - M_f(\theta)/M_{ult}]}} - \frac{M_e(\theta)}{M_y} \right\} d\theta$$

Since  $M_f(\theta)$  and  $M_e(\theta)$  are rather complicated functions, the integral is best evaluated numerically. In CANDE, Simpson's rule is used.

This completes the plastic rotation derivation and the yield-hinge theory.

## INCREMENTAL CONSTRUCTION TECHNIQUE

The term "incremental construction" is derived from the construction practice of building earth embankments in a series of soil lifts, where each lift is considered as an increment of construction (see Figure H-1). During the placement of each lift, the lift is brought up to some grade height. This implies that as the lift compresses due to compaction loads and under its own body weight, additional fill will be required to bring the top surface of the lift up to grade height.

Not too surprisingly, the analytical method that parallels this construction practice is called the "incremental construction technique." The basis of the technique is superposition of solutions from successive configurations, where each new configuration contains an additional soil lift combined into the global stiffness matrix. The only loads acting on each new configuration come from loads associated with the added lift. Specifically, the following steps are required:

- (1) Compute the stiffness matrix for the first soil lift and the associated loads (i.e., dead weight, etc.). Solve for displacements, strains, and stresses. Store them.

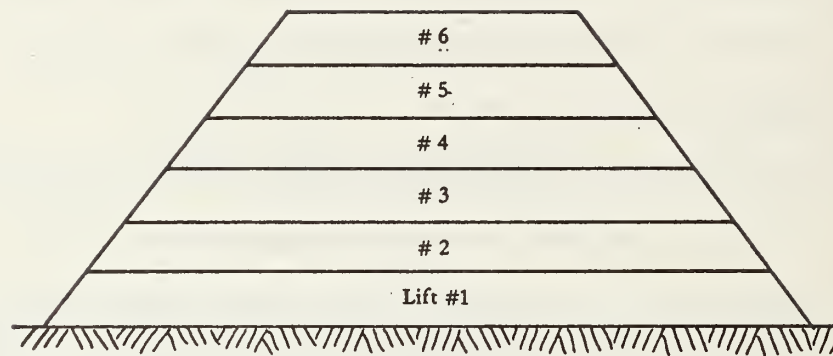


Figure H-1. Typical earth embankment in lifts.

- (2) Compute the combined stiffness matrix for the first and second lift. Determine the loads associated with the second lift. Solve this system for displacements, stresses, and strains. Add these responses to responses from (1), and store the resultant.
- (3) Continue in the same manner for each lift by, computing the global stiffness of all lifts up to and including the current lift and solving for the responses due to loads from the current lift. The sum of all responses is the final state of deformation.

It is a simple matter to redefine the material properties of any and all lifts as a function of the current fill height. This allows a simple method for handling material nonlinearity.

One may well wonder what are the consequences of analyzing an embankment as a single lift versus many lifts by the incremental construction technique. From an analytical viewpoint, the mechanical responses of an embankment constructed in a series of lifts are different from the responses of an equivalent embankment constructed in a single lift. The reason for this difference is inherent discontinuity in the deformation responses between lifts of a multilift embankment, whereas, the single lift embankment has continuous

deformations. To clarify this, consider the analysis of a multilift embankment. Imagine the first lift is set in place with a fictitious "gravity switch" turned off so that there are no deformations. Upon turning on the "gravity switch" the first lift compacts to the desired height, inducing deformations, stresses, and strains throughout the first lift. Next, let the second lift be set in place with its "gravity switch" turned off. Since the second lift is resting on the top of lift no. 1, it does not experience any initial deformation in mating with the first lift, even though the first lift has stresses and strains throughout. Upon turning on the "gravity switch" for lift no. 2, both lifts act as a continuous unit and deform together under the loads associated with lift no. 2. This induces initial deformations, stresses, and strains in lift no. 2, and additional deformations, stresses, and strains in lift no. 1. However, the previous discontinuity of deformations, stresses, and strains will always remain between lift no. 1 and lift no. 2. Similarly, when lift  $n + 1$  is placed on lift  $n$  there is discontinuity of deformation which will always remain.

On the other hand, an equivalent single lift analysis produces a continuous set of deformations and stresses throughout the embankment. Hence, it is evident that the responses of a multilift embankment will differ from those of a single lift one.

The extent of this difference is very pronounced with respect to displacements, but is much less pronounced with respect to stresses and strains. Surprisingly, maximum vertical displacements occur in



the central portion of embankments, when analyzed by the incremental construction technique, instead of at the top of the embankment as predicted from an equivalent single-lift solution. The reason for the multilift displacement pattern is simply due to the definition of the starting position of each lift. That is, when lift "n" is set in place (prior to turning on its "gravity switch"), no displacements are assumed even though displacements exist in the n-1 lifts below. Consequently, lift n does not experience pre-existing settlement. Negating this pre-existing settlement is akin to removing a rigid-body displacement from each lift and producing displacements significantly less than the equivalent single lift displacements. However, since stresses and strains are formed from the derivatives of displacements, the rigid-body effect does not influence these quantities. Thus, strains and stresses are only minorly affected by multilifts.

Examples of embankments analyzed by this method are reported in References H-1 and H-2. In the following, a very simple column example is presented that graphically demonstrates the consequences of incremental construction.

Consider a vertical column of total height,  $h$ , and divided into "N" individual blocks so that the length of each block is  $\ell = h/N$ .

This column is depicted in Figure H-2 as a homogeneous elastic column, loaded by its own body weight.

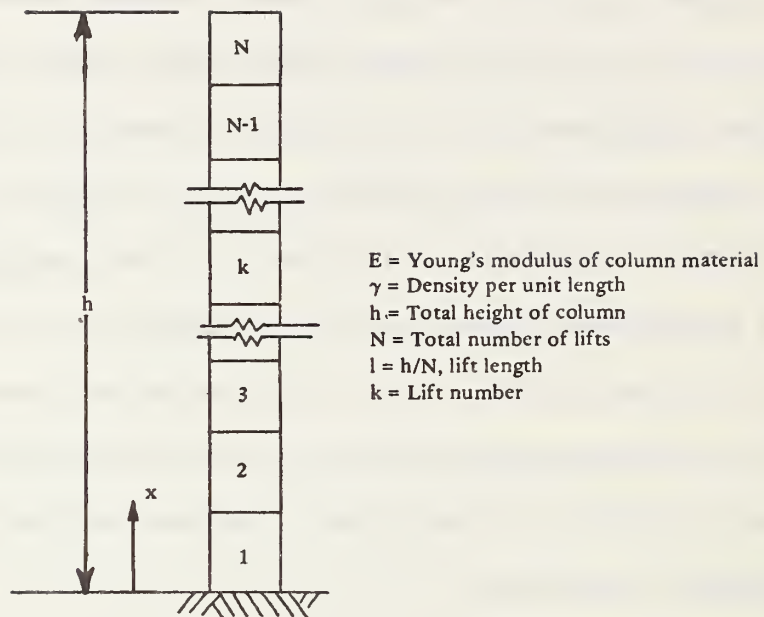


Figure H-2. Column of  $N$  increments.

Using simple one-dimensional elastic theory together with the incremental construction technique, the static equilibrium equation for the current construction increment,  $k$ , is:

$$\Delta u_k''(x) = \gamma_c/E \quad (k-1)\ell < x < k\ell \quad (H-1)$$

$$\Delta u_k''(x) = 0 \quad 0 < x < (k-1)\ell$$

where  $\Delta u_k(x)$  = displacement increment due to addition of lift,  $k$

$\gamma_c$  = body weight per unit length

$E$  = Young's modulus

$\ell$  = distance from base of column

$k$  = current lift number,  $1 \leq k \leq N$

The boundary conditions are: a fixed column base,  $\Delta u_k(0) = 0$ ; a traction free surface,  $\Delta u'(k\ell) = 1$ ; and continuity of displacement and strain between the current top lift and the lift below it. Upon integrating the equilibrium equations and applying the boundary conditions the solution for the displacement increments are:

$$\Delta u_k(x) = -\frac{\gamma_c}{E} \left[ k \ell x - \frac{x^2}{2} - \frac{(k-1)^2}{2} \ell^2 \right] \quad (k-1)\ell < x < k\ell$$

(H-2)

$$\Delta u_k(x) = -\frac{\gamma_c}{E} \ell x \quad 0 < x < (k-1)\ell$$

With Equation H-2, the displacement increments of all "N" lifts of the system can be calculated and added together to obtain the total displacement of any point in the system.

However, the summation of the displacement increments must be done with care because the addition of two or more displacement increments results in a discontinuous function. Table H-1 constitutes a conceptual tool for summing the displacement increments. The summation of all entries of a column is the total displacement function for the associated lift; i.e.,

$$u_k(x) = -\frac{\gamma_c}{E} \left[ f(k) + (N - k)b \right] \quad (k-1)\ell \leq x \leq k\ell \quad (H-3)$$

where  $u_k(x)$  = total displacement function in lift  $k$

$$f(k) = \ell k x - (x^2/2) - [(k-1)^2/2]\ell^2$$

$$b = \ell x$$

Table H-1. Summation Scheme of Displacement Increments

Displacement Increment *( $\gamma_c/E$ )	Lift Number				
	1	2	3	...k...	N
$\Delta u_1$	$f(1)$	0	0	0	0
$\Delta u_2$	b	$f(2)$	0	0	0
$\Delta u_3$	b	b	$f(3)$	0	0
$\cdot$ $\cdot$ $\cdot$ $\Delta u_k$ $\cdot$ $\cdot$ $\cdot$	b	b	b	$\cdots f(k)$ $\cdot$ $\cdot$ $\cdot$	0
$\Delta u_{n_i}$	b	b	b	$\cdots b \cdots$	$f(n)$

where  $b = \ell x$

$$f(k) = k \ell x - \frac{x^2}{2} - \frac{(k-1)^2}{2} \ell^2$$

Replacing  $\ell$  by  $h/N$  and rearranging terms, the final expression for total displacement in lift  $k$  is:

$$u_k(x) = \frac{\gamma_c}{E} \left[ h x - \frac{x^2}{2} - \frac{(k-1)^2}{2} \left( \frac{h}{N} \right)^2 \right] \quad \frac{h}{N} (k-1) < x < \frac{h}{N} k \quad (H-4)$$

Taking the derivative of  $u_k(x)$  gives the total strain in lift  $k$  as:

$$\epsilon_k(x) = - \frac{\gamma_c}{E} (h - x) \quad 0 < x < h \quad (H-5)$$

Note that the strain is independent of  $N$  and  $k$  so that Equation H-5 holds true for all  $x$  within  $h$ . Therefore, the strain is the same regardless of how many lifts are used to construct the total column.

By contrast, displacement is a function of both  $k$  and  $N$ . Figure H-3 shows plots of the displacement function for four values of  $N$ :  $N = 1, 3, 6$ , and  $\infty$ .

From the figure it is strikingly evident that the displacements are strongly influenced by the number of construction increments. Also, the discontinuous nature of the displacement functions is observable (except for the continuous cases:  $N = 1, \infty$ ). It is interesting to note that the discontinuities are not visible in a finite element solution because a given node only has one displacement



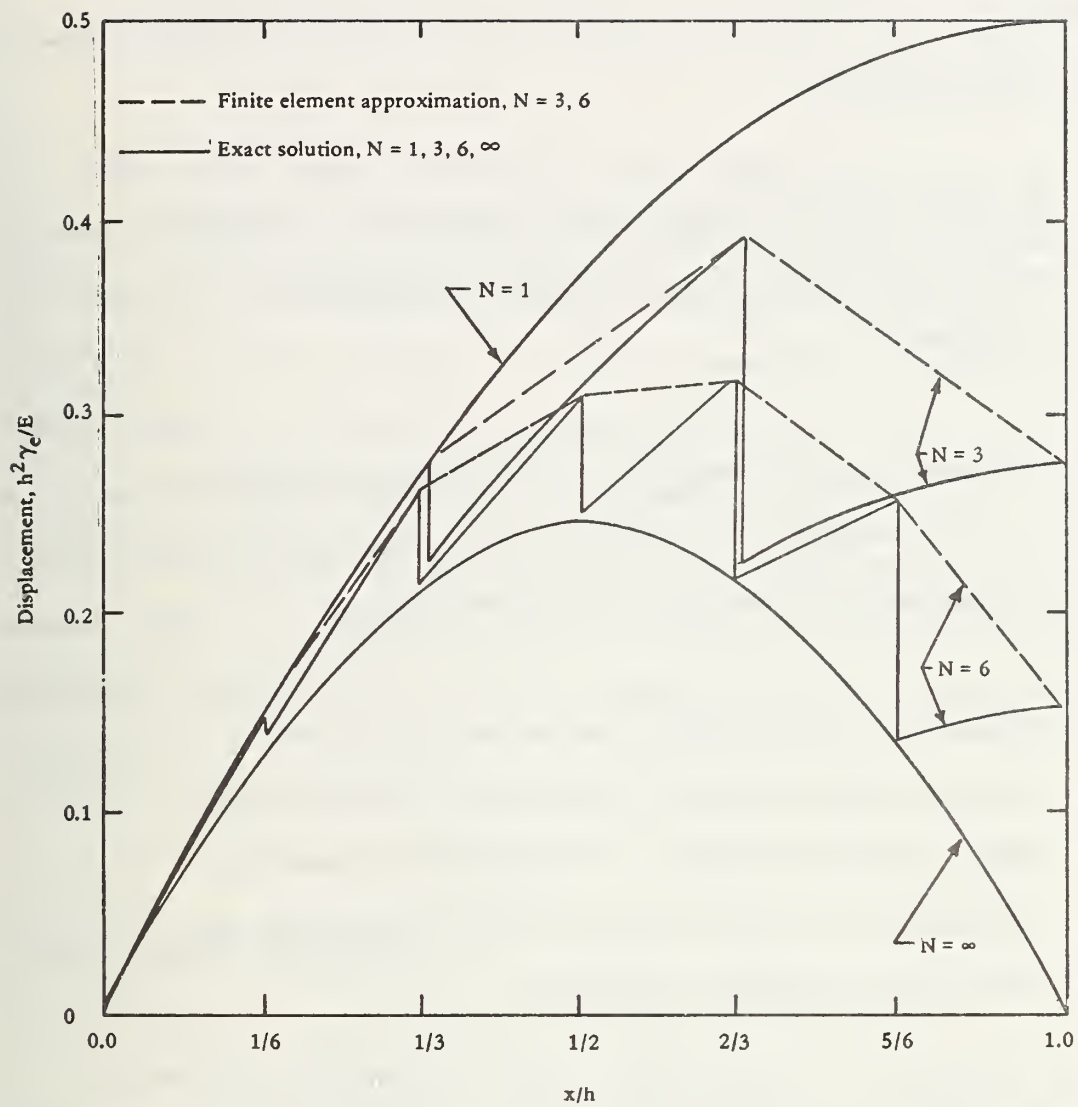


Figure H-3. Displacement distribution families for different numbers of lifts.

value assigned to it. Consequently, a finite element solution would have the appearance of a continuous solution, as indicated by the dashed lines in Figure H-3.

In summary, the incremental construction technique has the following characteristics:

- (1) It allows the consideration and evaluation of stresses and strains in the pipe-soil system as each lift is set in place.
- (2) Nonlinear material behavior can be easily accommodated by the "tangent" method, i.e., material properties can be changed after the solution for each lift.
- (3) Displacements are strongly influenced by the number of increments used, whereas stresses and strains are only weakly influenced thereby. In pipe-soil systems the technique has a more significant effect on stress and strains than in-plane embankments.
- (4) By definition, the technique produces discontinuous displacements between lifts; however, finite element solutions mask the discontinuity.

## APPENDIX I

### ELEMENT STIFFNESS DERIVATIONS

#### INTRODUCTION

The finite element methodology in this investigation employs three classes of elements: (1) a plane-strain bending element for modeling the pipe, (2) a plane-strain continuum element for modeling the soil, and (3) an interface element for treating interface conditions. The latter element is completely developed in the body of this report and will not be pursued further. In this appendix the basic finite element stiffness derivations for the bending and continuum elements are presented. Note the constitutive models for these two elements have been previously developed; thus, here the emphasis is on the spatial approximations.

#### BENDING ELEMENT DERIVATION

The bending element is a beam/column element in a plane-strain formulation, which simply implies that the beam theory is valid, providing the plane-strain equivalent of Young's modulus is used (i.e.,  $E_e = E/(1 - \nu^2)$ ). The bending element is assumed prismatic and of unit width with constant properties along the longitudinal beam axis.

Curvilinear pipe shapes are approximated with inscribed straightline segments.

With the above understanding, the traditional assumptions of Bernoulli-Euler beam theory without shear deformation are adopted as follows (see Figure I-1):

(a) Kinematics: By virtue of transverse planes remain plane in bending, longitudinal and transverse beam displacements are related by:

$$u(x,y) = u_0(x) + (\bar{y} - y)v'(x) \quad (I-1)$$

where  $u(x,y)$  = longitudinal displacement (i.e., in x-direction)

$v(x)$  = transverse displacement (i.e., in y-direction)

$u_0(x)$  = longitudinal displacement at axis of bending (i.e., at  $y = \bar{y}$ )

$x$  = beam coordinate in longitudinal direction

$y$  = beam coordinate in transverse direction  
measured from bottom fiber of beam

$\bar{y}$  = distance to axis of bending

$( )'$  = prime denotes derivative with respect to  $x$

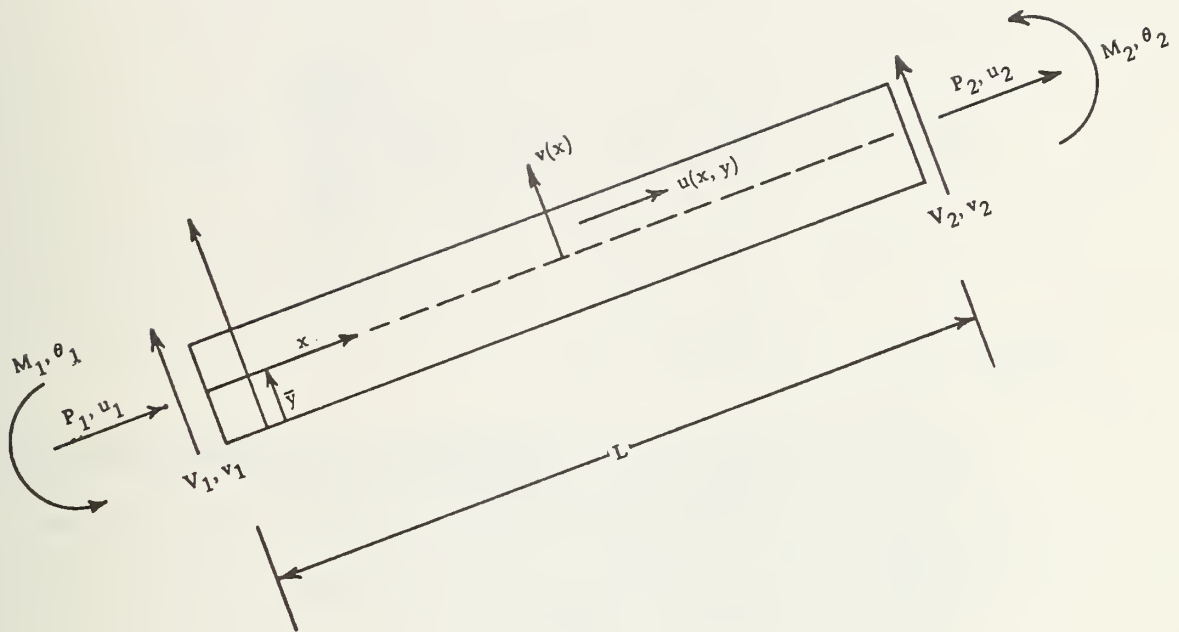


Figure I-1. Beam coordinates and definitions.

(b) Finite Element Approximation. The assumed interpolation functions for each element compatible with the assumption (a) are:

$$u_o(x) = \{\phi_1(x) \ \phi_2(x)\} \begin{Bmatrix} u_1 \\ u_2 \end{Bmatrix}$$

$$v(x) = \{\gamma_1(x) \ \gamma_2(x) \ \gamma_3(x) \ \gamma_4(x)\} \begin{Bmatrix} v_1 \\ \theta_1 \\ v_2 \\ \theta_2 \end{Bmatrix}$$

where  $\phi_1(x) = 1 - x/L$

$\phi_2(x) = x/L$

$\gamma_1(x) = 1 - 3(x/L)^2 + 2(x/L)^3$

$\gamma_2(x) = x(1 - x/L)^2$

$\gamma_3(x) = 3(x/L)^2 - 2(x/L)^3$

$\gamma_4(x) = (x - L)(x/L)^2$

$u_1, u_2 =$  axial displacements of end nodes

$v_1, v_2 =$  vertical displacements of end nodes

$\theta_1, \theta_2 =$  rotation of end nodes

$L =$  length of beam segment

Using the assumed interpolation functions, Equation I-1 may be written as:



$$u(x,y) = \{b(y)\}^T [H(x)] \{r\} \quad (I-2)$$

$$\text{where } \{b(y)\}^T = \{1, \bar{y}-y, \bar{y}-y, 1, \bar{y}-y, \bar{y}-y\}$$

$$\{r\}^T = \{u_1, v_1, \theta_1, u_2, v_2, \theta_2\}$$

$$\{ \}^T = \text{transpose of vector}$$

$$[H(x)] = \begin{bmatrix} \phi_1 & 0 & 0 & 0 & 0 & 0 \\ 0 & \gamma'_1 & 0 & 0 & 0 & 0 \\ 0 & 0 & \gamma'_2 & 0 & 0 & 0 \\ 0 & 0 & 0 & \phi_2 & 0 & 0 \\ 0 & 0 & 0 & 0 & \gamma'_3 & 0 \\ 0 & 0 & 0 & 0 & 0 & \gamma'_4 \end{bmatrix}$$

(c) Strain-Displacement Relationship. Longitudinal strains are given by the x derivative of longitudinal displacements, (i.e.,  $\epsilon = u'(x,y)$ ). All other strains are assumed zero. From Equation I-2 the strain is:

$$\epsilon = \{b(y)\}^T [H'(x)] \{r\} \quad (I-3)$$

(d) Stress-Strain Model. A general constitutive model was presented in detail in the main body of this report. The model relates increments of stress to increments of strain by the tangent modulus method, i.e.,

$$\Delta\sigma = E_e [1 - \alpha(\epsilon)] \Delta\epsilon \quad (I-4)$$

where  $E_e = E/(1 - \nu^2)$

$E$  = Young's elastic modulus

$\nu$  = Poisson's ratio

$\Delta\sigma$  = increment of stress

$\Delta\epsilon$  = increment of strain

$\alpha(\epsilon)$  = dimensionless function of total strain

The function  $\alpha(\epsilon)$  prescribes the reduction in the tangent modulus as a function of total strain. It was demonstrated that if the axis of bending,  $\bar{y}$ , is determined in a consistent manner,

$$y = \frac{\int_A [1 - \alpha(\epsilon)] y \, dA}{\int_A [1 - \alpha(\epsilon)] \, dA}$$

then the modified sectional properties are given as:

$$A^* = \int_A [1 - \alpha(\epsilon)] \, dA$$

$$I^* = \int_A [1 - \alpha(\epsilon)] (\bar{y} - y)^2 \, dA$$

where  $A$  is the actual cross-sectional area of the beam section, while  $A^*$  and  $I^*$  are modified values of cross-sectional area and moment of inertia consistent with the axis of bending. Note if the beam is linear elastic,  $\alpha(\epsilon) = 0$ , then  $A^*$  and  $I^*$  become the traditional  $I$  and  $A$  of beam theory. Furthermore, it should be recalled that the modified first moment is zero, i.e.,

$$\int_A [1 - \alpha(\epsilon)] (\bar{y} - y) dA = 0$$

These relationships are used in the following element stiffness derivation.

- (e) Element Stiffness by Virtual Work. The principle of virtual work may be used to equate an increment of virtual strain energy to an increment of virtual external work for one element as:

$$\int_V \delta \epsilon^T \Delta \sigma dV = \delta \{r\}^T \{\Delta F\}$$

where  $V$  = volume of beam element

$\delta$  = virtual movement symbol

$\{\Delta F\}^T = \{P_1, V_1, M_1, P_2, V_2, M_2\}$ , nodal loads

$P_1, P_2$  = axial loads at beam ends.

$V_1, V_2$  = shear load at beam ends

$M_1, M_2$  = moment load at beam ends

Inserting Equations I-2, I-3, and I-4 in the strain energy term, the virtual work statement provides the following element equilibrium equation:

$$[K_e] \{\Delta r\} = \{\Delta F\}$$

$$\text{where } [K_e] = \int_V [H'(x)]^T \{b(y)\} E_e [1 - \alpha(\epsilon)] \{b(y)\}^T [H'(x)] dV$$

In the above  $[K_e]$  is the element stiffness and could be evaluated by numerical quadrature. However, if it is assumed that  $\alpha(\epsilon)$  is relatively constant in the x-direction, an exact integration can be achieved by separating the volume integral into length and area integrations as follows:

$$[K_e] = \int_0^L [H'(x)]^T [G] [H'(x)] dx$$

$$\text{with } [G] = E_e \int_A \{b(y)\} [1 - \alpha(\epsilon)] \{b(y)\}^T dA$$

Substituting

$$\{b(y)\}^T = \{1, \bar{y}-y, \bar{y}-y, 1, \bar{y}-y, \bar{y}-y\}^T$$

into the integrand for the matrix  $[G]$  and recalling the definitions of  $A^*$  and  $I^*$ , we have upon integration:

$$[G] = \begin{bmatrix} A^* & 0 & 0 & A^* & 0 & 0 \\ 0 & I^* & I^* & 0 & I^* & I^* \\ 0 & I^* & I^* & 0 & I^* & I^* \\ A^* & 0 & 0 & A^* & 0 & 0 \\ 0 & I^* & I^* & 0 & I^* & I^* \\ 0 & I^* & I^* & 0 & I^* & I^* \end{bmatrix}$$

Lastly, inserting the component values for  $[H'(x)]$  in the expression for  $[K_e]$  and carrying out the indicated operations, the element stiffness may be explicitly expressed as:

$$[K_e] = E_e \begin{bmatrix} u_1 & v_1 & \theta_1 & u_2 & v_2 & \theta_2 \\ \frac{A^*}{L} & 0 & 0 & -\frac{A^*}{L} & 0 & 0 \\ 0 & \frac{12I^*}{L^3} & \frac{6I^*}{L^2} & 0 & -\frac{12I^*}{L^3} & \frac{6I^*}{L^2} \\ 0 & \frac{6I^*}{L^2} & \frac{4I^*}{L} & 0 & -\frac{6I^*}{L^2} & \frac{2I^*}{L} \\ -\frac{A^*}{L} & 0 & 0 & \frac{A^*}{L} & 0 & 0 \\ 0 & -\frac{12I^*}{L^3} & -\frac{6I^*}{L^2} & 0 & \frac{12I^*}{L^3} & -\frac{6I^*}{L^2} \\ 0 & \frac{6I^*}{L^2} & \frac{2I^*}{L} & 0 & -\frac{6I^*}{L^2} & \frac{4I^*}{L} \end{bmatrix} \quad (I-5)$$

The above element stiffness is valid for local beam coordinates. For assembling stiffnesses in global coordinates, standard coordinate transformations must be employed.

#### DEVELOPMENT OF AN INCOMPATIBLE ELEMENT

The following development is taken from Reference I-1. The material is duplicated here because it may not be readily available to readers. Moreover, the presentation is essential for the users who wish to extend or modify the element's capability.

The most straightforward procedure for developing two-dimensional quadrilateral elements is by sub-dividing the quadrilateral into two



or more triangular sub-regions and expressing the approximations within each triangular sub-region in terms of area coordinates (linear interpolation polynomials). The initial step, in such a development, is to decide upon the number of triangular sub-regions for each quadrilateral element and whether or not these sub-regions shall be sub-elements (i.e., capable of being independently used as triangular elements). The results of a preliminary investigation indicated that the most promising approach for the development of an incompatible quadrilateral element was to subdivide the quadrilateral into two triangular sub-regions (in CANDE this sub-division is performed so as to maximize the product of the areas of the two triangles). It should be noted that, by using this general approach, it is possible to develop several different types of convergent incompatible elements; of the elements investigated, the one presented herein displayed the best balance between accuracy and computational effort.

Figure I-2 illustrates the sub-division of the quadrilateral element and indicates the node numbering systems used for the element and the sub-regions. The area coordinates for sub-region 1 are defined as:

$$\begin{bmatrix} \xi_1 \\ \xi_2 \\ \xi_3 \end{bmatrix} = \frac{1}{2A} \begin{bmatrix} 2A_{23} & b_1 & a_1 \\ 2A_{31} & b_2 & a_2 \\ 2A_{12} & b_3 & a_3 \end{bmatrix} \begin{bmatrix} 1 \\ x \\ y \end{bmatrix} \quad (\text{I-6})$$

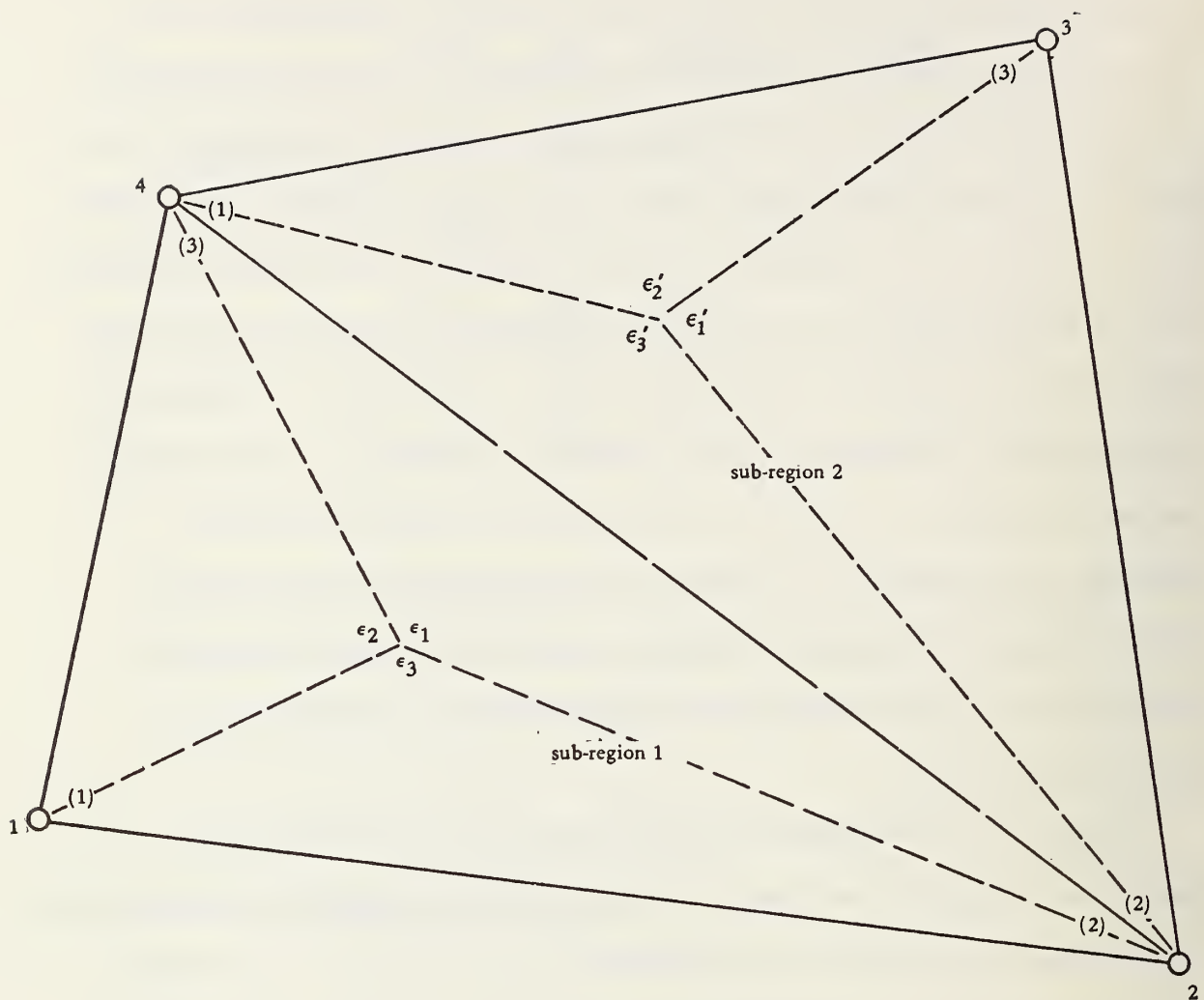


Figure I-2. Sub-division of quadrilateral element.

$$\text{where } A_{ij} = (x_i y_j - x_j y_i)/2 \quad (\text{I-7})$$

$$b_i = y_{J_i} - y_{K_i} \quad (\text{I-8})$$

$$a_i = x_{K_i} - x_{J_i} \quad (\text{I-9})$$

$$A = (1/2) x_\alpha b_\alpha \quad \alpha = \text{indicial summation } 1 \text{ to } 3 \quad (\text{I-10})$$

The repeated subscripts denote summation from 1 to 3,  $(x_i, y_i)$  denote the coordinates of triangle vertex "i," and

$$J_i = (2, 3, 1) \quad (\text{I-11})$$

$$K_i = (3, 1, 2) \quad (\text{I-12})$$

The expressions for the area coordinates of sub-region 2 are identical, with the exception that all quantities are primed.

Within each sub-region the displacements are initially approximated by complete quadratic expansions in  $x$  and  $y$ , i.e.,

Sub-region 1

$$u \approx u_i \xi_i + B_i \xi_{J_i} \xi_{K_i} \quad (\text{I-13})$$

$$v \approx v_i \xi_i + C_i \xi_{J_i} \xi_{K_i} \quad (\text{I-14})$$

Sub-region 2

$$u \approx u'_i \xi'_i + B'_i \xi'_{J_i} \xi'_{K_i} \quad (\text{I-15})$$

$$v \approx v'_1 \xi'_1 + C'_1 \xi'_{J_1} \xi'_{K_1} \quad (I-16)$$

$$\text{where } u_1 \equiv (u_{x_1}, u_{x_2}, u_{x_4}) \quad (I-17)$$

$$v_1 \equiv (u_{y_1}, u_{y_2}, u_{y_4}) \quad (I-18)$$

$$u'_1 \equiv (u_{x_4}, u_{x_2}, u_{x_3}) \quad (I-19)$$

$$v'_1 \equiv (u_{y_4}, u_{y_2}, u_{y_3}) \quad (I-20)$$

The  $u_{x_i}$  and  $u_{y_i}$  ( $i = 1 \rightarrow 4$ ) are the nodal point unknowns for the 4-node incompatible quadrilateral element. Unlike the compatible 8-node quadrilateral element, the  $B_i$ ,  $C_i$ ,  $B'_i$  and  $C'_i$  are treated as element unknowns, not midpoint node unknowns. It is easily seen that, if  $B_i = C_i = B'_i = C'_i = 0$ , the approximation becomes compatible (i.e., the displacement approximation becomes continuous for all points in the body). Thus, the convergence criterion requires that as the element size approaches zero,  $B_i \rightarrow 0$ ,  $B'_i \rightarrow 0$ ,  $C_i \rightarrow 0$ , and  $C'_i \rightarrow 0$ .

Assuming for the moment that the  $u_i$ ,  $v_i$ ,  $B_i$ , and  $C_i$  are independent, a 12 x 12-stiffness and a 12 x 1-load matrix for each of the triangular sub-regions can be developed in the usual manner. The matrices from the two sub-regions can now be combined to yield a 20 x 20-stiffness matrix and a 20 x 1-load matrix for the quadrilateral element. Denote these results as ( $\pi$  = element potential energy):

$$\begin{bmatrix} \frac{\partial \pi}{\partial \beta} \end{bmatrix} = \begin{bmatrix} S_{uu} & S_{u\psi} \\ S_{u\psi}^T & S_{\psi\psi} \end{bmatrix} \begin{bmatrix} U \\ \psi \end{bmatrix} = \begin{bmatrix} R_u \\ R_\psi \end{bmatrix} \quad (I-21)$$

$$\text{where } [U]^T = [u_{x_1}, u_{y_1}, u_{x_2}, u_{y_2}, u_{x_3}, u_{y_3}, u_{x_4}, u_{y_4}] \quad (I-22)$$

$$[\psi]^T = [B_1, B_2, B_3, C_1, C_2, C_3, B_1', B_2', B_3', C_1', C_2', C_3'] \quad (I-23)$$

$$[\beta] = \begin{bmatrix} U \\ \psi \end{bmatrix} \quad (I-24)$$

At this point the 12  $\psi$ 's could be treated as independent and eliminated at the element level to yield an 8 x 8-element stiffness matrix. The results, however, would not yield a convergent analysis, and, thus, it is now necessary to place certain constraints upon the admissible values of the  $\psi$ 's so as to assure convergence. The independence of the  $\psi$ 's is constrained by N constraints:

$$[\psi] = [T] [\phi] \quad (I-25)$$

$$\text{That is, } \psi_i = T_{ij} \phi_j \quad \begin{matrix} i = 1 \rightarrow 12 \\ j = 1 \rightarrow (12 - N) \end{matrix} \quad (I-26)$$

Introducing this transformation into Equation I-21 yields:

$$\begin{bmatrix} \frac{\partial \pi}{\partial \beta} \end{bmatrix} = \begin{bmatrix} S_{uu} & S_{u\phi} \\ S_{u\phi}^T & S_{\phi\phi} \end{bmatrix} \begin{bmatrix} U \\ \phi \end{bmatrix} = \begin{bmatrix} R_u \\ R_\phi \end{bmatrix} \quad (I-27)$$

$$\text{where } [\beta] = \left[ \frac{U}{\phi} \right] \quad (\text{I-28})$$

$$[S_{u\phi}] = [S_{u\psi}] [T] \quad (\text{I-29})$$

$$[S_{\phi\phi}] = [T]^T [S_{\psi\psi}] [T] \quad (\text{I-30})$$

$$[R_{\phi}] = [T]^T [R_{\psi}] \quad (\text{I-31})$$

Thus, a total of  $12-N$  element unknowns,  $(\phi)$ , remain; symbolically the elimination of these element unknowns can be expressed as:

$$[\phi] = -[S_{\phi\phi}]^{-1} \{[S_{u\phi}]^T [U] - [R_{\phi}]\} \quad (\text{I-32})$$

Convergence of the analysis requires that with vanishing element size, the  $\phi \rightarrow 0$ . As the element size decreases the strain state within the element approaches a constant strain state (i.e., first term in a Taylor's series expansion). The nodal displacements that correspond to an arbitrary constant strain state can be written as ( $\epsilon_{x_0}$ ,  $\epsilon_{y_0}$ , and  $\gamma_0$  are arbitrary):

$$\begin{aligned} [U]_{cs}^T = & [\epsilon_{x_0} x_1 + \gamma_0 y_1, \gamma_0 x_1 + \epsilon_{y_0} y_1, \epsilon_{x_0} x_2 \\ & + \dots, \gamma_0 x_4 + \epsilon_{y_0} y_4] \end{aligned} \quad (\text{I-33})$$

In addition, as the element size approaches zero, the norm of  $[S_{\phi\phi}]^{-1}$  remains bounded and  $[R_{\psi}] \rightarrow 0$  and, hence,  $[S_{\phi\phi}]^{-1} [R_{\phi}] \rightarrow 0$ . Thus, in



order to be assured that  $[\phi] \rightarrow 0$  with decreasing element size, it must be required that for an arbitrary constant strain state:

$$[S_{\phi\phi}]^{-1} [S_{u\phi}]^T [U]_{c.s.} = 0 \quad (I-34)$$

or 
$$[S_{u\phi}]^T [U]_{c.s.} = 0 \quad (I-35)$$

The above equation may be satisfied (for arbitrary values of  $\epsilon_{x_0}$ ,  $\epsilon_{y_0}$ , and  $\gamma_0$ ) if the transformation, Equation I-25, represented by the matrix  $[T]$  is such that the following three constraint equations are satisfied.

$$a_1 B_1 + a'_1 B'_1 = 0$$

$$b_1 C_1 + b'_1 C'_1 = 0 \quad (I-36)$$

$$b_1 B_1 + a_1 C_1 + b'_1 B'_1 + a'_1 C'_1 = 0$$

These constraints are satisfied if the transformation represented symbolically by Equation I-25 is:

$$B_1 = \phi_1 + \phi_5 + \frac{y_1}{A} (\phi_7 + \phi_8)$$

$$B_2 = \phi_1 + \frac{y_2}{A} (\phi_7 + \phi_8)$$

$$B_3 = \phi_1 + \frac{y_3}{A} (\phi_7 + \phi_8)$$

$$C_1 = \phi_3 + \phi_6 - \frac{x_1}{A} \phi_7$$

$$C_2 = \phi_3 - \frac{x_2}{A} \phi_7$$

$$C_3 = \phi_3 - \frac{x_3}{A} \phi_7$$

$$B'_1 = \phi_2 + \frac{y'_1}{A'} \phi_9$$

$$B'_2 = \phi_2 + \frac{y'_2}{A'} \phi_9$$

$$B'_3 = \phi_2 + \phi_5 + \frac{y'_3}{A'} \phi_9$$

$$C'_1 = \phi_4 - \frac{x'_1}{A'} (\phi_8 + \phi_9)$$

$$C'_2 = \phi_4 - \frac{x'_2}{A'} (\phi_8 + \phi_9)$$

$$C'_3 = \phi_4 + \phi_6 - \frac{x'_3}{A'} (\phi_8 + \phi_9)$$

Because the matrix [T] is quite sparse in actual practice the transformations given symbolically by Equations I-29, I-30, and I-31 are carried out so as to avoid the large number of trivial operations that would result if the matrix multiplications were performed directly.

The number of convergence constraints is three ( $N = 3$ ); thus, nine element unknowns remain ( $\phi_i, i = 1 \rightarrow 9$ ). The elimination of the element unknowns is carried out by Gaussian elimination; the results can symbolically be expressed in the form:

$$\begin{aligned} \left[ \frac{\partial \pi}{\partial U} \right] &= \{ [S_{uu}] - [S_{u\phi}] [S_{\phi\phi}]^{-1} [S_{u\phi}]^T \} [U] \\ &- \{ [R_u] - [S_{u\phi}] [S_{\phi\phi}]^{-1} [R_\phi] \} \end{aligned} \quad (I-38)$$

Thus, the final result is an eight-external degree-of-freedom (nine-internal degree-of-freedom) quadrilateral element that becomes compatible with its neighbors as the element sizes approach zero. In CANDE the above element stiffness is formed in the sub-routine STIFNS with the help of subroutines STFSUB, GEOM, and ESTAB.



## SOIL TEST DATA AND SOIL MODEL RESTRICTIONS

## SOIL TEST DATA

A comprehensive set of experimental data [J-1] on a uniform sand was available for the purposes of the soil study. This medium, known as Cook's bayou sand, was in a dense, dry condition. The characteristics of this material have been reported in the literature [J-2,J-3]; therefore, only that data pertaining to the final conclusions are included here. The available test data consisted of nine tests conducted using conventional triaxial apparatus. All test specimens were 2.8 inches in diameter by 6 inches high (7.1 cm x 16.8 cm) and were initially compacted to  $112 \pm 0.5$  pound per cubic foot ( $1,814 \pm \text{kg/m}^3$ ) dry density, resulting in void ratios of  $0.51 \pm 0.01$ . Since these specific test data had not been reported previously, a summary of the data for all nine tests is shown in Tables J-1, J-2, and J-3.

All calculations concerning specimen response assume a homogeneous state of stress and strain throughout the specimens. Although this is not precisely true, it is considered sufficiently accurate for prediction purposes. All correlations are based upon the levels of strain occurring during the first load cycle. For tests' cycled at various increments of loading the strains considered are those experienced by the soil the

Table J-1. Summary of Hydrostatic Compression Tests

Test No. 1		Test No. 2	
Confining Pressure (psi)	Volumetric Strain (in./in. x 10 <sup>-3</sup> )	Confining Pressure (psi)	Volumetric Strain (in./in. x 10 <sup>-3</sup> )
5.00	0.00	5.00	0.00
10.00	0.41	25.00	1.62
20.00	1.06	50.00	2.73
40.00	2.19	75.00	3.53
50.00	2.72	100.00	4.49
5.00	0.53	125.00	5.12
50.00	2.92	150.00	5.67
75.00	3.78	175.00	6.23
100.00	4.53	200.00	6.66
5.00	0.94	225.00	7.12
100.00	4.77	250.00	7.53
125.00	5.44		
150.00	6.00		
5.00	1.26		
150.00	6.24		
175.00	6.72		
250.00	7.23		
5.00	1.80		
200.00	7.70		
225.00	8.23		
250.00	8.52		



Table J-2. Summary of Uniaxial Strain Tests

Test No. 3			Test No. 4		
Axial Stress (psi)	Radial Stress (psi)	Axial Strain (in./in. x 10 <sup>-3</sup> )	Axial Stress (psi)	Radial Stress (psi)	Axial Strain (in./in. x 10 <sup>-3</sup> )
2.17	2.00	0.00	2.02	2.00	0.00
27.37	10.00	1.36	33.25	10.00	1.06
52.88	20.00	2.25	66.25	20.00	2.00
80.76	30.00	3.15	97.49	30.00	2.91
131.95	50.00	4.31	128.04	40.00	3.70
207.07	75.00	5.72	156.70	50.00	4.46
275.41	150.00	6.80	20.37	20.00	2.18
347.65	125.00	7.89	191.20	60.00	5.20
415.83	150.00	8.79	245.43	80.00	6.25
483.67	175.00	9.65	295.18	100.00	7.25
552.69	200.00	10.44	41.43	40.00	3.92
619.68	225.00	11.14	313.40	100.00	7.45
683.62	250.00	11.79	385.31	125.00	8.34
			460.13	150.00	9.19
			51.49	52.00	4.10
			461.16	150.00	9.58
			533.24	175.00	10.41
			597.24	200.00	11.10
			83.12	84.00	6.10
			603.60	200.00	11.40
			664.85	225.00	12.08
			734.87	250.00	12.72

Table J-3. Summary of Triaxial Shear Tests

Test No. 5 ( $\sigma_3 = 25$ psi)			Test No. 6 ( $\sigma_3 = 50$ psi)			Test No. 7 ( $\sigma_3 = 100$ psi)			Test No. 8 ( $\sigma_3 = 150$ psi)			Test No. 9 ( $\sigma_3 = 250$ psi)		
Deviator Stress (psi)	Axial Strain <sup>b)</sup> (in./in. x 10 <sup>-3</sup> )	Radial Strain <sup>b)</sup> (in./in. x 10 <sup>-3</sup> )	Deviator Stress (psi)	Axial Strain (in./in. x 10 <sup>-3</sup> )	Radial Strain (in./in. x 10 <sup>-3</sup> )	Deviator Stress (psi)	Axial Strain (in./in. x 10 <sup>-3</sup> )	Radial Strain (in./in. x 10 <sup>-3</sup> )	Deviator Stress (psi)	Axial Strain (in./in. x 10 <sup>-3</sup> )	Radial Strain (in./in. x 10 <sup>-3</sup> )	Deviator Stress (psi)	Axial Strain (in./in. x 10 <sup>-3</sup> )	Radial Strain (in./in. x 10 <sup>-3</sup> )
0.33	0.00	0.00	.16	0.00	- 0.00	0.99	0.00	- 0.00	2.71	0.00	- 0.00	8.58	0.00	- 0.00
15.13	0.41	- .04	13.27	.33	- .04	26.48	0.63	- .04	19.76	1.83	- .04	33.00	.25	- .07
32.13	.94	- .18	30.30	.65	- .11	77.44	1.91	- .22	70.88	2.49	- .15	118.38	1.08	- .18
49.11	1.57	- .40	64.33	1.74	- .37	128.31	3.33	- .58	138.96	3.98	- .44	220.73	2.24	- .44
66.05	2.48	- .80	98.26	3.23	- .91	179.01	5.04	- 1.24	206.88	5.80	- .95	322.86	3.91	- .88
82.91	3.92	- 1.54	132.01	5.61	- 1.87	229.30	7.31	- 2.48	291.22	8.62	- 2.20	424.56	5.90	- 1.61
99.51	7.40	- 3.33	164.98	10.30	- 4.83	278.72	10.75	- 4.86	357.59	12.27	- 4.32	541.90	9.39	- 3.33
111.17	13.01	- 6.40	196.14	20.58	- 11.45	376.16	17.08	- 9.57	421.84	18.07	- 8.31	639.89	14.71	- 6.34
						359.72	26.21	- 16.81	467.79	24.70	- 13.03	732.76	24.02	- 12.09
									496.53	31.00	- 17.64	802.56	38.64	- 20.73
												822.29	76.37	- 39.34

<sup>a)</sup> Deviator stress =  $\sigma_1 - \sigma_3$ .

<sup>b)</sup> Axial and radial strains do not include volumetric straining.

first time the load reached that level. Complete stress path and response history were recorded electronically for each test, and the experimental results were reasonably consistent between similar types of tests.

#### SOIL MODEL RESTRICTIONS

In Chapter 6 a variable modulus constitutive model (Extended-Hardin model) was proposed for characterizing the nonlinear behavior of soils for loading conditions representative of the culvert boundary value problem. The model was developed strictly for states of loading; no consideration is given to states of unloading. By definition, states of loading mean positive work is expended at every point in the system during each load step.

In the main text it is claimed that loading, i.e., positive work, is generally assured if the spherical and deviatoric stress components increase monotonically. The proof of this assertion follows.

The requirement of positive work over any load path is expressed as:

$$W = \int_{\text{path}} \sigma_{ij} d\epsilon_{ij} > 0 \quad (J-1)$$

where  $W$  = work per unit volume

$\sigma_{ij}$  = stress tensor

$\epsilon_{ij}$  = strain tensor

The subscripts denote standard indicial notation ( $i, j = 1, 2, 3$ ), and repeated indices imply summation.

The basic assumption of the variable modulus approach is that increments of strain are linearly related to increments of stress by an isotropic elastic relationship, i.e.,

$$d\epsilon_{ij} = \frac{1}{E} \left[ (1 + \nu) d\sigma_{ij} - \nu (d\sigma_{kk}) \delta_{ij} \right] \quad (J-2)$$

where  $E$  = Young's modulus

$\nu$  = Poisson's ratio

$$\delta_{ij} = \text{Kronecker delta} \quad \begin{cases} \delta_{ij} = 0 & i \neq j \\ \delta_{ij} = 1 & i = j \end{cases}$$

The elastic parameters,  $E$  and  $\nu$ , are dependent on the accumulated stress-strain state by a specified functional, such that  $E > 0$  and  $0 \leq \nu < 1/2$ . Within each load increment  $E$  and  $\nu$  are constant, so that Equation J-2 may be introduced into Equation J-1 to give work as a summation of  $N$  increments, i.e.,

$$W = \sum_{n=1}^N \Delta W_n > 0 \quad (J-3)$$

$$\text{where } \Delta W_n = \frac{1}{E} \int_{\bar{\sigma}_{ij}}^{\bar{\sigma}_{ij} + \Delta \bar{\sigma}_{ij}} \sigma_{ij} [(1 + \nu) d\sigma_{ij} - \nu \delta_{ij} d\sigma_{kk}] \quad (\text{J-4})$$

and  $\bar{\sigma}_{ij}$  = stress state at start of step n

$\Delta \bar{\sigma}_{ij}$  = stress increment over step n

Prior to integrating Equation J-4, it is convenient to decompose the stresses into spherical and deviatoric components:

$$\sigma_{ij} = s_{ij} + \sigma_o \delta_{ij} \quad (\text{J-5})$$

$$\text{where } \sigma_o = \frac{1}{3} \sigma_{kk} = \text{spherical stress} \quad (\text{J-6})$$

$$s_{ij} = \sigma_{ij} - \sigma_o \delta_{ij} = \text{deviatoric stresses} \quad (\text{J-7})$$

Using Equation J-5 in Equation J-4, noting  $\delta_{ij} s_{ij} = 0$ , and integrating  $ds_{ij}$  and  $d\sigma_o$  separately, the requirement for positive work increments (loading) may be written as:

$$\Delta W = \frac{1}{2E} [3(1 - 2\nu) \Delta B + (1 + \nu) \Delta Q] > 0 \quad (\text{J-8})$$

$$\text{where } \Delta B = 2 \bar{\sigma}_o \Delta \bar{\sigma}_o + (\Delta \bar{\sigma}_o)^2 \quad (\text{J-9})$$

$$\Delta Q = 2 \bar{s}_{ij} \Delta \bar{s}_{ij} + \Delta \bar{s}_{ij} \Delta \bar{s}_{ij} \quad (\text{J-10})$$

Recalling  $E > 0$  and  $0 \leq \nu < 1/2$  by construction, Equation J-8 is clearly positive for all stress increments,  $\Delta \bar{\sigma}_{ij} = \Delta \bar{s}_{ij} + \Delta \bar{\sigma}_o \delta_{ij}$ , such that  $\Delta B > 0$  and  $\Delta Q > 0$ . Upon inspecting the above equations for  $\Delta B$  and  $\Delta Q$ , it is evident the last term of each equation is positive for any stress increment. The first terms,  $2 \bar{\sigma}_o \Delta \bar{\sigma}_o$  and  $2 \bar{s}_{ij} \Delta \bar{s}_{ij}$ , are positive for all stress increments, where in  $\Delta \bar{\sigma}_o$  and  $\Delta \bar{s}_{ij}$  have the same sign as the corresponding components of the previous stress state,  $\bar{\sigma}_o$  and  $\bar{s}_{ij}$ . In other words, positive work is always expended when spherical and deviatoric stresses increase monotonically. Thus, the proof is complete. It should be evident that the requirement of monotonic stress paths is a sufficient but not necessary condition for positive work increments.

As a last comment, the culvert boundary value problem generally conforms to the requirement of monotonically increasing stress paths, because the loading is composed of monotonic increments of soil pressure placed uniformly on the system. Nonetheless, as a precautionary measure, the work increment,  $\Delta W_n$ , should be checked for each load step to assure positive work is expended.



## REFERENCES

- 1-1. Federally Coordinated Program of Research and Development in Highway Transportation. Improved structural design and construction techniques for culverts, Washington, D. C., Jul 1972.
- 1-2. National Cooperative Highway Research Program. Report No. 116: Structural analysis and design of pipe culverts, by R. J. Krizek et al. NAS/NAE Washington, D. C., 1971.
- 1-3. Highway Research Record No. 413, Soil Structure Interaction symposium, 1972. (All contributions are pertinent.)
- 1-4. Nataraja, M. "Finite element solution of stresses and displacements in a soil-culvert system," Ph D thesis, University of Pittsburg, 1973.
- 1-5. Marston, A. "The theory of external loads on closed conduits in the light of the latest experiments," Proc. HRB, vol 9, 1930, pp 138-170.
- 1-6. Marston, A. Second progress report to the joint concrete culvert pipe committee, Engineering Experiment Station, Iowa State College, Apr 1922.
- 1-7. Spangler, M. G. A preliminary experiment on the supporting strength of culvert pipes in an actual embankment, Bull. no. 76, Engineering Experiment Station, Iowa State College, 1926.
- 1-8. Spangler, M. G. "The structural design of flexible pipe culverts," Bull. no. 153, Engineering Experiment Station, Iowa State College, 1941.
- 1-9. American Concrete Pipe Association. Design Manual Concrete Pipe, Third printing (revised), Arlington, VI, 1974.
- 1-10. Watkins, R. K., and M. G. Spangler. "Some characteristics of the modulus of passive resistance of soil: A study in similitude," Proc. HRB, vol 37, 1958, pp 576-583.
- 1-11. White, H. L., and J. P. Layer. "The corrugated metal conduit as a compression ring," Proc. HRB, vol 39, 1960, pp 389-397.
- 1-12. Watkins, R. K. "Failure conditions of flexible culverts embedded in soil," Proc. HRB, vol 39, 1960, 361-371.

- 1-13. Meyerhof, G. G., and L. D. Baize. Strength of steel culvert sheets bearing against compacted sand backfill, Highway Research Record no. 30, 1963, pp 1-19.
- 1-14. Luscher, V. "Buckling of soil-surrounded tubes," Proc. ASCE, vol 92, SM6, Nov 1966.
- 1-15. Chelapati, C. V., and J. R. Allgood. Buckling of cylinders in a confining medium, Highway Research Record no. 413, 1972, pp 77-88.
- 1-16. Watkins, R. K. Structural design of buried circular conduits, Highway Research Record no. 145, 1966, pp 1-6.
- 1-17. Nielson, F. D. Soil structure arching analysis of buried flexible structures. Highway Research Record no. 185, 1967, pp 36-50.
- 1-18. American Iron and Steel Institute. Handbook of steel drainage and highway construction products. AISI, New York, 2nd ed, 1971.
- 1-19. American Association of State Highway Officials. Standard specifications for highway bridges. AASHTO, Washington, D. C., 10th ed, 1969.
- 1-20. U. S. Department of Transportation. Corrugated metal pipe-structural design criteria and recommended installation practice, USDOT, Federal Highway Admin., Bureau of Public Roads, Washington, D. C., 1970.
- 1-21. Savin, G. N. "Stress concentration around holes which are strengthened by elastic rings," International Series of Monographs in Aeronautics and Astronautics, vol 1, div 1, chapter V, 1961, pp 324-352.
- 1-22. Air Force Weapons Laboratory. Technical Report No. AFWL TR-65-98: Pressure distribution on underground structural cylinders, by K. Hoeg. Kirtland Air Force Base, NM, Apr 1966.
- 1-23. Burns, J. Q. "An analysis of circular cylindrical shells embedded in elastic media," Ph D thesis, University of Arizona, Tuscon, AZ.
- 1-24. Kay, J. N., and R. J. Krizek. "Adaptation of elastic theory to the design of circular conduits," Institution of Engineers, Australia, Civil Engineering Transactions, Apr 1970, pp 85-90.
- 1-25. Dar, S. M., and R. C. Bates. "Stress analysis of hollow cylindrical inculsions," Proc. ASCE, vol 100, no. GT2, Feb 1974, pp 123-138.

- 1-26. Nielson, F. D., and N. D. Statish. Design of circular soil-culvert systems, Highway Research Record no. 413, Soil-Structure Interaction Symposium, 1972, pp 67-76.
- 1-27. Civil Engineering Laboratory. Technical Report R-816: Soil structure interaction: Horizontal cylinders, by T. K. Lew. Port Hueneme, CA, Oct 1974.
- 1-28. Brown, C. B. "Forces on rigid culverts under high fills," Proc. ASCE, vol 93, no. ST5, Oct 1967, pp 195-215.
- 1-29. Brown, C. B, D. R. Green, and S. Pawsey. "Flexible culverts under high fills," Proc. ASCE, vol 94, no. ST4, Apr 1968, pp 905-917.
- 1-30. Allgood, J. R., and S. K. Takahashi. Balanced design and finite element analysis of culverts, Highway Research Record no. 413, Soil-Structure Interaction Symposium, 1972.
- 1-31. U. S. Army Waterways Experiment Station. Technical Report N-72-7: Fundamental studies of medium-structure interaction," by J. L. Kirkland and R. E. Walker. Vicksburg, MS, Jun 1972.
- 1-32. Anand, S. C. "Stress distributions around shallow buried rigid pipes," Proc. ASCE, ST1, Paper 10258, Jan 1974.
- 1-33. Duncan, J. M. "Finite element analysis of buried flexible metal culverts," paper to be published in Lauritis Bjerrum Memorial Volume, Norwegian Geotechnical Institute, Oslo, Norway (1976).
- 1-34. Abel, J. F., and R. Mark. "Soil stresses around flexible, elliptical pipes," Proc. ASCE, vol 99, no. SM7, Jul 1973, pp 509-526.
- 1-35. California Division of Highways, Bridge Department Report No. 73-6: Structural behavior of a flexible metal culvert under a deep earth embankment, by D. W. Spannagel, R. E. Davis, and A. E. Bacher, Jun 1973.
- 1-36. Duncan, J. M. "A design method for metal culvert structures based on finite element analyses" for Kaiser Aluminum and Chemical Sales, Inc. (presented at TRB-76), 1976.
- 1-37. Parmalee, R. A. "A new design method for buried concrete pipe," Symposium on Concrete Pipe and Soil-Structure System, ASTM, Committee C-13, Jun 1976.



1-38. Kay, N., and J. Abel. "A design approach for circular buried conduits," presented at Transportation Research Board Meeting, Committee A2K04, Jan 1976.

1-39. Civil Engineering Laboratory. Report to Federal Highway Administration, CANDE: User Manual, by M. G. Katona and J. M. Smith, Port Hueneme, CA, Jul 1976.

1-40. Civil Engineering Laboratory. Report to Federal Highway Administration, CANDE: System Manual, by M. G. Katona and J. M. Smith, Port Hueneme, CA, Jul 1976.

3-1. American Railway Engineering Association Committee. "Corrugated metal culverts for railroad purposes," Proc. AREA, vol 27, 1926, pp 794-798.

3-2. Spangler, M. G. "The structural design of flexible pipe culverts," Bull. no. 153, Engineering Experiment Station, Iowa State College, 1941.

3-3. White, H. L., and J. P. Layer. "The corrugated metal conduit as a compression ring," Proc. HRB, vol 39, 1960, pp 389-397.

3-4. Watkins, R. K. "Failure conditions of flexible culverts embedded in soil," Proc. HRB, vol 39, 1960, pp 361-371.

3-5. Meyerhof, G. G., and L. D. Baikié. Strength of steel culvert sheets bearing against compacted sand backfill, Highway Research Record no. 30, 1963, pp 1-19.

3-6. Luscher, V. "Buckling of soil-surrounded tubes," proc. ASCE, vol 92, SM6, Nov 1966.

3-7. Chelapati, C. V., and J. R. Allgood. Buckling of cylinders in a confining medium, Highway Research Record no. 413, 1972, pp 77-88.

3-8. American Association of State Highway Officials. "Standard specifications for highway bridges," AASHTO, Washington, D. C., 10th ed., 1969.

3-9. American Concrete Pipe Association, Design Manual Concrete Pipe, Third printing (revised), Arlington, VI, 1974.

3-10. National Cooperative Highway Research Program. Report no. 116: Structural analysis and design of pipe culverts, by R. J. Krizek et al. NAS/NAE, Washington, D. C., 1971 (Lum, p 21).

- 5-1. Burns, J. Q. "An analysis of circular cylindrical shells embedded in elastic media," Ph D thesis, University of Arizona, Tucson, AZ, 1965.
- 5-2. Herrmann, L. R. "User's manual for plane strain incremental construction program," University of California, Davis, 1972.
- 5-3. Zienkiewicz, O. C. "The finite element method in engineering science," McGraw-Hill, London, 1971.
- 5-4. Herrmann, L. R. "Efficiency evaluation of a two-dimensional incompatible finite element," Journal of Computers and Structures, vol 3, 1973, pp 1377-1395.
- 5-5. National Cooperative Highway Research Program. Report no. 116: Structural analysis and design of pipe culverts, by R. J. Krizek et al. NAS/NAE, Washington, D. C. 1971.
- 5-6. Chelapati, C. V., and J. R. Allgood. Buckling of cylinders in a confining medium, Highway Research Record no. 413, 1972, pp 77-88.
- 6-1. Truesdell, C., and W. Noll. "The nonlinear field theories of mechanics," Encyclopedia of Physics, vol III/3, Springer-Verlag, 1965.
- 6-2. Civil Engineering Laboratory. Technical Report R- : A viscoelastic-plastic constitutive model with a finite element solution methodology, by M. G. Katona. Port Hueneme, CA (to be published).
- 6-3. Zienkiewicz, O. C., and I. C. Cormeau. "Viscoplasticity, plasticity and creep in elastic solids, A unified numerical solution approach," International Journal for Numerical Methods in Engineering, vol 8, 1974, pp 821-845.
- 6-4. Ghaboussi, J., and E. L. Wilson. "Flow of compressible fluid in porous elastic media," UC-SESM Report 71-12, University of California Berkeley, Jul 1971.
- 6-5. Wong, Kai S., and J. M. Duncan. "Hyperbolic stress-strain parameters for nonlinear finite element analysis of stresses and movements in soil masses," Report TE-74-3 to National Science Foundation (Geotechnical Engineering), Department of Civil Engineering, University of California, Berkeley, Jul 1974.

- 6-6. Hardin, B. O. Constitutive relations for air field subgrade and base course materials, Technical Report UKY 32-71-CE5, University of Kentucky, College of Engineering, Soil Mechanics Series no. 4, Lexington, KY, 1970.
- 6-7. Air Force Weapons Laboratory. Technical Report AFWL-TR-72-201: Effects of strain amplitude on the shear modulus of soils, by B. O. Hardin. Kirtland Air Force Base, NM, Mar 1973.
- 6-8. Duncan, J. M., and Chin-Yung Chang. "Nonlinear analysis of stress and strain in soils," Journal of the Soil Mechanics and Foundations Division, ASCE, vol 96, no. SM5, Proc. Paper 7513, Sep 1970, pp 1629-1653.
- 6-9. Kulhawy, F. H., and J. M. Duncan. "Finite element analysis of stresses and movements in dams during construction," Report no. TE 69-4, Office of Research Services, University of California, Berkeley, 1970.
- 6-10. Konder, R. L. "Hyperbolic stress-strain response: Cohesive soils," Journal of the Soil Mechanics and Foundations Division, ASCE, vol 89, no. SM1, Proc. Paper 3429, 1963, pp 115-143.
- 6-11. Konder, R. L., and J. S. Zelasko. "A hyperbolic stress-strain formulation for sands," Proc. 2nd Pan-American Conference on Soil Mechanics and Foundation Engineering, Brazil, vol 1, 1963, pp 289-324.
- 6-12. Corotis, R. B., M. H. Farzin, and R. J. Krizek. Nonlinear stress-strain formulation for soils. Report by Northwestern University to the American Concrete Pipe Association, 1973.
- 6-13. Isenberg, J. "Nuclear Geoplosics, Part 2 mechanical properties of earth materials," DNA AD-755 488, Agababian Associates, Nov 1972.
- 6-14. Nayak, G. C., and O. C. Zienkiewicz. "Elasto-plastic stress analysis, generalization for various constitutive relations including strain softening," International Journal of Numerical Methods in Engineering, vol 5, 1972, pp 113-135.
- 6-15. Ballard, J. T. Personal Communication to the Naval Civil Engineering Laboratory, 6 Sep 1973.
- 7-1. Nataraja, M. "Finite element solution of stresses and displacements in a soil-culvert system," Ph D dissertation, Civil Engineering, University of Pittsburgh, 1973.



- 7-2. Leonards, J. "Performance of pipe culverts buried in soil," current research project at Purdue University, Department of Civil Engineering, Lafayette, IN, 1975.
- 7-3. Conry, T. F., and A. Seireg. "A mathematical programming method for design of elastic bodies in contact," Journal Applied Mechanics, vol 38, 1971, pp 387-392.
- 7-4. Chan, S. H., and I. S. Tuba. "A finite element method for contact problems of solid bodies," Int. Journal of Mechanical Sciences, vol 13, 1971, pp 615-639.
- 7-5. Hughes, T. J. R., R. L. Taylor, and J. L. Sackman. "A finite element method for a class of contact-impact problems," to appear in the Journal of Computer Methods in Applied Mechanics and Engineering (1975-76).
- 10-1. American Concrete Pipe Association. Design Manual Concrete Pipe, Third printing (revised), Arlington, VA, 1974.
- 10-2. American Association of State Highway Officials. "Standard specifications for highway bridges," AASHTO, Washington, D. C., 10th ed., 1969.
- 10-3. Spannagel, D., and R. Davis. Personal Communications to the Civil Engineering Laboratory from California Division of Highways, Bridge Department, 1976.
- A-1. National Cooperative Highway Research Program. Report No. 16: Structural analysis and design of pipe culverts, by R. J. Krizek et al. NAS, WAE, Washington, D.C., 1971.
- A-2. Haviland, J. E., P. V. Belair, and V. D. Morrell. Durability of corrugated metal culverts. New York State Department of Transportation, 1967.
- A-3. United States Steel Corporation Applied Research Laboratory. Steel products for culvert applications, by J. D. Swan. Presented at HRB Annual Meeting, 1972.
- A-4. Worley, H. E. Corrosion of corrugated metal pipe, State Highway Commission of Kansas, 1971.
- A-5. Utah State Department of Highways Report. Evaluation of aluminum alloy pipe for use in Utah's highways, by D. E. Peterson. Jun 1973.
- A-6. Koepf, A. H. The mechanisms of abrasion of aluminum alloy culverts, highway Research Record 262, 1969.

A-7. Butler, B. E. Structural design practice of pipe culverts, Highway Research Record No. 413, Soil-Structure-Interaction Symposium, 1972, pp 57-66.

B-1. National Cooperative Highway Research Program. Synthesis 8: "Construction of embankments," HRB/NRC/NAS/NAE, 1971.

B-2. Federal Highway Administration. Report No. FHWA-RD-73-8: The compaction of soil and rock materials for highway purposes, by H. E. Wahls, C. P. Fisher, and L. J. Langfelder. Aug 1966.

B-3. Yoder, E. J. Principles of pavement design. New York, Wiley. 1959.

C-1. National Cooperative Highway Research Program. Report No. 116: Structural analysis and design of pipe culverts, by R. J. Krizek et al. NAS, NAE, Washington, D.C., 1971.

C-2. Siko, A. "Practical method for the calculation of elastically supported culverts," Vizugyi Kozelmen-Yek No. 3-4, Budapest, 1958.

C-3. California Division of Highways, Bridge Department. Report No. 73-6: Structural behavior of a flexible metal culvert under a deep embankment using method A backfill, by D. W. Spannagel, R. E. Davis, and A. E. Baker, Jun 1973.

C-4. Tschebotarioff, G. Soil mechanics, foundations, and earth structures, McGraw-Hill, NY, 1951.

D-1. Department of Transportation, Bureau of Public Roads Manual: Corrugated metal pipe, structural design criteria, by W. E. Wolf and M. Townsend. Revised 1970.

D-2. Standard Specifications for Highway Bridges, The American Association of State Highway Officials, Tenth Edition, 1969.

D-3. Handbook of Steel Drainage and Construction Products, Second Edition, American Iron and Steel Institute, New York, NY, 1971.

D-4. National Clay Pipe Institute. Clay pipe engineering manual, 1972 edition.

D-5. Drawsky, R. H. Design method for buried flexible structures, Kaiser Aluminum and Chemical Co., Aug 1965.

D-6. Techite Pipe Installation Guide, United Technology Center, Sunnyvale, CA, 1972.

D-7. Concrete Pipe Design Manual, First Edition, American Concrete Pipe Association, VA, 1970.

D-8. Technical Manual: Corrugated steel pipe. California Corrugated Steel Pipe Association, San Francisco, CA.

E-1. Handbook of Steel Drainage and Construction Products. Second Edition, American Iron and Steel Institute, New York, 1971.

E-2. E. Silberman. "Effect of helix angle on flow in corrugated pipes," Journal of the Hydraulic Division, ASCE, vol 96, no. HY11, Nov 1970, pp 2253-2263.

E-3. Multi-Plate Super-Span Product Bulletin of Armco Steel Corporation, Metal Products Div., Middletown, OH.

E-4. Watkins, Reynold K. "Reinforced soil bridge," prepared for AASHTO Committee on Bridges and Structures, Apr 1974.

E-5. No Joint Cast-in-Place Concrete Pipe. Bulletin 33, No-Joint Pipe of Southern California, Anaheim, CA.

E-6. Composite Installed Pipe of Hydro Conduit Corporation. Newport Beach, CA, Mar 1973.

E-7. Pipe Technical Catalog. Ccr-Ban Industries, Tampa, FL.

E-8. Rib-Tite Product Information Brochure. Precision Polymers, Inc. Rockway, NJ.

E-9. "Squashed Pipe Market Ready to Go," Civil Engineering - ASCE, vol 43, no. 9, Sep 1973, p. 24.

E-10. Armco Truss Pipe Brochure, Armco Steel Corporation, Greencastle, PA, 1973.

E-11. Brookhaven National Laboratory, Concrete-Polymer Materials, Third Topical Report, Jan 1971.

E-12. Air Force Weapons Laboratory. TR 68-4D: Effect of backpacking on structure-medium-interaction, by D. A. Linger. Kirtland Air Force Base, NM, Jul 1968.

E-13. Allgood, J. R. Structures in soil under high loads, Proc. ASCE, vol 97, SM3, Mar 1971, pp 565-579.

E-14. Naval Civil Engineering Laboratory. TR-789: Effect of backpacking and internal pressurization on stresses transmitted to buried cylinders, by S. K. Takahashi. Port Hueneme, CA, May 1973.



E-15. Naval Civil Engineering Laboratory. TR-668: Response of buried capsules in the high-overpressure region, by R. J. Odello and J. R. Allgood. Port Hueneme, CA, 1970.

E-16. Air Force Weapons Laboratory. Technical Report No. AFWL TR-65-98: Pressure distribution on underground structural cylinders, by K. Hoeg. Kirtland Air Force Base, NM, Apr 1966.

E-17. Nataraja, M. "Finite element solution of stresses and displacements in a soil-culvert system," Ph D thesis, University of Pittsburg, 1973.

E-18. Iowa State College Engineering Experiment Station. Bulletin 96: The theory of loads on closed conduits in light of the latest experiments, by A. Marston, 1930.

E-19. Taylor, R. K. Induced trench method of culvert installation, Highway Research Record, no. 443, 1973.

F-1. U.S. Bureau of Reclamation. Engineering Monograph No. 6: Stress analysis of concrete pipe, by H. C. Olander. Denver, CO, Oct 1950.

F-2. Heger, F. J., E. G. Nawy, and R. B. Saba. Structural behavior of circular concrete pipe reinforcement with welded wire fabric, Title no. 60-60, ACI Journal, Oct 1963.

F-3. Katoh, J. Systematic stress analysis of circular pipe, Proc. ASCE, TE-4, Nov 1972.

F-4. Heger, F. J. Structural behavior of circular reinforced concrete pipe - development of theory, Title No. 60-67, ACI Journal, Nov 1963, p 1570.

F-5. California Division of Highways. Bridge Department Report No. 4-71: Structural behavior of a concrete pipe culvert, Mountainhouse Creek (Part 1), by R. E. Davis, A. E. Bacher, and J. C. Obermu. Apr 1971.

F-6. Nielsen, F. D. Experimental studies in soil-structure interaction, Highway Research Record no. 413: Soil-structure interaction symposium, 1972, p 30.

F-7. California Division of Highways. Bridge Department Report No. 73-6: Structural behavior of a flexible metal culvert under a deep earth embankment using method A backfill, by D. W. Spannagel, R. E. Davis, and A. E. Bacher. Jun 1973.

F-8. Spangler, M. G. Theory of loads on negative projecting conduits, Proc. HRB, vol 30, 1950, pp 153-161.

- F-9. Utah State University Engineering Experiment Station Report: The structural performance of buried corrugated steel pipes, by R. K. Watkins and A. P. Moser. Logan, UT, 1969.
- F-10. Utah State University Engineering Experiment Station Report: Response of corrugated steel pipe to external soil pressures, by. R. K. Watkins and A. P. Moser, Jun 1971.
- F-11. Parmalee, R. A., and R. B. Corotis. The Iowa Deflection formula: an appraisal, Highway Research Record no. 413, 1972, pp 89-101.
- F-12. Chelepati, C. V., and J. R. Allgood. Buckling of cylinders in a confining medium, Highway Research Record no. 413, 1972, pp 77-88.
- F-13. University of Detroit. Department of Engineering Mechanics. Report on Contract NBY-32254: Inelastic buckling of an elastically supported buried cylinder, by D. A. DaDeppo. Detroit, MI, Apr 1965.
- F-14. Callander, R. A. Hydraulics of culvert outlets, New Zealand Engineering, vol 28, no. 9, Sep 15, 1971, pp 261-265.
- F-15. Smith, G. L., and D. E. Hallmark. New developments in erosion control at culvert outlets, Highway Research Bulletin 286, Drainage Structures, Design and Performance, 1960: NAS/HRC Pub. 856, 1961, p 22.
- F-16. University of California Report EERC-69-16: The behavior of sand under seismic loading conditions, by M. L. Silver and H. B. Seed, Dec 1969.
- F-17. Montana State University Report: Large culvert studies in Montana, by A. C. Scheer. For Montana Highway Commission and the U.S. Department of Transportation, 1968.
- F-18. Peck, R. B., H. O. Ireland, and C. Y. Teng. A study of retaining failure, 2nd International Conference of S.M. and F.E., 1968.
- F-19. Singh, A., and J. K. Mitchell. Creep potential and creep rupture of soils, Proc. International conference on S.M. and F.E., 1969.
- F-20. Waterways Experiment Station Miscellaneous Paper S-73-28-1: Properties of expansive clay soils, Report 1, Jackson Field Test Section Study, NTIS AD 761-084, May 1973.
- F-21. National Cooperative Highway Research Program, Report No. 116: Structural Analysis and Design of Pipe Culverts, by R. J. Krizek et al. NAS, NAE, Washington, D.C., 1971.

H-1. Clough, R. W., and R. J. Woodward. "Analysis of Embankment Stresses and Deformations," Journal of Soil Mechanics and Foundations Division, Proc., ASCE, Jul 1967, pp 529-549.

H-2. Brown, C. B., "Forces on Rigid Culverts Under High Fills," Proc. ASCE, vol 93, no. ST5, Oct 1967, pp 195-215.

I-1. Herrmann, L. R. "Efficiency Evaluation of a Two Dimensional Incompatible Finite Element," Journal of Computers and Structures, vol 3, 1973, pp 1377-1395.

J-1. Ballard, J. T. Personal Communication to the Naval Civil Engineering Laboratory, Sep 6, 1973.

J-2. U.S. Army Engineer Waterways Experiment Station. Technical Report No. 1-683: Response of horizontally oriented buried cylinders to static and dynamic loading, by A. F. Dorris. Vicksburg, MS, Jul 1965.

J-3. U.S. Army Engineer Waterways Experiment Station. C. E. Technical Report No. 1-821: Behavior of flexible cylinders buried in sand under static and dynamic loading, by G. E. Albritton. Vicksburg, MS, Apr 1968.



y Administration.  
RD-77-5.

ELEPHONE	DATE
<del>285-2009</del>	<del>1-18-93</del>

GP 0 896.099

DOT LIBRARY



00055914

